Ministère de l'Enseignement Supérieur et de la Recherche Scientifique
Université Mohamed Khider - Biskra
Faculté des Sciences et de la Technologie
Département de Génie Électrique

Thèse de Doctorat

En vue de l'obtention du diplôme de docteur LMD en électrotechnique

Contribution à l'estimation d'état des systèmes non linéaires décrits par les multi-modèles flous

Réalisé par: **Wail HAMDI**

Soutenue publiquement le: 11/11/2024

Devant le jury composé de:

Mohamed BOUMEHRAZ	Professeur	Université de Biskra	Président
Mohamed Yacine HAMMOUDI	Professeur	Université de Biskra	Rapporteur
Mostefa Mohamed TOUBA	MCA	Université de Biskra	Examinateur
Kheireddine CHAFAA	Professeur	Université de Batna	Examinateur
Okba KRAA	MCA	Université de Biskra	Examinateur

Année Universitaire 2024/2025

Ministry of Higher Education and Scientific Research
Mohamed khider university of biskra
Faculty of Sciences and Technology
Department of Electrical Engineering

LMD Doctoral Thesis

To obtain the LMD doctor's degree in electrical engineering

Contribution to the state estimation of nonlinear systems described by fuzzy multi-models

By: **Wail HAMDI**

Publicly defended on: 11/11/2024

In front of the committee consisting of:

Mohamed BOUMEHRAZ	Professor	University of Biskra	President
Mohamed Yacine HAMMOUDI	Professor	University of Biskra	Thesis Supervisor
Mostefa Mohamed TOUBA	MCA	University of Biskra	Examiner
Kheireddine CHAFAA	Professor	University of Batna	Examiner
Okba KRAA	MCA	University of Biskra	Examiner

Academic Year 2024/2025

Dedication

To my dear parents,

To my dear family,

To all my friends.

Acknowledgment

I begin by expressing my gratitude to God Almighty for bestowing upon me this significant blessing and success on the path I have chosen. Without His grace, reaching this stage and completing it would not have been possible. I extend my sincere thanks to God for all His blessings. It is essential to acknowledge that the worldly means we employed were not the contributors to our progress; rather, it was the grace of God that served as the foundation for our success and accomplishment in this endeavor.

My profound gratitude and appreciation extend to my thesis director, Dr. Hammoudi Mohamed Yacine, a member of the LMSE Laboratory at the University of Biskra. His availability, unwavering support, and, most importantly, patience were key factors in the success of my thesis.

I wish to express my sincerest appreciation to Mr. Boumehraz Mohamed, the head of the LMSE laboratory, for all the assistance he provided me and for allocating his time to answering all the inquiries I presented to him within the scope of my research. I thank him again as well as Mrs. Betka, the laboratory engineer, for providing an ideal environment for research and experimental work. The completion of this work would not have been possible without their assistance and the support of all members of the LMSE.

I extend my sincere thanks to the esteemed members of my jury: Boumehraz Mohamed, from the University of biskra, who did me the honor of chairing my thesis; Professors Mostefa Mohamed touba and Okba Kraa, also from the University of biskra; and Professor Kheireddine CHAFAA, from the University of batna, for their gracious agreement to be part of my jury.

Undoubtedly, I cannot conclude without expressing my heartfelt gratitude to my parents for their unwavering support throughout this journey. Their collaborative efforts alongside me played a crucial role in helping me successfully complete this endeavor. I am truly thankful for the conducive conditions they provided and the invaluable assistance they offered.

To everyone who offered help without exception through a smile, words of encouragement, or provision of information; to all who showed confidence in me and provided the energy I needed to persevere and achieve success, I offer my sincerest thanks.

Abstract

The research work presented in this thesis focuses on the state estimation of nonlinear systems described by the Takagi-Sugeno multi-model with unmeasurable premise variables. The primary contribution of this work lies in mitigating conservatism in the stability conditions of the state estimation error dynamics. To alleviate this conservatism, the poly-quadratic Lyapunov function was employed, specifically to reduce the conservatism associated with the quadratic approach. Various methodologies have been presented based on this function, encompassing the Lipschitz method, $\mathcal{L}_2$-gain synthesis, and the differential mean value theorem. We derived linear and bilinear stability conditions for the convergence of the estimation error dynamics, and we have introduced an efficient algorithm for solving the bilinear one, which was then compared to other existing solvers. In the second part of this work, the challenges of unknown inputs have been addressed. We presented different observer designs, including proportional integral, proportional multi-integral, and decoupled unknown input observers. Furthermore, we tackled the challenge of the real-time applicability of the observer by optimizing the observer's Lyapunov matrix. This methodology was implemented and tested for unknown input observers in real-time examples, and a comprehensive discussion comparing the performance of the various unknown input observers was provided. Overall, this research contributes to advancing the understanding and practical implementation of state and unknown input estimation techniques in complex nonlinear systems.

Key words: Nonlinear system, Takagi-Sugeno multi-model, state estimation, Unknown input estimation, Linear matrix inequalities, Bilinear matrix inequalities, poly-quadratic Lyapunov function.

Résumé

Le travail de recherche présenté dans cette thèse se concentre sur l'estimation de l'état des systèmes non linéaires décrits par le multi-modèle de Takagi-Sugeno avec des variables de prémisse non mesurables. La principale contribution de ce travail réside dans l'atténuation du conservatisme dans les conditions de stabilité de la dynamique de l'erreur d'estimation d'état. Pour atténuer ce conservatisme, la fonction de Lyapunov poly-quadratique a été employée, spécifiquement pour réduire le conservatisme associé à l'approche quadratique. Diverses méthodologies ont été présentées sur la base de cette fonction, notamment la méthode de Lipschitz, la synthèse du gain $\mathcal{L}_2$ et le théorème de la valeur moyenne différentielle. Nous avons dérivé des conditions de stabilité linéaires et bilinéaires pour la convergence de la dynamique de l'erreur d'estimation, et nous avons introduit un algorithme efficace pour résoudre le cas bilinéaire, qui a ensuite été comparé à d'autres solveurs existants. Dans la deuxième partie de ce travail, les défis posés par les entrées inconnues ont été abordés. Nous avons présenté différentes conceptions d'observateurs, notamment des observateurs proportionnel integral, proportionnel multi-integral et des observateurs à entrées inconnues découplés. En outre, nous avons relevé le défi de l'applicabilité en temps réel de l'observateur en optimisant la matrice de Lyapunov de l'observateur. Cette méthodologie a été mise en oeuvre et testée pour les observateurs à entrée inconnue dans des exemples en temps réel, et une discussion complète comparant les performances des différents observateurs à entrée inconnue a été fournie. Dans l'ensemble, cette recherche contribue à faire progresser la compréhension et la mise en oeuvre pratique des techniques d'estimation de l'état et des entrées inconnues dans les systèmes non linéaires complexes.

Mots-Clés: Système non linéaire, multi-modèle de Takagi-Sugeno, estimation d'état, estimation d'entrée inconnue, inégalités matricielles linéaires, inégalités matricielles bilinéaires, fonction de Lyapunov poly-quadratique.

ملخص

يركز العمل البحثي المقدم في هذه الأطروحة على تقدير الحالة للأنظمة غير الخطية الموصوفة بنموذج تاكاجي-سوجينو المتعدد مع متغيرات قرار غير قابلة للقياس. تكمن المساهمة الأساسية لهذا العمل في التخفيف من التحفظ في شروط استقرار ديناميكيات خطأ تقدير الحالة. وللتخفيف من هذا التحفظ، تم استخدام دالة Lyapunov متعددة التربيعات، وتحديدًا لتقليل التحفظ المرتبط بالنهج التربيعي. تم تقديم منهجيات مختلفة استنادًا إلى هذه الدالة، بما في ذلك طريقة Lipschitz، وL_2-gain synthesis، ونظرية القيمة المتوسطة التفاضلية. لقد اشتققنا شروط الاستقرار الخطية والثنائية الخطية من اجل تقارب ديناميكيات خطأ التقدير، وقدمنا خوارزمية فعالة لحل ثنائية الخط، والتي تمت مقارنتها بعد ذلك مع غيرها من أدوات الامثلة الأخرى الموجودة. في الجزء الثاني من هذا العمل، تمت معالجة تحديات المدخلات المجهولة. قدمنا تصاميم مختلفة للمراقب، بما في ذلك مراقب تناسبي تكاملي، والتناسبي متعدد التكاملات، ومراقب فصل المداخل المجهولة. علاوة على ذلك، تعاملنا مع التحدي المتمثل في قابلية تطبيق المراقب في الوقت الحقيقي من خلال تحسين مصفوفة Lyapunov للمراقب. تم تنفيذ هذه المنهجية واختبارها لمراقبي المدخلات المجهولة في أمثلة في الوقت الحقيقي، وتم تقديم مناقشة شاملة تقارن أداء مختلف مراقبي المدخلات المجهولة. وبشكل عام، يساهم هذا البحث في تطوير الفهم والتنفيذ العملي لتقنيات تقدير الحالة والمدخلات المجهولة في الأنظمة غير الخطية المعقدة.

كلمات مفتاحية: النظام غير الخطي، نموذج تاكاجي-سوجينو المتعدد، تقدير الحالة، تقدير المدخلات غير المعروفة، متباينات المصفوفة الخطية، متباينات المصفوفة الخطية الثنائية، دالة Lyapunov متعددة التربيعات.

Table of Contents

List of Figures

Nomenclature

Acronyms

T-S	**T**akagi-**S**ugeno
MPV	**M**easurable **P**remise **V**ariables
UPV	**U**nmeasurable **P**remise **V**ariables
LMI	**L**inear **M**atrix **I**nequality
BMI	**B**ilinear **M**atrix **I**nequality
MVT	**M**ean **V**alue **T**heorem
PIO	**P**roportional **I**ntegral **O**bserver
PMIO	**P**roportional **M**ulti-**I**ntegral **O**bserver
DUIO	**D**ecoupled **U**nknown **I**nput **O**bserver

List of Publications

International Journal publications

- **Hamdi, W.**, Hammoudi, M. Y., & Hamiane, M. (2024). Proportional multi-integral observer design for Takagi-Sugeno systems with unmeasurable premise variables: Conservatism reduction via polyquadratic Lyapunov function. European Journal of Control,75, 100915.

- **Hamdi, W.**, Saadi, R., Hammoudi, M. Y., Houili, R., Benbouzid, M., Himeur, Y., Miniaoui, S., Atalla , S., & Mansoor, W. (2024). Enhanced State and Unknown Input Estimation for Synchronous Reluctance Motor using Takagi-Sugeno Fuzzy Proportional Multi-Integral Observer. IEEE Access, 12, 42908-42920.

- **Hamdi, W.**, Saadi, R., Hammoudi, M. Y., & Hamiane, M. (2024). Decoupled Unknown Input Observer for Takagi-Sugeno Systems: Hardware-in-the-Loop Validation to Synchronous Reluctance Motor. Elektronika ir elektrotechnika, 30(3), 23-31.

- **Hamdi, W.**, Hammoudi, M. Y., & Hamiane, M. (2024). Observer Design for Takagi-Sugeno Systems with Unmeasurable Premise Variables using a Non-Quadratic Lyapunov Function. ISA transactions.

- Mimoune, K., Hammoudi, M. Y., **Hamdi, W.**, & Mimoune, S. M. (2023). Observer design for Takagi-Sugeno fuzzy systems with unmeasured premise variables: Conservatism reduction using line integral Lyapunov function. ISA transactions, 142, 626-634.

Papers published in international conferences

- **Hamdi, W.**, Hammoudi, M. Y., Okba, S. & Saadi, R. (2023). Decoupled Unknown-Input Observer for Takagi-Sugeno Systems: Application to Three Phase Interleaved Boost Converter. In 2023 International Conference on Electrical Engineering and Advanced Technology (ICEEAT) (Vol. 1, pp. 1-6). IEEE.

- **Hamdi, W.**, Hammoudi, M. Y., Boukhlouf, A. & Saadi, R. (2023). Robust Observer for Takagi-Sugeno Systems based on $\mathcal{L}_2$-attenuation approach: Application to Separately Excited DC Motor. In 2023 International Conference on Electrical Engineering and Advanced Technology (ICEEAT) (Vol. 1, pp. 1-6). IEEE.

- **Hamdi, W.**, Hammoudi, M. Y., & Meredef, I.E. (2023). Observer Design for Takagi-Sugeno Fuzzy Systems Using Poly-Quadratic Lyapunov Function Based On Lipschitz Approach. In 2023 International Conference on Electrical Engineering and Advanced Technology (ICEEAT) (Vol. 1, pp. 1-5). IEEE.

- **Hamdi, W.**, Hammoudi, M. Y., & BOUKHLOUF, A. (2023). Observer Design for Takagi-Sugeno Fuzzy Systems with Unmeasurable Premise Variables based on Differential Mean Value Theorem. Engineering Proceedings, 58(1), 28.

- **Hamdi, W.**, Hammoudi, M. Y., & Betka, A. (2023). Sensorless Speed Control of Induction Motor Using Model Reference Adaptive System and Deadbeat Regulator. Engineering Proceedings, 56(1), 16.

- **Hamdi, W.**, Hammoudi, M. Y., Betka, A. & Saadi, R. (2024). Energy optimization of induction motor in transient state under field oriented control. In 2024 8th International Conference on Image and Signal Processing and their Applications (ISPA) (pp. 1-7). IEEE.

- Okba, S., Saadi, R., Hammoudi, M. Y. & **Hamdi, W**. (2024). Enhancing the Potential of PEMFC EVs with Cutting-Edge FOPI Control based PDO Algorithme for a Three-Phase Interleaved Boost Converter. In 2024 8th International Conference on Image and Signal Processing and their Applications (ISPA) . IEEE.

- Mimoune, K., Hammoudi, M. Y., Saadi, R., & **Hamdi, W.** (2024, April). Estimating Actuator Fault Through the Utilization of a Proportional Integral Observer with Quadratic Lyapunov Functions. In 2024 8th International Conference on Image and Signal Processing and their Applications (ISPA) (pp. 1-6). IEEE.

- Mimoune, K., Hammoudi, M. Y., Saadi, R., **Hamdi, W.**, & Mimoune, S. M. (2024, April). State Estimation for Nonlinear System Using Line Integral Lyapunov Function: A Polytopic Approach With Unmeasurable Premises. In 2024 8th International Conference on Image and Signal Processing and their Applications (ISPA) (pp. 1-6). IEEE.

- Mimoune, K., Hammoudi, M. Y., & **Hamdi, W.** (2023). Designing Unknown Input Observers for Fault Reconstruction in Disturbed Takagi-Sugeno Fuzzy Systems. Engineering Proceedings, 58(1), 132.

Papers published in national conferences

- **Hamdi, W.**, Hammoudi, M. Y., Boukhlouf, A. & Benaissa, I. (2023). Design and Evaluation of a Decoupled Unknown-Input Observer for the Synchronous Reluctance Motor Using Takagi-Sugeno Fuzzy Representation. In NATIONAL CONFERENCE ON MECHANICS AND MATERIALS, NCMM2023/ Boumerdes- Algeria, 06 -07 December 2023.

- **Hamdi, W.**, Hammoudi, M. Y., MIMOUNE, K. (2023). Design and Evaluation of Takagi-Sugeno Fuzzy Observer for Induction Motor. In 1ST NATIONAL CONFERENCE ON EMERGENT TECHNOLOGIES IN ELECTRICAL ENGINEERING NCETEE'23/ Setif, Algeria, 16 -17 December 2023.

- **Hamdi, W.**, Hammoudi, M. Y., BOUSSABEUR, M.T. & Benaissa, I. (2023). Design and Evaluation of a Proportional Multi-Integral Observer for the Synchronous Reluctance Motor Using Takagi-Sugeno Fuzzy Representation. In 1ST NATIONAL CONFERENCE ON EMERGENT TECHNOLOGIES IN ELECTRICAL ENGINEERING NCETEE'23/ Setif, Algeria, 16 -17 December 2023.

- **Hamdi, W.**, Hammoudi, M. Y., Boukhlouf, A. & Benaissa, I. (2023). Observer design for Takagi-Sugeno Systems with Unmeasurable Premise Variables based on $\mathcal{L}_2$-Attenuation Approach: Application to DC Motor. In 1ST NATIONAL CONFERENCE ON EMERGENT TECHNOLOGIES IN ELECTRICAL ENGINEERING NCETEE'23/ Setif, Algeria, 16 -17 December 2023.

- **Hamdi, W.**, Hammoudi, M. Y. & Fettah, K. (2023). State Estimation Of Fuel Cell-Interleaved Boost Converter Using Takagi-Sugeno Fuzzy Observer. In THE FIRST NATIONAL CONFERENCE ON MATTER SCIENCES NCSM2023/ Djelfa, Algeria, 20 December 2023.

- Mimoune, K., Hammoudi, M. Y., **Hamdi, W.** & Mimoune, S.M. (2023). Nonlinear System State Estimation With Unmeasurable Premises: A Novel Approach Using Line Integral Lyapunov Function. In NATIONAL CONFERENCE ON MECHANICS AND MATERIALS, NCMM2023/ Boumerdes- Algeria, 06 -07 December 2023.

- Okba, S., Saadi, R., Hammoudi, M. Y. & **Hamdi, W.** (2023). Enhancing the Potential of PEMFC EVs with Cutting-Edge FOPI Control based PDO Algorithm for a Three-Phase Interleaved Boost Converter. In the first international Conference on Advances in Electronics, Control and Computer Technology, ICAECCT2023/ Mascara, Algeria, 25 -27 October 2023.

General Introduction

Introduction

Engineering plays a pivotal role in the development and control of systems, striving to attain optimal performance and efficiency. Historically, linear systems and their associated control mechanisms have been the cornerstone of this domain, primarily due to their simplicity and the straightforward nature of their mathematical models. Linear control systems, with their predictable and uniform behavior, have allowed engineers to design and implement effective control strategies with relative ease. However, the inherent complexity of the real world often defies this simplicity. Most physical systems exhibit nonlinear characteristics, making them significantly more complex and challenging to model and control. The nonlinear nature of these systems introduces a wide array of difficulties in system design and control, necessitating advanced strategies to accurately predict and manage their behaviors.

A fundamental aspect of controlling any system is the accurate knowledge of its states. State estimation is typically achieved through the use of an auxiliary system known as an observer. The seminal works in observer design, attributed to Luenberger in [Luenberger, 1971] and Kalman in [Kalman, 1960], laid the foundation for state estimation. However, these initial frameworks were confined only to linear systems. This limitation led to the development of extended observers, extended Luenberger observer and extended Kalman filter, which employ linearization techniques to make nonlinear systems amenable to the existing linear observer designs.

Linearization, despite offering benefits such as the simplification of complex systems, entails the significant drawback of overlooking the intricacies inherent in exact nonlinear models, which results in degraded estimation performance. This trade-off highlights a critical challenge in observer design: the difficulty of developing observers that can directly utilize nonlinear models without resorting to simplifications. Therefore, the design of observers is intrinsically linked to the mathematical model of the system, as the process of modeling plays a crucial role in understanding the dynamics of a system and deriving its states. An accurate model is essential for comprehending the system's behavior, enhancing its performance, and achieving effective control.

While the analysis of linear systems has reached a significant level of maturity, the study of nonlinear systems presents more complexity, and research in this area continues to evolve. Analysis of nonlinear systems often necessitates customized approaches for specific types of systems, such as Lipschitz, Hammerstein-Wiener and bilinear systems. In response to these challenges, the multi-model approach has emerged as a promising strategy for representing nonlinear systems. This approach decomposes a nonlinear system into a collection of linear models, each corresponding to specific operating conditions of the system. This provides a more manageable framework for analysis and control, facilitating the extension of linear control techniques to nonlinear systems.

Among the various multi-model frameworks, this work leverages the capabilities of the Takagi-Sugeno (T-S) fuzzy multi-model. This approach is renowned for its ability to accurately capture nonlinear system dynamics using the sector nonlinearity approach, while maintaining precision and avoiding information loss due to linearization. It employs fuzzy-set theory to depict nonlinear systems as a combination of time-invariant local linear models. These models are integrated using weights determined by fuzzy-set membership functions. Such an approach offers significant advantages in the design of observers for nonlinear systems. It enables precise system modeling and facilitates the derivation of simple stability conditions, similar to those established for linear systems.

In this context, two categories of systems are distinguished based on the variables in the weight functions: Measurable Premise Variables (MPV) and Unmeasurable Premise Variables (UPV). Systems with UPV represent a broader class and have thus garnered substantial research interest. However, designing observers for UPV systems poses greater challenges than for those with MPV.

To examine the stability of state estimation errors, the application of the second Lyapunov theorem with a quadratic candidate function provides simple stability conditions in the form of Linear Matrix Inequalities (LMIs). Nonetheless, this approach encounters difficulties with larger systems as identifying a common matrix satisfying all LMIs becomes increasingly challenging [Elias et al., 2021]. Consequently, recent research has shifted towards less conservative Lyapunov functions, such as the poly-quadratic Lyapunov function [Tanaka et al., 2003]. While this approach reduces conservatism compared to its quadratic counterpart, and facilitates solution finding, it nevertheless introduces greater complexity, specially with the emergence of Bilinear Matrix Inequalities (BMIs).

To implement an observer effectively, it is essential to have knowledge of all its inputs. However, in practical scenarios, systems often encounter unknown inputs that can significantly influence their behavior. This reality necessitates the design of robust observers capable of handling such unknown inputs. The estimation of these unknown inputs is

crucial, as it enables a more comprehensive understanding and control of the system's behavior. This, in turn, leads to enhanced efficiency and prolongs the system's operational life. Robust observers play a pivotal role in maintaining system integrity and performance, even in the face of unforeseen or unpredictable external influences.

Contributions

The main goal of this thesis is to contribute in improving the state estimation process of nonlinear systems described by T-S multi-model with UPV, specifically by reducing the conservatism inherent in existing methodologies. The principal contributions of this thesis are summarized as follows:

- ❖ The principal contribution of our work is the development of a novel observer for T-S fuzzy systems with UPV. This observer addresses the conservatism that results from the mismatching terms and the employment of the quadratic candidate Lyapunov function. Our method overcomes these challenges by adopting the differential mean value theorem coupled with the poly-quadratic Lyapunov function.

- ❖ The second contribution is the formulation of an iterative LMI algorithm to solve the bilinear constraints that emerge from combining the mean value theorem with the poly-quadratic Lyapunov function. This algorithm facilitates solving these constraints through linear optimization solvers, offering enhanced outcomes compared to existing BMI optimization solvers.

- ❖ Our third contribution addresses the conservatism arising from the high Lipschitz gain in existing Lipschitz-assumption-based observers for T-S systems with UPV. The proposed observer outperforms its predecessor primarily due to the effective employment of the completion of square property. The obtained results demonstrate an expanded feasibility domain for stability conditions, particularly concerning higher Lipschitz gain, compared to the previous approach.

- ❖ The fourth contribution in our work is the reduction of conservatism in simultaneous state and unknown input observers. This is achieved by addressing the mismatching terms of the premise variables using the mean value theorem, a significant improvement over the Lipschitz-based observers used in earlier studies. Additionally, the use of the poly-quadratic Lyapunov function further diminishes conservatism compared to the traditional quadratic approach.

Organization

This thesis is structured into four main chapters, organized as follows:

- **Chapter 1:** This chapter introduces the fundamental concepts of multi-model representation using the T-S approach. It begins with an exploration of the mathematical model structure based on fuzzy theory and progresses to its construction using various methods, evaluating their limitations and determining the most suitable approach. Additionally, this chapter delves into the principal aspects of convexity in T-S representation and the LMI optimization problems. Various relaxation methods designed to lessen conservatism in stability conditions are also discussed.

- **Chapter 2:** The focus of this chapter is on the principal aspects of observability and detectability in T-S multi-models. It presents stability conditions for systems with MPV, along with strategies to enhance state estimation performance by adapting the pole placement method, traditionally used in linear systems, for nonlinear systems characterized by T-S fuzzy representation.

- **Chapter 3:** This chapter outlines the primary contributions of this thesis. It addresses the class of T-S systems with UPV, which poses significant challenges in stability analysis due to the presence of the mismatching terms. Various methods to mitigate the effects of these terms are explored, highlighting the limitations of each and proposing improvements to reduce associated conservatism. The iterative method for solving the resulting BMIs is presented in this chapter.

- **Chapter 4:** This chapter focuses on improving the observers discussed in the previous chapter to address the issue of unknown inputs affecting the system, such as faults, noise, uncertainties, etc. It presents different types of proposed observers and provides a thorough comparative analysis between theme. The chapter culminates with real-time application scenarios, discussing the practical implementation and benefits of the developed observers in real-world settings. A method to make the observer gains applicable in real world scenarios is proposed.

Chapter 1

Generalities of multi-model representation

1.1 Introduction

The art and science of representing systems have always been centered around understanding and describing the dynamical characteristics of those systems. In the pursuit of comprehending any system, a primary objective is to accurately represent its behavior through mathematical models. These models serve as the foundation in numerous applications, spanning from engineering and biology to economics and beyond. They not only capture the essence of how a system behaves but also provide a platform for prediction, control, and optimization. However, finding the optimal model is a delicate balancing act. Three main pillars guide this process:

- **Validity:** Every model functions within a specific boundary of applicability. This boundary is often delineated by the system's inherent physical properties or the assumptions made during the modeling phase. The constraints, whether driven by tangible realities or hypothetical conditions, determine the model's scope and relevance.
- **Precision:** At its core, precision in modeling emphasizes detailed and faithful representation of a system's dynamics and interactions among its different characteristic quantities. A precise model adeptly captures these interactions as well as the input-output behaviors, delivering predictions that closely match observed real-world data. However, this depth might increase computational demands.
- **Simplicity:** Often, the goal in modeling is to capture the essence of a system without unnecessary complexities. A simpler model, if valid, can be more interpretable and easier to work with. Yet, oversimplification risks missing crucial dynamics of the system.

The principles of validity, precision, and simplicity not only guide the modeling process but also deeply influence the choices we make regarding the model's structure. This balance is paramount when aiming to accurately depict a system's dynamic behavior. In light of these guiding principles, we can categorize mathematical models into two prominent structural types: linear and nonlinear models.

1.1.1 Linear models

Due to their simplicity and ease of handling, linear models offer numerous benefits. They often form the foundation of theory across various fields, thanks to their analytical

solvability and the abundance of specialized tools and methodologies designed for them. Fundamentally, linear models are distinguished by two primary properties: additivity and homogeneity. If a system adheres to both of these principles, then it is said to obey the principle of superposition.

Definition 1.1. *(Additivity) Let $y_1(t)$ and $y_2(t)$ be the outputs of a system corresponding to the inputs $u_1(t)$ and $u_2(t)$, respectively. A system is said to exhibit additivity if, when subjected to combined inputs given by*

$$u(t) = u_1(t) + u_2(t), \tag{1.1}$$

the resulting response is

$$y(t) = y_1(t) + y_2(t), \tag{1.2}$$

which is the summation of its individual responses to each separate input.

Definition 1.2. *(Homogeneity) Let $y(t)$ be the output of a system corresponding to the input $u(t)$. A system is said to exhibit homogeneity if, when subjected to input given by*

$$\alpha u(t), \alpha \in \mathbb{R}, \tag{1.3}$$

the resulting response is

$$\alpha y(t), \tag{1.4}$$

which scales proportionally with the input.

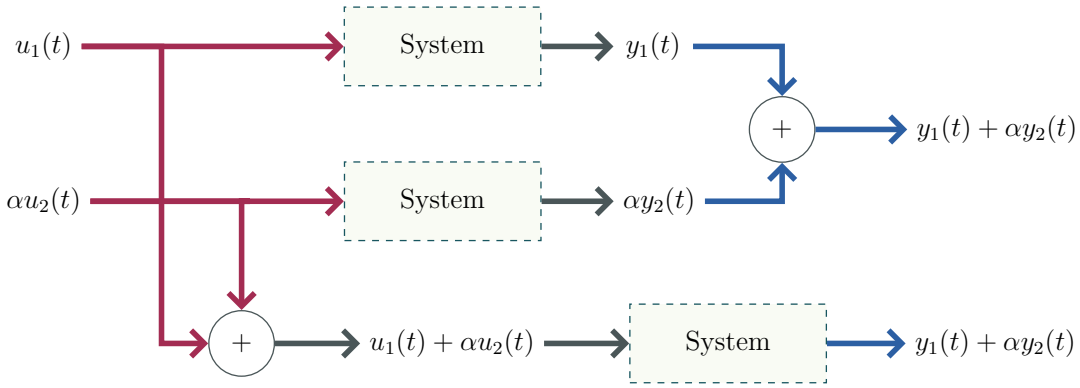

Fig 1.1: Linear system

Linear systems are typically represented using the following state-space form:

$$\begin{cases} \dot{x}(\mathrm{t}) = Ax(\mathrm{t}) + Bu(\mathrm{t}) \\ y(\mathrm{t}) = Cx(\mathrm{t}) + Du(\mathrm{t}) \end{cases} \tag{1.5}$$

where $x(t) \in \mathbb{R}^{n_x}$ is the state vector, $u(t) \in \mathbb{R}^{n_u}$ is the input vector and $y(t) \in \mathbb{R}^{n_y}$ represents the output vector. $A \in \mathbb{R}^{n_x \times n_x}, B \in \mathbb{R}^{n_x \times n_u}, C \in \mathbb{R}^{n_y \times n_x}$ and $D \in \mathbb{R}^{n_y \times n_u}$ are known matrices.

1.1.2 Nonlinear models

While linear models offer numerous advantages in terms of simplicity and analytical solvability, it's imperative to recognize that most physical systems encountered in nature are inherently nonlinear. The presence of nonlinearity introduces a level of dynamical richness that isn't found in linear systems.

The standard form for representing nonlinear systems is as follows:

$$\begin{cases} \dot{x}(t) = f(x(t), u(t)) \\ y(t) = h(x(t), u(t)) \end{cases} \tag{1.6}$$

where: f is the state function. It describes how the state vector $x(t)$ of the system evolves over time given a certain input $u(t)$. This function represents the dynamics of the system. h is the output function. It relates the state vector $x(t)$ and the input $u(t)$ to the output $y(t)$. This function determines how the states are measured.

However, the richness introduced by nonlinearity introduces significant challenges in terms of analysis, control, and prediction. The lack of linear properties, like superposition, amplifies this complexity. As a result, there's a pressing need for specialized tools and techniques tailored to navigate and comprehend these intricate nonlinear dynamics. Among of which two are particularly noteworthy:

Linearization: A widely-adopted method, linearization aims to approximate the nonlinear dynamics around a specific operating point. While this technique greatly simplifies the modeling process, especially for systems operating near a steady state, its accuracy diminishes as the system's behavior deviates from this chosen point. This limitation is particularly pronounced in systems with stark nonlinear characteristics.

Multi-model representation: As an alternative to linearization, the multi-model representation decomposes a complex nonlinear system into a series of local linear models, each tailored to a different operating point. The succeeding section will delve deeper into the intricacies of the multi-model approach, providing a comprehensive exploration.

1.2 Multi-model representation

In the pursuit of comprehending nonlinear systems, the multi-model representation emerges as a powerful tool. By segmenting the overall behavior of a system into smaller, more manageable sub-models, multi-model approaches simplify complexities, enabling easier analysis and control. It's like assembling a complex puzzle game, where each individual piece reveals a portion of the broader picture . This chapter aims to provide a comprehensive exploration of the multi-model approach, shedding light on its principles,

methodologies, and applications. As we dive deeper, we will unveil how multi-model representation bridges the gap between the desire for simplicity and the inherent complexity of nonlinear systems.

Before delving into the intricacies of multi-model representation, it's essential to introduce and define foundational terms. These key definitions will guide the subsequent discussions, ensuring clarity and depth of understanding.

1.2.1 Sub-Model

A system can be described using a series of local models: $M_1, M_2, ..., M_r$, each describes the behavior of the global system in a specific domain of validity.

1.2.2 Domains of validity

Each sub model is associated with its unique domain of validity (operational zone): $D_1, D_2, ..., D_r$. Every domain is centered around a specific operating point. These domains might either be disjoint, implying no overlap, or they might overlap [Ksouri, 1999]. In situations where domains overlap, they share common regions, creating overlapping validity domains, as illustrated in Figure 1.2. The union of these domains constitutes the system's operating space $\mathcal{D} = \mathcal{D}_1 \cup \mathcal{D}_2 \cup \ldots \mathcal{D}_r$.

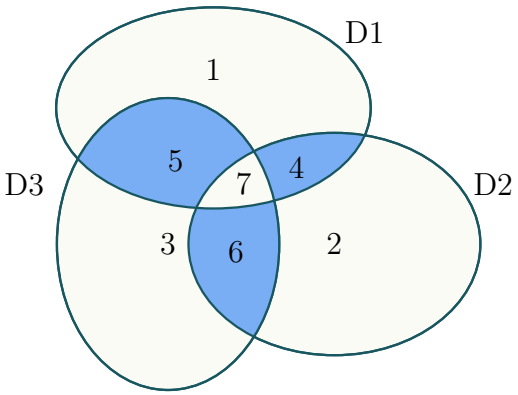

Fig 1.2: Overlapping domains of validity illustration

1.2.3 Multi-model

Multi-model refers to the integration of various sub-models using a meticulous interpolation mechanism (weighting functions), to capture the overall dynamic behavior of the entire system. While each sub-model focuses on specific facets or regions of operation, the multi-model seamlessly merges them, presenting a holistic depiction of the system's dynamics.

1.2.4 Weighting functions

Weighting functions $\mu_i(t)$ play a pivotal role in determining the contribution of each individual sub-model M_i. Essentially, these functions assign a weight or "importance factor" to each sub-model based on the current operating point or condition. By design, these functions are bounded within the range [0, 1].

Considering the example in Figure 1.2:

- In regions 1, 2, and 3, a singular model is deemed valid, bearing a weight coefficient of 1, while the remaining models carry a coefficient of zero.
- For regions 4, 5, and 6, two models concurrently possess partial validity, exhibiting non-zero weights whose cumulative value is 1.
- Region 7 showcases a scenario where three or more models have overlapping validity.

These weighting functions are also referred to as "Activation functions" [Chadli and Borne, 2012] due to their role in ascertaining the activation level of their linked local sub-model. Subsequent sections will provide an in-depth exploration of the methods to determine these functions.

1.3 Different multi-model structures

Multi-model systems primarily fall into two categories, distinguished by the design and interaction of their sub-models. Each structure offers unique approaches to encapsulate and represent system dynamics, accompanied by their inherent strengths and challenges [Orjuela, 2008].

In the following illustration, we present a detailed scheme that represents the construction of the Takagi-Sugeno multi-model. Among the various methods available, we've chosen to emphasize sector nonlinearity specifically for its potential to reduce the error between the actual model and its representation to the greatest extent possible.

- **Coupled Multi-model Structure (Homogeneous Structure):** Often referred to as the **"Takagi-Sugeno multi-model"**, this structure is characterized by its shared and unified state vector $x(t)$. All the sub-models in this structure possess the same form, ensuring homogeneity across the multi-model system. The strength of this method lies in its uniformity, which can often simplify analysis and control design. However, this strict structure might not always provide the flexibility needed for more complex systems.

❖ **Decoupled Multi-model Structure (Heterogeneous Structure):** Contrary to the homogeneous structure, the decoupled multi-model structure allows for a diverse and flexible representation. Here, each sub-model is unique, possessing its distinct state vector $x_i(t)$ and structural form. This approach provides a broader framework, accommodating a vast array of system behaviors and characteristics. It is especially useful for representing systems where different regions of operation have inherently different dynamics. Nonetheless, this flexibility might come at the cost of increased complexity in analysis and control.

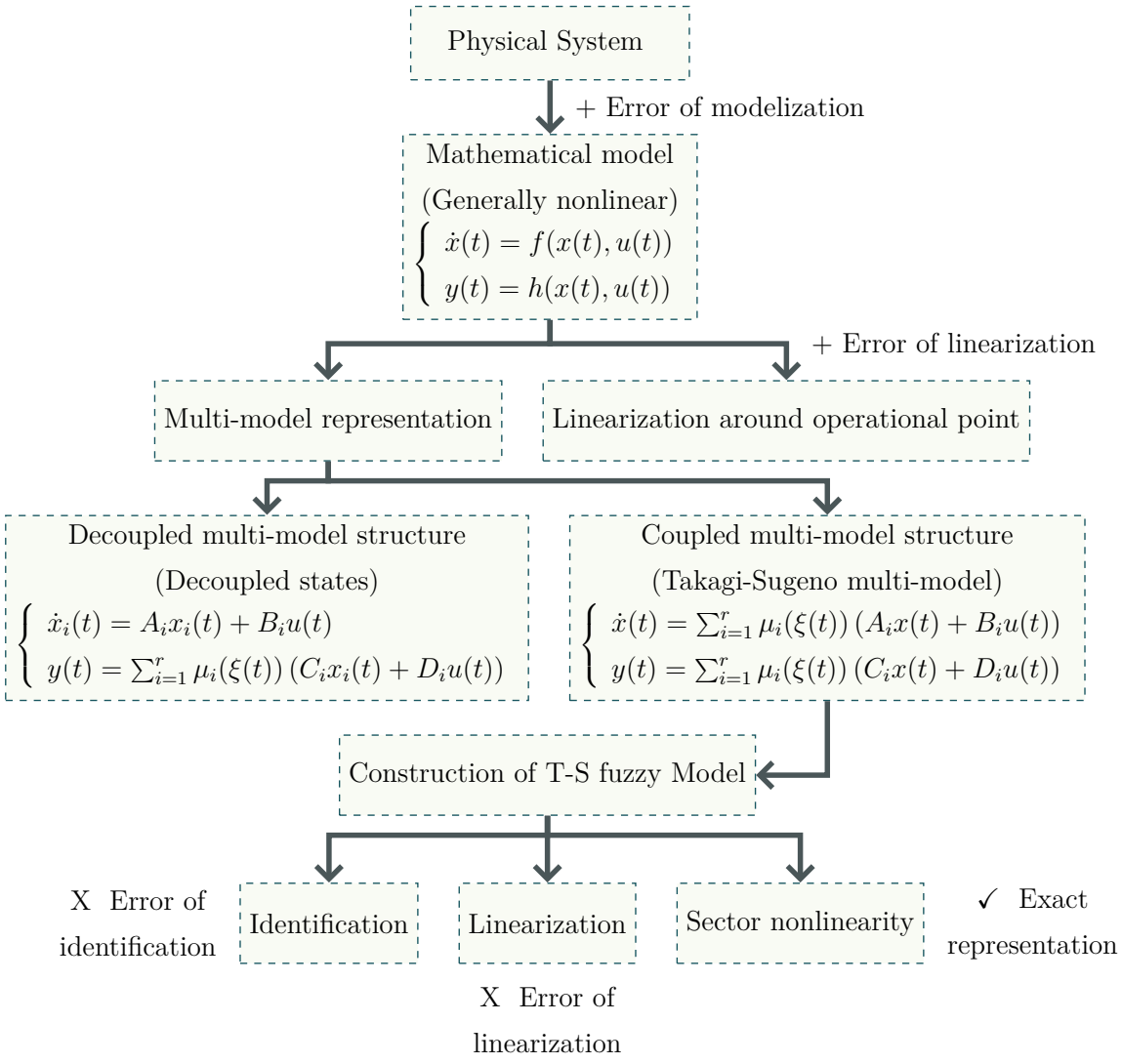

Fig 1.3: Multi-model construction scheme

1.3.1 Takagi-Sugeno multi-model (Coupled structure)

The Takagi-Sugeno (T-S) fuzzy multi-model has its roots in the late 20th century, emerging as a prominent approach in the domain of fuzzy systems and control. Introduced

by Takagi and Sugeno in 1985 in [Takagi and Sugeno, 1985], this model was designed as a systematic method to handle the complexities and nonlinearities found in various systems. Over the years, the T-S model has gained traction due to its capacity to provide an intuitive representation of nonlinear systems using linear subsystems guided by fuzzy logic principles.

In its foundational form, the T-S model operates on the principles of fuzzy logic. At its core lies the inference of a set of r fuzzy rules. These rules adopt the "**IF** (premise) **THEN** (consequence)" structure:

- **Premise (Antecedent):** This is the "IF" part of the rule. It contains conditions that are checked. These conditions are based on the premise variables and their corresponding fuzzy sets.
- **Premise variables:** Also known as "decision variables" [Chadli and Borne, 2012], refer to the variables that appear in the "IF" part (the Premise) of the fuzzy rules. They are called "premise" variables because they set the conditions or premises for each rule.
- **Fuzzy Sets:** In the context of the T-S model, fuzzy sets represent categories or classes that the premise variables can belong to, albeit to varying degrees. The degree to which a premise variable belongs to a fuzzy set is determined by the membership function associated with that set.
- **Membership Functions:** These functions define how a premise variable is mapped to a membership value between 0 and 1. Essentially, they quantify the degree to which a specific premise variable belongs to a particular fuzzy set. The shapes and forms of these functions will be further detailed later in this work, using the sector nonlinearity approach.
- **Consequent:** This is the "THEN" part of the rule. In Takagi-Sugeno systems, the consequents describe linear dynamic models that are valid under the conditions specified by the antecedents.

These rules collectively characterize the nonlinear behavior and its segmented linear approximations. A typical representation is given by the i^{th} fuzzy rule, for $i = 1, \ldots, r$:

$$\textbf{If } \xi_1(t) \text{ is } M_{i1} \text{ and } \ldots \text{ and } \xi_k(t) \text{ is } M_{ik},$$

$$\textbf{Then } \begin{cases} \dot{x}(t) = A_i x(t) + B_i u(t), \\ y(t) = C_i x(t) + D_i u(t), \end{cases} \tag{1.7}$$

here, ξ_j represents the premise variable, with k denoting their total number. M_{ij} signifies the fuzzy set of the i^{th} fuzzy rule associated with the j^{th} premise variable. Furthermore, r stands for the number of fuzzy rules, which corresponds to the number of sub-models.

Upon employing "Weighted average method", this allows the expression of a T-S model in the compact form:

$$\begin{cases} \dot{x}(t) = \sum_{i=1}^{r} \mu_i(\xi(t)) \left(A_i x(t) + B_i u(t)\right) \\ y(t) = \sum_{i=1}^{r} \mu_i(\xi(t)) \left(C_i x(t) + D_i u(t)\right) \end{cases} \tag{1.8}$$

In this representation, $x(t) \in \mathbb{R}^{n_x}$ stands as the state vector, $u(t) \in \mathbb{R}^{n_u}$ represents the input vector, and $y(t) \in \mathbb{R}^{n_y}$ is the output vector. The matrices A_i, B_i, C_i, and D_i detail the local dynamics. The functions $\mu_i(\xi(t)) \geq 0$ are normalized membership functions, also known as weighting functions as described in Section 1.2.4, abiding by the convex sum properties (later, in Section 1.5, we will provide a detailed definition of what "convex" means):

$$\begin{cases} \sum_{i=1}^{r} \mu_i(\xi(t)) = 1 \\ 0 \leq \mu_i(\xi(t)) \leq 1, \quad \forall i = 1, ..r \end{cases} \tag{1.9}$$

These weighting functions are obtained based on the "weighted average method" and given as follows:

$$\begin{cases} w_i(\xi(t)) = \prod_{j=1}^{k} M_{ij}\left(\xi_j(t)\right) \\ \mu_i(\xi(t)) = \dfrac{w_i(\xi(t))}{\sum_{i=1}^{r} w_i(\xi(t))} \end{cases} \tag{1.10}$$

where the term $M_{ij}\left(\xi_j(t)\right)$ is the membership function of the premise variable $\xi(t)$ in the fuzzy set M_{ij}. This membership function verifies as well the convex sum property given in (1.9).

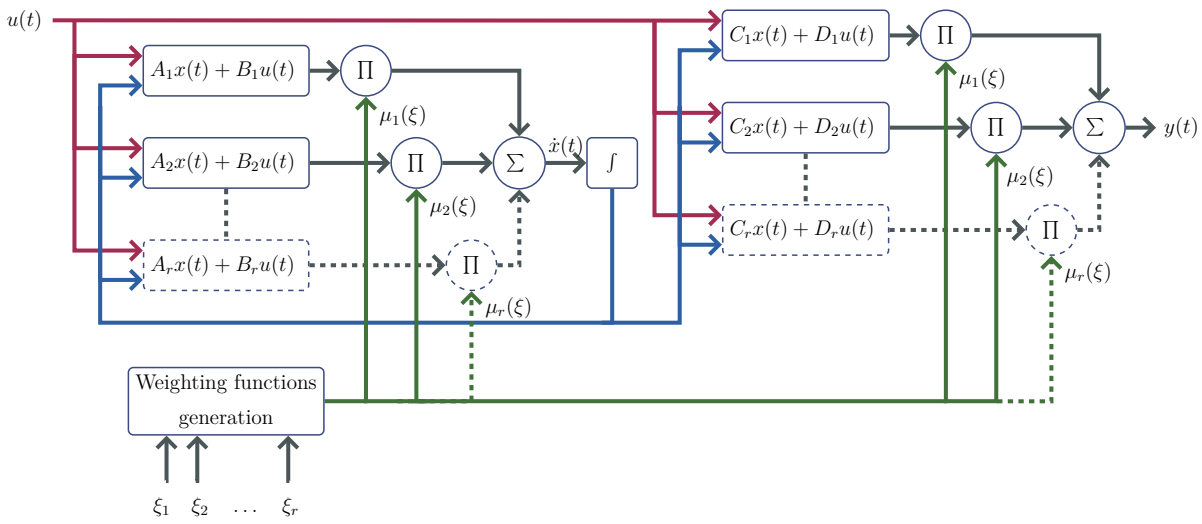

Fig 1.4: Takagi-Sugeno multi-model structure

1.3.2 Decoupled Multi-model Structure

The decoupled structure presents a different take on multi-model representations. Proposed by Filev [Filev, 1991], this type is characterized by each sub-model having its unique state vector $x_i(t) \in \mathbb{R}^{n_{x_i}}$ and structural formation. These individual sub-models are tailored to symbolize the system's behavior in the vicinity of specific operational points. Consequently, the comprehensive behavior of the overarching system is articulated by interpolating the outputs of these sub-models. It's important to note that the local state vectors $x_i(t)$ do not necessarily have a physical meaning in structure [Akhenak, 2004].

A notable aspect of this structure is the distinct local state for each sub-model, emphasizing the system's behavior in a defined operational domain. The sub-model's dynamics can be represented as:

$$\begin{cases} \dot{x}_i(t) = A_i x_i(t) + B_i u(t) \\ y_i(t) = C_i x_i(t) + D_i u(t) \end{cases} \tag{1.11}$$

Integrating these sub-models, the global representation of the multi-model is given by:

$$\begin{cases} \dot{x}_i(t) = A_i x_i(t) + B_i u(t), \quad i = 1, \ldots, r \\ y(t) = \sum_{i=1}^{r} \mu_i(\xi(t)) \left(C_i x_i(t) + D_i u(t)\right) \end{cases} \tag{1.12}$$

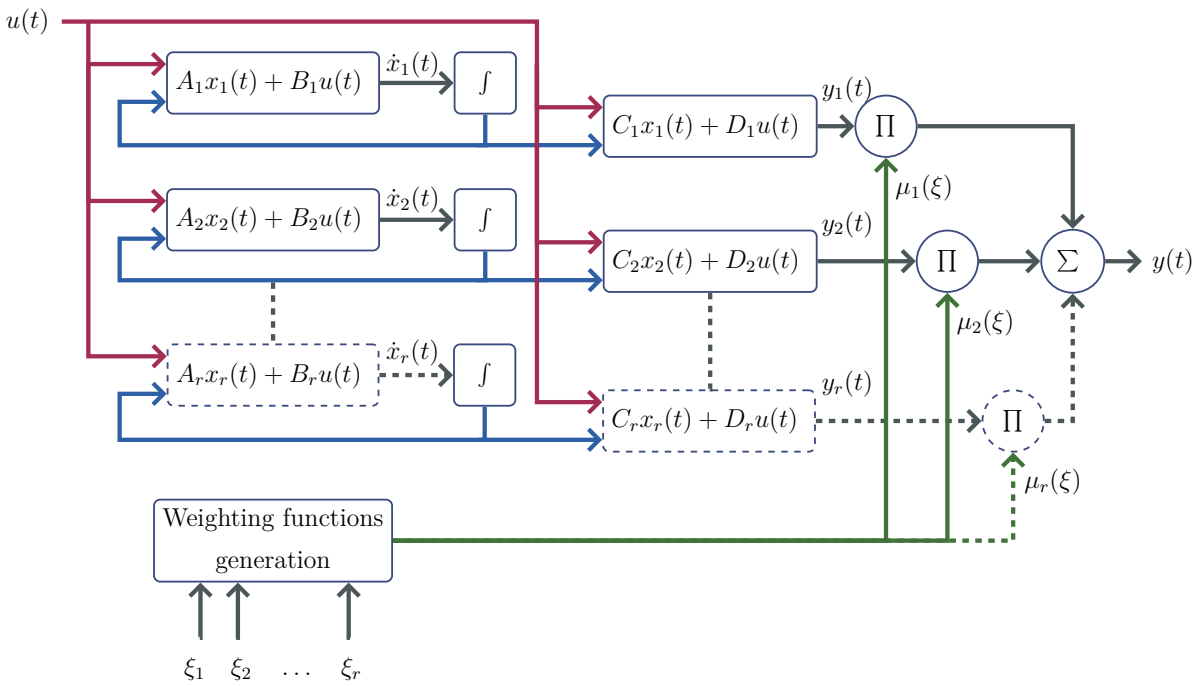

Fig 1.5: Decoupled multi-model structure

1.4 Construction of Takagi-Sugeno fuzzy Model

The process of constructing a Takagi-Sugeno multi-model is a sensitive step, particularly in the realm of observer design. By meticulously tailoring the multi-model, it's aligned to reflect the intrinsic behaviors of the original nonlinear model with heightened precision, a fundamental requirement for the successful design of observers. This process encompasses specifying the premise variables involved, determining the number of sub-models and determining the matrices A_i, B_i, C_i, and D_i that best describe the system's behavior. The subsections that follow will explore the mainly methodologies documented in literature for this construction which are: identification, linearization, and the sector nonlinearity approach which will be adopted in this work.

1.4.1 Identification

The identification process in the context of multi-models is a systematic approach to derive appropriate sub-models from experimental or observational data. It involves segmenting this data based on varying operating conditions or regimes. Each distinct regime or segment is then encapsulated by its unique sub-model. Then the identification of the unknown parameters is based on the minimization of a criterion (global, local or combined [Orjuela, 2008]) of the difference between the estimated output of the multi-model and the measured output of the system . The identification method for fuzzy modeling is appropriate for systems that are challenging to represent through analytical and/or physical models, often referred to as "black box" systems [Tanaka and Wang, 2004].

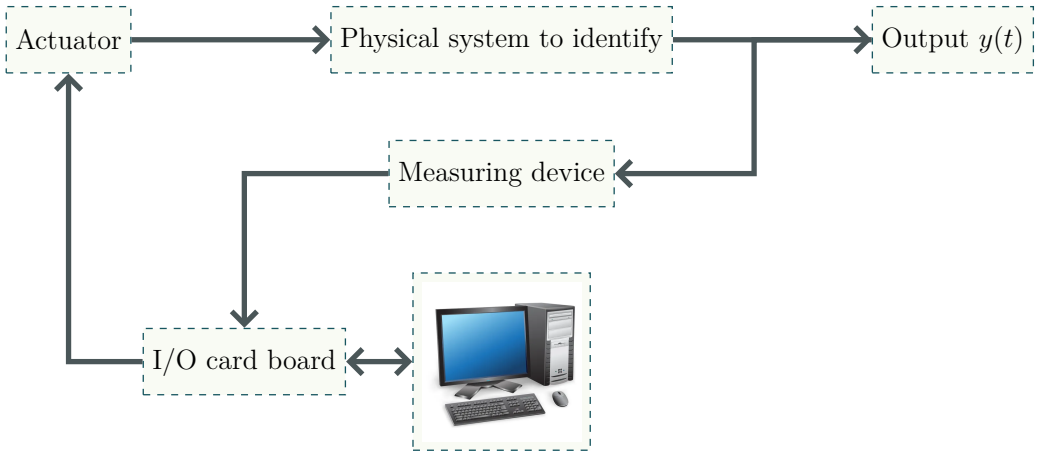

Fig 1.6: System identification setup

The development of a multi-model through identification raises three major issues [Orjuela, 2008]:

- The choice of the characteristic variable (i.e., the premise variable "ξ" of the system used to index the weighting functions).
- Decomposing the system's operating space into a finite number of operating zones. This step may be accompanied by an optimization of the weight functions associated with each zone.
- Identification of each sub-model structure and parameters.

Remark 1.1

The identification approach in constructing the Takagi-Sugeno multi-model has its limitations:

- ❖ Relying on identification with "non-persistent input signals" can lead to a multi-model that fits the training data exceptionally well but fails to generalize to unseen data or different operating conditions. This over-reliance on observed data can obscure underlying system dynamics, making the model less robust in real-world applications.
- ❖ Identification process can be computationally intensive, especially for complex systems with a vast amount of data.
- ❖ The choice of the appropriate identification method and its parameters can be non-trivial, often requiring expert knowledge and trial-and-error.
- ❖ Models derived purely from identification might lack the intuitive or physical interpretability that analytical models provide.

1.4.2 Linearization

Linearization is a mathematical tool used to simplify nonlinear systems by approximating them with linear equations around an operational point. In essence, it corresponds on approximating a nonlinear function using its tangent in this operational point as illustrated in Figure 1.7, thereby simplifying complex behaviors into more tractable forms. In the context of constructing a Takagi-Sugeno multi-model through the linearization approach, each sub-model can be seen as a representation of the system's behavior linearized around a specific operational point [Johansen et al., 2000].

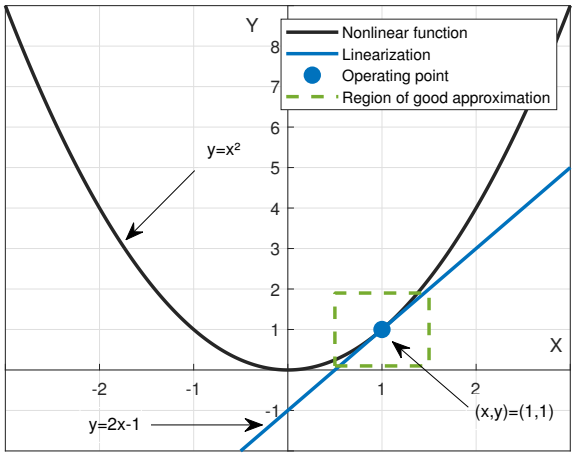

Fig 1.7: Linearization of nonlinear function illustration

One of the most common techniques employed for linearization is to use the first term of the Taylor series expansion [Johansen and Foss, 1993], [Gasso, 2000]. Lets define the linearization L_i of the nonlinear system $f(x(t), u(t))$ given in (1.6) around operational points (x_i, u_i) as follows:

$$L_i(x(t), u(t)) = f(x_i, u_i) + \left.\frac{\partial f(x,u)}{\partial x}\right|_{(x,u)=(x_i,u_i)} (x(t) - x_i) + \left.\frac{\partial f(x,u)}{\partial u}\right|_{(x,u)=(x_i,u_i)} (u(t) - u_i) \tag{1.13}$$

This expression can be written as :

$$L_i(x(t), u(t)) = A_i x(t) + B_i u(t) + f(x_i, u_i) - A_i x_i - B_i u_i \tag{1.14}$$

where:

$$A_i = \frac{\partial f(x,u)}{\partial x}|_{(x,u)=(x_i,u_i)} \ , \ B_i = \frac{\partial f(x,u)}{\partial u}|_{(x,u)=(x_i,u_i)} \tag{1.15}$$

The non linear system (1.6) will then be represented by the multi-model (1.16) composed of several local linear or affine models obtained by linearizing the nonlinear system around an arbitrary operating point $(x_i, u_i) \in \mathbb{R}^{n_x} \times \mathbb{R}^{n_u}$:

$$\begin{cases} \dot{x}(t) = \sum_{i=1}^{r} \mu_i(\xi(t))(A_i x(t) + B_i u(t) + D_i) \\ y(t) = \sum_{i=1}^{r} \mu_i(\xi(t))(C_i x(t) + E_i u(t) + N_i) \end{cases} \tag{1.16}$$

where:

$$A_i = \frac{\partial f(x,u)}{\partial x}|_{(x,u)=(x_i,u_i)} \ , \ B_i = \frac{\partial f(x,u)}{\partial u}|_{(x,u)=(x_i,u_i)}, D_i = f(x_i, u_i) - A_i x_i - B_i u_i$$

$$C_i = \frac{\partial h(x,u)}{\partial x}|_{(x,u)=(x_i,u_i)} \ , \ E_i = \frac{\partial h(x,u)}{\partial u}|_{(x,u)=(x_i,u_i)}, \ N_i = h(x_i, u_i) - C_i x_i - E_i u_i$$

Remark 1.2

The linearization approach, when employed in the construction of the Takagi-Sugeno multi-model, brings with it certain limitations:

- ❖ Linearization inherently involves approximation, and while it simplifies the representation of nonlinear systems, it may not capture the full dynamics accurately, especially when the system exhibits strong non-linearities.
- ❖ The reliance on the first term of the Taylor series expansion might miss higher-order dynamics crucial to certain applications.
- ❖ Choosing an appropriate linearization point or determining the number of linearization points needed can be challenging. The number of local models is not only dictated by the modeling accuracy desired but also by the system's complexity and the choice of activation function.

1.4.3 Sector nonlinearity approach

Sector nonlinearity is an approach based on the knowledge of the mathematical model of the system. It constrains the system's nonlinearities within specific bounds or sectors. This leads to a set of linear models that provide an exact representation, which aligns optimally with the real system. This contrasts with the other two methods, Identification and Linearization, which offer only approximations. This approach either determines the global sector covering the entire nonlinearity, as illustrated in Figure 1.8, or considers local sector nonlinearity when it's challenging to identify global sectors, as shown in Figure 1.9. It's important to to clarify that contrary to what's depicted in Figures 1.8 and 1.9, nonlinear equations don't necessarily intersect the origin, as will be further demonstrated in the proof of Lemma 1.1.

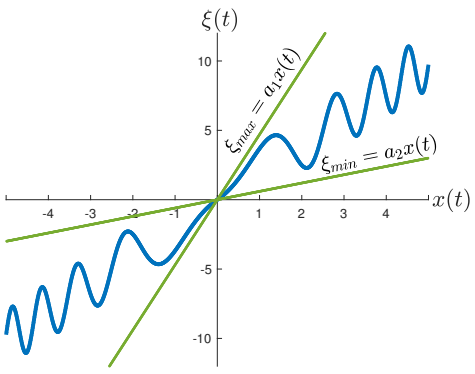

Fig 1.8: Global sector nonlinearity

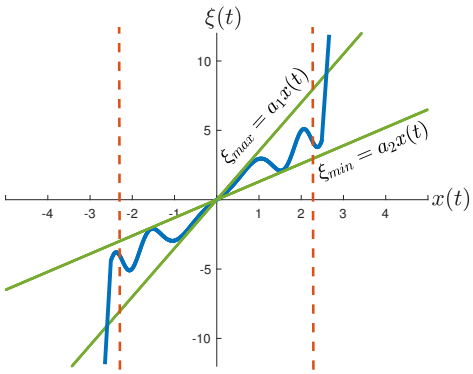

Fig 1.9: Local sector nonlinearity

Lemma 1.1. *(Sector nonlinearity) [Tanaka and Wang, 2004] Let us consider a bounded function* $\xi(x) \in [\xi_{\min} \quad \xi_{\max}]$*, there always exist two functions* $M_1(\xi(x))$ *and* $M_2(\xi(x))$ *such that:*

$$\xi(x) = M_1(\xi(x))\xi_{\max} + M_2(\xi(x))\xi_{\min} \tag{1.17}$$

where:

$$0 \leq M_1(\xi(x)) \leq 1, \quad 0 \leq M_2(\xi(x)) \leq 1, \quad M_1(\xi(x)) + M_2(\xi(x)) = 1$$

and

$$M_1(\xi(x)) = \frac{\xi(x) - \xi_{\min}}{\xi_{\max} - \xi_{\min}}, \quad M_2(\xi(x)) = \frac{\xi_{\max} - \xi(x)}{\xi_{\max} - \xi_{\min}}.$$

Proof. Under the assumption that the function $\xi(x)$ is bounded, it is then possible to write:

$$\xi(x) = \xi(x)\left(\frac{\xi_{\max} - \xi_{\min}}{\xi_{\max} - \xi_{\min}}\right) + \left(\frac{\xi_{\max}\xi_{\min}}{\xi_{\max} - \xi_{\min}} - \frac{\xi_{\max}\xi_{\min}}{\xi_{\max} - \xi_{\min}}\right) \tag{1.18}$$

After factorization, Equation (1.18) becomes:

$$\xi(x) = \underbrace{\frac{\xi(x) - \xi_{\min}}{\xi_{\max} - \xi_{\min}}}_{M_1(\xi(x))}\xi_{\max} + \underbrace{\frac{\xi_{\max} - \xi(x)}{\xi_{\max} - \xi_{\min}}}_{M_2(\xi(x))}\xi_{\min} \tag{1.19}$$

□

This property can be written in summation formula as follows:

$$\xi(x) = \sum_{i=1}^{2} M_i(\xi(t))\xi_i, \tag{1.20}$$

where: $\xi_1 = \xi_{\max}$ and $\xi_2 = \xi_{\min}$.

To construct the multi-model using this approach, we first reformulate the nonlinear system (1.6) using a basic factorization. The formulation is:

$$\begin{cases} \dot{x}(t) = A(\xi(t))x(t) + B(\xi(t))u(t) \\ y(t) = C(\xi(t))x(t) + D(\xi(t))u(t) \end{cases} \tag{1.21}$$

where $A(\xi(t))$, $B(\xi(t))$, $C(\xi(t))$ and $D(\xi(t))$ are matrices that depend on the premise variable $\xi(t)$. In the simple case where there is only one premise variable, these functions can be expressed using the sector nonlinearity approach to define the membership functions as follows:

$$\begin{array}{ll} A(\xi(t)) = \sum_{i=1}^{2} M_i(\xi(t))A_i, & B(\xi(t)) = M_{i=1}^{2} M_i(\xi(t))B_i \\ C(\xi(t)) = \sum_{i=1}^{2} M_i(\xi(t))C_i, & D(\xi(t)) = \sum_{i=1}^{2} M_i(\xi(t))D_i \end{array} \tag{1.22}$$

Thus, the system (1.21) becomes:

$$\begin{cases} \dot{x}(t) = \sum_{i=1}^{2} M_i(\xi(t)) \left(A_i x(t) + B_i u(t)\right) \\ y(t) = \sum_{i=1}^{2} M_i(\xi(t)) \left(C_i x(t) + D_i u(t)\right) \end{cases} \tag{1.23}$$

In the general case where there are k premise variables, the number of rules is defined by $r = 2^k$. The corresponding nonlinear functions are given by:

$$\begin{aligned} A(\xi(t)) &= \sum_{i=1}^{r} \mu_i(\xi(t)) A_i, \quad & B(\xi(t)) &= \sum_{i=1}^{r} \mu_i(\xi(t)) B_i \\ C(\xi(t)) &= \sum_{i=1}^{r} \mu_i(\xi(t)) C_i, \quad & D(\xi(t)) &= \sum_{i=1}^{r} \mu_i(\xi(t)) D_i \end{aligned} \tag{1.24}$$

where μ_i represents the activation function of the i^{th} fuzzy rule. This function is the product of the membership functions from distinct premise variables $\xi_j(t)$:

$$\mu_i(\xi(t)) = \prod_{j=1}^{k} M_{\sigma_{ij}}^{j} \left(\xi_j(t)\right) \tag{1.25}$$

here, $M_{\sigma_{ij}}^{j}$ refers to the membership function for the j^{th} premise variable. The index σ_{ij} can be either 1 or 2, indicating which partition (either M_1^j for max or M_2^j for min) defines the activation function μ_i. The indexing is detailed in the table below:

$M_{\sigma_{ij}}^{j}$ / μ_i	$M_{\sigma_{ij}}^{1}$	$M_{\sigma_{ij}}^{2}$	$\dots$	$M_{\sigma_{ij}}^{k-1}$	$M_{\sigma_{ij}}^{k}$
μ_1	$\sigma_{ij} = 1$	$\sigma_{ij} = 1$	$\dots$	$\sigma_{ij} = 1$	$\sigma_{ij} = 1$
μ_2	$\sigma_{ij} = 1$	$\sigma_{ij} = 1$	$\dots$	$\sigma_{ij} = 1$	$\sigma_{ij} = 2$
$\vdots$	$\vdots$	$\vdots$	$\ddots$	$\vdots$	$\vdots$
μ_{r-1}	$\sigma_{ij} = 2$	$\sigma_{ij} = 2$	$\dots$	$\sigma_{ij} = 2$	$\sigma_{ij} = 1$
μ_r	$\sigma_{ij} = 2$	$\sigma_{ij} = 2$	$\dots$	$\sigma_{ij} = 2$	$\sigma_{ij} = 2$

Table 1.1: Definition of the membership functions corresponding to the fuzzy rules

Given this, the system (1.21) can be expressed as:

$$\begin{cases} \dot{x}(t) = \sum_{i=1}^{r} \mu_i(\xi(t)) \left(A_i x(t) + B_i u(t)\right) \\ y(t) = \sum_{i=1}^{r} \mu_i(\xi(t)) \left(C_i x(t) + D_i u(t)\right) \end{cases} \tag{1.26}$$

Example 1: Multi-model construction of induction motor using sector nonlinearity

The dynamical model of the induction motor is typically described in the rotational d-q reference frame. Below are the specific equations that described this nonlinear system:

$$\begin{cases} \dfrac{di_{sd}}{dt} = -\gamma i_{sd} + \omega_s i_{sq} + \dfrac{K_s}{T_r}\Psi_{rd} + K_s\omega\Psi_{rq} + \dfrac{1}{\sigma L_s}u_{sd} \\ \dfrac{di_{sq}}{dt} = -\omega_s i_{sd} - \gamma i_{sq} - K_s\omega\Psi_{rd} + \dfrac{K_s}{T_r}\Psi_{rq} + \dfrac{1}{\sigma L_s}u_{sq} \\ \dfrac{d\Psi_{rd}}{dt} = \dfrac{L_m}{T_r}i_{sd} - \dfrac{1}{T_r}\Psi_{rd} + (\omega_s - \omega)\,\Psi_{rq} \\ \dfrac{d\Psi_{rq}}{dt} = \dfrac{L_m}{T_r}i_{sq} - (\omega_s - \omega)\,\Psi_{rd} - \dfrac{1}{T_r}\Psi_{rq} \\ \dfrac{d\omega}{dt} = \alpha i_{sq}\Psi_{rd} - \alpha i_{sd}\Psi_{rq} - \dfrac{f}{J_m}\omega - \dfrac{p}{J_m}T_L \end{cases} \tag{1.27}$$

where:

$$\alpha = \frac{3}{2}p\frac{L_m}{L_r}\frac{p}{J_m};\ K_s = \frac{1}{\sigma L_s}\frac{L_m}{L_r};\gamma = \frac{1}{\sigma L_s}\left(R_s + \frac{1}{T_r}\frac{{L_m}^2}{L_r}\right);T_r = \frac{L_r}{R_r};\sigma = 1 - \frac{{L_m}^2}{L_s L_r}$$

here, u_{sd} and u_{sq} are the direct and the quadrature stator voltages respectively. i_{sd} and i_{sq} are the direct and the quadrature stator currents. ω is the rotor electrical angular speed. $T_L(t)$ is the resistant torque. The rest of the parameters are defined in Table 1.2:

Parameters	**Values**
Stator resistance	$R_s = 1.4\ [\Omega]$
Rotor resistance	$R_r = 1.7\ [\Omega]$
Stator inductance	$L_s = 0.2419\ [H]$
Rotor inductance	$L_r = 0.2554\ [H]$
Mutual inductance	$L_m = 0.24\ [H]$
Moment of inertia	$J_m = 0.0096\ [kg.\ m^2]$
Number of pole pairs	$p = 2$
Friction coefficient	$f = 0.0017[Nm]$

Table 1.2: Induction motor parameters

By defining $x\,(t) = \begin{bmatrix} i_{sd} & i_{sq} & \Psi_{rd} & \Psi_{rq} & \omega \end{bmatrix}^T$, $u\,(t) = \begin{bmatrix} u_{sd} & u_{sq} \end{bmatrix}^T$ and $y\,(t) = [\omega(t)]$ the nonlinear model of the induction machine in the $d-q$ axes is presented as follows:

$$\begin{cases} \dot{x}(t) = A(x)x(t) + Bu(t) + ET_L(t) \\ y = Cx(t) \end{cases} \tag{1.28}$$

where:

$$A(x) = \begin{bmatrix} -\gamma & \omega_s & \frac{K_s}{T_r} & K_s\omega & 0 \\ -\omega_s & -\gamma & -K_s\omega & \frac{K_s}{T_r} & 0 \\ \frac{L_m}{T_r} & 0 & -\frac{1}{T_r} & \omega_s - \omega & 0 \\ 0 & \frac{L_m}{T_r} & -(\omega_s - \omega) & -\frac{1}{T_r} & 0 \\ 0 & 0 & \alpha i_{sq} & -\alpha i_{sd} & -\frac{f}{J_m} \end{bmatrix}, B = \begin{bmatrix} \frac{1}{\sigma L_s} & 0 \\ 0 & \frac{1}{\sigma L_s} \\ 0 & 0 \\ 0 & 0 \\ 0 & 0 \end{bmatrix}, E = \begin{bmatrix} 0 \\ 0 \\ 0 \\ 0 \\ -\frac{p}{J_m} \end{bmatrix},$$

$$C = \begin{bmatrix} 0 & 0 & 0 & 0 & 1 \end{bmatrix}$$

As shown, the nonlinearities of this model are presented in the matrix $A(x)$ where there are three premise variables defined as : $\xi_1 = i_{sd}$, $\xi_2 = i_{sq}$ and $\xi_3 = \omega$. In order to apply the sector nonlinearity to these premise variables, two steps can be followed:

1 - First step:

It consists of separating the nonlinearities individually and then applying the sector nonlinearity to each part. Let's write $A(x)$ as follows:

$$A(\xi) = A_{cst} + A_1(\xi_1) + A_2(\xi_2) + A_3(\xi_3), \tag{1.29}$$

where:

$$A_{cst} = \begin{bmatrix} -\gamma & \omega_s & \frac{K_s}{T_r} & 0 & 0 \\ -\omega_s & -\gamma & 0 & \frac{K_s}{T_r} & 0 \\ \frac{L_m}{T_r} & 0 & -\frac{1}{T_r} & \omega_s & 0 \\ 0 & \frac{L_m}{T_r} & -\omega_s & -\frac{1}{T_r} & 0 \\ 0 & 0 & 0 & 0 & -\frac{f}{J_m} \end{bmatrix}, A_1(\xi_1) = \begin{bmatrix} 0 & 0 & 0 & 0 & 0 \\ 0 & 0 & 0 & 0 & 0 \\ 0 & 0 & 0 & 0 & 0 \\ 0 & 0 & 0 & 0 & 0 \\ 0 & 0 & 0 & -\alpha i_{sd} & 0 \end{bmatrix},$$

$$A_2(\xi_2) = \begin{bmatrix} 0 & 0 & 0 & 0 & 0 \\ 0 & 0 & 0 & 0 & 0 \\ 0 & 0 & 0 & 0 & 0 \\ 0 & 0 & 0 & 0 & 0 \\ 0 & 0 & \alpha i_{sq} & 0 & 0 \end{bmatrix}, A_3(\xi_3) = \begin{bmatrix} 0 & 0 & 0 & K_s\omega & 0 \\ 0 & 0 & -K_s\omega & 0 & 0 \\ 0 & 0 & 0 & -\omega & 0 \\ 0 & 0 & \omega & 0 & 0 \\ 0 & 0 & 0 & 0 & 0 \end{bmatrix}$$

Next, the sector nonlinearity approach is applied to each separated nonlinear term using Lemma 1.1 as follows:

$$\begin{cases} A_1(\xi_1) = \sum_{i=1}^{2} M_{1i}(\xi_1) A_{1i}, \\ A_2(\xi_2) = \sum_{i=1}^{2} M_{2i}(\xi_2) A_{2i}, \\ A_3(\xi_3) = \sum_{i=1}^{2} M_{3i}(\xi_3) A_{3i}, \end{cases} \tag{1.30}$$

where the sub-matrices are given by:

$$A_{11}=\begin{bmatrix}0&0&0&0&0\\0&0&0&0&0\\0&0&0&0&0\\0&0&0&0&0\\0&0&0&-\alpha i_{sd_{\max}}&0\end{bmatrix},A_{12}=\begin{bmatrix}0&0&0&0&0\\0&0&0&0&0\\0&0&0&0&0\\0&0&0&0&0\\0&0&0&-\alpha i_{sd_{\min}}&0\end{bmatrix}$$

$$A_{21}=\begin{bmatrix}0&0&0&0&0\\0&0&0&0&0\\0&0&0&0&0\\0&0&0&0&0\\0&0&\alpha i_{sq_{\max}}&0&0\end{bmatrix},A_{22}=\begin{bmatrix}0&0&0&0&0\\0&0&0&0&0\\0&0&0&0&0\\0&0&0&0&0\\0&0&\alpha i_{sq_{\min}}&0&0\end{bmatrix}$$

$$A_{31}=\begin{bmatrix}0&0&0&K_s\omega_{\max}&0\\0&0&-K_s\omega_{\max}&0&0\\0&0&0&-\omega_{\max}&0\\0&0&\omega_{\max}&0&0\\0&0&0&0&0\end{bmatrix},A_{32}=\begin{bmatrix}0&0&0&K_s\omega_{\min}&0\\0&0&-K_s\omega_{\min}&0&0\\0&0&0&-\omega_{\min}&0\\0&0&\omega_{\min}&0&0\\0&0&0&0&0\end{bmatrix}$$

and the membership functions are defined by:

$$\begin{cases}M_{11}(\xi_1)=\frac{i_{sd}-i_{sd_{\min}}}{i_{sd_{\max}}-i_{sd_{\min}}}\\M_{12}(\xi_1)=\frac{i_{sd_{\max}}-i_{sd}}{i_{sd_{\max}}-i_{sd_{\min}}}\end{cases},\begin{cases}M_{21}(\xi_2)=\frac{i_{sq}-i_{sq_{\min}}}{i_{sq_{\max}}-i_{sq_{\min}}}\\M_{22}(\xi_2)=\frac{i_{sq_{\max}}-i_{sq}}{i_{sq_{\max}}-i_{sq_{\min}}}\end{cases},\begin{cases}M_{31}(\xi_3)=\frac{\omega-\omega_{\min}}{\omega_{\max}-\omega_{\min}}\\M_{32}(\xi_3)=\frac{\omega_{\max}-\omega}{\omega_{\max}-\omega_{\min}}\end{cases}$$

2 - Second Step:

This step consists of combining the separated parts to obtain a compact form. By substituting (1.30) in equation (1.29), the matrix $A(\xi)$ can be written as follows:

$$A(\xi)=A_{cst}+\sum_{i=1}^{2}M_{1i}(\xi_1)A_{1i}+\sum_{i=1}^{2}M_{2i}(\xi_2)A_{2i}+\sum_{i=1}^{2}M_{3i}(\xi_3)A_{3i} \tag{1.31}$$

By benefiting from the convex sum property giving in (1.9), the equation (1.31) can be written as follows:

$$A(\xi)=\sum_{i=1}^{2}\sum_{j=1}^{2}\sum_{k=1}^{2}M_{1i}(\xi_1)M_{2j}(\xi_2)M_{3k}(\xi_3)(A_{cst}+A_{1i}+A_{2j}+A_{3k})=\sum_{i=1}^{r=2^3}\mu_i(\xi)A_i, \tag{1.32}$$

where the sub-matrices are given by:

$$A_1=\begin{bmatrix}-\gamma&\omega_s&\frac{K_s}{T_r}&K_s\omega_{\max}&0\\-\omega_s&-\gamma&-K_s\omega_{\max}&\frac{K_s}{T_r}&0\\\frac{L_m}{T_r}&0&-\frac{1}{T_r}&\omega_s-\omega_{\max}&0\\0&\frac{L_m}{T_r}&-(\omega_s-\omega_{\max})&-\frac{1}{T_r}&0\\0&0&\alpha i_{sq_{\max}}&-\alpha i_{sd_{\max}}&-\frac{f}{J_m}\end{bmatrix},A_2=\begin{bmatrix}-\gamma&\omega_s&\frac{K_s}{T_r}&K_s\omega_{\min}&0\\-\omega_s&-\gamma&-K_s\omega_{\min}&\frac{K_s}{T_r}&0\\\frac{L_m}{T_r}&0&-\frac{1}{T_r}&\omega_s-\omega_{\min}&0\\0&\frac{L_m}{T_r}&-(\omega_s-\omega_{\min})&-\frac{1}{T_r}&0\\0&0&\alpha i_{sq_{\max}}&-\alpha i_{sd_{\max}}&-\frac{f}{J_m}\end{bmatrix}$$

$$A_3 = \begin{bmatrix} -\gamma & \omega_s & \frac{K_s}{T_r} & K_s\omega_{\max} & 0 \\ -\omega_s & -\gamma & -K_s\omega_{\max} & \frac{K_s}{T_r} & 0 \\ \frac{L_m}{T_r} & 0 & -\frac{1}{T_r} & \omega_s - \omega_{\max} & 0 \\ 0 & \frac{L_m}{T_r} & -(\omega_s - \omega_{\max}) & -\frac{1}{T_r} & 0 \\ 0 & 0 & \alpha i_{sq_{\min}} & -\alpha i_{sd_{\max}} & -\frac{f}{J_m} \end{bmatrix}, A_4 = \begin{bmatrix} -\gamma & \omega_s & \frac{K_s}{T_r} & K_s\omega_{\min} & 0 \\ -\omega_s & -\gamma & -K_s\omega_{\min} & \frac{K_s}{T_r} & 0 \\ \frac{L_m}{T_r} & 0 & -\frac{1}{T_r} & \omega_s - \omega_{\min} & 0 \\ 0 & \frac{L_m}{T_r} & -(\omega_s - \omega_{\min}) & -\frac{1}{T_r} & 0 \\ 0 & 0 & \alpha i_{sq_{\min}} & -\alpha i_{sd_{\max}} & -\frac{f}{J_m} \end{bmatrix}$$

$$A_5 = \begin{bmatrix} -\gamma & \omega_s & \frac{K_s}{T_r} & K_s\omega_{\max} & 0 \\ -\omega_s & -\gamma & -K_s\omega_{\max} & \frac{K_s}{T_r} & 0 \\ \frac{L_m}{T_r} & 0 & -\frac{1}{T_r} & \omega_s - \omega_{\max} & 0 \\ 0 & \frac{L_m}{T_r} & -(\omega_s - \omega_{\max}) & -\frac{1}{T_r} & 0 \\ 0 & 0 & \alpha i_{sq_{\max}} & -\alpha i_{sd_{\min}} & -\frac{f}{J_m} \end{bmatrix}, A_6 = \begin{bmatrix} -\gamma & \omega_s & \frac{K_s}{T_r} & K_s\omega_{\min} & 0 \\ -\omega_s & -\gamma & -K_s\omega_{\min} & \frac{K_s}{T_r} & 0 \\ \frac{L_m}{T_r} & 0 & -\frac{1}{T_r} & \omega_s - \omega_{\min} & 0 \\ 0 & \frac{L_m}{T_r} & -(\omega_s - \omega_{\min}) & -\frac{1}{T_r} & 0 \\ 0 & 0 & \alpha i_{sq_{\max}} & -\alpha i_{sd_{\min}} & -\frac{f}{J_m} \end{bmatrix}$$

$$A_7 = \begin{bmatrix} -\gamma & \omega_s & \frac{K_s}{T_r} & K_s\omega_{\max} & 0 \\ -\omega_s & -\gamma & -K_s\omega_{\max} & \frac{K_s}{T_r} & 0 \\ \frac{L_m}{T_r} & 0 & -\frac{1}{T_r} & \omega_s - \omega_{\max} & 0 \\ 0 & \frac{L_m}{T_r} & -(\omega_s - \omega_{\max}) & -\frac{1}{T_r} & 0 \\ 0 & 0 & \alpha i_{sq_{\min}} & -\alpha i_{sd_{\min}} & -\frac{f}{J_m} \end{bmatrix}, A_8 = \begin{bmatrix} -\gamma & \omega_s & \frac{K_s}{T_r} & K_s\omega_{\min} & 0 \\ -\omega_s & -\gamma & -K_s\omega_{\min} & \frac{K_s}{T_r} & 0 \\ \frac{L_m}{T_r} & 0 & -\frac{1}{T_r} & \omega_s - \omega_{\min} & 0 \\ 0 & \frac{L_m}{T_r} & -(\omega_s - \omega_{\min}) & -\frac{1}{T_r} & 0 \\ 0 & 0 & \alpha i_{sq_{\min}} & -\alpha i_{sd_{\min}} & -\frac{f}{J_m} \end{bmatrix}$$

and the activation functions are defined by:

$$\begin{cases} \mu_1(\xi) = M_{11}(\xi_1)M_{21}(\xi_2)M_{31}(\xi_3), \mu_2(\xi) = M_{11}(\xi_1)M_{21}(\xi_2)M_{32}(\xi_3), \\ \mu_3(\xi) = M_{11}(\xi_1)M_{22}(\xi_2)M_{31}(\xi_3), \mu_4(\xi) = M_{11}(\xi_1)M_{22}(\xi_2)M_{32}(\xi_3), \\ \mu_5(\xi) = M_{12}(\xi_1)M_{21}(\xi_2)M_{31}(\xi_3), \mu_6(\xi) = M_{12}(\xi_1)M_{21}(\xi_2)M_{32}(\xi_3), \\ \mu_7(\xi) = M_{12}(\xi_1)M_{22}(\xi_2)M_{31}(\xi_3), \mu_8(\xi) = M_{12}(\xi_1)M_{22}(\xi_2)M_{32}(\xi_3) \end{cases}$$

The rest of the sub-matrices are defined as follows:

$$B_i = \begin{bmatrix} \frac{1}{\sigma L_s} & 0 \\ 0 & \frac{1}{\sigma L_s} \\ 0 & 0 \\ 0 & 0 \\ 0 & 0 \end{bmatrix}, E_i = \begin{bmatrix} 0 \\ 0 \\ 0 \\ 0 \\ -\frac{p}{J_m} \end{bmatrix}, \; C_i = \begin{bmatrix} 0 & 0 & 0 & 0 & 1 \end{bmatrix} \quad \forall i = 1, ..r.$$

Hence, the T-S multi-model of the induction motor is given by:

$$\begin{cases} \dot{x}(t) = \sum_{i=1}^{r} \mu_i(\xi(t)) \left(A_i x(t) + B_i u(t) + E_i T_L(t)\right) \\ y(t) = \sum_{i=1}^{r} \mu_i(\xi(t)) \left(C_i x(t)\right) \end{cases} \tag{1.33}$$

The subsequent figures present the results derived from the nonlinear model of the induction motor given in (1.28) in comparison to those from the T-S multi-model provided in (1.33):

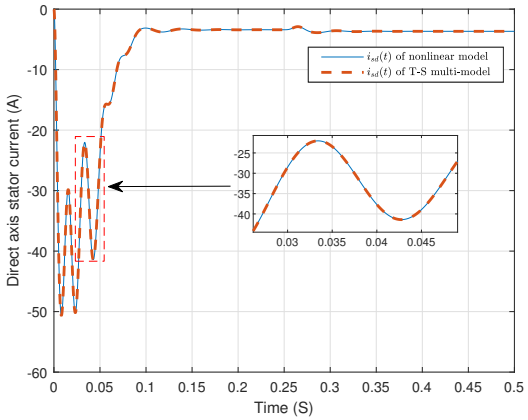

Fig 1.10: Direct axis stator current.

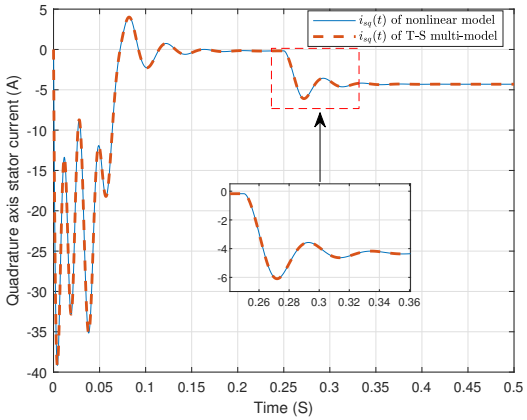

Fig 1.11: Quadrature axis stator current.

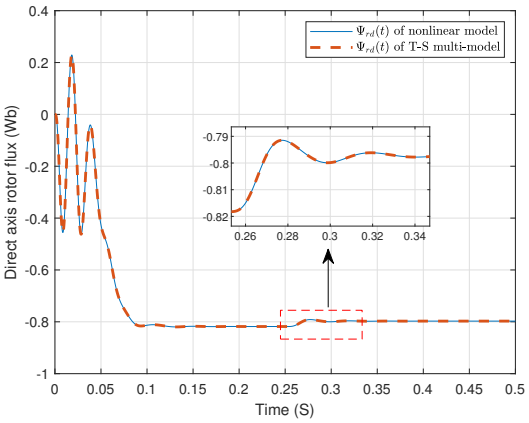

Fig 1.12: Direct axis rotor flux.

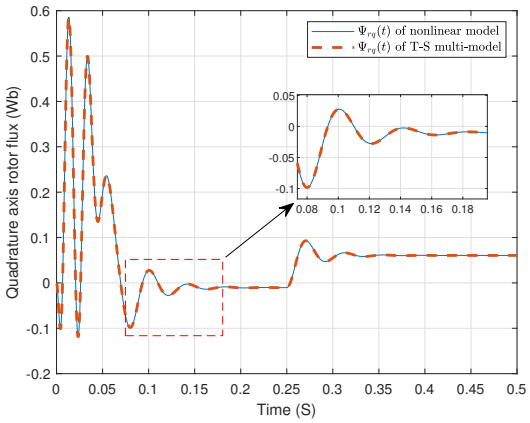

Fig 1.13: Quadrature axis rotor flux.

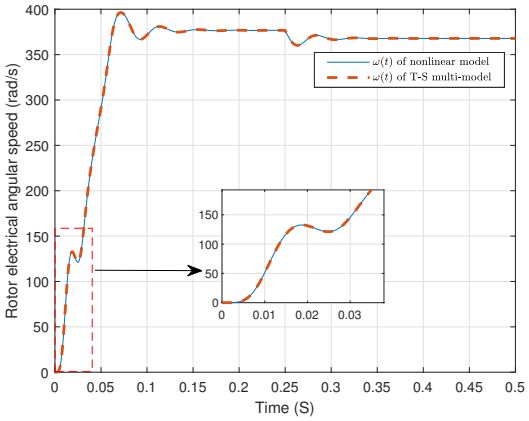

Fig 1.14: Rotor electrical angular speed.

Based on these results, it's evident that the T-S multi-model offers an accurate representation of the nonlinear model using the sector nonlinearity approach, without any errors or loss of information, in contrast to the identification or linearization methods. Consequently, this approach will be adopted in this work when constructing T-S multi-models.

1.5 Preliminaries on Convex analysis

1.5.1 Convex sets

A set C is said to be convex if the line segment between any two points in C is entirely contained within C. If this is not the case, the set is termed non-convex. The distinction between convex and non-convex sets can be visualized as shown in the figures below:

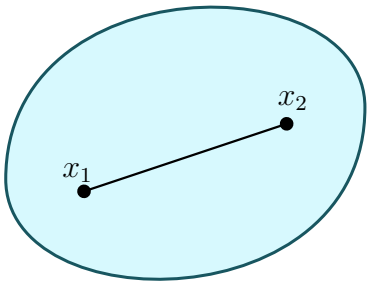

Fig 1.15: Convex set illustration.

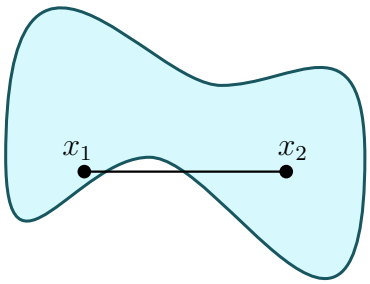

Fig 1.16: Non-convex set illustration.

In Figure 1.15, the line segment connecting points x_1 and x_2 is entirely contained within the set, which is depicted in blue. Given that this is true for any possible pair of points in the set, it is deemed convex.

In contrast, Figure 1.16 displays a line segment between points x_1 and x_2 that extends beyond the set boundaries, indicating that the set is non-convex.

Thus, the formal definition of a convex set is:

Definition 1.3. *[Boyd and Vandenberghe, 2004] A set C is convex if:*

$$\forall\,(x_1, x_2) \in C^2, \quad \lambda \in [0,1] \implies \lambda x_1 + (1-\lambda)x_2 \in C. \tag{1.34}$$

1.5.2 Convex functions

A function is deemed to be convex if, and only if, its epigraph, the set of points lying on or above the graph of the function, is a convex set. An illustration of a convex function is depicted in the following figure:

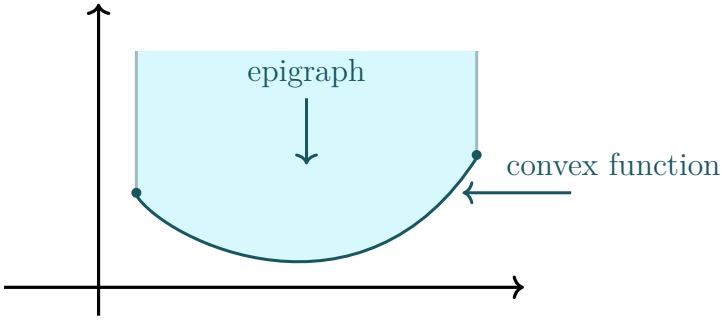

Fig 1.17: Illustration of a convex function

A more formal definition of a convex function is provided as:

Definition 1.4. *[Boyd and Vandenberghe, 2004] Given a convex set C, a function f is convex if the following condition is satisfied:*

$$\forall (x_1, x_2) \in C^2, \quad \lambda \in [0,1] \implies f\left((1-\lambda)x_1 + \lambda x_2\right) \leq (1-\lambda)f(x_1) + \lambda f(x_2) \tag{1.35}$$

1.5.3 Convex combination

A convex combination of a set of points x_i refers to their linear combination where each coefficient λ_i is non-negative and their sum equals 1.

The formal definition of a convex combination is as follows:

Definition 1.5. *[Boyd and Vandenberghe, 2004] Given a set of points x_i, for $i = 1, \ldots, r$, a convex combination of these points is a point y defined as:*

$$y = \sum_{i=1}^{r} \lambda_i x_i, \tag{1.36}$$

such that $\lambda_i \geq 0$ and $\sum_{i=1}^{r} \lambda_i = 1$.

Hence, another definition pertaining to convex sets is provided:

Definition 1.6. *[Boyd and Vandenberghe, 2004] A set C is convex if and only if it contains every convex combination of its points.*

The figures below provide an illustration of a convex combination in relation to both convex and non-convex sets:

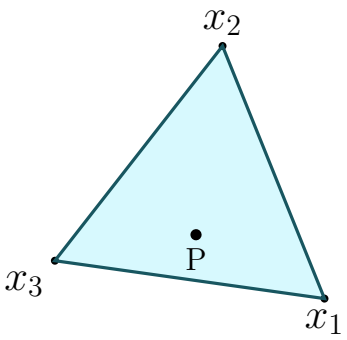

Fig 1.18: Convex combination and convex set.

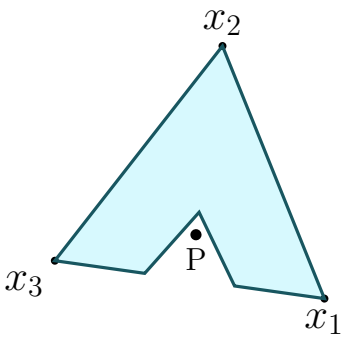

Fig 1.19: Convex combination and non-convex set.

In both Figures 1.18 and 1.19, the point P represents a convex combination of the three points x_1, x_2, and x_3. The set (depicted in blue) in Figure 1.18 is convex as it contains all the convex combinations of its points. Conversely, in Figure 1.19, the set is non-convex because point P, despite being a convex combination of points from the set, lies outside of it.

1.5.4 Convex hull

The convex hull of a set C, which doesn't necessarily have to be convex, represents the smallest convex set that encompasses or contains C. For a tangible understanding, consider a finite set of points P, as demonstrated in Figure 1.20. One can envisage the convex hull as the shape produced when a tight rubber band is stretched around the given points of P. This form ensures that any line segment drawn between any pair of points within the convex hull remains entirely contained within the hull. Thus, the convex hull of a finite set of points becomes the unique convex polytope (referred to as a polygon in 2D) that not only has its vertices among the points of P but also encapsulates every point from P [De Berg, 2000]. The vertices of this minimal convex polytope are termed as the extreme points. The quest to pinpoint the minimal convex polytope for a finite set of points essentially becomes an endeavor to identify these extreme points [Anstett et al., 2009].

(a) Set of points (b) Its convex hull

Fig 1.20: Convex hull illustration

Formally, the definition of convex hull is given by:

Definition 1.7. *[Boyd and Vandenberghe, 2004] The convex hull of a set C, symbolized by* $\operatorname{conv} C$*, is the set of all convex combinations of points in C:*

$$\operatorname{conv} C = \{\lambda_1 x_1 + \cdots + \lambda_r x_r \mid x_i \in C, \lambda_i \geq 0, i = 1, \ldots, r, \lambda_1 + \cdots + \lambda_r = 1\} \tag{1.37}$$

1.5.5 Takagi-Sugeno system and convex combination

The T-S fuzzy representation of a system leverages local time-invariant systems combined using weighting functions, denoted as μ_i. As previously discussed in Section 1.3.1, these weighting functions satisfy the convex sum property:

$$\sum_{i=1}^{r} \mu_i(\xi(t)) = 1, \quad 0 \leq \mu_i(\xi(t)) \leq 1, \quad \forall i = 1, \ldots, r. \tag{1.38}$$

Therefore, the T-S representation of a system can be conceptualized as a convex combination of sub-systems. Each sub-system delineates a vertex of a convex polytope, and the real-time value of the system navigates within this polytope.

Given the outlined structure of the T-S system, its polytope representation can be framed using the concept of a convex hull. At any given time t, the system can be represented by $M(t)$, which is a convex combination of the vertices M_i. Mathematically, this relationship is given by:

$$M(t) \in \operatorname{conv}\{M_1, \ldots, M_r\} = \left\{ \sum_{i=1}^{r} \mu_i(\xi(t)) M_i \mid \sum_{i=1}^{r} \mu_i(\xi(t)) = 1, 0 \leq \mu_i(\xi(t)) \leq 1 \right\}, \tag{1.39}$$

where each M_i is represented by the matrix:

$$M_i = \begin{bmatrix} A_i & B_i \\ C_i & D_i \end{bmatrix}. \tag{1.40}$$

To visually represent the discussed concepts, the polytopic structure of the T-S system is illustrated below:

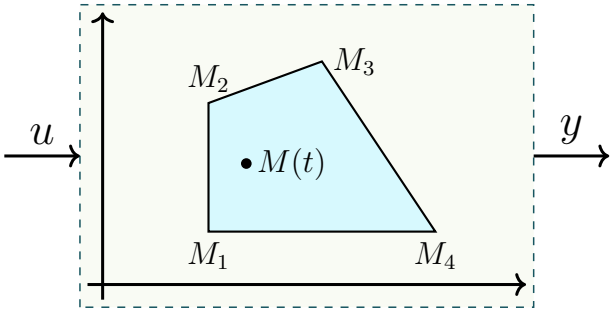

Fig 1.21: Polytopic structure of the T-S system

1.6 Preliminaries on Matrix Inequality

Matrix comparisons can be understood in different ways based on context. One can compare matrices element-wise, where each element of one matrix is compared with the corresponding element of another. Specifically, for a symmetric matrix $P \in \mathbb{R}^{n_x \times n_x}$, the notation $P > 0_{n_x \times n_x}$ (where $0_{n_x \times n_x}$ is the zero matrix) indicates that all the elements of P are strictly greater than 0.

However, comparing a matrix with a scalar directly, as in $P > 0$ where 0 is a scalar, doesn't have a straightforward element-wise meaning. Instead, the notation $P > 0$ typically means that the matrix P is positive definite. This is a more intricate concept and is not merely a comparison of individual matrix elements with a scalar.

Definition 1.8. *(Positive definite matrix) A symmetric matrix $P \in \mathbb{R}^{n_x \times n_x}$ is said to be positive definite if $x^T Px > 0$ for all non-zero column vector $x \in \mathbb{R}^{n_x}$:*

$$P > 0 \quad \Longleftrightarrow \quad \mathbf{x}^{\mathrm{T}} P\mathbf{x} > 0 \quad \forall \mathbf{x} \neq 0 \tag{1.41}$$

Among the properties of the positive definite matrix:

- ❖ All eigenvalues are positive.
- ❖ All sub-determinants are positive.
- ❖ All the diagonal components are positive.

For a positive semi-definite matrix P, the sign $>$ is replaced with $\geq$:

Definition 1.9. *(Positive semi-definite matrix) A symmetric matrix $P \in \mathbb{R}^{n_x \times n_x}$ is said to be positive semi-definite if $x^T Px \geq 0$ for all non-zero column vector $x \in \mathbb{R}^{n_x}$:*

$$P \geq 0 \quad \Longleftrightarrow \quad \mathbf{x}^{\mathrm{T}} P\mathbf{x} \geq 0 \quad \forall \mathbf{x} \neq 0 \tag{1.42}$$

Similarly, the definition of negative definite and negative semi-definite matrices can be deduced:

Definition 1.10. *(Negative definite matrix) A symmetric matrix $P \in \mathbb{R}^{n_x \times n_x}$ is said to be negative definite if $x^T Px < 0$ for all non-zero column vector $x \in \mathbb{R}^{n_x}$:*

$$P < 0 \quad \Longleftrightarrow \quad \mathbf{x}^{\mathrm{T}} P\mathbf{x} < 0 \quad \forall \mathbf{x} \neq 0 \tag{1.43}$$

Definition 1.11. *(Negative semi-definite matrix) A symmetric matrix $P \in \mathbb{R}^{n_x \times n_x}$ is said to be negative semi-definite if $x^T Px \leq 0$ for all non-zero column vector $x \in \mathbb{R}^{n_x}$:*

$$P \leq 0 \quad \Longleftrightarrow \quad \mathbf{x}^{\mathrm{T}} P\mathbf{x} \leq 0 \quad \forall \mathbf{x} \neq 0 \tag{1.44}$$

It is worth noting that for scalars, based on the "Law of Trichotomy", if $a \ngeq b$ means $a < b$ and $a \nleq b$ means $a \geq b$. However, for matrices this is not true:

Definition 1.12. *For a symmetric matrix $P \in \mathbb{R}^{n_x \times n_x}$, if $P \nleqslant 0$ then it is not imperative that $P > 0$:*

$$P \nleqslant 0 \quad \not\Rightarrow \quad P > 0 \tag{1.45}$$

Remark 1.3

In certain literature, the notation $\succ$ is adopted to indicate a matrix being positive definite, rather than using $>$. Similarly, $\succeq$ is used to denote a matrix as positive semi-definite in place of $\geq$.

1.7 Preliminaries on Linear Matrix Inequality

1.7.1 Definition of Linear Matrix Inequality

A Linear Matrix Inequality (LMI) represents an inequality that involves matrices and is linear in its unknowns. Given a set of constant symmetric matrices $F_0, F_1, \ldots, F_m$ and a vector of decision variables (in any optimization problem, the unknown variables that need to be determined are referred to as "decision variables") $x = [x_1, x_2, \ldots, x_m]^T \in \mathbb{R}^m$, an LMI can be formulated as:

$$F(x) = F_0 + x_1 F_1 + x_2 F_2 + \cdots + x_m F_m \geq 0 \tag{1.46}$$

Here, the symbol "≥ 0" indicates that the resulting matrix $F(x)$ is positive semi-definite, implying that all its eigenvalues are non-negative. The matrices F_i are provided and are symmetric, which ensures $F_i = F_i^T$. As any matrix variable can be decomposed into a base of symmetric matrices, the definition (1.46) involving scalars is easily extended to matrices [Lendek et al., 2011].

Historical records trace the origins of LMIs to the 1890s, credited to Lyapunov. He introduced a seminal concept concerning the stability of dynamical systems. Specifically, he asserted that the ordinary differential equation

$$\frac{d}{dt}x(t) = Ax(t), \tag{1.47}$$

is asymptotically stable if there exists a solution to the matrix inequalities

$$PA + A^T P < 0 \quad \text{and} \quad P = P^T > 0, \tag{1.48}$$

with the matrix P being the sought-after decision variable, readers interested in the history of LMI are encouraged to refer to [Boyd et al., 1994].

The LMI formulation has gained considerable attention among control engineers in recent years. This can be attributed to the LMI's capability to seamlessly integrate various design constraints or objectives in a numerically efficient manner.

The set of solutions for the LMI (1.46) is called the "feasibility set" and is denoted by $S = \{x \mid x \in \mathbb{R}^m, F(x) \geq 0\}$ which constitutes a convex subset of $\mathbb{R}^m$. Finding a solution to the LMI (1.46) is a convex optimization problem avoiding local minima and guaranteeing finite feasibility tests. If a solution to this problem exists, it is said to be "feasible"; otherwise, it is classified as "infeasible" [Lendek et al., 2011]. Later, in Section 1.7.4, we will provide a detailed definition of the convex optimization problem, along with an exploration of some of its various types.

1.7.2 Properties used in Linear Matrix Inequalities

LMI constraints do not "naturally" arise in control problems. However, due to the availability of optimization solutions, one objective when addressing control problems is to reformulate them in terms of LMI expressions. This is achieved by leveraging the properties of LMIs, some of which are listed below.

Lemma 1.2. *(Completion of squares) [Lendek et al., 2011]*

For two appropriately sized matrices X and Y, and given $Q = Q^T > 0$, the subsequent inequality is valid:

$$X^T Y + Y^T X \leq X^T Q X + Y^T Q^{-1} Y \tag{1.49}$$

Lemma 1.3. *(Schur complement) [Lendek et al., 2011]*

Consider a matrix $M = M^T = \begin{bmatrix} M_{11} & M_{12} \\ M_{12}^T & M_{22} \end{bmatrix}$ with M_{11} and M_{22} being square matrices. Then:

$$M < 0 \Leftrightarrow \begin{cases} M_{22} < 0 \\ M_{11} - M_{12} M_{22}^{-1} M_{12}^T < 0 \end{cases} \tag{1.50}$$

1.7.3 Relaxation Methods for Parameterized LMI

Many stability conditions in control and observation problems can be formulated as an LMI that depends on parameters $\mu(\xi)$. Consequently, they are referred to as Parameterized Linear Matrix Inequalities (PLMI). Recently proposed stability approaches are often represented with double parameters, also known as double summation. This is depicted by:

$$\sum_{i=1}^{r} \sum_{j=1}^{r} \mu_i(\xi)\, \mu_j(\xi)\, \mathcal{K}_{ij}(x) < 0, \tag{1.51}$$

where $\mathcal{K}_{ij}(x)$ are symmetric matrices affinely dependent on unknown decision variables $x \in \mathbb{R}^m$. Here, x signifies the decision variables of the optimization problem, not the state variable of a system's state-space representation. The functions $\mu_i(\xi)$ are nonlinear and satisfy the convex sum property $\sum_{i=1}^{r} \mu_i(\xi) = 1$ and $0 \leq \mu_i(\xi) \leq 1$.

A trivial solution to the LMI problem (1.51) is given by:

$$\mathcal{K}_{ij}(x) < 0, \ \forall i, j = 1, \ldots, r \tag{1.52}$$

Proof. Consider the expansion of inequality (1.51):

$$\underbrace{\mu_1(\xi)\, \mu_1(\xi)}_{+} \mathcal{K}_{11}(x) + \underbrace{\mu_1(\xi)\, \mu_2(\xi)}_{+} \mathcal{K}_{12}(x) + \cdots + \underbrace{\mu_r(\xi)\, \mu_r(\xi)}_{+} \mathcal{K}_{rr}(x) < 0 \tag{1.53}$$

Given that the activation functions yield positive values, the negativity of inequality (1.53) can be verified if each term $\mathcal{K}_{ij}$ is negative as given in condition (1.52). □

However, these conditions can sometimes be conservative. In the context of this discussion, the definition of conservatism is provided as:

Definition 1.13. *"Conservatism" denotes the tendency to stipulate stability conditions or margins that are more restrictive than the true stability limits of the system. While a conservative analysis ensures stability if its conditions are met, the system may remain stable even if those conditions are slightly exceeded. This is because the analysis might not accurately define the entire stability boundary, focusing instead on a narrower range for simplicity or guaranteed safety. Such an approach, while possibly making analysis easier or ensuring safety, might overlook feasible and potentially more efficient solutions by not capturing the system's full stability limits.*

The objective, therefore, is to identify the least conservative (or more relaxed) conditions on $\mathcal{K}_{ij}$ that still ensure the negativity of the double sum in equation (1.51), leveraging only the convex sum property of the functions $\mu_i(\xi)$. Subsequent Lemmas offer stability conditions for the LMI given in (1.51) that are less conservative than those in (1.52):

Lemma 1.4. *[Wang et al., 1996] The PLMI given in (1.51) is satisfied if the following conditions are met:*

$$\begin{cases} \mathcal{K}_{ii} < 0, & i = 1, \dots, r \\ \mathcal{K}_{ij} + \mathcal{K}_{ji} < 0, & i, j = 1, \dots, r \text{ and } i < j \end{cases} \tag{1.54}$$

Proof. Considering the symmetry of the parameters, i.e., $\mu_i \mu_j = \mu_j \mu_i$, from expression (1.51), we derive the following LMI:

$$\sum_{i=1}^{r} \sum_{j=1}^{r} \mu_i(\xi)\mu_j(\xi)\mathcal{K}_{ij}(x) = \sum_{i=1}^{r} \mu_i^2(\xi)\mathcal{K}_{ii}(x) + \sum_{i=1}^{r} \sum_{j>i}^{r} \mu_i(\xi)\mu_j(\xi) \left(\mathcal{K}_{ij}(x) + \mathcal{K}_{ji}(x)\right). \tag{1.55}$$

In the above expression, we distinguish between the coupled terms in both i and j (represented by $\mathcal{K}_{ij}$) and the non-coupled terms that depend solely on i (represented by $\mathcal{K}_{ii}$). The conditions given in (1.54) ensure the negativity of (1.55).

□

In comparison to the trivial conditions outlined in (1.52), the relaxation is achieved through benefiting from the symmetric property of the coupled terms. This obviates the need for $\mathcal{K}_{ij}(x) < 0$ and $\mathcal{K}_{ji}(x) < 0$ for every i, j. Instead, we are only required to satisfy the more lenient condition $\mathcal{K}_{ij}(x) + \mathcal{K}_{ji}(x) < 0$ for all $i < j$.

Lemma 1.5. *[Tuan et al., 2001] The PLMI given in (1.51) is satisfied if the following conditions are met:*

$$\begin{cases} \mathcal{K}_{ii} < 0, & i = 1, \ldots, r \\ \frac{1}{r-1}\mathcal{K}_{ii} + \frac{1}{2}\left(\mathcal{K}_{ij} + \mathcal{K}_{ji}\right) < 0, & 1 \leq i \neq j \leq r \end{cases} \tag{1.56}$$

It is evident that the coupled terms in Lemma 1.5 offer more relaxed conditions than those in Lemma 1.4. Rather than strictly requiring $\mathcal{K}_{ij}(x) + \mathcal{K}_{ji}(x)$ to be negative, they only need to be less than the positive value $\frac{-2}{r-1}\mathcal{K}_{ii}$.

Xiaodong and Qingling proposed another relaxation method in [Xiaodong and Qingling, 2003]. While this method offers less conservative conditions compared to previous ones, it comes at a substantial increase in computational cost due to the greater number of decision variables. In contrast, Tuan's lemma establishes a favorable balance between conservatism and computational cost, achieving satisfactory levels of conservatism without introducing new decision variables [DUONG, 2013]. In [Sala and Ariño, 2007], another relaxation method was introduced, leveraging Polya's theorem. Central to this method is the property $(\sum_{i=1}^{r} \mu_i(\xi))^p = 1$, where p is a positive integer. This allows for the multiplication of the LMI given in (1.51) by this term. When grouping all terms on the left-hand side of the inequality with identical coefficients, the result is less conservative LMI conditions than those presented in (1.52). Furthermore, it has been demonstrated that as the value of p increases, even less restrictive conditions can be achieved. However, an increase in p also amplifies the computational complexity of the optimization problem due to the increase in the number of LMIs. This complexity can be particularly challenging when dealing with higher-order systems.

1.7.4 Convex optimization problem

LMIs inherently represent convex constraints. Consider x_1 and x_2 as two feasible solutions for the LMI (1.46). Given that $F(x_1) \geq 0$ and $F(x_2) \geq 0$, any convex combination of those solutions $x = (1-\lambda)x_1 + \lambda x_2$, where $\lambda \in [0, 1]$, will also be a feasible solution to the LMI:

$$F(x) = F\left((1-\lambda)x_1 + \lambda x_2\right) = (1-\lambda)F(x_1) + \lambda F(x_2) \geq 0 \tag{1.57}$$

Given this convex nature, many optimization problems with convex objective functions and LMI constraints can be efficiently addressed using available software. Some of the most adept algorithms for tackling LMI challenges employ interior point methods. These methods operate iteratively, with each iteration encompassing a least squares minimization problem [Zhang et al., 2016, Vandenberghe and Balakrishnan, 1997].

The standard form of an optimization problem is defined as follows:

$$\begin{cases} \text{minimize} & f(x) \\ \text{subject to} & g_i(x) \leq 0, \quad i = 1, \ldots, l. \\ & h_j(x) = 0, \quad j = 1, \ldots, p. \end{cases} \tag{1.58}$$

where the vector x represents the optimization variable of the problem (decision variable). The function f is the objective function. The functions g_i, for $i = 1, \ldots, l$, are the inequality constraint functions. The functions h_j, for $j = 1, \ldots, p$, are the equality constraint functions.

A vector $x^\star$ is deemed optimal or a solution to the problem (1.58) if it yields the minimum value for the objective function among all vectors that meet the constraints. Formally, for any vector z such that $g_i(z) \leq 0$ and $h_j(z) = 0$, it must be true that $f(z) \geq f(x^\star)$.

Optimization problems are typically grouped into families or classes based on the characteristics of their objective and constraint functions. These classes help in categorizing problems for the purpose of applying specialized solution techniques. In this context, we are particularly interested in the class of convex optimization problems.

Definition 1.14. *A convex optimization problem is one in which the objective and constraint functions are convex.*

Among the types of convex optimization problems discussed in [Boyd and Vandenberghe, 2004, Bockmayr et al., 2001], some prominent ones are:

1. **Linear Program (LP)**: The optimization problem (1.58) is Linear Program if the objective and all constraint functions are linear:

$$\begin{cases} \text{minimize} & c_1x_1 + c_2x_2 + \cdots + c_mx_m \\ \text{subject to} & a_{i1}x_1 + a_{i2}x_2 + \cdots + a_{im}x_m \leq b_i \quad \text{for } i = 1, 2, \ldots, l \\ & 0 \leq x_j \quad \text{for } j = 1, 2, \ldots, m \end{cases} \tag{1.59}$$

   Using matrix notation, we can rewrite this LP as:

$$\begin{cases} \text{minimize} & c^T x \\ \text{subject to} & Ax \leq b \\ & x \geq 0 \end{cases} \tag{1.60}$$

   where $c = [c_1 \ldots c_m]^T$ and $b = [b_1 \ldots b_l]^T$ are given vectors, $x = [x_1 \ldots x_m]^T$ is a vector of decision variables and A is a matrix. The inequalities $Ax \leq b$ and $x \geq 0$ are to be interpreted componentwise (comparison of element by element from both sides of the inequality).

2. **Quadratic Program (QP)**: The optimization problem (1.58) is quadratic program if the objective is a quadratic function, and constraints are linear:

$$\begin{cases} \text{minimize} & \frac{1}{2}x^T Q x + c^T x \\ \text{subject to} & Ax \leq b \\ & x \geq 0 \end{cases} \tag{1.61}$$

The convexity of the objective function depends on the matrix Q:

- ❖ If Q is positive semidefinite, the function is convex.
- ❖ If Q is negative semidefinite, the function is concave.
- ❖ If Q has both positive and negative eigenvalues, the function is neither strictly convex nor concave.

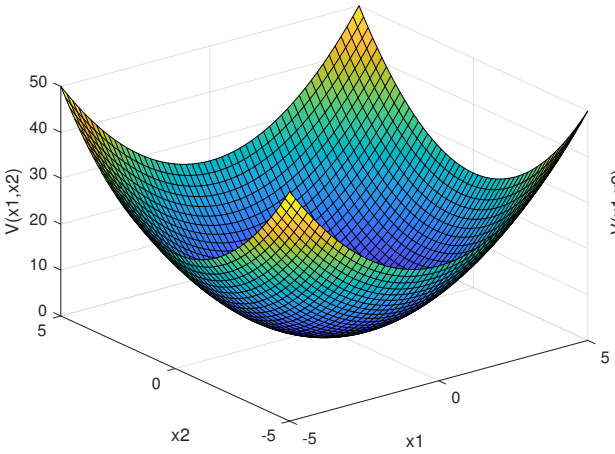

Fig 1.22: Positive definite quadratic function (convex).

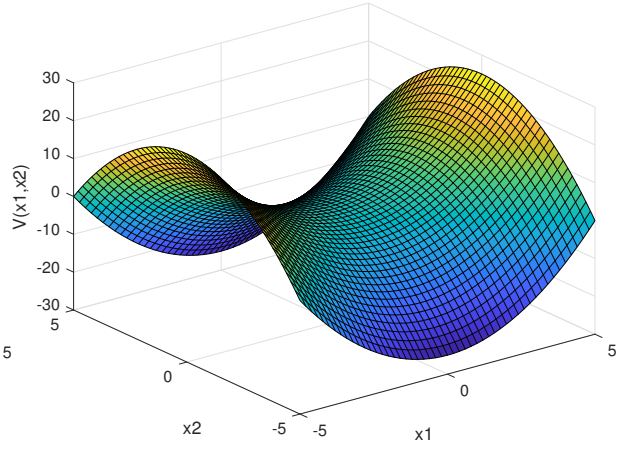

Fig 1.23: Indefinite quadratic function (non-convex).

For a quadratic program to be a convex optimization problem ,the quadratic objective function must be convex (i.e., Q should be positive semidefinite) and the constraints must also define a convex feasible set (linear constraints always define convex sets).

So, while quadratic program is nonlinear due to its quadratic objective function, it can still be convex if the conditions mentioned above are met.

3. **Semi-Definite Program (SDP)**: Semidefinite program is an extension of linear program where the componentwise inequalities between vectors are replaced by matrix inequalities [Bockmayr et al., 2001]. The optimization problem (1.58) is semi-definite program if it has the form:

$$\begin{cases} \text{minimize} & c^T x \\ \text{subject to} & F_0 + x_1 F_1 + x_2 F_2 + \cdots + x_m F_m \leq 0 \\ & x \geq 0 \end{cases} \tag{1.62}$$

Unlike in linear programming, in this context, the notations $F(x) \leq 0$ and $x \geq 0$ denote that the matrix $F(x)$ is negative semi-definite and the matrix x is positive semi-definite, respectively.

Various solvers are capable of addressing these optimization problems, including Mosek, LMILAB, SeDuMi, and SDPT3. To utilize these solvers, the YALMIP [1] toolbox is employed (refer to Appendix A for additional details about this toolbox).

1.8 Stability of Takagi-Sugeno fuzzy systems

In control theory, ensuring the stability of a system is of paramount importance. Stability denotes that, a system return to a steady state or equilibrium after experiencing disturbances, ensuring that it does not display erratic or unbounded behavior regardless of its initial conditions. One prominent method for assessing stability is the Lyapunov theorem. It employs specific functions, known as Lyapunov functions, to evaluate whether a system will remain stable or converge to an equilibrium over time. For T-S fuzzy systems, the Lyapunov method is especially beneficial because it can establish stability conditions as LMIs. Due to their standard convex structure, LMIs can be more easily handled and solved using advanced convex optimization methods. This not only simplifies the stability analysis process but also offers computational efficiency, a significant advantage when analyzing complex non-linear systems.

However, like many techniques in control theory, the LMI-based stability conditions for T-S systems come with their own set of challenges. One significant challenge is their conservative nature. This conservatism can sometimes restrict the design space or provide an excessively cautious representation of the system's actual capabilities. This has the potential to stifle innovation or lead to sub-optimal designs.

Yet, the research community remains proactive and adaptive. In order to bypass the constraints introduced by conservatism, numerous techniques have been investigated. Broadly, these approaches can be categorized into three groups:

1. **Relaxation methods for parameterized linear matrix inequalities:** This category have been discussed before in Section 1.7.3. This methodology employs several mathematical relaxation techniques such as Tuan, Xiaodong and Polya's theorems which yielded significant results. Given its relative simplicity and efficiency, Tuan's theorem is typically preferred over Xiaodong's and Polya's theorems. These latter

[1] The list of available solvers integrated with YALMIP is available at the following link.

tend to complicate the optimization process by increasing the number of LMI, which could be particularly challenging when dealing with higher-order systems.

2. **Membership function-dependent (MFD) stability:** It modifies the stability conditions depending on the specific membership function employed. The MFD stability is often not the preferred choice due to its dependence on the form of each system's membership function. This not only complicates the stability analysis but it also limits its universal applicability across various systems.

3. **Non-quadratic Lyapunov functions:** It including approaches such as Piecewise Lyapunov Functions and Poly-quadratic Lyapunov Functions (PQLF). The Piecewise method is utilized to decrease conservatism by subdividing the system's state space. However, this method is not suitable for systems represented by the sector nonlinearity technique. Alternatively, PQLF assign different decision variables, denoted as P_i, to each subsystem rather than seeking a single unique variable for all, which contributes to a reduction in conservatism.

In the following sections, the stability conditions based on both quadratic and non-quadratic Lyapunov functions are presented.

1.8.1 Stability using quadratic Lyapunov function

Consider the following autonomous unforced system:

$$\dot{x}(t) = \sum_{i=1}^{r} \mu_i(\xi(t)) \left(A_i x(t)\right) \tag{1.63}$$

Theorem 1.1

The system described by (1.63) is asymptotically stable if there exists a symmetric positive definite matrix $P = P^T > 0 \in \mathbb{R}^{n_x \times n_x}$ and the following LMI holds :

$$A_i^T P + P A_i < 0 \quad i = 1, \ldots, r \tag{1.64}$$

Proof. Let's define the quadratic Lyapunov function as follows:

$$V(t) = x(t)^T P x(t) \tag{1.65}$$

The time derivative of $V(t)$ is given by:

$$\dot{V}(t) = \dot{x}(t)^T P x(t) + x(t)^T P \dot{x}(t) \tag{1.66}$$

By substituting (1.63) in (1.66), the following equation is obtained:

$$\dot{V}(t) = \sum_{i=1}^{r} \mu_i(\xi(t)) x(t)^T \left(A_i^T P + P A_i\right) x(t) \tag{1.67}$$

Given that the weighting functions $\mu_i(\xi(t))$ are positive, if the matrices $(A_i^T P + P A_i)$ are negative definite, then $\dot{V}(t)$ will also be negative. Thus, the condition in (1.64) ensures this property. □

Remark 1.4

As stipulated by the condition in (1.64), merely interpolating stable sub-systems does not guarantee their stability. It's imperative to identify and verify a common positive definite matrix P that satisfies the derived stability condition.

Remark 1.5

Employing a quadratic Lyapunov function allows for deriving simple stability conditions expressed as LMIs. Nonetheless, this approach tends to be conservative, especially for larger systems. The difficulty arises when attempting to find a common matrix P that simultaneously satisfies all the r inequalities as presented in (1.64) [Tanaka et al., 1998].

In recent years, to address the issue of conservatism, research has shifted towards more flexible approaches, such as the poly-quadratic Lyapunov function [Tanaka et al., 2003].

1.8.2 Stability using poly-quadratic Lyapunov function

The fuzzy Lyapunov function, also known as poly-quadratic Lyapunov function, is used to reduce the conservatism caused by the quadratic Lyapunov function. It associates a different matrix P_i to each sub-system, which contributes to reducing the conservatism, instead of finding a unique matrix P for all sub-systems as the possibility to find only one decreases when the number of sub-systems is important.

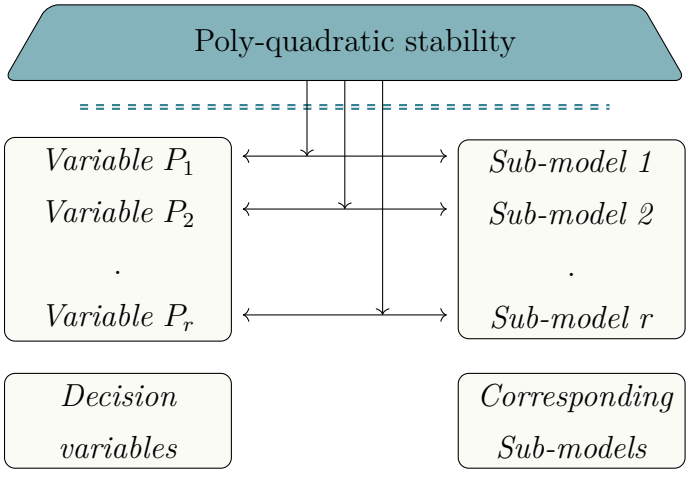

Fig 1.24: Conservatism reduction principal of poly-quadratic Lyapunov function based on non-coupled terms

By adopting the approach proposed by Mozelli et al. in [Mozelli et al., 2009], the time derivative of the membership functions $\mu_k(\xi(t))$ are upper bounds:

$$|\dot{\mu}_k(\xi)| \leq \emptyset_k \tag{1.68}$$

and by defining in prior the value of $\emptyset_k$, then the following theorem provides sufficient conditions described as LMI to ensure the stability of the system (1.63):

Theorem 1.2

The system described by (1.63) is asymptotically stable if there exists symmetric positive definite matrices $P_j \in \mathbb{R}^{n_x \times n_x}$ and a symmetric matrix $P_0 \in \mathbb{R}^{n_x \times n_x}$, such that:

$$P_i \geq P_0, \qquad i = 1, \ldots, r \tag{1.69}$$

$$\mathcal{K}_{ii} < 0, \qquad i = 1, \ldots, r \tag{1.70}$$

$$\frac{1}{r-1}\mathcal{K}_{ii} + \frac{1}{2}(\mathcal{K}_{ij} + \mathcal{K}_{ji}) < 0, \qquad 1 \leq i \neq j \leq r \tag{1.71}$$

where:

$$\mathcal{K}_{ij} = A_i^T P_j + P_j A_i + \sum_{k=1}^{r} \emptyset_k (P_k - P_0) \tag{1.72}$$

Proof. Let us define the poly-quadratic candidate Lyapunov function as follows:

$$V(t) = x(t)^T P_\mu x(t), \tag{1.73}$$

where:

$$P_\mu = \sum_{j=1}^{r} \mu_j(\xi(t)) P_j \tag{1.74}$$

The time derivative of $V(t)$ is given by:

$$\dot{V}(t) = \dot{x}(t)^T P_\mu x(t) + x(t)^T P_\mu \dot{x}(t) + x(t)^T \dot{P}_\mu x(t) \tag{1.75}$$

Upon substituting (1.63) and (1.74) into (1.75), the subsequent expression is derived:

$$\dot{V}(t) = \sum_{i=1}^{r}\sum_{j=1}^{r} \mu_i(\xi(t))\mu_j(\xi(t)) x(t)^T \left(A_i{}^T P_j + P_j A_i + \dot{P}_\mu\right) x(t) \tag{1.76}$$

From this expression, the value of employing the poly-quadratic Lyapunov function becomes evident. The presence of symmetric parameters in equation (1.76) suggests that it offers an avenue to relax the stability conditions, particularly by leveraging one of the relaxation techniques delineated in Section 1.7.3.

However, before opting for any of the double summation relaxation techniques, we will first implement another method aimed at reducing conservatism. The negativity of (1.76) can be assured if the subsequent matrix inequalities hold true:

$$A_i{}^T P_j + P_j A_i + \dot{P}_\mu < 0 \tag{1.77}$$

To mitigate the conservatism associated with the time derivatives of the membership functions, Mozelli et al. introduced a novel relaxation technique, as discussed in [Mozelli et al., 2009]. This method represents an improvement of the one initially proposed by Tanaka et al. in [Tanaka et al., 2001]. This technique is centered around the introduction of a symmetric matrix $P_0 \in \mathbb{R}^{n_x \times n_x}$, employing the convex sum property (1.9) as follows:

$$\sum_{k=1}^{r} \dot{\mu}_k(\xi) = 0 \Rightarrow \sum_{k=1}^{r} \dot{\mu}_k(\xi) = \sum_{k=1}^{r} \dot{\mu}_k(\xi) P_0 \tag{1.78}$$

Hence, we obtain:

$$\sum_{k=1}^{r} \dot{\mu}_k(\xi)\, x^T P_k x = \sum_{k=1}^{r} \dot{\mu}_k(\xi)\, x^T (P_k - P_0)\, x, \tag{1.79}$$

where the terms $(P_k - P_0)$ have to be minimized.

The derivatives with respect to time for the membership functions are assumed bounded:

$$\sum_{k=1}^{r} \dot{\mu}_k(\xi)\,(P_k - P_0) \leq \sum_{k=1}^{r} |\dot{\mu}_k(\xi)|\,(P_k - P_0) = \sum_{k=1}^{r} \emptyset_k\,(P_k - P_0) \tag{1.80}$$

such that the matrix P_0 has to verify $P_k - P_0 \geq 0$.

Then, the inequality (1.77) becomes:

$$K_{ij} = A_i^T P_j + P_j A_i + \sum_{k=1}^{r} \emptyset_k\,(P_k - P_0) < 0 \tag{1.81}$$

Now, to harness the advantages of the poly-quadratic Lyapunov function, we can employ one of the relaxation methods detailed in Section 1.7.3. As previously mentioned, we will adopt Lemma 1.5. This leads us to the stability conditions outlined in Theorem 1.2. □

The idea of associating a different matrix P_i to each LMI becomes evident in the stability condition (1.70). This equation corresponds to the non-coupled terms, where each matrix P_i is associated to different LMI. Consequently, the conservatism is reduced in comparison to the case where identifying a single matrix P satisfying all LMIs proves unattainable. The stability condition (1.71) addresses the coupled terms, and a discussion on these terms is provided in Section 1.7.3.

1.9 Conclusion

In this chapter, we explored the principles underlying multi-model representation, underscoring the vital role that these mathematical models play in capturing system dynamics, all the way leveraging their inherent simplicity. The Takagi-Sugeno fuzzy systems, in particular, took center stage in our discussion. As we delved deeper, various construction methods for designing these systems were introduced. Notably, the sector nonlinearity approach stood out as the preferred choice due to its ability to offer an accurate representation of the original nonlinear system. As we moved forward, through an in-depth exploration of convex analysis and matrix inequalities, we established the foundational comncepts essential for grasping the design and stability intricacies of these systems. The chapter concluded with a focus on the stability analysis of T-S systems, spotlighting the importance of quadratic and poly-quadratic Lyapunov functions.

Chapter 2

Introduction to the state estimation of Takagi-Sugeno fuzzy systems

2.1 Introduction

In the realm of control systems and diagnostics, knowledge of a system's state variables is paramount. These variables embody all the necessary information needed to navigate and predict the system's trajectory. With an accurate read on the system's states, engineers and technicians can expertly navigate its functionality, optimizing its operation, and preemptively addressing issues before they escalate into serious malfunctions. It's a proactive approach, analogous to charting a course with a detailed map; without such guidance, the path to maintaining efficiency and reliability is obscured.

However, the real-world application of state measurement is fraught with practical challenges. In many instances, it is difficult or outright impossible to measure all the system's states directly due to limitations in sensor technology or the system's complexity. Furthermore, even when technically possible, economic factors weigh heavily in this arena; the high cost of state sensor equipment can render comprehensive direct state measurement inefficient and cost-prohibitive. Consequently, this leaves system operators searching for alternative methods to glean the necessary information. It is here where we encounter the necessity for innovation in system state estimation.

It is within this context of constraint and necessity that the concept of the observer comes to the fore. The observer fulfills a critical function by enabling state estimation where direct measurement is unfeasible. The observer is an auxiliary dynamical system conceived to deduce the internal states of a system by integrating the system's inputs and the available measurements in the output with a dynamic model of the system, utilizing computational techniques to estimate those states that are not directly measurable. This methodological approach not only enhances the feasibility of state monitoring in complex systems but also optimizes resource allocation by reducing the dependence on extensive sensor networks. Observers, thus, provide a practical and efficient means to achieve comprehensive system state awareness, ensuring control and diagnostic processes remain robust and reliable.

The historical development of observers has been a journey of continuous innovation that goes back to the groundbreaking works of Kalman and Luenberger in their seminal papers [Kalman, 1960] and [Luenberger, 1971]. Rudolf Kalman published his famous paper where he presented a filter, particularly effective for systems with stochastic disturbances or noise. It provided a recursive solution to the discrete-data linear filtering problem, allowing for real-time state estimation in noisy environments, which was a significant advancement for both control and diagnostic applications. Following the development of the Kalman filter, the Luenberger observer emerged as another significant development

in the field of state estimation. The central concept of the Luenberger observer is its ability to estimate system states based on accurately modeling the system's dynamics. In this observer, the choice of observer gain is critical, as it is fine-tuned to match the specific dynamics of the system, ensuring that the state estimates converge effectively and reliably. This approach employs a deterministic framework for its gain calculation, contrasting with the Kalman filter.

These seminal works were designed for linear systems; however, real-world systems often exhibit nonlinear behaviors, which poses a substantial challenge to the linear assumption. To address this issue, extended observers such as the extended Luenberger observer and the extended Kalman filter have emerged. These were developed based on the linearization method around an operational point, allowing them to handle mild nonlinearities. This approach enables the principles of the Kalman filter and the Luenberger observer to be applied to a broader class of systems. Despite their widespread use, these methods can struggle with highly nonlinear dynamics or systems that are not well-suited for linearization. In response to these limitations, several alternative methods have been developed. The high-gain observer has emerged as an effective solution for state estimation in nonlinear systems that adhere to global Lipschitz condition [Orjuela, 2008]. It guarantees exponential convergence thanks to the tuning of a single parameter, which must be sufficiently large [Zemouche, 2017]. This gain increases in accordance to the increase in the Lipschitz constant. However, it is well-known in observer theory that a trade-off exists between the speed of state reconstruction and immunity to measurement noise. Consequently, the high-gain observer is sensitive to output measurement noises [Ahrens and Khalil, 2009, Khalil and Praly, 2014]. The sliding mode observer represents another innovative approach, distinguished by its ability to estimate states in systems characterized by pronounced nonlinearities and uncertainties. Unlike sliding mode control, this observer utilizes a similar principle of sliding mode but specifically for state estimation. It involves constructing a sliding surface in the state space and employing a discontinuous algorithm to drive the estimation errors to reach and remain on this surface. Once the errors are confined to the sliding surface, they converge to zero, enabling accurate state estimation. This robust mechanism renders the sliding mode observer highly effective in dynamic environments laden with significant uncertainties and external disturbances. It provides reliable state estimation even in scenarios where conventional linear observers prove inadequate [Yan and Utkin, 2002, Wu et al., 2008]. However, it's important to note that while sliding mode observers are robust, they can also induce chattering effects due to their discontinuous control action. This chattering can sometimes be undesirable in practical applications. Therefore, while sliding mode observers are highly

effective for systems with pronounced nonlinearities and uncertainties, their implementation should be carefully considered in the context of the specific system and application requirements.

Subsequently, the field has expanded to incorporate more sophisticated observers like the T-S fuzzy observers, which offer robustness and adaptability by handling nonlinear systems. These modern observers leverage fuzzy logic to extend the Luenberger observer for nonlinear systems without losing informations unlike those who are based on linearization. For instance, Yang et at [Yang et al., 2019] designed a Lipschitz-observer to estimate the states of a four-wheeled omni-directional mobile robot in the presence of disturbances affecting the system. The challenge of uncertain systems has also been addressed, with authors in [Nacer et al., 2021] developing a robust observer design for induction motors. Observers dealing with unknown inputs have been extensively studied, as demonstrated in [Boukhlouf et al., 2023], where a proportional integral observer is applied for the observation of synchronous reluctance motor states. The domain of fault detection has also seen the practical application of observers. For example, their usage in a three-tank hydraulic system is detailed in [Yan et al., 2021]. In the field of detection and mitigation of cyber-attacks, the unknown input observers have provided significant results [Pan et al., 2023]. The T-S fuzzy observers can accommodate as well with other techniques as the sliding mode approach (see, e.g., [Akhenak, 2004, Amel, 2020]). These diverse applications highlight the crucial role T-S observers play in enhancing state estimation of nonlinear systems. They offer precise results and straightforward stability conditions, which are described as LMIs and solvable using convex optimization solvers.

In the realm of T-S observers, systems can be broadly classified into two categories based on the variables involved in their weighting functions: Measurable Premise Variables (MPV) and Unmeasurable Premise Variables (UPV). The latter category represents a larger class of systems, and hence, has led to increased scientific research interest. However, designing observers for systems featuring UPV proves more challenging than for systems with measurable variables. Hence, this chapter aims to provide an introduction to observer design for T-S systems. It begins by discussing criterion for observability in T-S systems and then delves into the distinctions between MPV and UPV systems. The primary focus of this chapter is on the MPV case, detailing how to design an observer for these systems using quadratic Lyapunov functions and enhancing observer performance through pole placement methods. The subsequent chapter will explore observer design for UPV systems.

2.2 Notations on observers and observability

2.2.1 Definitions

In the realm of control theory and systems engineering, a fundamental question is whether it's possible to accurately reconstruct the internal states of the system or not. This capability is encapsulated in the concept of a system's "observability". The formal definitions of observability is given as follows:

Definition 2.1. *(Observability) [Yves and Granjon, 2001] A system is said to be observable at time t_0, if knowledge of the input signal $u(t)$ and the output signal $y(t)$ over a time interval $[t_0, t_1]$ makes it possible to calculate the state of the system at time t_0 ($x(t_0)$). If a system is observable at any time t_0, it is said to be completely observable.*

The reconstruction of a system's states can be achieved through the use of an observer. The formal definition of an observer is as follows:

Definition 2.2. *(Observer) [Fossard and Normand-Cyrot, 1993] we call an observer of a dynamic system:*

$$\mathcal{S} : \begin{cases} \dot{x}(t) = f(x(t), u(t)) \\ y(t) = h(x(t)) \end{cases} \tag{2.1}$$

an auxiliary dynamic system $\mathcal{O}$ whose inputs are constituted of the input vectors and the output of the system to be observed and whose output vector $\hat{x}(t)$ is the estimated state:

$$\mathcal{O} : \begin{cases} \dot{z}(t) = \hat{f}(z(t), u(t), y(t)) \\ \hat{x}(t) = \hat{h}(z(t), u(t), y(t)) \end{cases} \tag{2.2}$$

such that the error between the state vector $x(t)$ and $\hat{x}(t)$ asymptotically tends towards zero.

$$\|e(t)\| = \|x(t) - \hat{x}(t)\| \to 0 \quad when \quad t \to \infty. \tag{2.3}$$

The diagram of such an observer is given in Figure 2.1:

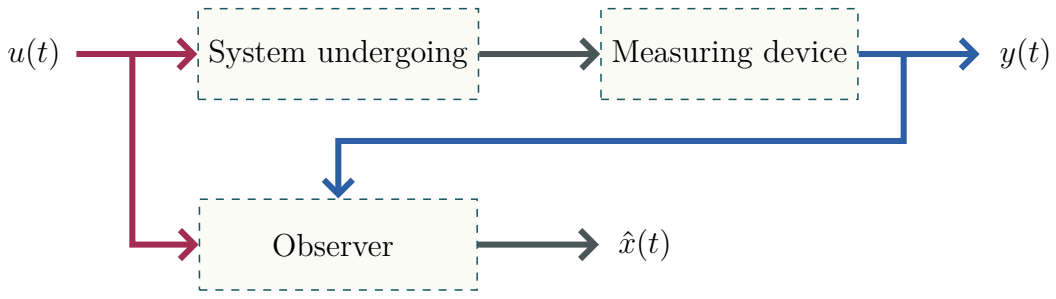

Fig 2.1: Observer structure.

However, observability can be a restrictive condition for designing an observer. In cases where the system is not fully observable, meaning there are unobservable states, a less restrictive and more practical condition for designing an observer, known as detectability, can be introduced. Detectability allows for the design of observers in systems where not all states are observable, offering a feasible solution when full observability is not possible [Zhou et al., 2022, Tanwani and Trenn, 2019, Schaum, 2018, Długosz and Baranowski, 2020]. The concept of detectability can be defined as follows:

Definition 2.3. *(Detectability) [Naidu, 2002] A system is said to be detectable if its unobservable states are stable. Its observable states may be stable or unstable.*

Given that the unobservable states of a detectable system are stable, they will naturally converge to the equilibrium point. This characteristic allows for the construction of an auxiliary system (observer) whose unobservable states are designed to converge to the same equilibrium point as those of the original system. Consequently, the estimation error in the observer system will asymptotically converge towards zero. This highlights the practicality of detectability as a criterion in observer design, especially in complex systems where full observability is not attainable.

In the following sections, we will discuss both the observer structure and the observability criterion for Takagi-Sugeno fuzzy systems.

2.2.2 Observer structure for Takagi-Sugeno fuzzy systems

Let us consider the T-S multi-model given as follows:

$$\begin{cases} \dot{x}(t) = \sum_{i=1}^{r} \mu_i(\xi(t)) \left(A_i x(t) + B_i u(t)\right) \\ y(t) = \sum_{i=1}^{r} \mu_i(\xi(t)) \left(C_i x(t) + D_i u(t)\right) \end{cases} \tag{2.4}$$

Here, $x(t) \in \mathbb{R}^{n_x}$ represent the state vector, $u(t) \in \mathbb{R}^{n_u}$ represent the input vector and $y(t) \in \mathbb{R}^{n_y}$ represent the output vector. The known matrices are represented by $A_i \in \mathbb{R}^{n_x \times n_x}, B_i \in \mathbb{R}^{n_x \times n_u}, D_i \in \mathbb{R}^{n_y \times n_u}$ and $C_i \in \mathbb{R}^{n_y \times n_x}$. Lastly, $\xi(t)$ represent the premise variables and $\mu_i\left(\xi\left(t\right)\right)$ are the weighting functions that verify the convex sum property:

$$\sum_{i=1}^{r} \mu_i(\xi(t)) = 1, \quad 0 \leq \mu_i(\xi(t)) \leq 1, \quad \forall i = 1, \ldots r. \tag{2.5}$$

The observer structure used for the fuzzy system (2.4) in literature is given by:

$$\begin{cases} \dot{\hat{x}}(t) = \sum_{i=1}^{r} \mu_i(\hat{\xi}(t)) \left(A_i \hat{x}(t) + B_i u(t) + \ L_i(y(t) - \hat{y}(t))\right) \\ \hat{y}(t) = \sum_{i=1}^{r} \mu_i(\hat{\xi}(t)) \left(C_i \hat{x}(t) + D_i u(t)\right) \end{cases} \tag{2.6}$$

where the hat $\hat{}$ corresponds to the estimated variable, and L_i are the observer gains.

The diagram of this observer is given in the following figure:

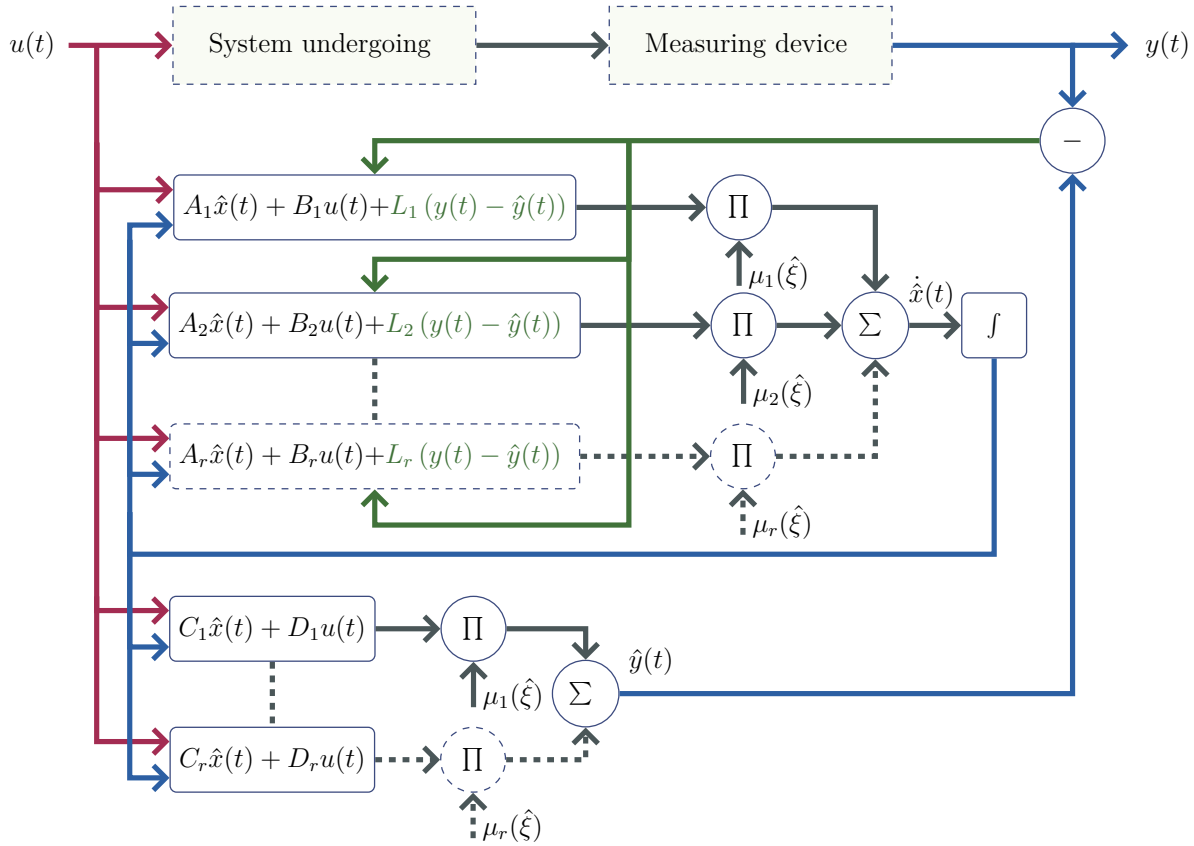

Fig 2.2: Takagi-Sugeno observer structure

It is important to highlight that this observer operates as a T-S fuzzy system. Essentially, it represents an extension of the traditional Luenberger observer, adapted for application in fuzzy systems. This adaptation involves each sub-model of the fuzzy system being associated with a distinct observer gain, denoted as L_i.

Prior to deriving the observer gains, it's essential to verify the system's observability, adhering to the definition of observability discussed earlier. Therefore, the subsequent section will detail the specific criterion used for testing the observability of Takagi-Sugeno fuzzy systems.

2.2.3 Criterion for Observability in Takagi-Sugeno Fuzzy Systems

Considering the nonlinear nature of T-S systems, one might initially consider applying nonlinear observability criteria directly. However, the specific design of their observers, as indicated in (2.6) and characterized by each rule having a local gain, shifts the focus to ensuring the observability or detectability of the individual local models rather than

the whole nonlinear system. It is important to emphasize that this criteria is neither sufficient nor necessary for the overall system's observability or detectability. However, in the context of T-S systems, considering their specific observer structure, this requirement become sufficient and necessary. For the design, it is implicitly assumed that the local models are observable [Lendek et al., 2011].

Theorem 2.1

The T-S system defined in (2.4) is observable if and only if each pair (A_i, C_i) is observable $\forall i = 1, \dots r$. This condition holds true if and only if the observability matrix for each pair (A_i, C_i) has full rank:

$$\text{rank}\left(\mathcal{O}_{bs}\right) = \text{rank}\begin{pmatrix} C_i \\ C_iA_i \\ \vdots \\ C_iA_i^{n-1} \end{pmatrix} = n, \quad \forall i = 1, \dots, r \tag{2.7}$$

Proof. [Amel, 2020] By utilizing the convex sum property (2.5) to $x(t)$, the following result is obtained :

$$\sum_{i=1}^{r} \mu_i(\xi(t))x(t) = x(t) \tag{2.8}$$

By defining $\mu_i(\xi(t))x(t) = x_i(t)$, the equation in (2.8) can be reformulated as follows:

$$\sum_{i=1}^{r} x_i(t) = x(t) \tag{2.9}$$

Each individual sub-model within the rules of the T-S multi-model is given as follows:

$$\begin{cases} \dot{x}(t) = A_ix(t) + B_iu(t), \\ y(t) = C_ix(t) + D_iu(t), \end{cases} \tag{2.10}$$

By executing a series of successive derivations, starting with y and utilizing the state equation, the following system is derived:

$$\begin{cases} C_ix(t) = y(t) - D_iu(t) = \bar{y}_0(t) \\ C_iA_ix(t) = \bar{y}_1(t) = \dot{\bar{y}}_0(t) - C_iB_iu(t) \\ C_iA_i^2x(t) = \bar{y}_2(t) = \dot{\bar{y}}_1(t) - C_iA_iB_iu(t) \\ \vdots \\ C_iA_i^{n-1}x(t) = \bar{y}_{n-1}(t) = \dot{\bar{y}}_{n-2}(t) - C_iA_i^{n-2}B_iu(t) \end{cases} \tag{2.11}$$

The system described in (2.11) can be represented in matrix form as follows:

$$\begin{pmatrix} C_i \\ C_iA_i \\ C_iA_i^2 \\ \vdots \\ C_iA_i^{n-1} \end{pmatrix} x(t) = \begin{pmatrix} \bar{y}_0(t) \\ \dot{\bar{y}}_0(t) - C_iB_iu(t) \\ \dot{\bar{y}}_1(t) - C_iA_iB_iu(t) \\ \vdots \\ \dot{\bar{y}}_{n-2}(t) - C_iA_i^{n-2}B_iu(t) \end{pmatrix} \tag{2.12}$$

By multiplying both sides of the system (2.12) by $\mu_i(\xi(t))$, this system can be reformulated as follows:

$$\begin{pmatrix} C_i \\ C_iA_i \\ C_iA_i^2 \\ \vdots \\ C_iA_i^{n-1} \end{pmatrix} x_i(t) = \mu_i(\xi(t)) \begin{pmatrix} y(t) - D_iu(t) \\ \dot{y}(t) - D_i\dot{u}(t) - C_iB_iu(t) \\ \dot{\bar{y}}_1(t) - C_iA_iB_iu(t) \\ \vdots \\ \dot{\bar{y}}_{n-2}(t) - C_iA_i^{n-2}B_iu(t) \end{pmatrix} \tag{2.13}$$

Assuming $\mu_i(\xi(t)) \neq 0$, the system (2.13) becomes:

$$\frac{1}{\mu_i(\xi(t))} \begin{pmatrix} C_i \\ C_iA_i \\ C_iA_i^2 \\ \vdots \\ C_iA_i^{n-1} \end{pmatrix} x_i(t) = \begin{pmatrix} y(t) - D_iu(t) \\ \dot{y}(t) - D_i\dot{u}(t) - C_iB_iu(t) \\ \dot{\bar{y}}_1(t) - C_iA_iB_iu(t) \\ \vdots \\ \dot{\bar{y}}_{n-2}(t) - C_iA_i^{n-2}B_iu(t) \end{pmatrix} \tag{2.14}$$

where a weight $\mu_i(\xi(t)) = 0$ corresponds to a null contribution from the i^{th} local model in the state of the global model.

Let us define:

$$P = \frac{1}{\mu_i(\xi)} \underbrace{\begin{pmatrix} C_i \\ C_iA_i \\ \vdots \\ C_iA_i^{n-1} \end{pmatrix}}_{\mathcal{O}_{bs}} \tag{2.15}$$

Using the following rank invariance property: Multiplying a row by a non-zero scalar preserves the rank of the matrix, we get $\text{rank}\,(\mathcal{O}_{bs}) = \text{rank}(P)$. Thus, if the observability matrix has a full rank, i.e. $\text{rank}\,(\mathcal{O}_{bs}) = n$, the system (2.14) admits a unique solution $x_i(t)$, with the variables $y(t)$ and $u(t)$ known. Thus, the observability of the pair (A_i, C_i) is necessary and sufficient to ensure the observability of the corresponding sub-model (2.10).

So, if the pairs $(A_i, C_i)\,, i = 1, \ldots, r$, are observable, the sub-models (2.10) $i = 1, \ldots, r$, are observable and, consequently, the states $x_i(t), i = 1, \ldots, r$, can be reconstructed as well as the state $x(t)$ of the global system according to (2.9). □

After elucidating the observability criterion of T-S systems, it becomes pertinent to elucidate its interplay with the concept of detectability.

Remark 2.1

In light of the definitions of observability and detectability, along with the inherently linear nature of each sub-model within T-S systems, the following can be concluded:

- If A_i is stable $\Longrightarrow$ (A_i, C_i) is detectable.
- If (A_i, C_i) is observable $\Longrightarrow$ (A_i, C_i) is detectable as well.
- If (A_i, C_i) is not observable $\Longrightarrow$ (A_i, C_i) could still be detectable.

With these insights, the criterion for designing an observer for T-S systems can be formally stated:

Theorem 2.2

An observer for a T-S system exists if all pairs (A_i, C_i) within the system are detectable.

2.3 Observer design for Takagi-Sugeno fuzzy systems

Following the design of the T-S system and the verification of observability for all pairs (A_i, C_i) (or at least its detectability), the subsequent step involves determining the observer gains L_i in order to implement the observer and estimating the system's states.

Consider the observer (2.6) designed for the T-S system (2.4). In order to determine the values of the observer gains, the second Lyapunov theorem is applied to the state estimation error, which is presented as follows:

$$e(t) = x\,(t) - \hat{x}\,(t) \tag{2.16}$$

At first let us rewrite the dynamic state of the system (2.4) as a perturbated system with the following representation:

$$\begin{cases} \dot{x}(t) = \sum_{i=1}^{r} \mu_i(\hat{\xi}(t))\,(A_i x(t) + B_i u(t) + \omega_1(t)) \\ y(t) = \sum_{i=1}^{r} \mu_i(\hat{\xi}(t))\,(C_i x(t) + D_i u(t) + \omega_2(t)) \end{cases} \tag{2.17}$$

here, the perturbation term $\omega_i\,(t)$ is referred to as the "mismatching term" due to its

composition of two mismatched functions.

$$\begin{cases} \omega_1(t) = \sum_{i=1}^{r} \left(\mu_i(\xi(t)) - \mu_i\left(\hat{\xi}(t)\right)\right)(A_i x(t) + B_i u(t)) \\ \omega_2(t) = \sum_{i=1}^{r} \left(\mu_i(\xi(t)) - \mu_i\left(\hat{\xi}(t)\right)\right)(C_i x(t) + D_i u(t)) \end{cases} \tag{2.18}$$

The purpose of formulating the dynamic state of the system (2.4) as a perturbated system (2.17) is to obtain the same weighting functions as those of the observer (2.6) in order to simplify the expression of the error dynamic.

The representation of the estimation error dynamics is now given by:

$$\dot{e}(t) = \dot{x}(t) - \dot{\hat{x}}(t) = \sum_{i=1}^{r}\sum_{j=1}^{r} \mu_i(\hat{\xi}(t))\mu_j(\hat{\xi}(t))\left[(A_i - L_i C_j)e(t) + \omega_1(t) - L_i\omega_2(t)\right] \tag{2.19}$$

Based on the premise variables of the weighting functions, two cases can be distinguished:

- ❖ Measurable premise variables.
- ❖ Unmeasurable premise variables.

2.3.1 Measurable premise variables

The MPV corresponds to the case where the premise variable are measured (known). Consequently, the weighting functions utilized in the observer implementation are derived from the measurements obtained from the system:

$$\mu_i\left(\hat{\xi}(t)\right) = \mu_i(\xi(t)) \tag{2.20}$$

In this scenario, the mismatching terms are null, leading to:

$$\omega_1(t) = \omega_2(t) = 0 \tag{2.21}$$

Therefore, the dynamics of the estimation error can be simplified as follows:

$$\dot{e}(t) = \dot{x}(t) - \dot{\hat{x}}(t) = \sum_{i=1}^{r}\sum_{j=1}^{r} \mu_i(\hat{\xi}(t))\mu_j(\hat{\xi}(t))\left[(A_i - L_i C_j)e(t)\right] \tag{2.22}$$

2.3.1.1 Observer design using quadratic Lyapunov function

In the case of MPV, the stability analysis of the estimation error dynamics is conducted straightforwardly by employing the quadratic Lyapunov function. The stability conditions are expressed as LMI in the following theorem [Tanaka and Wang, 2004]:

Theorem 2.3

The estimation error converges asymptotically towards zero if there exist matrices $P = P^T \in \mathbb{R}^{n_x \times n_x} > 0$ and $M_i \in \mathbb{R}^{n_x \times n_y}$ such that the following LMIs hold $\forall i, j = 1, ..., r$:

$$(PA_i - M_iC_i)^T + (PA_i - M_iC_i) < 0, \quad i = 1, \ldots, r \tag{2.23}$$

$$(PA_i - M_iC_j + A_j - M_jC_i)^T + (PA_i - M_iC_j + PA_j - M_jC_i) < 0, \quad i < j \tag{2.24}$$

where the observer gains are given by $L_i = P^{-1}M_i$.

Proof. Let us define the quadratic Lyapunov function as follows:

$$V(t) = e(t)^T P e(t) \tag{2.25}$$

The time derivative of $V(t)$ is:

$$\dot{V}(t) = \dot{e}(t)^T P e(t) + e(t)^T P \dot{e}(t) \tag{2.26}$$

By substituting (2.22) in (2.26), the following equation is obtained:

$$\dot{V}(t) = \sum_{i=1}^{r}\sum_{j=1}^{r} \mu_i(\hat{\xi}(t))\mu_j(\hat{\xi}(t)) e(t)^T \left[(PA_i - PL_iC_j)^T + (PA_i - PL_iC_j)\right] e(t) \tag{2.27}$$

Since the equation (2.27) involves two symmetric parameters, μ_i and μ_j, its negativity can be determined by applying the relaxation method described in Lemma 1.4 as follows:

$$(PA_i - PL_iC_i)^T + (PA_i - PL_iC_i) < 0, \quad i = 1, \ldots, r \tag{2.28}$$

$$(PA_i - PL_iC_j + PA_j - PL_jC_i)^T + (PA_i - PL_iC_j + PA_j - PL_jC_i) < 0, \quad i < j \tag{2.29}$$

These inequalities involve the product of two decision variables, P and L_i. Consequently, they are not considered as LMI; instead, they fall under the category of Bilinear Matrix Inequalities (BMIs). In optimization problems, BMIs present challenges due to their lack of convexity, making them unsuitable for straightforward resolution using traditional convex optimization solvers discussed in Chapter 1. To address this, a method is employed to convert these bilinear inequalities into linear ones. The selected approach for this transformation is the "change of variable method".

Let us define the following change of variables:

$$M_i = PL_i \tag{2.30}$$

By substituting the change of variable from (2.30) into (2.28) and (2.29), we arrive at Theorem 2.3. □

Example 2: Observer design of three phase interleaved boost converter in the case of MPV using quadratic Lyapunov function

1 - Modeling of the interleaved boost converter

Figure 2.3 presents the design of a three-phase interleaved boost converter (3P-IBC) setup. This assembly comprises three conventional boost converters, all linked in parallel to a shared DC-bus. Here, V_{in} signifies the input voltage of the converter, and V_{out} denotes the output voltage. Main switches are represented as S_1, S_2, and S_3. The diodes are referred as D_1, D_2 and D_3 whereas L_1, L_2, and L_3 stand for the inductors. The capacitor in this configuration is denoted as C_{ap} and R symbolizes the DC-load.

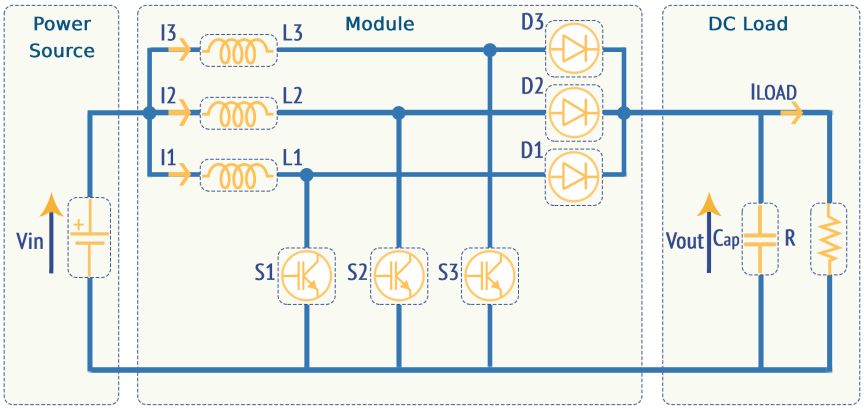

Fig 2.3: Three-phase interleaved boost converter

The mathematical model of this converter is giving as follows, where the load current $I_{Load}(t)$ is considered as a known input affecting the state dynamics (later in Section 4.3.1.2 we will use this example where the load current will be considered as unknown input):

$$\begin{cases} L_1 \frac{dI_{L_1}(t)}{dt} &= V_{in} - (1 - S_1) D_1 V_{out} - r_{L_1} I_{L_1} \\ L_2 \frac{dI_{L_2}(t)}{dt} &= V_{in} - (1 - S_2) D_2 V_{out} - r_{L_2} I_{L_2} \\ L_3 \frac{dI_{L_3}(t)}{dt} &= V_{in} - (1 - S_3) D_3 V_{out} - r_{L_3} I_{L_3} \\ C_{ap} \frac{dV_{out}(t)}{dt} &= (1 - S_1) D_1 I_{L_1} + (1 - S_2) D_2 I_{L_2} + (1 - S_3) D_3 I_{L_3} - I_{Load} \end{cases} \tag{2.31}$$

where D_i represent the behavior of the diode, allowing the flow of positive current while preventing the negative one:

$$D_i = \begin{cases} 1 \text{ if } I_i \geq 0 \\ 0 \text{ if } I_i < 0 \end{cases} \tag{2.32}$$

By defining $x(t) = \begin{bmatrix} I_1 & I_2 & I_3 & V_{out} \end{bmatrix}^T$, $u(t) = \begin{bmatrix} S_1 & S_2 & S_3 & V_{in} \end{bmatrix}^T$ the state space representation of the 3P-IBC is presented as follows:

$$\begin{cases} \dot{x}(t) = A(u)\,x(t) + Bu(t) + EI_{Load}(t) \\ y(t) = Cx(t) \end{cases} \tag{2.33}$$

where:

$$A(u) = \begin{bmatrix} -\frac{r_{L1}}{L_1} & 0 & 0 & -\frac{(1-S_1)}{L_1} \\ 0 & -\frac{r_{L2}}{L_2} & 0 & -\frac{(1-S_2)}{L_2} \\ 0 & 0 & -\frac{r_{L3}}{L_3} & -\frac{(1-S_3)}{L_3} \\ \frac{1-S_1}{C_{ap}} & \frac{1-S_2}{C_{ap}} & \frac{1-S_3}{C_{ap}} & 0 \end{bmatrix}, B = \begin{bmatrix} 0 & 0 & 0 & \frac{1}{L_1} \\ 0 & 0 & 0 & \frac{1}{L_2} \\ 0 & 0 & 0 & \frac{1}{L_3} \\ 0 & 0 & 0 & 0 \end{bmatrix}, \; E = \begin{bmatrix} 0 \\ 0 \\ 0 \\ -\frac{1}{C_{ap}} \end{bmatrix},$$

$$C = \begin{bmatrix} 0 & 0 & 0 & 1 \end{bmatrix}$$

The parameters of this system are : $L_i = 0.0011$ $[H]$, $r_{Li} = 0.0071$ $[\Omega]$ and $C_{ap} = 484$ $[\mu F]$.

2 - Takagi-Sugeno fuzzy representation of the system

The T-S multi-model is given as follows:

$$\begin{cases} \dot{x}(t) = \sum_{i=1}^{r} \mu_i(\xi(t)) \left(A_i x(t) + B_i u(t) + E_i I_{Load}(t)\right) \\ y(t) = \sum_{i=1}^{r} \mu_i(\xi(t)) \left(C_i x(t)\right) \end{cases} \tag{2.34}$$

By defining the premise variables as $\xi_1 = (1 - S_1)D_1$, $\xi_2 = (1 - S_2)D_2$ and $\xi_3 = (1-S_3)D_3$ as the nonlinear terms in the dynamical model of the 3P-IBC in (2.33), which are measurable, the weighting functions can be described as follows:

$$\mu_i(\xi(t)) = \prod_{j=1}^{3} M_{ij}(\xi_j), \tag{2.35}$$

where the membership functions of the fuzzy rules are:

$$\begin{aligned}
&\textbf{Rule1}\text{: } M_{11} = W_1(\xi_1), \quad M_{12} = W_1(\xi_2), \quad M_{13} = W_1(\xi_3) \\
&\textbf{Rule2}\text{: } M_{21} = W_1(\xi_1), \quad M_{22} = W_1(\xi_2), \quad M_{23} = W_2(\xi_3) \\
&\textbf{Rule3}\text{: } M_{31} = W_1(\xi_1), \quad M_{32} = W_2(\xi_2), \quad M_{33} = W_1(\xi_3) \\
&\textbf{Rule4}\text{: } M_{41} = W_1(\xi_1), \quad M_{42} = W_2(\xi_2), \quad M_{43} = W_2(\xi_3) \\
&\textbf{Rule5}\text{: } M_{51} = W_2(\xi_1), \quad M_{52} = W_1(\xi_2), \quad M_{53} = W_1(\xi_3) \\
&\textbf{Rule6}\text{: } M_{61} = W_2(\xi_1), \quad M_{62} = W_1(\xi_2), \quad M_{63} = W_2(\xi_3) \\
&\textbf{Rule7}\text{: } M_{71} = W_2(\xi_1), \quad M_{72} = W_2(\xi_2), \quad M_{73} = W_1(\xi_3) \\
&\textbf{Rule8}\text{: } M_{81} = W_2(\xi_1), \quad M_{82} = W_2(\xi_2), \quad M_{83} = W_2(\xi_3)
\end{aligned}$$

And using the sector nonlinearity approach the following functions are obtained:

$$W_1(\xi_i) = \frac{\xi_i - \xi_{imin}}{\xi_{imax} - \xi_{imin}}, W_2(\xi_i) = \frac{\xi_{imax} - \xi_i}{\xi_{imax} - \xi_{imin}}$$

By defining the limits of the premise variables as follows: $\xi_1 \in \begin{bmatrix}0 & 1\end{bmatrix}, \xi_2 \in \begin{bmatrix}0 & 1\end{bmatrix}$ and $\xi_3 \in \begin{bmatrix}0 & 1\end{bmatrix}$. Hence, the sub-matrices A_i, B_i, C_i and E_i of the multi-model (2.34) can be given as follows:

$$A_1 = \begin{bmatrix} -\frac{r_{L1}}{L_1} & 0 & 0 & -\frac{\xi_{1max}}{L_1} \\ 0 & -\frac{r_{L2}}{L_2} & 0 & -\frac{\xi_{2max}}{L_2} \\ 0 & 0 & -\frac{r_{L3}}{L_3} & -\frac{\xi_{3max}}{L_3} \\ \frac{\xi_{1max}}{C_{ap}} & \frac{\xi_{2max}}{C_{ap}} & \frac{\xi_{3max}}{C_{ap}} & 0 \end{bmatrix}, A_2 = \begin{bmatrix} -\frac{r_{L1}}{L_1} & 0 & 0 & -\frac{\xi_{1max}}{L_1} \\ 0 & -\frac{r_{L2}}{L_2} & 0 & -\frac{\xi_{2max}}{L_2} \\ 0 & 0 & -\frac{r_{L3}}{L_3} & -\frac{\xi_{3min}}{L_3} \\ \frac{\xi_{1max}}{C_{ap}} & \frac{\xi_{2max}}{C_{ap}} & \frac{\xi_{3min}}{C_{ap}} & 0 \end{bmatrix}$$

$$A_3 = \begin{bmatrix} -\frac{r_{L1}}{L_1} & 0 & 0 & -\frac{\xi_{1max}}{L_1} \\ 0 & -\frac{r_{L2}}{L_2} & 0 & -\frac{\xi_{2min}}{L_2} \\ 0 & 0 & -\frac{r_{L3}}{L_3} & -\frac{\xi_{3max}}{L_3} \\ \frac{\xi_{1max}}{C_{ap}} & \frac{\xi_{2min}}{C_{ap}} & \frac{\xi_{3max}}{C_{ap}} & 0 \end{bmatrix}, A_4 = \begin{bmatrix} -\frac{r_{L1}}{L_1} & 0 & 0 & -\frac{\xi_{1max}}{L_1} \\ 0 & -\frac{r_{L2}}{L_2} & 0 & -\frac{\xi_{2min}}{L_2} \\ 0 & 0 & -\frac{r_{L3}}{L_3} & -\frac{\xi_{3min}}{L_3} \\ \frac{\xi_{1max}}{C_{ap}} & \frac{\xi_{2min}}{C_{ap}} & \frac{\xi_{3min}}{C_{ap}} & 0 \end{bmatrix}$$

$$A_5 = \begin{bmatrix} -\frac{r_{L1}}{L_1} & 0 & 0 & -\frac{\xi_{1min}}{L_1} \\ 0 & -\frac{r_{L2}}{L_2} & 0 & -\frac{\xi_{2max}}{L_2} \\ 0 & 0 & -\frac{r_{L3}}{L_3} & -\frac{\xi_{3max}}{L_3} \\ \frac{\xi_{1min}}{C_{ap}} & \frac{\xi_{2max}}{C_{ap}} & \frac{\xi_{3max}}{C_{ap}} & 0 \end{bmatrix}, A_6 = \begin{bmatrix} -\frac{r_{L1}}{L_1} & 0 & 0 & -\frac{\xi_{1min}}{L_1} \\ 0 & -\frac{r_{L2}}{L_2} & 0 & -\frac{\xi_{2max}}{L_2} \\ 0 & 0 & -\frac{r_{L3}}{L_3} & -\frac{\xi_{3min}}{L_3} \\ \frac{\xi_{1min}}{C_{ap}} & \frac{\xi_{2max}}{C_{ap}} & \frac{\xi_{3min}}{C_{ap}} & 0 \end{bmatrix}$$

$$A_7 = \begin{bmatrix} -\frac{r_{L1}}{L_1} & 0 & 0 & -\frac{\xi_{1min}}{L_1} \\ 0 & -\frac{r_{L2}}{L_2} & 0 & -\frac{\xi_{2min}}{L_2} \\ 0 & 0 & -\frac{r_{L3}}{L_3} & -\frac{\xi_{3max}}{L_3} \\ \frac{\xi_{1min}}{C_{ap}} & \frac{\xi_{2min}}{C_{ap}} & \frac{\xi_{3max}}{C_{ap}} & 0 \end{bmatrix}, A_8 = \begin{bmatrix} -\frac{r_{L1}}{L_1} & 0 & 0 & -\frac{\xi_{1min}}{L_1} \\ 0 & -\frac{r_{L2}}{L_2} & 0 & -\frac{\xi_{2min}}{L_2} \\ 0 & 0 & -\frac{r_{L3}}{L_3} & -\frac{\xi_{3min}}{L_3} \\ \frac{\xi_{1min}}{C_{ap}} & \frac{\xi_{2min}}{C_{ap}} & \frac{\xi_{3min}}{C_{ap}} & 0 \end{bmatrix}$$

$$C_i = \begin{bmatrix}0 & 0 & 0 & 1\end{bmatrix}, B_i = \begin{bmatrix} 0 & 0 & 0 & \frac{1}{L_1} \\ 0 & 0 & 0 & \frac{1}{L_2} \\ 0 & 0 & 0 & \frac{1}{L_3} \\ 0 & 0 & 0 & 0 \end{bmatrix}, E_i = \begin{bmatrix} 0 \\ 0 \\ 0 \\ -\frac{1}{C_{ap}} \end{bmatrix}, \quad \forall i = 1, \ldots, r.$$

3 - Observer design for three-phase interleaved boost converter

By considering the output as the output voltage V_{out}, Theorem 2.3 is applied to derive the following observer gains:

$$L_1 = \begin{bmatrix} -926.2329 \\ -926.2329 \\ -926.2329 \\ 9390.6915 \end{bmatrix}, L_2 = \begin{bmatrix} -926.2014 \\ -926.2014 \\ -1.1935 \\ 9329.2412 \end{bmatrix}, L_3 = \begin{bmatrix} -926.2014 \\ -1.1935 \\ -926.2014 \\ 9329.2412 \end{bmatrix}, L_4 = \begin{bmatrix} -926.1702 \\ -1.1781 \\ -1.1781 \\ 9270.9647 \end{bmatrix},$$

$$L_5 = \begin{bmatrix} -1.1935 \\ -926.2014 \\ -926.2014 \\ 9329.2412 \end{bmatrix}, L_6 = \begin{bmatrix} -1.1781 \\ -926.1702 \\ -1.1781 \\ 9270.9647 \end{bmatrix}, L_7 = \begin{bmatrix} -1.1781 \\ -1.1781 \\ -926.1702 \\ 9270.9647 \end{bmatrix}, L_8 = \begin{bmatrix} -1.1562 \\ -1.1562 \\ -1.1562 \\ 9214.7198 \end{bmatrix}.$$

$$P = \begin{bmatrix} 2.6506 & 0.0710 & 0.0710 & 0.0004 \\ 0.0710 & 2.6506 & 0.0710 & 0.0004 \\ 0.0710 & 0.0710 & 2.6506 & 0.0004 \\ 0.0004 & 0.0004 & 0.0004 & 0.0018 \end{bmatrix}$$

4 - Simulation results

Figure 2.4 depicts a schematic of the Dual-loop control dedicated to the three-phase interleaved boost converter. In this topology, two imbricated loops are used: an outer voltage loop and an inner current loop. The four involved controllers are of type "PI", used in a conventional manner to synthesize the duty cycle control signals S_1, S_2 and S_3 where the parameters of the regulators are given as follows: $K_{pV} = 0.1834, K_{iV} = 16.6301, K_{pI} = 0.4242$ and $K_{iI} = 41.9135$, and the frequency of the PWM is $f_c = 20(Khz)$.

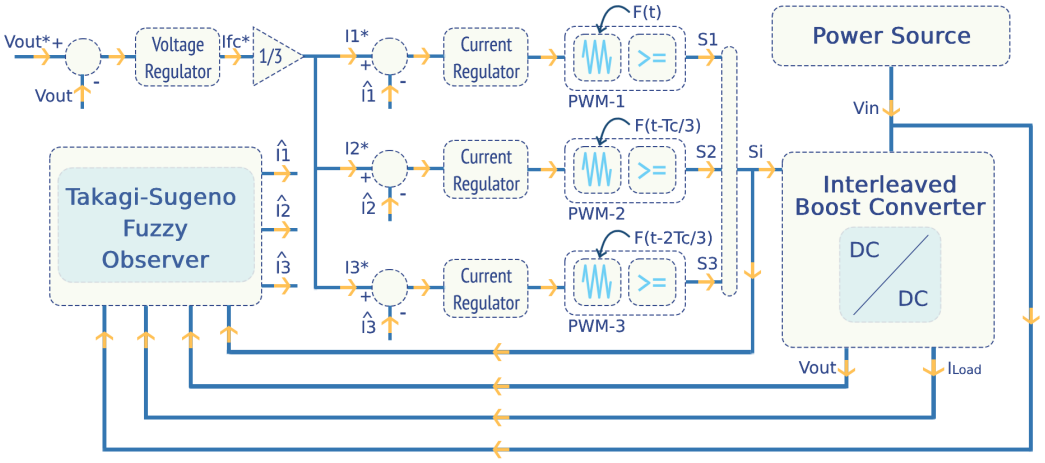

Fig 2.4: Dual-loop control scheme of three-phase interleaved boost converter

In order to demonstrate the stability of the error dynamic, the system's initial conditions were set as $x_0(t) = \begin{bmatrix} 0.5 & 1.5 & -1 & 7.5 \end{bmatrix}^T$ while those of the observer are $\hat{x}_0(t) = \begin{bmatrix} 0 & 0 & 0 & 0 \end{bmatrix}^T$. The load resistance commences with $R = 20(\Omega)$, undergoes a decrease to $R = 15(\Omega)$ at $t = 0.4(s)$, and then returns to the initial $R = 20(\Omega)$ at $t = 0.8(s)$. The estimated states are shown in Figure 2.5 through Figure 2.8, while the estimation error is represented in Figure 2.9.

The obtained results display the successful tracking of the estimated states to the actual ones, regardless of the different initial conditions set for the system and the observer. This consistency, as evidenced in Figure 2.9, shows the estimation error curves converging asymptotically towards zero, thereby affirming the efficacy of the proposed observer.

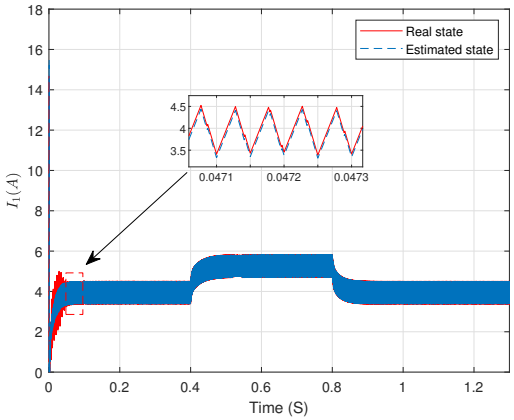

Fig 2.5: Interleaved boost converter phase current I_1.

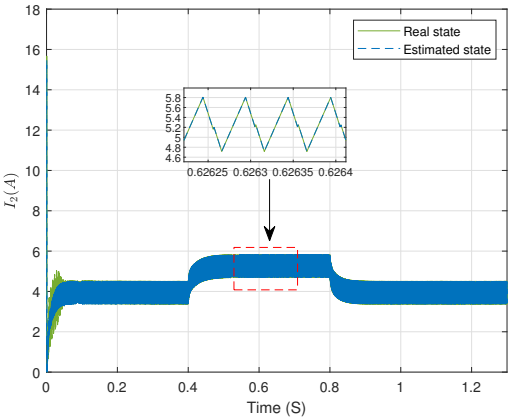

Fig 2.6: Interleaved boost converter phase current I_2.

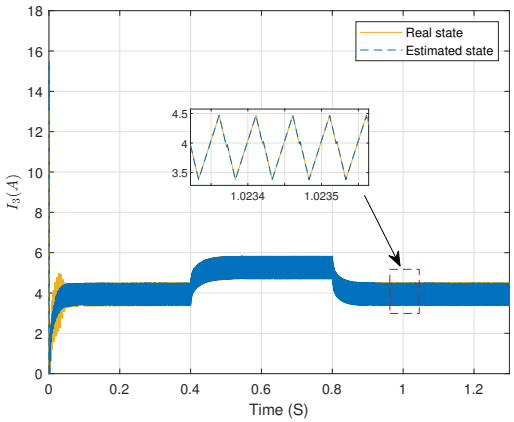

Fig 2.7: Interleaved boost converter phase current I_3.

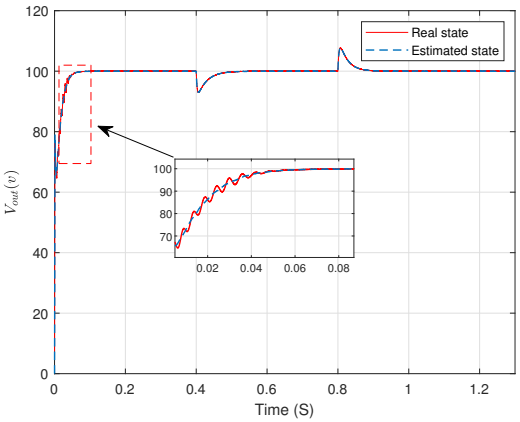

Fig 2.8: Interleaved boost converter output voltage V_{out}.

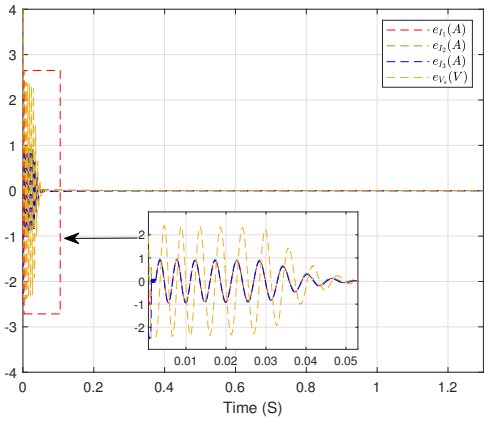

Fig 2.9: State estimation error.

Remark 2.2

In the case where the achieved results are not satisfactory, the pole placement method can be applied on the LMIs specified in the theorem. This approach is designed to optimize the results by identifying new observer gains. A detailed explanation of this method will be provided later in Section 2.4.

Remark 2.3

It is important to note that when the premise variables depend on the input signal, $\xi = f(u(t))$, as in the previous example, the parallel distributed compensation (PDC) control, defined as $u(t) = -(\sum_{i=1}^{r} \mu_i(\xi(t))K_i)x(t)$, cannot be applied. This limitation arises because it introduces an algebraic loop: the control signal at the current time step is calculated using its own value at the same time step, $u(t) = -(\sum_{i=1}^{r} \mu_i(u(t))K_i)x(t)$. Consequently, a causality problem arises, rendering the controller implementation infeasible.

2.3.1.2 Summarize of the observer design process

The diagram below serves as a comprehensive guide to the systematic approach employed in designing an observer for T-S systems. It distinguishes between the initial offline phase, which is dedicated to developing the observer gains, and the subsequent online phase, where these gains are applied in real-time to estimate the system's states.

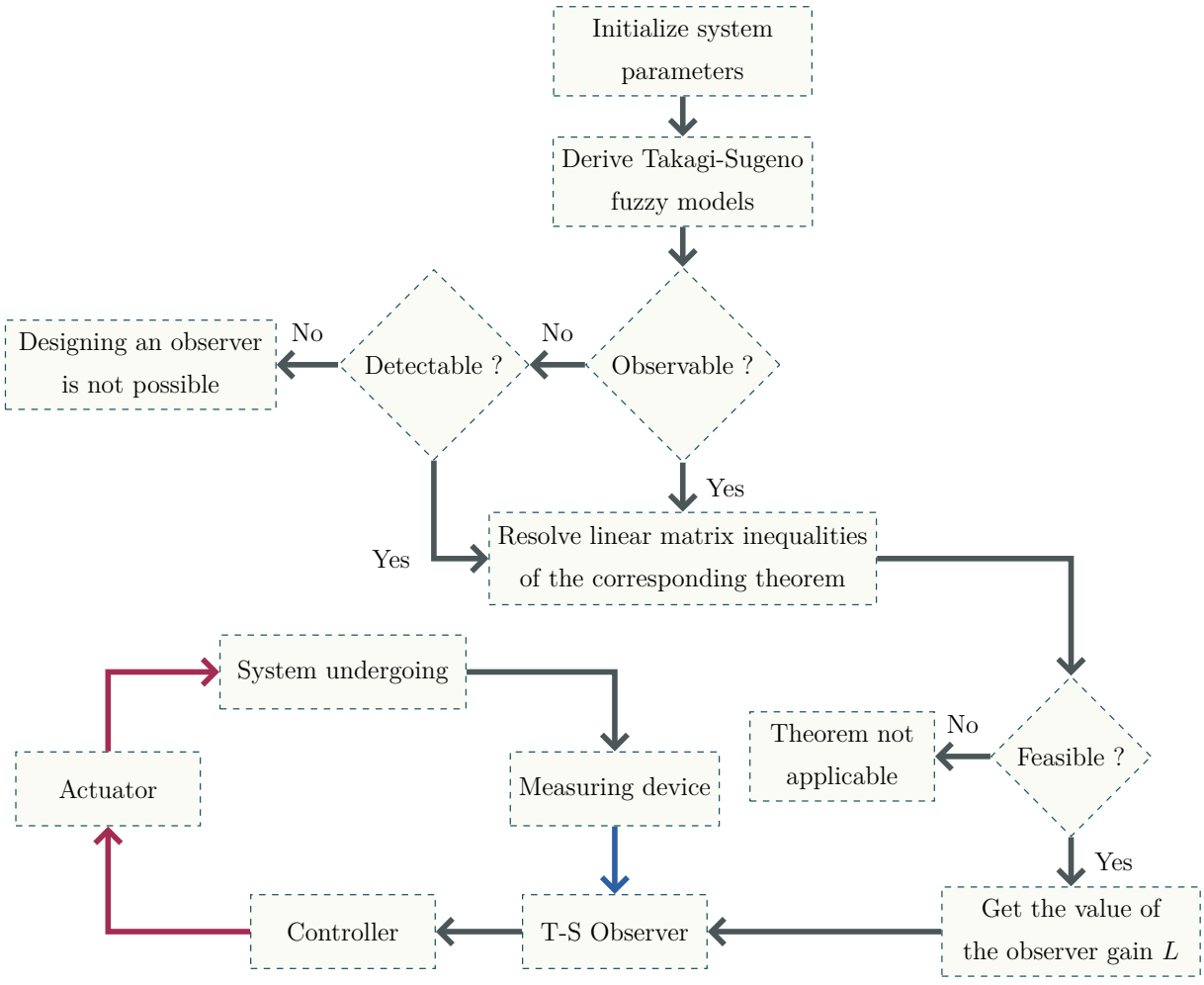

Fig 2.10: Overall schematic diagram of observer design and implementation.

2.3.2 Unmeasurable premise variables

The UPV corresponds to the case where part of the premise variables or all of them are unmeasured. Consequently, the weighting functions utilized in the observer implementation can't be derived from the measurements obtained from the system:

$$\mu_i\left(\hat{\xi}\left(t\right)\right) \neq \mu_i\left(\xi\left(t\right)\right) \tag{2.36}$$

In this scenario, the mismatching terms are not equal until the estimation error tends towards zero:

$$\textbf{WHEN} \quad \hat{x}\left(t\right) \rightarrow x\left(t\right), \quad \textbf{THEN} \quad \omega_i\left(t\right) \rightarrow 0 \tag{2.37}$$

Therefore, the dynamics of the estimation error is still given by (2.19).

To analyze the stability of state estimation error in the case of UPV, various methodologies have been developed by the research community over the years. These approaches will be discussed comprehensively in the forthcoming chapter.

2.4 Enhancing the Performance of Observer Dynamics using pole placement method

In this section, we delve into advanced strategies for enhancing observer gains, with the primary aim of improving the dynamic performance of state estimation errors. This involves a meticulous focus on critical dynamics aspects such as augmenting damping levels, curtailing overshoot, and accelerating convergence speed or decay rate. These improvements are vital for the optimized functioning of the observer system.

Central to these performance enhancements is the understanding of the system's poles λ_i (the eigenvalues of the state matrix) and their positions in the complex plane. According to control theory, a linear system achieves stability when all its poles are situated in the left half of the complex plane, a condition indicating that the state matrix is Hurwitz (all eigenvalues have negative real parts). However, achieving mere stability is not sufficient for enhanced performance. Additional criteria regarding the placement of these poles within the complex plane must be considered, as the locations of these poles are intrinsically linked to the system's dynamic behaviors and capabilities [Yves and Granjon, 2001, Hendricks et al., 2008].

Hence, a key strategy for achieving desired performance levels is through the "pole placement" method, which involves strategically placing the poles of estimation error dynamics in specific regions of the complex plane. Therefore, the concept of "regional pole

placement" is introduce in this section, which contrasts with "pointwise pole placement" by not assigning poles to exact locations but within specified regions in the complex plane. Such regions could be disks, conic sectors, vertical strips, etc. Constraining the poles of the system in specific regions allows us to impose specific bounds on performance measures, ensuring a satisfactory transient response [Chilali and Gahinet, 1996, Chilali et al., 1999].

Generally, the concept of poles and zeros is not applicable in nonlinear systems [Byrnes et al., 1999]. However, the application of the T-S multi-model approach to these systems enables the use of pole placement techniques. This becomes feasible as it allows nonlinear systems to be represented as a combination of local linear models. Each of these models is characterized by its own distinct set of poles, bridging the gap between linear and nonlinear system analysis.

The stability region defined by the classical Lyapunov function applied to autonomous unforced linear system $\dot{x} = Ax(t)$, characterized by the condition

$$A^T P + PA < 0, \tag{2.38}$$

corresponds to the situation where the poles of the matrix A reside in the left half-plane. Therefore, in this section, we will explore how to modify the stability conditions derived from the Lyapunov method to cater to specific regions.

2.4.1 Definitions

2.4.1.1 Kronecker product

The Kronecker product, represented by the symbol $\otimes$, is a mathematical operation applied to two matrices A_{mn} and B_{pq}. This operation results in a larger block matrix. Each element a_{ij} of matrix A is multiplied by the entire matrix B to form the corresponding block in the resultant matrix:

$$A \otimes B = \begin{bmatrix} a_{11}B & \cdots & a_{1n}B \\ \vdots & \ddots & \vdots \\ a_{m1}B & \cdots & a_{mn}B \end{bmatrix} \tag{2.39}$$

2.4.1.2 LMI regions

The LMI region is a region of the complex plain that is characterized by an LMI in function of the complex number z.

Definition 2.4. *(LMI region) [Chilali and Gahinet, 1996] An LMI region is any subset $\mathcal{D} \in \mathbb{C}$ of the complex plane that can be defined as:*

$$\mathcal{D} = \{z = x + jy \in \mathbb{C} : \quad f_{\mathcal{D}}(z) = \gamma + z\beta + z^*\beta < 0\} \tag{2.40}$$

where, $\gamma = \gamma^T \in \mathbb{R}^{m\times m}$ and $\beta \in \mathbb{R}^{m\times m}$. Here, z^* denotes the complex conjugate of z. The matrix valued function $f_{\mathcal{D}}(z)$ is called the characteristic function of $\mathcal{D}$ and < 0 stands for negative definite.

2.4.1.3 $\mathcal{D}$-Stability

$\mathcal{D}$-Stability is a concept used to describe the relationship between the LMI region and the eigenvalues of a matrix. It is formally defined as follows:

Definition 2.5. *($\mathcal{D}$-Stability) [Chilali et al., 1999] A real matrix A is said to be $\mathcal{D}$-stable if all of its eigenvalues are located within the LMI region denoted as $\mathcal{D}$.*

2.4.2 LMI region examples

Below are a few interesting examples of LMI regions, each illustrating a unique aspect of these regions in complex analysis:

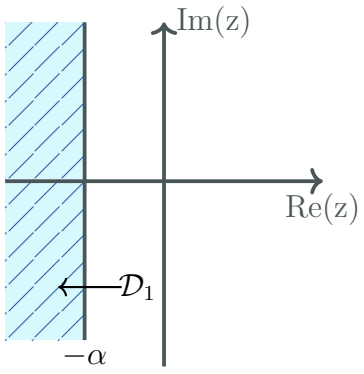

Fig 2.11: Half-plane.

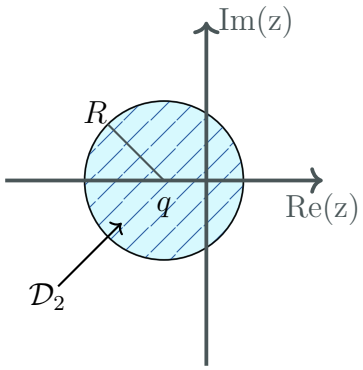

Fig 2.12: Disk.

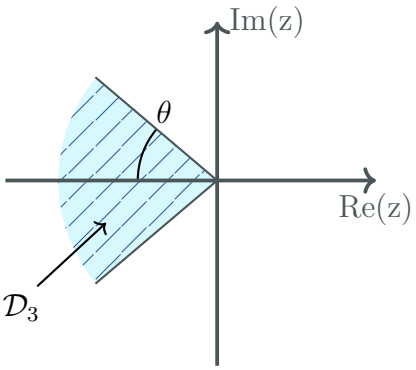

Fig 2.13: Conical sector.

1 - Biased left half-plane: The region $\mathcal{D}_1$ represents a left half-plane that is biased by a value α. To define this region, we consider the real part x of the complex number z and shift it to the left by α. The region is then described by the condition:

$$x < -\alpha \iff \frac{z^* + z}{2} < -\alpha \iff z^* + z < -2\alpha \tag{2.41}$$

The characteristic function $f_{\mathcal{D}}(z)$ for this region is obtained by setting $\gamma = 2\alpha$ and $\beta = 1$, resulting in:

$$f_{\mathcal{D}}(z) = 2\alpha + z + z^* < 0 \tag{2.42}$$

2 - Disk centered at (q,0) with radius R: The region $\mathcal{D}_2$ is a disk in the complex plane centered at the point $(q, 0)$ with radius R. The condition defining this disk, using complex numbers, is given by:

$$(z - q)(z^* - q) < R^2 \tag{2.43}$$

This equation represents all complex numbers z whose distance from the point q is less than R.

Applying the Schur complement, as stated in Lemma 1.3, the inequality (2.43) is equivalent to:

$$\begin{bmatrix} -R & (z-q) \\ (z^*-q) & -R \end{bmatrix} < 0 \tag{2.44}$$

Consequently, the characteristic function $f_{\mathcal{D}}(z)$ for this region can be derived by setting $\gamma = \begin{bmatrix} -R & -q \\ -q & -R \end{bmatrix}$ and $\beta = \begin{bmatrix} 0 & 1 \\ 0 & 0 \end{bmatrix}$. Thus, we obtain:

$$f_{\mathcal{D}}(z) = \begin{bmatrix} -R & -q \\ -q & -R \end{bmatrix} + z \begin{bmatrix} 0 & 1 \\ 0 & 0 \end{bmatrix} + z^* \begin{bmatrix} 0 & 0 \\ 1 & 0 \end{bmatrix} = \begin{bmatrix} -R & (z-q) \\ (z^*-q) & -R \end{bmatrix} \tag{2.45}$$

3 - Conic sector: The region $\mathcal{D}_3$ is a conic sector centered around the negative direction of the real axis, with the apex at the origin and an inner angle of 2θ, where $0 < \theta < \frac{\pi}{2}$. This region is defined by the condition:

$$|y| < -xtan(\theta) \Longleftrightarrow y^2 < x^2 tan(\theta)^2 \tag{2.46}$$

Utilizing the properties

$$x = \frac{z + z^*}{2}, \quad y = \frac{z - z^*}{2j},$$

the inequality given in (2.46) can be reformulated as:

$$sin(\theta)(z + z^*) + cos(\theta)(z - z^*)(sin(\theta)(z + z^*))^{-1} cos(\theta)(z - z^*) < 0 \tag{2.47}$$

Applying the Schur complement, the inequality in (2.47) is equivalent to:

$$\begin{bmatrix} sin(\theta)(z+z^*) & cos(\theta)(z-z^*) \\ -cos(\theta)(z-z^*) & sin(\theta)(z+z^*) \end{bmatrix} < 0 \tag{2.48}$$

Consequently, the characteristic function $f_{\mathcal{D}}(z)$ for this region can be obtained by setting $\gamma = \begin{bmatrix} 0 & 0 \\ 0 & 0 \end{bmatrix}$ and $\beta = \begin{bmatrix} sin(\theta) & cos(\theta) \\ -cos(\theta) & sin(\theta) \end{bmatrix}$, resulting in:

$$f_{\mathcal{D}}(z) = z \begin{bmatrix} sin(\theta) & cos(\theta) \\ -cos(\theta) & sin(\theta) \end{bmatrix} + z^* \begin{bmatrix} sin(\theta) & -cos(\theta) \\ cos(\theta) & sin(\theta) \end{bmatrix} = \begin{bmatrix} sin(\theta)(z+z^*) & cos(\theta)(z-z^*) \\ -cos(\theta)(z-z^*) & sin(\theta)(z+z^*) \end{bmatrix} \tag{2.49}$$

4 - Intersection of LMI regions: The intersections of r LMI sub-regions $\mathcal{D}_i$ forms another LMI region, denoted as $\mathcal{D}$. The characteristic function for this intersected region is a diagonal matrix constructed from the characteristic functions of each individual sub-region. Mathematically, it is represented as:

$$f_{\mathcal{D}}(z) = diag(f_{\mathcal{D}_1}(z), \ldots, f_{\mathcal{D}_r}(z)) \tag{2.50}$$

For illustration, consider the LMI region $\mathcal{D}_4$, which represents the intersection of the LMI sub-regions $\mathcal{D}_1$, $\mathcal{D}_2$ and $\mathcal{D}_3$:

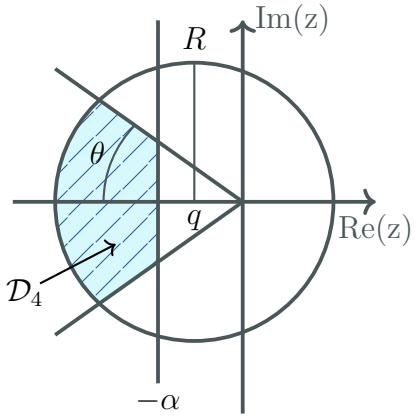

Fig 2.14: Intersection of LMI regions

Therefore, for a complex number z to belong to the intersection region $\mathcal{D}_4$, it must simultaneously satisfy the conditions of all sub-regions $\mathcal{D}_i$.

For further exploration and a more comprehensive list of LMI regions, interested readers are referred to the work presented in [Chadli and Borne, 2012].

2.4.3 Pole clustering in LMI regions

This section focuses on the analysis of pole clustering within specific LMI regions, emphasizing the concept of quadratic $\mathcal{D}$-stability for a matrix A. The theoretical foundation for this approach is rooted in the research of Chilali in [Chilali and Gahinet, 1996], which provides stability conditions to ensure that the poles of the state matrix A are confined within the LMI region $\mathcal{D}$. When the region $\mathcal{D}$ encompasses the entire left-half plane, $\mathcal{D}$-stability is equivalent to asymptotic stability, aligning with employing the quadratic Lyapunov function as detailed in (2.38). Moreover, if $\mathcal{D}$ corresponds to a biased left-half plane, as illustrated in Figure 2.11, the matrix A is then termed α-stable. The following theorem announced this concept:

Theorem 2.4

A matrix A is $\mathcal{D}$-stable if and only if there exists a symmetric positive definite matrix P such that:

$$M_{\mathcal{D}}(A,P) = \gamma \otimes P + \beta \otimes AP + \beta^T \otimes PA^T < 0, \quad P > 0 \tag{2.51}$$

Proof. Let λ be any eigenvalue of A, and let $v \in \mathbb{C}^n$ be a nonzero vector such that $v^H A = \lambda v^H$. Using the identity:

$$\left(I_m \otimes v^H\right) M_{\mathcal{D}}(A,P) \left(I_m \otimes v\right) = \left(v^H P v\right) f_{\mathcal{D}}(\lambda) \tag{2.52}$$

it follows that if $M_{\mathcal{D}}(A,P) < 0$ and $P > 0$, then $f_{\mathcal{D}}(\lambda) < 0$. This implies that λ is located within the region $\mathcal{D}$. Therefore, the condition in (2.51) guarantees the $\mathcal{D}$-stability of the matrix A. □

By applying the definition of the Kronecker product as described in equation (2.39), the inequality presented in (2.51) can be reformulated as follows:

$$\begin{bmatrix} \gamma_{11}P + \beta_{11}AP + \beta_{11}(AP)^T & \cdots & \gamma_{1n}P + \beta_{1n}AP + \beta_{1n}(AP)^T \\ \vdots & \ddots & \vdots \\ \gamma_{n1}P + \beta_{n1}AP + \beta_{n1}(AP)^T & \cdots & \gamma_{nn}P + \beta_{nn}AP + \beta_{nn}(AP)^T \end{bmatrix} < 0 \tag{2.53}$$

The fundamental principles of $\mathcal{D}$-stability outlined in Theorem 2.4 have been further expanded beyond quadratic Lyapunov functions. This broader scope, as detailed in [Nguang and Shi, 2006], allows for the inclusion of various types of Lyapunov functions, including but not limited to the fuzzy Lyapunov function, as demonstrated in the studies by Cherifi in [Cherifi et al., 2017, Cherifi et al., 2019]. This generalization is encapsulated in the following theorem:

Theorem 2.5

For a given LMI region defined by (2.40), a nonlinear system characterized by $\dot{x} = f(x)x$ is considered $\mathcal{D}$-stable if there exist a Lyapunov function $V(x(t))$ satisfying $\frac{1}{2}\frac{\dot{V}(x(t))}{V(x(t))} \in \mathcal{D}$, i.e:

$$\gamma \otimes V(x(t)) + \beta \otimes \frac{1}{2}\dot{V}(x(t)) + \beta^T \otimes \frac{1}{2}\dot{V}(x(t)) < 0 \tag{2.54}$$

2.4.4 Examples of pole clustering in LMI regions

This section presents examples of pole placement within the LMI regions described in Section 2.4.2.

It is essential to understand the relationship between the characteristic function of the LMI region $f_{\mathcal{D}}(z)$ in (2.40) and the $\mathcal{D}$-stability condition $M_{\mathcal{D}}(A, P)$ in (2.51). This relationship is established by the substitution:

$$(P, AP, PA^T) \longleftrightarrow (1, z, z^*) \tag{2.55}$$

Using this substitution, the poles of the state matrix A can be clustered within the designated LMI region.

1 - Clustering the poles in the left half-plane:

Theorem 2.6

Consider an LMI region $\mathcal{D}$ that includes the entire left half of the complex plane. A matrix A is said to be $\mathcal{D}$-stable if it satisfies the stability condition obtained by setting $\gamma = 0$ and $\beta = 1$ in (2.51). This stability condition is expressed as follows:

$$AP + PA^T < 0, \quad P > 0 \tag{2.56}$$

It is known from control theory that placing the eigenvalues of a system in the left half-plane corresponds to the asymptotic stability, which can be achieved by employing a quadratic Lyapunov function as represented in (2.38).

The inequality expressed in (2.38) utilizes the matrix product order (PA), while the inequality in (2.56) uses the order (AP). To demonstrate that these two inequalities are equivalent, it suffices to multiply (2.56) from both the left and right sides by P^{-1}. Following this, the substitution $Q = P^{-1}$ leads to the reformulated expression:

$$QA + A^T Q < 0, \quad Q > 0 \tag{2.57}$$

2 - Clustering the poles in the Biased left half-plane:

Theorem 2.7

Consider the LMI region $\mathcal{D}$ as illustrated in Figure 2.11 and characterized by the characteristic function (2.42). A matrix A is said to be $\mathcal{D}$-stable if it satisfies the stability condition derived either by setting $\gamma = 2\alpha$ and $\beta = 1$ in (2.51), or by directly substituting (2.55) into the characteristic function (2.42). This results in the following stability condition:

$$2\alpha P + AP + PA^T < 0 \tag{2.58}$$

This form of stability is referred to as "Exponential convergence" characterized by a decay rate denoted by α, and is also known as "α-stability". This concept is described

using the Lyapunov function as follows:

$$2\alpha V(t) + \dot{V}(t) \leq 0 \tag{2.59}$$

The inequality (2.59) emerges from the general stability condition presented in (2.54) by setting the parameters $\gamma = 2\alpha$ and $\beta = 1$.

3 - Clustering the poles in a disk centered at (q,0) with radius R:

Theorem 2.8

Consider the LMI region $\mathcal{D}$ as illustrated in Figure 2.12 and characterized by the characteristic function (2.45). A matrix A is said to be $\mathcal{D}$-stable if it satisfies the stability condition derived either by setting $\gamma = \begin{bmatrix} -R & -q \\ -q & -R \end{bmatrix}$ and $\beta = \begin{bmatrix} 0 & 1 \\ 0 & 0 \end{bmatrix}$ in (2.51), or by directly substituting (2.55) into the characteristic function (2.45). This results in the following stability condition:

$$\begin{bmatrix} -RP & (AP - qP) \\ (PA^T - qP) & -RP \end{bmatrix} < 0 \tag{2.60}$$

4 - Clustering the poles in a conic sector:

Theorem 2.9

Consider the LMI region $\mathcal{D}$ as illustrated in Figure 2.13 and characterized by the characteristic function (2.49). A matrix A is said to be $\mathcal{D}$-stable if it satisfies the stability condition derived either by setting $\gamma = \begin{bmatrix} 0 & 0 \\ 0 & 0 \end{bmatrix}$ and $\beta = \begin{bmatrix} sin(\theta) & cos(\theta) \\ -cos(\theta) & sin(\theta) \end{bmatrix}$ in (2.51), or by directly substituting (2.55) into the characteristic function (2.49). This results in the following stability condition:

$$\begin{bmatrix} sin(\theta)(AP + PA^T) & cos(\theta)(AP - PA^T) \\ -cos(\theta)(AP - PA^T) & sin(\theta)(AP + PA^T) \end{bmatrix} < 0 \tag{2.61}$$

For further exploration and a more comprehensive list of examples of pole clustering in LMI regions, interested readers are referred to the work presented in [Chadli and Borne, 2012].

Now, to improve the observer's performance, the eigenvalues of the state estimation error, giving in the equation (2.22), can be assigned to any of the previously discussed LMI regions. This is accomplished by substituting the matrix A with $(A_i - L_i C_j)$ in the general stability condition described in (2.51), leading to the following modified stability condition:

$$M_{\mathcal{D}}((A_i - L_i C_j), P) = \gamma \otimes P + \beta \otimes (A_i - L_i C_j) P + \beta^T \otimes P (A_i - L_i C_j)^T < 0, \quad P > 0 \tag{2.62}$$

By appropriately setting the values of γ and β, the poles of the system can be clustered within the desired LMI region.

Clustering the eigenvalues of the state matrix in the left half-plane ensures the asymptotic stability and leading to the convergence of the estimation error dynamics towards zero. However, this stability condition alone does not guarantee optimal dynamic performance. For this reason, it is advisable to employ the α-stability condition. The α-stability condition enforces a specific decay rate of the Lyapunov function, thereby controlling the convergence speed of the estimation error.

Despite these measures, oscillatory behavior in the estimation error dynamics can still occur due to the imaginary parts of the eigenvalues. To mitigate this, it is recommended to impose bounds on the imaginary parts of the eigenvalues. This can be accomplished by using disk or conic sector LMI regions, which help in ensuring not only stability but also adequate damping in the estimation error dynamics.

For instance, consider the case of the conical sector described in Theorem 2.9. By substituting the matrix A with $(A_i - L_i C_j)$, the following result is obtained:

$$\begin{bmatrix} sin(\theta)((A_i - L_i C_j)P + P(A_i - L_i C_j)^T) & cos(\theta)((A_i - L_i C_j)P - P(A_i - L_i C_j)^T) \\ -cos(\theta)((A_i - L_i C_j)P - P(A_i - L_i C_j)^T) & sin(\theta)((A_i - L_i C_j)P + P(A_i - L_i C_j)^T) \end{bmatrix} < 0 \tag{2.63}$$

This inequality represents a BMI in terms of the product of two decision variables, P and L_i. To transform it into an LMI, it must first be multiplied from the left and the right by $Q = P^{-1}$. Subsequently, employing the change of variables given by

$$M_i = Q L_i, \tag{2.64}$$

leads to the following LMI:

$$\begin{bmatrix} sin(\theta)(QA_i - M_i C_j + A_i^T Q - C_j^T M_i^T) & cos(\theta)(QA_i - M_i C_j - A_i^T Q - C_j^T M_i^T) \\ -cos(\theta)(QA_i - M_i C_j - A_i^T Q - C_j^T M_i^T) & sin(\theta)(QA_i - M_i C_j + A_i^T Q - C_j^T M_i^T) \end{bmatrix} < 0 \tag{2.65}$$

It is important to highlight that the $\mathcal{D}$-stability condition expressed in this inequality has been employed in the example of the 3P-IBC in Section 2.3.1.1 where the set angle is $\theta = 20$.

2.5 Conclusion

In this chapter, we delved deeply into the intricacies of observer design for Takagi-Sugeno fuzzy systems, starting with a fundamental analysis of observability and detectability. These initial steps were crucial for assessing the feasibility of constructing an observer for the corresponding system. As we moved forward, we have addressed the two pivotal categories faced in observer design: the measurable and unmeasurable premise variables, with the chapter primarily concentrating on the MPV aspect and the derivation of the corresponding observer gains. An example was presented to demonstrate the observer's design and its implementation in the system's control process. Notably, the observer's performance was enhanced through pole placement in LMI regions. We discussed various LMI regions and elaborated on how clustering the eigenvalues of the state estimation error within these regions can further refine the observer's performance.

Chapter 3

State estimation of Takagi-Sugeno fuzzy systems with UPV

3.1 Introduction

As discussed in the previous chapter, two categories of T-S systems can be identified: those with measurable premise variables and those with unmeasurable premise variables. The MPV category pertains to systems where premise variables can be directly measured. However, this scenario is not always the case. In contrast, systems falling under the UPV category are more prevalent, as they encompass a broader range of real-world situations. This prevalence of UPV systems has led recent research towards enhancing their control and observer design methodologies. However, designing observers for systems featuring unmeasurable premise variables proves more challenging than for systems with measurable ones, especially in the context of state estimation problems, where the presence of the mismatching terms in the error dynamics poses significant challenges.

To analyze the stability of these dynamics, a variety of methods have been proposed. Notably, the Lipschitz-based method stands out. This method involves applying the Lipschitz condition to the mismatching terms, which allows for the factorization of stability conditions in terms of the estimation error. Initial research efforts, such as those cited in [Ichalal et al., 2009b, Bergsten et al., 2002] laid the foundation for designing observers for T-S systems with UPV using Lipschitz condition. Subsequent studies, including those by [Louzimi et al., 2017, Ouzaz et al., 2021], have further expanded the use of this method. They applied it to estimate both the system's states and unknown inputs, especially in the context of fault detection. The author in [Ouhib, 2020] further contributed to this field by designing an unknown input observer where relaxed stability conditions, through the injection of output error into the premise variable, have been obtained, demonstrating the versatility and effectiveness of this approach.

Despite the success of the Lipschitz-based method, challenges arise when the Lipschitz constant exceeds an acceptable threshold, leading to pronounced conservatism in the LMI constraints, thus rendering the method infeasible [Ichalal et al., 2018]. Efforts to reduce this conservatism, notably through the introduction of a poly-quadratic Lyapunov function, are documented in [Ichalal et al., 2012]. This led to the development of two distinct approaches: the first aimed at ensuring asymptotic convergence of the estimation error, which unfortunately did not meet the desired target; and a second approach that focused on input to state stability to eliminate the need for the Lipschitz constant in the stability condition. This latter approach successfully achieved the desired objective, thus reducing the conservatism, however, it did not verify asymptotic convergence.

Alternative approaches have been developed to address the limitations of the Lipschitz-based method, including the $\mathcal{L}_2$-attenuation approach, as detailed in [Pérez-Estrada et al., 2018,

Ouhib and Kara, 2023]. This method does not rely on the Lipschitz assumption, eliminates the need for the Lipschitz constant calculations of the mismatching terms, minimizes their effect, and additionally, isn't dependent on the knowledge of the system's input bounds, an assumption required in the Lipschitz approach, thereby reducing the conservatism of the Lipschitz-based method. The efficacy of this approach in addressing the challenges of the Lipschitz assumption was addressed in various studies. Notably, in [Ichalal et al., 2008], it was proposed as a solution to these challenges, yielding promising results. This approach was further applied by the same authors to manage the unknown inputs affecting the system in [Ichalal et al., 2009a]. Furthermore, its utility in diminishing the impact of disturbances on measurements has been demonstrated in several studies, in which several studies have employed this principle [Boukhlouf et al., 2023, Guzman et al., 2021, Youssef et al., 2017, Chaves Jr et al., 2021].

While typically simpler and less conservative than the Lipschitz method, the $\mathcal{L}_2$-attenuation approach sometimes fails to achieve a sufficiently low attenuation level, even with successful simulations. This limitation has led to the adoption of the Mean Value Theorem (MVT) method, as seen in [Pan et al., 2022, Pan et al., 2023], allowing the factorization of the estimation error dynamics, which leads to making it proportional completely to the estimation error. Hence, the mismatching terms disappeared from the estimation error dynamics. Due to its advantageous properties over the previous methods, the MVT has been applied in a variety of applications. For instance, Mimoune et al. [Mimoune et al., 2023] demonstrated a real-time implementation of a controller that uses an MVT-based observer on an induction motor, yielding significant results. Similarly, the study in [Allag et al., 2019] introduced a robust H^{∞} Field Oriented Control using MVT for an induction motor. In [Hamidani et al., 2019], a sensorless non-linear control was proposed for a Permanent Magnet Synchronous Motor. Additionally, the authors in [Pan et al., 2022] presented an empirical study focusing on fault detection in steering and torque actuators of autonomous ground vehicles. In the field of detection and mitigation of cyber-attacks, the mean value theorem was helpful in handling the mismatching terms for the unknown inputs estimation [Pan et al., 2023]. All of these studies employ the second Lyapunov theorem with quadratic candidate function to analyze the stability of the state estimation error, resulting in a sufficient stability condition described as LMI. However, this candidate function is known for its conservative nature, which requires determining a common decision variable for the entire set of LMI, hence making it unsuitable for several systems. To overcome this problem, research in recent years has focused on lesser restrictive approaches such as the poly-quadratic Lyapunov function.

This chapter delves into the methods previously outlined for designing observers in T-S

systems with UPV. Initially, the problem statement is presented in Section 3.2. Subsequently, Section 3.3 explores the Lipschitz-based method using a poly-quadratic Lyapunov function, offering an enhanced solution compared to that detailed in [Ichalal et al., 2012]. Section 3.4 presents the $\mathcal{L}_2$-attenuation approach, used for reducing the conservatism inherent in the Lipschitz-based method and enhancing robustness against measurement noises. Finally, Section 3.5 discusses the application of the Mean Value Theorem to both quadratic and poly-quadratic Lyapunov functions, focusing on the non-quadratic approach to diminish the conservatism observed in previous works reliant on the quadratic method, such as in [Mimoune et al., 2023, Allag et al., 2019], and the others.

3.2 Problem statement

Consider a nonlinear system that is modeled using the T-S multi-model approach, which is described as follows:

$$\begin{cases} \dot{x}(t) = \sum_{i=1}^{r} \mu_i(\xi(t)) \left(A_i x(t) + B_i u(t)\right) \\ y(t) = \sum_{i=1}^{r} \mu_i(\xi(t)) \left(C_i x(t) + D_i u(t)\right) \end{cases} \tag{3.1}$$

here, $x(t) \in \mathbb{R}^{n_x}$ represent the state vector, $u(t) \in \mathbb{R}^{n_u}$ represent the input vector and $y(t) \in \mathbb{R}^{n_y}$ represent the output vector. The known matrices are represented by $A_i \in \mathbb{R}^{n_x \times n_x}, B_i \in \mathbb{R}^{n_x \times n_u}, D_i \in \mathbb{R}^{n_y \times n_u}$ and $C_i \in \mathbb{R}^{n_y \times n_x}$. Lastly, $\xi(t)$ represent the premise variables and $\mu_i\left(\xi\left(t\right)\right)$ are the weighting functions that verify the convex sum property:

$$\begin{cases} \sum_{i=1}^{r} \mu_i(\xi(t)) = 1 \\ 0 \leq \mu_i(\xi(t)) \leq 1, \quad \forall i = 1, ..r \end{cases} \tag{3.2}$$

This system can be described as a perturbed system, represented by the following equations:

$$\begin{cases} \dot{x}(t) = \sum_{i=1}^{r} \mu_i(\hat{\xi}(t)) \left(A_i x(t) + B_i u(t) + \omega_1(t)\right) \\ y(t) = \sum_{i=1}^{r} \mu_i(\hat{\xi}(t)) \left(C_i x(t) + D_i u(t) + \omega_2(t)\right) \end{cases} \tag{3.3}$$

In this model, $\mu_i\left(\hat{\xi}\left(t\right)\right)$ denotes the weighting function of the observer, and $\omega_i\left(t\right)$ represents the perturbation term, which accounts for the mismatching term:

$$\begin{cases} \omega_1\left(t\right) = \sum_{i=1}^{r} \left(\mu_i\left(\xi\left(t\right)\right) - \mu_i\left(\hat{\xi}\left(t\right)\right)\right) \left(A_i x\left(t\right) + B_i u\left(t\right)\right) \\ \omega_2\left(t\right) = \sum_{i=1}^{r} \left(\mu_i\left(\xi\left(t\right)\right) - \mu_i\left(\hat{\xi}\left(t\right)\right)\right) \left(C_i x\left(t\right) + D_i u\left(t\right)\right) \end{cases} \tag{3.4}$$

Designing an observer for the T-S system described in (3.3) depends on which Lyapunov function will be used, whether it be the quadratic or the poly-quadratic one. Generally, the observer's structure is defined as follows:

$$\begin{cases} \dot{\hat{x}}(t) = \sum_{i=1}^{r} \mu_i(\hat{\xi}(t)) \left(A_i\hat{x}(t) + B_iu(t) + L_i(t)(y(t) - \hat{y}(t))\right) \\ \hat{y}(t) = \sum_{i=1}^{r} \mu_i(\hat{\xi}(t)) \left(C_i\hat{x}(t) + D_iu(t)\right) \end{cases} \tag{3.5}$$

where, $L_i(t)$ represents the observer gains in the general case.

In order to determine the values of the observer gains, the second Lyapunov theorem is applied to the state estimation error, which is presented as follows:

$$e(t) = x\,(t) - \hat{x}\,(t) \tag{3.6}$$

By substituting the expressions from (3.3) and (3.5) into (3.6), the dynamics of the estimation error can be derived as follows:

$$\begin{aligned} \dot{e}(t) &= \sum_{i=1}^{r} \mu_i(\hat{\xi}(t)) \left[A_ie(t) + \omega_1(t)\right] - \sum_{i=1}^{r}\sum_{j=1}^{r} \mu_i(\hat{\xi}(t))\mu_j(\hat{\xi}(t)) \left[L_i(t)\left(C_je(t) + \omega_2(t)\right)\right] \\ &= \sum_{i=1}^{r}\sum_{j=1}^{r} \mu_i(\hat{\xi}(t))\mu_j(\hat{\xi}(t)) \left[A_ie(t) + \omega_1(t) - L_j(t)\left(C_ie(t) + \omega_2(t)\right)\right] \\ &= \sum_{i=1}^{r}\sum_{j=1}^{r} \mu_i(\hat{\xi}(t))\mu_j(\hat{\xi}(t)) \left[(A_i - L_j(t)C_i)e(t) + \omega_1(t) - L_j(t)\omega_2(t)\right] \end{aligned} \tag{3.7}$$

In the case where the output equation is linear, corresponding to $C_1 = \cdots = C_r = C$ and $D_1 = \cdots = D_r = D$, the mismatching term $\omega_2(t)$ becomes zero. Consequently, the estimation error dynamics depicted in (3.7) can be expressed as follows:

$$\dot{e}(t) = \sum_{i=1}^{r} \mu_i(\hat{\xi}(t)) \left[(A_i - L_i(t)C)e(t) + \omega_1(t)\right] \tag{3.8}$$

3.2.1 Observer structure in the case of using the quadratic Lyapunov function:

In the case of designing an observer for a T-S system using the quadratic Lyapunov function, the observer gains $L_i(t)$ are selected as constant. These gains are defined as follows:

$$L_i(t) = L_i, \quad \forall i = 1, \ldots, r, \tag{3.9}$$

where, L_i represent the local observer gains for each sub-model individually.

By substituting the expression of the observer gain from (3.9) into (3.5), the following observer structure is obtained:

$$\begin{cases} \dot{\hat{x}}(t) = \sum_{i=1}^{r} \mu_i(\hat{\xi}(t)) \left(A_i\hat{x}(t) + B_iu(t) + L_i(y(t) - \hat{y}(t))\right) \\ \hat{y}(t) = \sum_{i=1}^{r} \mu_i(\hat{\xi}(t)) \left(C_i\hat{x}(t) + D_iu(t)\right) \end{cases} \tag{3.10}$$

and the estimation error dynamics, as outlined in (3.7), are now given by:

$$\dot{e}(t) = \sum_{i=1}^{r}\sum_{j=1}^{r} \mu_i(\hat{\xi}(t))\mu_j(\hat{\xi}(t)) \left[(A_i - L_jC_i)e(t) + \omega_1(t) - L_j\omega_2(t)\right] \tag{3.11}$$

while in the case of a linear output equation, the estimation error dynamics, as outlined in (3.8), are given by:

$$\dot{e}(t) = \sum_{i=1}^{r} \mu_i(\hat{\xi}(t)) \left[(A_i - L_i C)e(t) + \omega_1(t)\right] \tag{3.12}$$

This employment of the quadratic Lyapunov function corresponds to the structure described in Section 2.2.2.

3.2.2 Observer structure in the case of using the poly-quadratic Lyapunov function:

In the case of using the Poly-quadratic Lyapunov function, which provides less conservatism compared to the quadratic one, the observer structure given in (3.10) cannot be used because it does not provide LMI stability conditions. The implications of this limitation and the associated discussion will be addressed later in Section 3.5.3. To derive LMI stability conditions, a specific observer structure is necessary. This particular structure has been utilized in several literature, such as [Ichalal et al., 2012], [Wang et al., 2016], and [Guzman et al., 2021]. This observer is obtained by defining the observer gains $L_i(t)$ as follows:

$$L_i(t) = P_\mu(t)^{-1} L_i, \quad \forall i = 1, \ldots, r, \tag{3.13}$$

where, L_i represent the local observer gains for each sub-model individually, and $P_\mu(t)$ is given by:

$$P_\mu(t) = \sum_{j=1}^{r} \mu_j \left(\hat{\xi}\,(t)\right) P_j \tag{3.14}$$

here, P_j represents the matrices of the Poly-quadratic Lyapunov function to be determined.

By substituting the expression of the observer gain from (3.13) into (3.5), the following observer structure is obtained:

$$\begin{cases} \dot{\hat{x}}(t) = \sum_{i=1}^{r} \mu_i(\hat{\xi}(t)) \left(A_i \hat{x}(t) + B_i u(t) + P_\mu(t)^{-1}\ L_i(y(t) - \hat{y}(t))\right) \\ \hat{y}(t) = \sum_{i=1}^{r} \mu_i(\hat{\xi}(t)) \left(C_i \hat{x}(t) + D_i u(t)\right) \end{cases} \tag{3.15}$$

and the estimation error dynamics, as outlined in (3.7), are now given by:

$$\dot{e}(t) = \sum_{i=1}^{r} \sum_{j=1}^{r} \mu_i(\hat{\xi}(t)) \mu_j(\hat{\xi}(t)) \left[(A_i - P_\mu(t)^{-1}\ L_j C_i)e(t) + \omega_1(t) - P_\mu(t)^{-1}\ L_j \omega_2(t)\right] \tag{3.16}$$

while in the case of a linear output equation, the estimation error dynamics, as outlined in (3.8), are given by:

$$\dot{e}(t) = \sum_{i=1}^{r} \mu_i(\hat{\xi}(t)) \left[(A_i - P_\mu(t)^{-1}\ L_i C)e(t) + \omega_1(t)\right] \tag{3.17}$$

The diagram of this observer is presented in Figure 3.1 below:

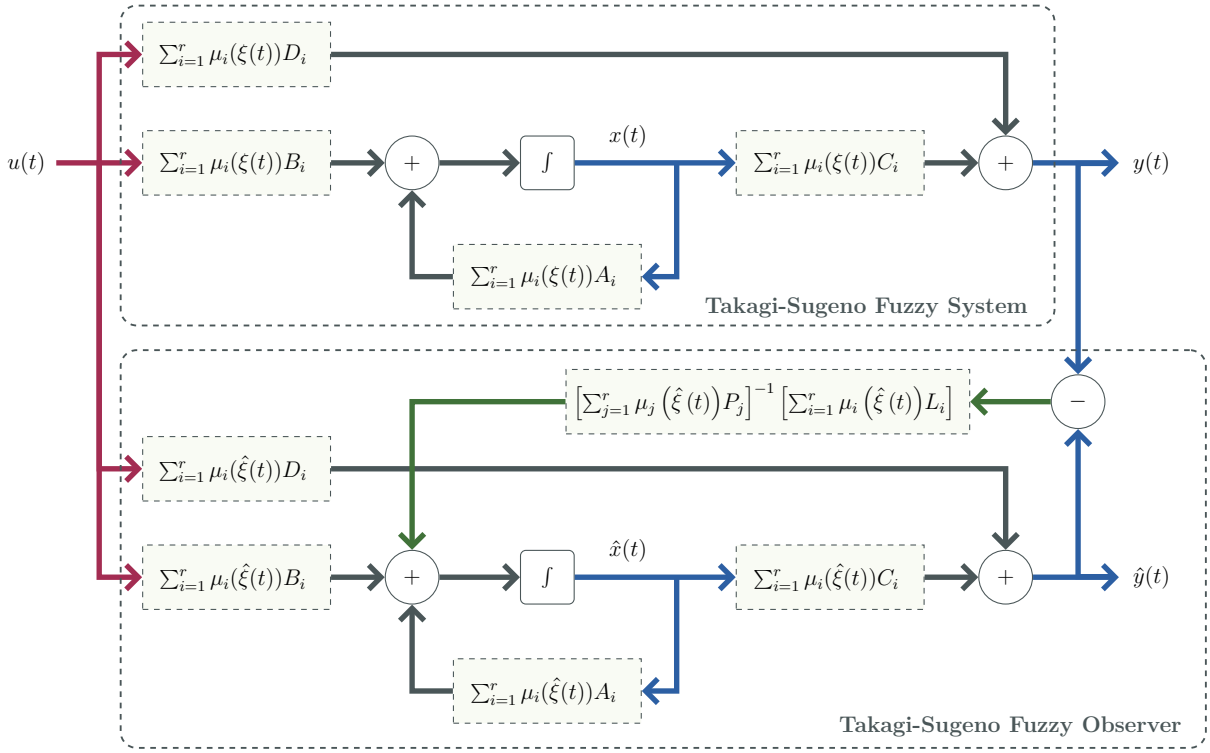

Fig 3.1: Takagi-Sugeno observer structure in the case of using a poly-quadratic Lyapunov function

In the subsequent sections, methods for analyzing the stability of estimation error dynamics in T-S systems with UPV are presented. These methods are applicable in cases using either the quadratic Lyapunov function or the poly-quadratic Lyapunov function.

3.3 Lipschitz based observer

This section introduces an enhancement aimed at reducing the conservatism of the observer based on the Lipschitz method detailed in [Ichalal et al., 2012]. The proposed methodology is built upon the judicious use of the completion of squares property, which is a critical Lemma in observer design based on the Lipschitz assumption (see Lemma 1.2). The proposed observer in this section is based on the poly-quadratic Lyapunov function, hence, the observer structure used is the one presented in (3.15)

3.3.1 Definitions

A Lipschitz function is a real-valued function defined on a metric space where there exists a positive constant δ such that for all pairs of points x, y in the domain, the absolute

difference in the function's values at those points is no greater than δ times the distance between the points.

Definition 3.1. *(Lipschitz Function) [Sohrab, 2003] Let I be an interval in the set of real numbers, $f : I \to \mathbb{R}$, and $\delta \in \mathbb{R}_+$. We say that f is Lipschitz function with Lipschitz constant δ if for all $x, y \in I$:*

$$|f(x) - f(y)| \leq \delta |x - y| \tag{3.18}$$

Consequently, a function that is differentiable on the interval I is Lipschitz on that interval if and only if its derivative remains bounded there.

The evaluation of the Lipschitz constant δ is detailed in Appendix B.

Before proceeding with the observer design, it is imperative to define the Lipschitz constant for the mismatching term. Therefore, the following assumptions are posited:

Assumption 3.1. *The weighting functions $\mu_i(\xi(t))$ are Lipschitz:*

$$|\mu_i(\xi(t)) - \mu_i\left(\hat{\xi}(t)\right)| \leq \delta_i |x(t) - \hat{x}(t)| \tag{3.19}$$

Assumption 3.2. *The system's state $x(t)$ is bounded:*

$$|x(t)| \leq \alpha_x, \tag{3.20}$$

Assumption 3.3. *The system's input $u(t)$ is bounded:*

$$|u(t)| \leq \alpha_u, \tag{3.21}$$

Based on the stated assumptions, the mismatching term $\omega_1(t)$ is bounded as follows:

$$\left| \sum_{i=1}^{r} \left(\mu_i(\xi(t)) - \mu_i\left(\hat{\xi}(t)\right)\right) (A_i x(t) + B_i u(t)) \right| \leq \beta |x(t) - \hat{x(t)}| \tag{3.22}$$

here, the value of β is determined by:

$$\beta = \sum_{i=1}^{r} \delta_i \rho_i, \tag{3.23}$$

with the terms ρ_i adhering to the constraints:

$$|(A_i x(t) + B_i u(t))| \leq \rho_i \tag{3.24}$$

The specifications for ρ_i are given by:

$$\rho_i = (\sigma_{max}(A_i)\alpha_x + \sigma_{max}(B_i)\alpha_u) \tag{3.25}$$

where, $\sigma_{max}(M)$ represents the largest singular value of the matrix M.

3.3.2 Observer design based on the poly-quadratic Lyapunov function

Consider the case of the state estimation error described (3.17). In order to study the stability of this system, the Lipschitz-based method is employed, with reliance on the following assumptions:

Assumption 3.4. *The mismatching term is Lipschitz:*

$$|\omega_1(t)| \leq \beta |e(t)| \Longleftrightarrow \omega_1(t)^T \omega_1(t) \leq \beta^2 e(t)^T e(t), \tag{3.26}$$

where β , positive scalar, is the Lipschitz constant.

Assumption 3.5. *The derivatives with respect to time for the weighting functions are constrained by positive constants, represented as $\emptyset_i$, described below:*

$$\left|\dot{\mu}_i\left(\hat{\xi}\right)\right| \leq \emptyset_i \tag{3.27}$$

Assumption 3.6. *The pairs (A_i, C) are observable (or at least detectable).*

The subsequent theorem offers adequate conditions for the stability of the estimation error dynamics, described as LMI:

Theorem 3.1

The estimation error converges asymptotically towards zero if there exist matrices $P_j = {P_j}^T \in \mathbb{R}^{n_x \times n_x} > 0, P_0 = {P_0}^T \in \mathbb{R}^{n_x \times n_x}, Q = Q^T \in \mathbb{R}^{n_x \times n_x} > 0$ and $L_i \in \mathbb{R}^{n_x \times n_y}$ such that $P_j \geq P_0$ and the following LMIs hold $\forall i, j = 1, ..., r$:

$$\mathcal{K}_{ii} < 0, \qquad i = 1, \ldots, r \tag{3.28}$$

$$\tfrac{1}{r-1}\mathcal{K}_{ii} + \tfrac{1}{2}\left(\mathcal{K}_{ij} + \mathcal{K}_{ji}\right) < 0, \qquad 1 \leq i \neq j \leq r \tag{3.29}$$

where:

$$\mathcal{K}_{ij} = \begin{bmatrix} M_{ij} & P_j \\ P_j & -Q \end{bmatrix} \tag{3.30}$$

$$M_{ij} = \left(P_j A_i - L_i C\right)^T + \left(P_j A_i - L_i C\right) + \beta^2 Q + \sum_{k=1}^{r} \emptyset_k \left(P_k - P_0\right) \tag{3.31}$$

Proof. Let us define the poly-quadratic candidate Lyapunov function as follows:

$$V(t) = e(t)^T P_\mu(t) e(t), \tag{3.32}$$

where $P_\mu(t)$ is defined in (3.14).

The time derivative of $V(t)$ is given by:

$$\dot{V}\left(t\right) = \dot{e}\left(t\right)^{T} P_{\mu} e\left(t\right) + e\left(t\right)^{T} P_{\mu} \dot{e}\left(t\right) + e\left(t\right)^{T} \dot{P}_{\mu} e\left(t\right) \tag{3.33}$$

Upon substituting (3.17) and (3.14) into (3.33), the subsequent expression is derived:

$$\begin{aligned} \dot{V}(t) = \sum_{i=1}^{r}\sum_{j=1}^{r} \mu_i(\hat{\xi}(t))\mu_j(\hat{\xi}(t)) \Big[e(t)^T \left({A_i}^T P_j - C^T L_i^T + P_j A_i - L_i C + \dot{P}_{\mu} \right) e(t) \\ + \omega_1(t)^T P_j e(t) + e(t)^T P_j \omega_1(t) \Big] \end{aligned} \tag{3.34}$$

By defining $X = \omega_1(t)$ and $Y = P_j e(t)$, Lemma 1.2 is employed as follows:

$$\omega_1(t)^T P_j e(t) + e(t)^T P_j \omega_1(t) \leq \omega_1(t)^T Q \omega_1(t) + e^T P_j Q^{-1} P_j e(t) \tag{3.35}$$

Consequently, the derivative of the Lyapunov function $\dot{V}\left(t\right)$ is constrained as follows:

$$\begin{aligned} \dot{V}(t) \leq \sum_{i=1}^{r}\sum_{j=1}^{r} \mu_i(\hat{\xi}(t))\mu_j(\hat{\xi}(t)) \Big[e(t)^T \left(A_i^T P_j - C^T L_i^T + P_j A_i - L_i C + \dot{P}_{\mu} \right) e(t) \\ + \omega_1(t)^T Q \omega_1(t) + e(t)^T P_j Q^{-1} P_j e(t) \Big] \end{aligned} \tag{3.36}$$

In contradiction to the method proposed in [Ichalal et al., 2012], here the matrix Q is used as a symmetric definite positive matrix, as described in Lemma 1.2, instead of as an identity matrix multiplied by a scalar. This choice offers more flexibility in defining appropriate values for the stability conditions, thereby reducing conservatism compared to the restriction of using a diagonal matrix with identical elements.

By using the Lipschitz condition specified in Assumption 3.4 on inequality (3.36), the negative value of $\dot{V}\left(t\right)$ is given by:

$$\sum_{i=1}^{r}\sum_{j=1}^{r} \mu_i(\hat{\xi}(t))\mu_j(\hat{\xi}(t)) \left[e^T \left({A_i}^T P_j - C^T {L_i}^T + P_j A_i - L_i C + \dot{P}_{\mu} + P_j Q^{-1} P_j + \beta^2 Q \right) e \right] < 0 \tag{3.37}$$

The conservatism associated with the time derivatives of the membership functions is mitigated by introducing a slack variable P_0 and employing Assumption 3.5, similarly to the proof of Theorem 1.2, as follows:

$$\textstyle\sum_{k=1}^{r} \dot{\mu}_k \left(\hat{\xi} \right) e^T P_k e = \sum_{k=1}^{r} \dot{\mu}_k \left(\hat{\xi} \right) e^T \left(P_k - P_0 \right) e, \tag{3.38}$$

the objective here is to identify the matrix P_0 such that the terms $(P_k - P_0)$ are minimized.

The time derivatives of the membership functions, being variable over time, will be systematically constrained as follows:

$$\sum_{k=1}^{r} \dot{\mu}_k(\hat{\xi}) \left(P_k - P_0 \right) \leq \sum_{k=1}^{r} \left| \dot{\mu}_k(\hat{\xi}) \right| \left(P_k - P_0 \right) = \sum_{k=1}^{r} \emptyset_k \left(P_k - P_0 \right), \tag{3.39}$$

such that the matrix P_0 has to verify $P_k - P_0 \geq 0$.

Then, the inequality (3.37) becomes:

$$\sum_{i=1}^{r}\sum_{j=1}^{r}\mu_i(\hat{\xi}(t))\mu_j(\hat{\xi}(t))\left[e^T\left(A_i^TP_j - C^TL_i^T + P_jA_i - L_iC + \sum_{k=1}^{r}\emptyset_k\left(P_k - P_0\right) + P_jQ^{-1}P_j + \beta^2Q\right)e\right] < 0 \tag{3.40}$$

Due to the non-linear nature of the product between decision variables $P_jQ^{-1}P_j$, this inequality does not present a linear form. To address this, the Schur complement, as outlined in Lemma 1.3, is employed, yielding the subsequent result:

$$\sum_{i=1}^{r}\sum_{j=1}^{r}\mu_i(\hat{\xi}(t))\mu_j(\hat{\xi}(t))\left[K_{ij}\right] < 0, \tag{3.41}$$

where K_{ij} is given in (3.30).

The advantage of employing the poly-quadratic Lyapunov function is evident here. The stability condition presented in (3.41) utilizes two symmetric parameters, μ_j and μ_j. As a result, the relaxation technique outlined in Lemma 1.5 can be applied, leading to the formulation presented in Theorem 3.1. □

Example 3: Lipschitz-based observer design for the Lorenz's chaotic system

In order to study the feasibility of the proposed observer, let us consider the same example used in [Ichalal et al., 2012] given as follows:

$$\begin{cases}\dot{x}_1 = \sigma(x_2 - x_1)\\ \dot{x}_2 = x_1(\rho - x_3) - x_2\\ \dot{x}_3 = x_1x_2 - \beta x_3\end{cases} \tag{3.42}$$

By defining $x\left(t\right) = \begin{bmatrix}x_1 & x_2 & x_3\end{bmatrix}^T$, the state space representation of the Lorenz's chaotic system is presented as follows:

$$\begin{cases}\dot{x}\left(t\right) = A\left(x\right)x\left(t\right)\\ y(t) = Cx\left(t\right)\end{cases} \tag{3.43}$$

where:

$$A\left(x\right) = \begin{bmatrix}-\sigma & \sigma & 0\\ \rho & -1 & -x_1\\ 0 & x_1 & -\beta\end{bmatrix}, C = \begin{bmatrix}0 & 1 & 0\\ 0 & 0 & 1\end{bmatrix}$$

The parameters of Lorenz's chaotic system are: $\sigma = 10$, $\rho = 28$ and $\beta = 8/3$.

By defining the premise variable as $\xi = x_1$ and using the sector nonlinearity method, the following results are obtained:

$$A_1 = \begin{bmatrix} -\sigma & \sigma & 0 \\ \rho & -1 & -x_{1max} \\ 0 & x_{1max} & -\beta \end{bmatrix}, A_2 = \begin{bmatrix} -\sigma & \sigma & 0 \\ \rho & -1 & -x_{1min} \\ 0 & x_{1min} & -\beta \end{bmatrix},$$

$$B_1 = B_2 = \begin{bmatrix} 0 \\ 0 \\ 0 \end{bmatrix}, C = \begin{bmatrix} 0 & 1 & 0 \\ 0 & 0 & 1 \end{bmatrix}, \mu_1(\xi) = \frac{x_1(t) - x_{1min}}{x_{1max} - x_{1min}}, \quad \mu_2(\xi) = 1 - \mu_1(\xi)$$

where $x_1(t)$ is bounded as $-20 \leq x_1(t) \leq 20$ and the derivatives with respect to time for the membership functions are bounded by $\emptyset_k = 30$, $k \in \{1, 2\}$.

Theorem 1 given in [Ichalal et al., 2012] is not applicable for the computed Lipschitz constant $\beta = 173.35$, where it is only applicable for values smaller than 29.73. On the other hand, Theorem 3.1 proposed in our work is applicable for $\beta = 173.35$ or even bigger values. Applying this theorem to the example yields the following matrices:

$$P_1 = \begin{bmatrix} 0.0022 & -0.0748 & 0.0007 \\ -0.0748 & 3.3876 & -0.0330 \\ 0.0007 & -0.0330 & 1.9444 \end{bmatrix}, P_2 = \begin{bmatrix} 0.0052 & -0.1042 & -0.0006 \\ -0.1042 & 3.0826 & 0.0236 \\ -0.0006 & 0.0236 & 1.9434 \end{bmatrix}$$

$$P_0 = \begin{bmatrix} -0.0091 & -0.0883 & 0.0002 \\ -0.0883 & 0.0697 & -0.0053 \\ 0.0002 & -0.0053 & -2.5386 \end{bmatrix}, Q = \begin{bmatrix} 0.0001 & -0.0004 & 0 \\ -0.0004 & 0.0287 & 0 \\ 0 & 0 & 0.0270 \end{bmatrix}$$

$$L_1 = \begin{bmatrix} 74.9403 & 0.7897 \\ 911.4833 & -15.8440 \\ -15.8440 & 874.5624 \end{bmatrix}, L_2 = \begin{bmatrix} 61.4690 & -1.3963 \\ 908.8857 & 12.9959 \\ 12.9959 & 874.5045 \end{bmatrix}$$

To illustrate the convergence of the estimation error, the initial conditions of the system were set to $x_0 = \begin{bmatrix} 10 & -3 & 10 \end{bmatrix}^T$, while the observer's initial conditions were defined as $\hat{x}_0 = \begin{bmatrix} 0 & 10 & 40 \end{bmatrix}^T$. The following results were obtained:

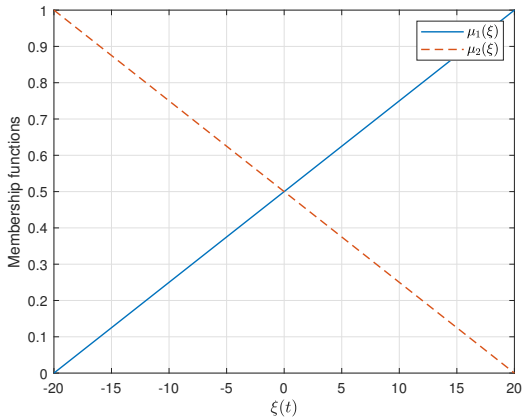

Fig 3.2: Membership functions $\mu_1(\xi(t))$ and $\mu_2(\xi(t))$.

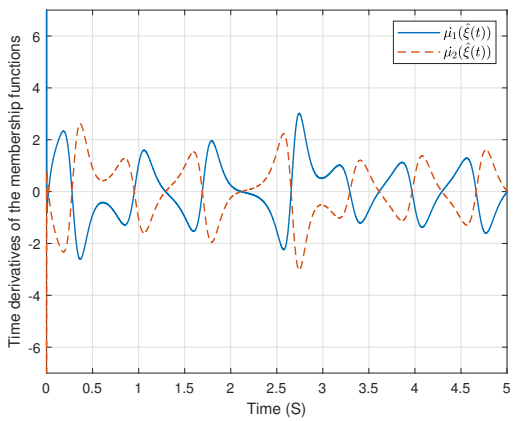

Fig 3.3: Time derivatives of the membership functions.

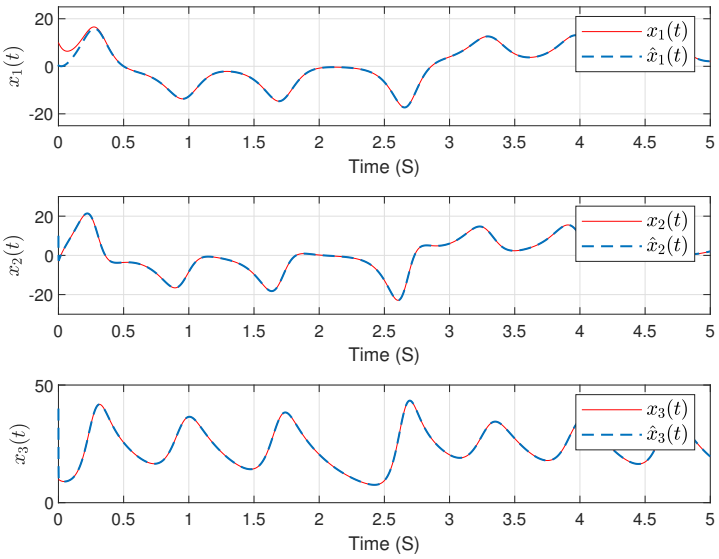

Fig 3.4: Real states and their estimations.

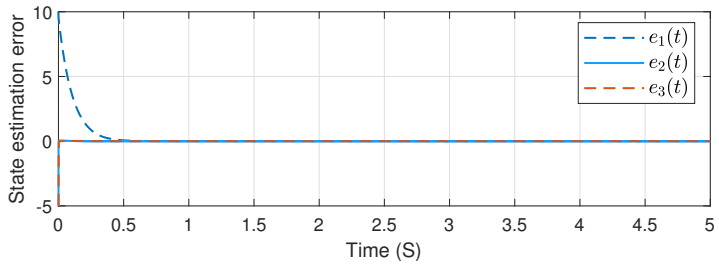

Fig 3.5: State estimation error.

Figure Figure 3.2 presents the membership function curves. The results indicate that these functions satisfy the convex sum property described in equation (3.2), as they are positive and their sum equals one. Additionally, Figure 3.3 illustrates the time derivatives of these membership functions. The results confirm that their upper absolute values are consistent with those defined earlier in the design process of the observer.

As illustrated in Figure 3.4, the estimated states tracked the real ones despite the different initial conditions of both of them, which proves the convergence of the state estimation error to zero and at the same time proves the feasibility of the relaxation proposed in this paper compared to Theorem 1 given in [Ichalal et al., 2012].

3.4 $\mathcal{L}_2$-attenuation approach based observer

Despite efforts to enhance the performance of the Lipschitz-based observer, it continues to demonstrate significant limitations, particularly when the Lipschitz constant surpasses acceptable threshold [Ichalal et al., 2007, Ichalal et al., 2008]. To address these challenges, the $\mathcal{L}_2$-attenuation approach has been introduced as an alternative. Unlike its predecessor, this method does not depend on the Lipschitz condition, thereby offering increased flexibility and reduced conservatism. The subsequent section will elaborate on how this method effectively mitigates the challenges associated with mismatching terms and addresses the impact of noise on measurements.

3.4.1 Definitions

The $\mathcal{L}_2$-gain synthesis is a robust method that focuses on optimizing the worst-case performance of a system against disturbances. Fundamentally, the $\mathcal{L}_2$-gain of a system is a measure of the maximum energy amplification a system can exhibit in response to an external disturbance, with the aim to minimize (attenuate) this gain to improve system robustness. By reducing this amplification factor, the system becomes better equipped to maintain its performance and stability, even when faced with unpredictable external inputs or disturbances. The concept of $\mathcal{L}_2$-gain synthesis is an extension of H_∞ norm of linear systems. Hence, $\mathcal{L}_2$-gain synthesis problem is usually called the nonlinear H_∞ control problem.

In observer design, employing the $\mathcal{L}_2$-attenuation involves creating an observer capable of estimating system states through the determination of observer gains $L_i(t)$, which are optimized to minimize sensitivity to disturbances $d(t)$ (mismatching terms, noise, etc.). Therefore, the stability of the estimation error dynamics can be studied by minimizing the $\mathcal{L}_2$-gain , denoted γ, which reflects the effect of the disturbance $d(t)$ on the estimation error $e(t) = x(t) - \hat{x}(t)$.

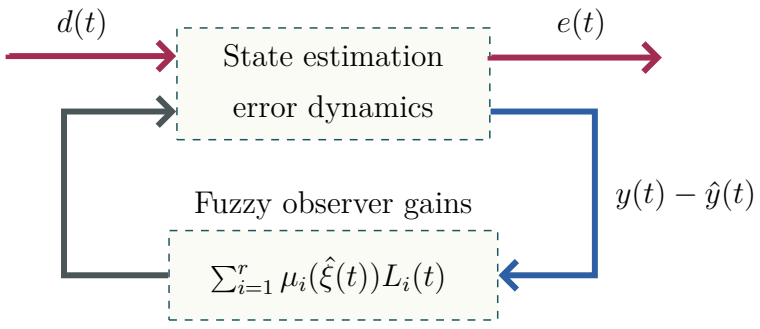

Fig 3.6: Robust Observation problem.

In order to design an observer based on the $\mathcal{L}_2$-attenuation approach, the following definitions are necessary:

Definition 3.2. *($\mathcal{L}_2$-norm). The $\mathcal{L}_2$-norm of signal $d(t)$, denoted $\|d(t)\|_2$ is defined by:*

$$\|d(t)\|_2 = \left(\int_{-\infty}^{+\infty} d(t)^T d(t) dt\right)^{1/2} \tag{3.44}$$

Definition 3.3. *($\mathcal{L}_2$-gain). The $\mathcal{L}_2$-gain of the system with input $d(t)$ and output $e(t)$ is:*

$$\gamma = sup\ \frac{\|e(t)\|_2}{\|d(t)\|_2} \tag{3.45}$$

Lemma 3.1. *The amplification from $d(t)$ to $e(t)$ is bounded by γ as $\frac{\|e(t)\|_2}{\|d(t)\|_2} \leq \gamma$ if there exists a Lyapunov function $V(t)$, such that:*

$$\dot{V}(t) + e(t)^T e(t) - \gamma^2 d(t)^T d(t) < 0 \tag{3.46}$$

3.4.2 Observer design by attenuating the mismatching terms

Consider the case of the state estimation error described in (3.12), which corresponds to the use of the quadratic Lyapunov function in the case of a linear output equation. In order to study its stability, the $\mathcal{L}_2$-attenuation method is employed by defining the disturbance $d(t)$ as the mismatching term $\omega_1(t)$, and with reliance on the following assumptions:

Assumption 3.7. *The nonlinear system is stable which leads to bounded state.*

Assumption 3.8. *The system's input $u(t)$ is bounded.*

Assumption 3.9. *The pairs (A_i, C) are observable (or at least detectable).*

The subsequent theorem offers adequate conditions for the stability of the estimation error dynamics, described as LMI:

Theorem 3.2

The estimation error is asymptotically stable and the $\mathcal{L}_2$ performance is guaranteed with an attenuation level γ, if there exist matrices $P = P^T \in \mathbb{R}^{n_x \times n_x} > 0, M_i \in \mathbb{R}^{n_x \times n_y}$ and positive scalar $\bar{\gamma}$ such that the following minimization problem holds $\forall i = 1, ..., r$:

$$\min \bar{\gamma} \tag{3.47}$$

$$\begin{bmatrix} A_i{}^T P + P A_i - M_i C - C^T M_i{}^T + I & P \\ P & -\bar{\gamma} I \end{bmatrix} < 0 \tag{3.48}$$

where the observer gains are given by $L_i = P^{-1} M_i$.

Proof. The stability of the estimation error dynamics is studied using the quadratic Lyapunov function $V(t) = e(t)^T P e(t)$, where its derivative is given by:

$$\dot{V}(t) = \dot{e}(t)^T P e(t) + e(t)^T P \dot{e}(t) \tag{3.49}$$

Upon substituting (3.12) into (3.49), the subsequent expression is derived:

$$\dot{V}(t) = \sum_{i=1}^{r} \mu_i \left(\hat{\xi}(t)\right) e(t)^T ((A_i - L_i C)^T P + P(A_i - L_i C)) e(t) + \omega_1(t)^T P e(t) + e(t)^T P \omega_1(t) \tag{3.50}$$

Substituting (3.50) in (3.46), where $d(t) = \omega_1(t)$, we obtain the following inequality:

$$\sum_{i=1}^{r} \mu_i \left(\hat{\xi}(t)\right) \begin{bmatrix} e \\ d \end{bmatrix}^T \begin{bmatrix} A_i{}^T P + P A_i - P L_i C - C^T L_i{}^T P + I & P \\ P & -\gamma^2 I \end{bmatrix} \begin{bmatrix} e \\ d \end{bmatrix} < 0 \tag{3.51}$$

By using the change of variables $M_i = P L_i$ and $\bar{\gamma} = \gamma^2$, Theorem 3.2 is obtained. □

Example 4: $\mathcal{L}_2$-attenuation based observer design for separately excited DC motor

1 - Modeling of the Separately Excited Dc Motor

Figure 3.7 showcases the Separately Excited DC Motor (SE-DCM), which comprises two core components: the stator, a stationary part, and the armature, a rotating element. The stator establishes a magnetic field utilizing an external DC source, represented as V_f, with i_f denoting the current flowing through it. On the other hand, the armature yields mechanical output, powered by a separate DC source, symbolized as V_a. The current flowing through the armature is indicated as i_a. Within this context, ω signifies the electrical angular speed, and T_L designates the load torque applied to the rotating part. The definitions for the remaining parameters can be found in Table 3.1.

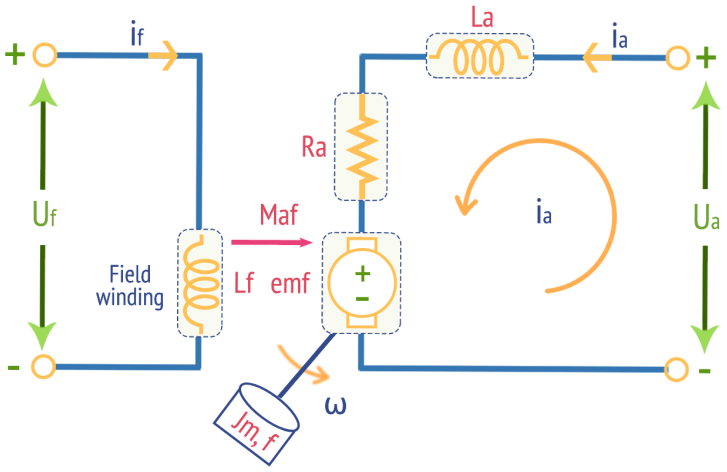

Fig 3.7: Separately Excited DC Motor Structure.

Based on the equivalent circuit expressed in Figure 3.7, the mathematical model of the motor is giving as follows:

$$\begin{cases} V_f &= R_f i_f + L_f \frac{di_f}{dt} \\ V_a &= R_a i_a + L_a \frac{di_a}{dt} + \omega M_{af} i_f \\ \frac{J_m}{p}\frac{d\omega}{dt} &= M_{af} i_f i_a - \frac{f}{p}\omega - T_L \end{cases} \tag{3.52}$$

By defining $x(t) = \begin{bmatrix} i_f & i_a & \omega \end{bmatrix}^T$, $u(t) = \begin{bmatrix} V_f & V_a \end{bmatrix}^T$, the state space representation of the SE-DCM is presented as follows:

$$\begin{cases} \dot{x}(t) = A(x)\,x(t) + Bu(t) + ET_L(t) \\ y(t) = Cx(t) \end{cases} \tag{3.53}$$

where:

$$A(x) = \begin{bmatrix} -\frac{R_f}{L_f} & 0 & 0 \\ 0 & -\frac{R_a}{L_a} & -\frac{M_{af}}{L_a} i_f \\ 0 & \frac{p}{J_m} M_{af} i_f & -\frac{f}{J_m} \end{bmatrix}, B = \begin{bmatrix} \frac{1}{L_f} & 0 \\ 0 & \frac{1}{L_a} \\ 0 & 0 \end{bmatrix}, E = \begin{bmatrix} 0 \\ 0 \\ -\frac{p}{J_m} \end{bmatrix}, C = \begin{bmatrix} 1 & 0 & 0 \\ 0 & 1 & 0 \end{bmatrix}$$

The parameters of the motor are giving in the following table:

Parameters	**Values**
Armature resistance	$R_a = 6.67\ [\Omega]$
Field resistance	$R_f = 880\ [\Omega]$
Armature inductance	$L_a = 0.198\ [H]$
Field inductance	$L_f = 55.366\ [H]$
Armature-field mutual inductance	$M_{af} = 5.213\ [H]$
Moment of inertia	$J_m = 0.0398\ [kg.\ m^2]$
Number of pole pairs	$p = 2$
Viscous friction coefficient	$f = 0.001\ [Nm]$

Table 3.1: Separately Excited DC Motor parameters

2 - Takagi-Sugeno fuzzy representation of the system

The T-S multi-model is given as follows:

$$\begin{cases} \dot{x}(t) = \sum_{i=1}^{r} \mu_i(x(t)) \left(A_i x(t) + B_i u(t) + E_i T_L(t)\right) \\ y(t) = Cx(t) \end{cases} \tag{3.54}$$

By defining the premise variable as $\xi = i_f$ as the nonlinear terms in the dynamical model of the SE-DCM in (3.53), the weighting functions can be described as follows:

$$\mu_1(x(t)) = W_1(\xi) \text{ and } \mu_2(x(t)) = W_2(\xi)$$

where using the sector nonlinearity approach, the following functions are obtained:

$$W_1(\xi) = \frac{\xi - \xi_{min}}{\xi_{max} - \xi_{min}}, W_2(\xi_i) = \frac{\xi_{max} - \xi}{\xi_{max} - \xi_{min}}$$

The sub-matrices A_i, B_i and E_i of the multi-model (3.54) are giving using the sector nonlinearity approach as follows:

$$A_1 = \begin{bmatrix} -\frac{R_f}{L_f} & 0 & 0 \\ 0 & -\frac{R_a}{L_a} & -\frac{M_{af}}{L_a} i_{f\,max} \\ 0 & \frac{p}{J_m} M_{af} i_{f\,max} & -\frac{f}{J_m} \end{bmatrix}, A_2 = \begin{bmatrix} -\frac{R_f}{L_f} & 0 & 0 \\ 0 & -\frac{R_a}{L_a} & -\frac{M_{af}}{L_a} i_{f\,min} \\ 0 & \frac{p}{J_m} M_{af} i_{f\,min} & -\frac{f}{J_m} \end{bmatrix}$$

$$B_i = \begin{bmatrix} \frac{1}{L_f} & 0 \\ 0 & \frac{1}{L_a} \\ 0 & 0 \end{bmatrix}, E_i = \begin{bmatrix} 0 \\ 0 \\ -\frac{p}{J_m} \end{bmatrix} \quad \forall i = 1 \ldots 2.$$

3 - Observer design for the separately excited DC motor

By considering the output as field and armature currents $y(t) = \begin{bmatrix} i_f & i_a \end{bmatrix}^T$, Theorem 3.2 is applied to derive the following gains:

$$L_1 = \begin{bmatrix} 617.4613 & 0 \\ 0 & 607.0818 \\ 0 & -2.4956 \times 10^6 \end{bmatrix}, L_2 = \begin{bmatrix} 617.4613 & 0 \\ 0 & 607.0818 \\ 0 & 2.4956 \times 10^6 \end{bmatrix},$$

$$P = \begin{bmatrix} 3.8394 & 0 & 0 \\ 0 & 3.7766 & 0 \\ 0 & 0 & 0.0004 \end{bmatrix} \times 10^5, \qquad \gamma = 39.8002$$

4 - Simulation results

To demonstrate the stability of the error dynamics, the initial conditions of the system were set to $x_0(t) = \begin{bmatrix} 0 & 0 & 0 \end{bmatrix}^T$, while the initial conditions of the observer were defined as $\hat{x}_0(t) = \begin{bmatrix} 0.2 & 5 & 10 \end{bmatrix}^T$. The results obtained from this test are depicted in Figure 3.8 through Figure 3.10. Figure 3.8 and Figure 3.9, individually illustrate the actual currents and their respective estimations, while Figure 3.10 displays the estimation of the electrical speed.

As observed, despite the differing initial conditions between the system and the observer, the observer still managed to accurately estimate the real states of the system. The estimation error asymptotically converged to zero, affirming the efficacy of the theorem.

On the other hand, the results demonstrate that the derived observer gains have successfully ensured that the amplification from the mismatching term $\omega_1(t)$ to the

estimation error $e(t)$ is minimized and bounded by γ, Consequently, this proves the feasibility of using the $\mathcal{L}_2$-gain synthesis to design an observer for the SE-DCM. Notably, employing the Lipschitz-based method for designing the observer was found to be inapplicable.

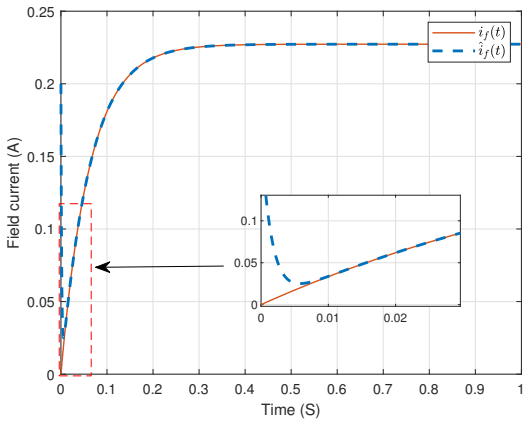

Fig 3.8: Field current estimation.

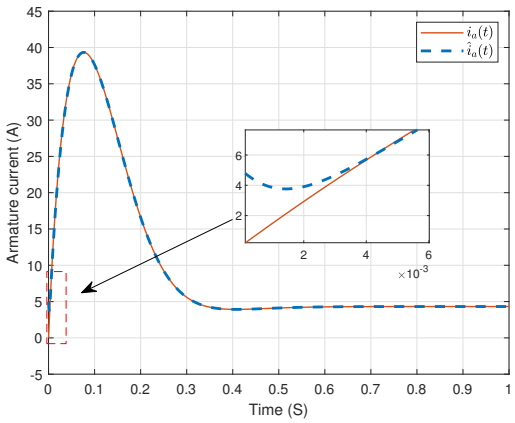

Fig 3.9: Armature current estimation.

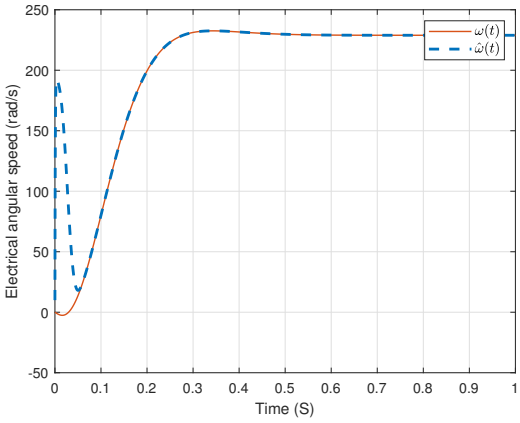

Fig 3.10: Electrical angular speed estimation.

3.4.3 Observer design in the presence of measurement noise

In this section, the case of measurements affected by noise, denoted as $\varphi(t) \in \mathbb{R}^{n_\varphi}$, will be studied. The focus is on the scenario where the output equation of the T-S multi-model is linear ($C_i = C$ and $D_i = D$):

$$\begin{cases} \dot{x}(t) = \sum_{i=1}^{r} \mu_i \left(\hat{\xi}(t)\right) \left(A_i x(t) + B_i u(t) + \omega_1(t)\right) \\ y(t) = Cx(t) + Du(t) + W_y \varphi(t) \end{cases} \tag{3.55}$$

where, $W_y \in \mathbb{R}^{n_y \times n_\varphi}$ is the influence matrix of the noise $\varphi(t)$ on the measurements.

The observer considered for this system is given by:

$$\begin{cases} \dot{\hat{x}}(t) = \sum_{i=1}^{r} \mu_i \left(\hat{\xi}(t)\right) \left(A_i \hat{x}(t) + B_i u(t) + L_i \left(y(t) - \hat{y}(t)\right)\right) \\ \hat{y}(t) = C\hat{x}(t) + Du(t) \end{cases} \tag{3.56}$$

which is the same observer given in (3.10) but in the case of linear output equation.

The subsequent theorem offers adequate conditions for the stability of the estimation error dynamics, described as LMI:

Theorem 3.3

The estimation error is asymptotically stable and the $\mathcal{L}_2$ performance is guaranteed with an attenuation level γ, if there exist matrices $P = P^T \in \mathbb{R}^{n_x \times n_x} > 0, M_i \in \mathbb{R}^{n_x \times n_y}$ and positive scalar $\bar{\gamma}$ such that the following minimization problem holds $\forall i = 1, ..., r$:

$$\min \bar{\gamma} \tag{3.57}$$

$$\begin{bmatrix} {A_i}^T P + P A_i - M_i C - C^T {M_i}^T + I & P & -M_i W_y \\ P & -\bar{\gamma} I & 0 \\ -{W_y}^T {M_i}^T & 0 & -\bar{\gamma} I \end{bmatrix} < 0 \tag{3.58}$$

where the observer gains are given by $L_i = P^{-1} M_i$.

Proof. The dynamics of the estimation error $e(t) = x(t) - \hat{x}(t)$ are given as follows:

$$\dot{e}(t) = \sum_{i=1}^{r} \mu_i \left(\hat{\xi}(t)\right) \left((A_i - L_i C) e(t) + \left(\widetilde{W}_x - L_i \widetilde{W}_y\right) d(t) \right), \tag{3.59}$$

where:

$$\widetilde{W}_x = \begin{bmatrix} I & 0 \end{bmatrix}, \ \widetilde{W}_y = \begin{bmatrix} 0 & W_y \end{bmatrix}, \ d(t) = \begin{bmatrix} \omega_1(t) \\ \varphi(t) \end{bmatrix}$$

To study the stability of the error dynamics, the quadratic Lyapunov function is used:

$$V(t) = e(t)^T P e(t) \tag{3.60}$$

The derivative of $V(t)$ with respect to t is:

$$\begin{aligned} \dot{V}(t) = & \textstyle\sum_{i=1}^{r} \mu_i \left(\hat{\xi}(t)\right) e(t)^T \left((A_i - L_i C)^T P + P (A_i - L_i C) \right) e(t) \\ & + d(t)^T \left(\widetilde{W}_x - L_i \widetilde{W}_y\right)^T P e(t) + e(t)^T P \left(\widetilde{W}_x - L_i \widetilde{W}_y\right) d(t) \end{aligned} \tag{3.61}$$

To achieve the $\mathcal{L}_2$ performance, we substitute (3.61) into (3.46) to obtain the following inequality:

$$\sum_{i=1}^{r} \mu_i \left(\hat{\xi}(t)\right) \begin{bmatrix} e \\ d \end{bmatrix}^T \begin{bmatrix} {A_i}^T P + P A_i - P L_i C - C^T {L_i}^T P + I & P \left(\widetilde{W}_x - L_i \widetilde{W}_y\right) \\ \left(\widetilde{W}_x - L_i \widetilde{W}_y\right)^T P & -\gamma^2 I \end{bmatrix} \begin{bmatrix} e \\ d \end{bmatrix} < 0 \tag{3.62}$$

Using the change of variables $M_i = P L_i$ and $\bar{\gamma} = \gamma^2$, and replacing $\widetilde{W}_x$ and $\widetilde{W}_y$ by their values, Theorem 3.3 is obtained. □

Example 5: Robust observer design for separately excited DC motor

The same system from the previous example will be employed here, maintaining the same initial conditions for both the system and the observer.

1 - Observer design for the separately excited DC motor

By considering the output as field and armature currents $y(t) = \begin{bmatrix} i_f & i_a \end{bmatrix}^T$, and defining the influence matrix W_y as:

$$W_y = \begin{bmatrix} 1 \\ 1 \end{bmatrix},$$

the method outlined in Theorem 3.3 is applied to derive the following results:

$$L_1 = \begin{bmatrix} 66.7819 & -66.7294 \\ -107.5522 & 107.6149 \\ 3.8664 \times 10^5 & -3.8664 \times 10^5 \end{bmatrix}, L_2 = \begin{bmatrix} 66.7819 & -66.7294 \\ -107.5522 & 107.6149 \\ -3.8664 \times 10^5 & 3.8664 \times 10^5 \end{bmatrix},$$

$$P = \begin{bmatrix} 8.8287 & -5.8449 & 0 \\ -5.8449 & 5.8845 & 0 \\ 0 & 0 & 0.0040 \end{bmatrix} \times 10^4$$

2 - Simulation results

In studying the observer's reliability against sensor noise, a random noise amplitude of $2(A)$ was introduced to the system's output vector. The results obtained from this are depicted in Figure 3.11 through Figure 3.14. Figure 3.11 presents the noise-distorted measured currents alongside the real currents and their estimations. Figure 3.12 and Figure 3.13, individually illustrate the actual currents and their respective estimations, while Figure 3.14 displays the estimation of the electrical speed.

As observed, despite the presence of noise in the measurements and the differing initial conditions between the system and the observer, the observer still managed to accurately estimate the real states of the system. The estimation error asymptotically converged to zero, affirming the efficacy of the proposed theorem.

The T-S representation of the SE-DCM, as depicted in (3.54), utilizes i_f as its premise variable, which is measurable in this example. This naturally allows observer design to be based on MPV approach discussed in Chapter 2. However, these measurements are distorted by noise interference, rendering them unsuitable for use. As a solution, the proposed observer design navigates around this issue by dealing with an unmeasurable premise variable. This approach circumvents the use of noisy measured current and concurrently ensures the observer's robustness, guaranteeing accurate acquisition of the system's states.

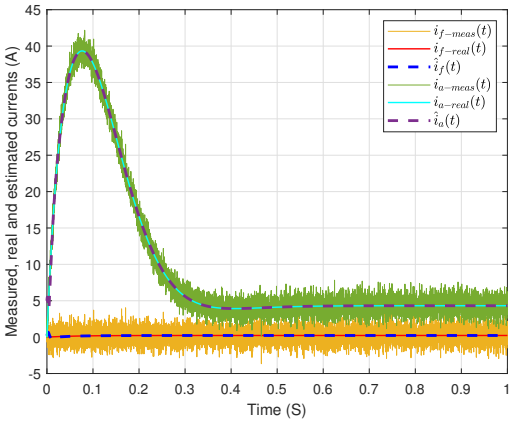

Fig 3.11: Measured, real and estimated currents.

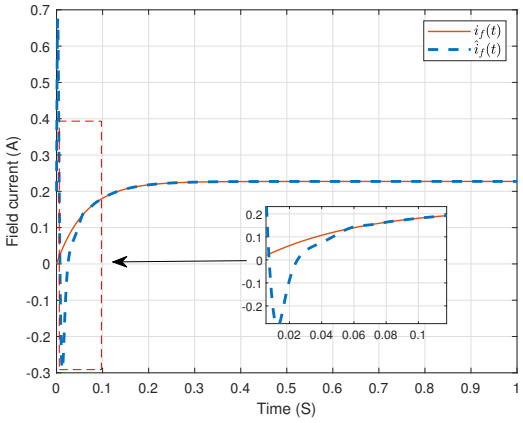

Fig 3.12: Field current estimation.

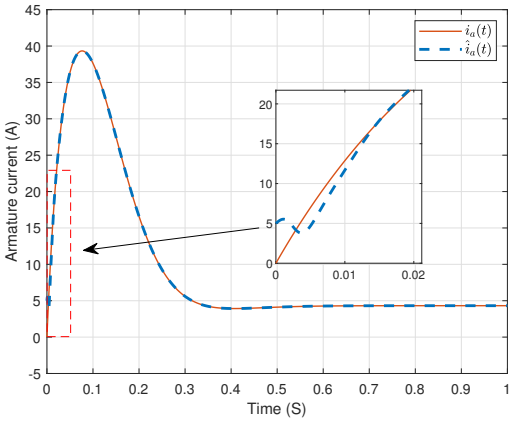

Fig 3.13: Armature current estimation.

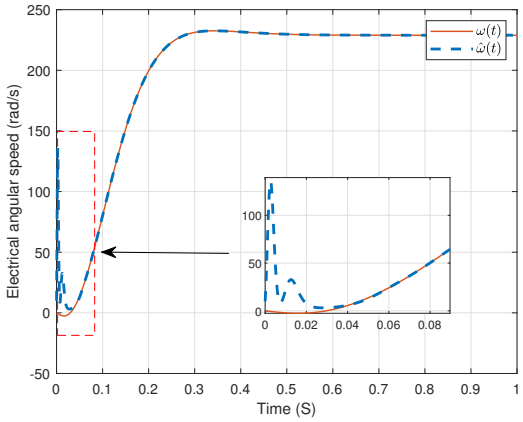

Fig 3.14: Electrical angular speed estimation.

3.4.4 Observer design for fuzzy output equation based on the poly-quadratic Lyapunov function

In this section, the study focuses on the case of fuzzy output equations. Consideration is given to the T-S system (3.3) and its corresponding observer (3.15). This scenario pertains to the state estimation error outlined in (3.16). To analyze the system's stability, the $\mathcal{L}_2$-attenuation method is employed, based on the following assumptions:

Assumption 3.10. *The nonlinear system is stable and the input $u(t)$ is bounded.*

Assumption 3.11. *The derivatives with respect to time for the weighting functions are constrained by positive constants, represented as $\emptyset_i$, described below:*

$$\left|\dot{\mu}_i\left(\hat{\xi}\right)\right| \leq \emptyset_i \tag{3.63}$$

Assumption 3.12. *The pairs (A_i, C_i) are observable (or at least detectable).*

The subsequent theorem offers adequate conditions for the stability of the estimation error dynamics, described as LMI:

Theorem 3.4

The estimation error is asymptotically stable and the $\mathcal{L}_2$ performance is guaranteed with an attenuation level γ, if there exist matrices $P_j = {P_j}^T \in \mathbb{R}^{n_x \times n_x} > 0, P_0 = {P_0}^T \in \mathbb{R}^{n_x \times n_x}, L_j \in \mathbb{R}^{n_x \times n_y}$ and positive scalar $\bar{\gamma}$ such that $P_j \geq P_0$ and the following minimization problem holds $\forall i, j = 1, ..., r$:

$$\min \bar{\gamma} \tag{3.64}$$

$$\mathcal{K}_{ii} < 0, \qquad i = 1, \ldots, r \tag{3.65}$$

$$\tfrac{1}{r-1}\mathcal{K}_{ii} + \tfrac{1}{2}\left(\mathcal{K}_{ij} + \mathcal{K}_{ji}\right) < 0, \qquad 1 \leq i \neq j \leq r \tag{3.66}$$

where:

$$\mathcal{K}_{ij} = \begin{bmatrix} {A_i}^T P_j + P_j A_i - L_j C_i - C_i^T {L_j}^T + I & P_j & -L_j \\ P_j & -\bar{\gamma} I & 0 \\ -{L_j}^T & 0 & -\bar{\gamma} I \end{bmatrix} \tag{3.67}$$

Proof. Let us define the poly-quadratic candidate Lyapunov function as follows:

$$V\left(t\right) = e\left(t\right)^T P_\mu(t) e\left(t\right), \tag{3.68}$$

where $P_\mu(t)$ is defined in (3.14).

The time derivative of $V(t)$ is given by:

$$\dot{V}\left(t\right) = \dot{e}\left(t\right)^T P_\mu e\left(t\right) + e\left(t\right)^T P_\mu \dot{e}\left(t\right) + e\left(t\right)^T \dot{P}_\mu e\left(t\right) \tag{3.69}$$

Upon substituting (3.16) and (3.14) into (3.69), the subsequent expression is derived:

$$\begin{aligned} \dot{V}(t) = \sum_{i=1}^{r}\sum_{j=1}^{r} \mu_i(\hat{\xi}(t))\mu_j(\hat{\xi}(t)) \Big[& e(t)^T \left({A_i}^T P_j - C_i^T L_j^T + P_j A_i - L_j C_i + \dot{P}_\mu \right) e(t) \\ & + \omega_1(t)^T P_j e(t) + e(t)^T P_j \omega_1(t) + \omega_2(t)^T (-L_j)^T e(t) + e(t)^T (-L_j)\omega_2(t) \Big] \end{aligned} \tag{3.70}$$

This equation can be formulated as follows:

$$\begin{aligned} \dot{V}(t) = \sum_{i=1}^{r}\sum_{j=1}^{r} \mu_i(\hat{\xi}(t))\mu_j(\hat{\xi}(t)) \Big[& e(t)^T \left(A_i^T P_j - C_i^T L_j^T + P_j A_i - L_j C_i + \dot{P}_\mu \right) e(t) \\ & + d(t)^T \left(P_j \widetilde{W}_x - L_j \widetilde{W}_y \right)^T e(t) + e(t)^T \left(P_j \widetilde{W}_x - L_j \widetilde{W}_y \right) d(t) \Big] \end{aligned} \tag{3.71}$$

where:

$$\widetilde{W}_x = \begin{bmatrix} I & 0 \end{bmatrix}, \ \widetilde{W}_y = \begin{bmatrix} 0 & I \end{bmatrix}, \ d\left(t\right) = \begin{bmatrix} \omega_1(t) \\ \omega_2(t) \end{bmatrix}$$

To achieve the $\mathcal{L}_2$ performance, we substitute (3.71) into (3.46) to obtain the following inequality:

$$\sum_{i=1}^{r}\sum_{j=1}^{r}\mu_i(\hat{\xi}(t))\mu_j(\hat{\xi}(t))\begin{bmatrix}e\\d\end{bmatrix}^T \begin{bmatrix}A_i^TP_j - C_i^TL_j^T + P_jA_i - L_jC_i + I + \dot{P}_\mu & \left(P_j\widetilde{W}_x - L_j\widetilde{W}_y\right)\\ \left(P_j\widetilde{W}_x - L_j\widetilde{W}_y\right)^T & -\gamma^2 I\end{bmatrix}\begin{bmatrix}e\\d\end{bmatrix} < 0 \tag{3.72}$$

Using the change of variables $\bar{\gamma} = \gamma^2$, substituting $\widetilde{W}_x$ and $\widetilde{W}_y$ with their values, and introducing the slack variable P_0 similarly to the proof of Theorem 3.1, Theorem 3.4 is derived. □

Example 6:

To examine the feasibility of the observer, consider the following system:

$$A_1 = \begin{bmatrix}-10 & -1\\ -20 & -20\end{bmatrix}, A_2 = \begin{bmatrix}-10 & 15\\ -10 & 6\end{bmatrix}, C_1 = \begin{bmatrix}0 & 1\\ 0 & -6\end{bmatrix}, C_2 = \begin{bmatrix}2 & 0\\ -2 & -5\end{bmatrix},$$

$$B_1 = B_2 = \begin{bmatrix}-0.2\\ 0.03\end{bmatrix}, \mu_1(\xi) = \frac{sin(0.2x_1(t))}{2}, \quad \mu_2(\xi) = 1 - \mu_1(\xi)$$

where the time derivatives of the membership functions are bounded by $\emptyset_k = 40$.

Applying Theorem 3.4 to this example yields the following results:

$$P_1 = \begin{bmatrix}1\times10^7 & 6.288\times10^6\\ 6.288\times10^6 & 1.9966\times10^7\end{bmatrix}, P_2 = \begin{bmatrix}9.9997\times10^6 & 6.2277\times10^6\\ 6.2277\times10^6 & 1.1898\times10^7\end{bmatrix}$$

$$L_1 = \begin{bmatrix}3.2796\times10^7 & 1.4204\times10^6\\ 3.0603\times10^7 & -1.9690\times10^8\end{bmatrix}, L_2 = \begin{bmatrix}3.0283\times10^7 & -1.2946\times10^7\\ -1.7123\times10^7 & -2.2219\times10^8\end{bmatrix}$$

To illustrate the convergence of the estimation error, the initial conditions of the system were set to $x_0 = \begin{bmatrix}0.2 & 5\end{bmatrix}^T$, while the observer's initial conditions were defined as $\hat{x}_0 = \begin{bmatrix}0 & 0\end{bmatrix}^T$. The following results were obtained:

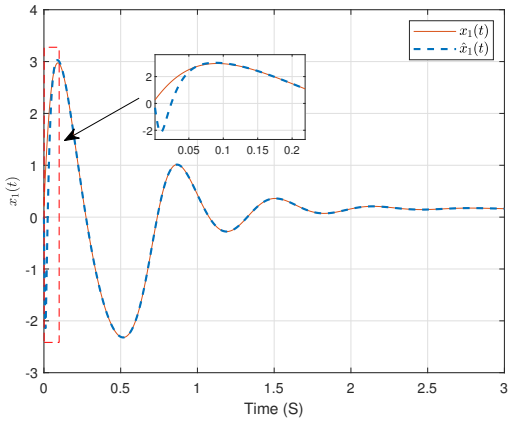

Fig 3.15: State $x_1(t)$ and its estimation.

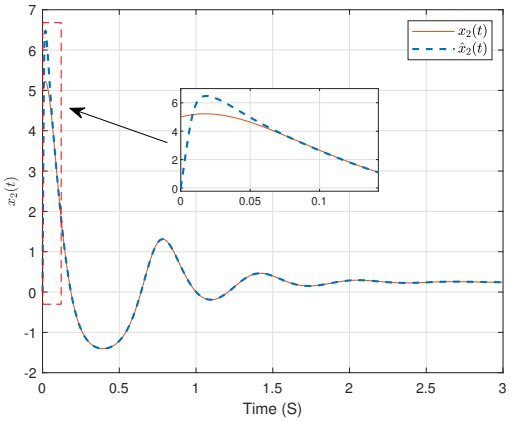

Fig 3.16: State $x_2(t)$ and its estimation.

3.5 Mean Value Theorem based observer

While the $\mathcal{L}_2$-gain synthesis is typically less conservative than the Lipschitz method, there are cases where it fails to provide an adequately low attenuation level, rendering it unsatisfactory even in successful simulations. Moreover, since the disturbance explicitly depends on the system state and control input, its effects on the error dynamics strongly depend on the behaviors of the nonlinear system [Nguyen et al., 2021]. Consequently, this section introduces an alternative formulation of the Lipschitz method: the Differential Mean Value Theorem. As explained in the introduction, this approach allows for the factorization of the estimation error dynamics, making it proportional completely to the estimation error. Therefore, effectively eliminating the mismatching terms from the error dynamics.

3.5.1 Definitions

The mean value theorem states that for a given curve $f(x)$ connecting two points a and b, there exists at least one point z on the curve at which the tangent is parallel to the secant line drawn between these two points. This theorem is a consequence of Rolle's Theorem.

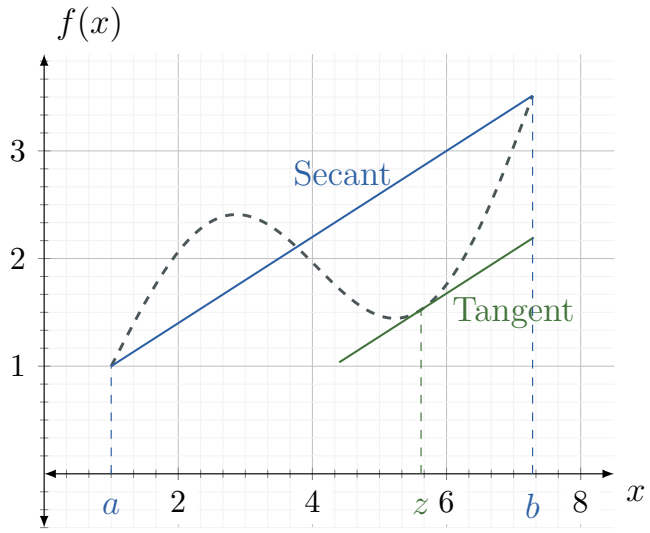

Fig 3.17: Graph of mean value theorem

The following Lemmas provide the mathematical description of MVT:

Lemma 3.2. *(MVT for one dimension) [Zemouche et al., 2005] Let $f : [a, b] \longrightarrow \mathbb{R}$ be continuous on $[a, b]$ and differentiable on (a, b). Then, there is some z with $a < z < b$ such that*

$$f(a) - f(b) = f'(z)(a - b) \tag{3.73}$$

For higher-dimension, the following definition and Lemma are stated:

Definition 3.4. *Let x, y be two elements in $\mathbb{R}^n$. We define by $conv(x, y)$ the convex hull of the set $\{x, y\}$, i.e.*

$$conv(x, y) = \{\lambda x + (1 - \lambda)y, \lambda \in [0, 1]\} \tag{3.74}$$

Lemma 3.3. *(MVT for higher-dimension) [Zemouche et al., 2005] Let $f : \mathbb{R}^n \to \mathbb{R}$. Let a, b be two elements in $\mathbb{R}^n$. We assume that f is differentiable on $conv(a, b)$. Then, there is a constant $z \in conv(a, b), z \neq a, z \neq b$ such that :*

$$f(a) - f(b) = f'(z)(a - b) \tag{3.75}$$

where

$$f' = \left[\frac{\partial f}{\partial x_1} \cdots \frac{\partial f}{\partial x_n}\right] \tag{3.76}$$

For higher-dimensional vector-valued functions, the mean value theorem is stated by the following Lemmas:

Lemma 3.4. *(Canonical basis) [Zemouche et al., 2005] Let $f(x) : R^n \to R^n$ be a vector function, $f_i(x) : \mathbb{R}^n \to \mathbb{R}$ the i^{th} component of f, and E_n is the canonical basis of the vectorial space $\mathbb{R}^n$ for all $n \geq 1$:*

$$E_n = \{e_n(i) | \, e_n(i) = (0, \ ..., \ 0, \ \underbrace{1}_{i}, \ 0, \ ..., \ 0)^T, \ i = 1, \ ..., \ n\} \tag{3.77}$$

Therefore, $f(x)$ can be written as:

$$f(x) = \sum_{i=1}^{n} e_n(i) \, f_i(x) \tag{3.78}$$

Lemma 3.5. *(MVT for higher-dimension vector-valued functions) [Zemouche et al., 2005] Let $a, \ b \in \mathbb{R}^n$ and assume that f is differentiable on $conv(a, b)$. It follows that there exist constant vectors $z_1, \ ..., \ z_n \in conv(a, b)$ with $z_i \neq a$, and $z_i \neq b$ for each $i = 1, \ ..., \ n$ such that:*

$$f(a) - f(b) = \sum_{i=1}^{n} \sum_{j=1}^{n} e_n(i) \, e_n(j)^T \frac{\partial f_i(z_i)}{\partial x_j} (a - b) \tag{3.79}$$

Applying Lemma 1.1 allows us to rewrite the equation (3.79) in terms of T-S representation

$$f(a) - f(b) = \sum_{i=1}^{q \leq 2^{n^2}} h_i(z(t)) \, \mathcal{H}_i . (a - b) \tag{3.80}$$

where $\mathcal{H}_i$ represents the sub-model of the nonlinear term $\sum_{i=1}^{n} \sum_{j=1}^{n} e_n(i) e_n(j)^T \frac{\partial f_i(z_i)}{\partial x_j}$, and $h_i(z(t))$ are its weighting functions, while q represents the number of sub-models.

3.5.2 Observer design using the quadratic Lyapunov function

When using the MVT, the system is maintained in its original form as indicated in (3.1), rather than in a perturbed form as shown in (3.3). Let's consider the following observer:

$$\begin{cases} \dot{\hat{x}}(t) = \sum_{i=1}^{r} \mu_i(\hat{\xi}(t)) \left(A_i\hat{x}(t) + B_iu(t)\right) + L(t)(y(t) - \hat{y}(t)) \\ \hat{y}(t) = \sum_{i=1}^{r} \mu_i(\hat{\xi}(t)) \left(C_i\hat{x}(t) + D_iu(t)\right) \end{cases} \tag{3.81}$$

The dynamics of the estimation error $e(t) = x\left(t\right) - \hat{x}(t)$ are given as follows:

$$\begin{aligned} \dot{e}(t) = &\underbrace{\sum_{i=1}^{r} \mu_i(\xi(t)) \left(A_ix(t) + B_iu(t)\right)}_{\Phi_1(x(t))} - \underbrace{\sum_{i=1}^{r} \mu_i(\hat{\xi}(t)) \left(A_i\hat{x}(t) + B_iu(t)\right)}_{\Phi_1(\hat{x}(t))} \\ &- L[\underbrace{\sum_{i=1}^{r} \mu_i(\xi(t)) \left(C_ix(t) + D_iu(t)\right)}_{\Phi_2(x(t))} - \underbrace{\sum_{i=1}^{r} \mu_i(\hat{\xi}(t)) \left(C_i\hat{x}(t) + D_iu(t)\right)}_{\Phi_2(\hat{x}(t))}] \end{aligned} \tag{3.82}$$

By defining $a = x(t)$ and $b = \hat{x}(t)$, the mean value theorem is applied to the terms Φ_1 and Φ_2, utilizing Lemma 3.5, to derive the subsequent result:

$$\dot{e}\left(t\right) = \sum_{i=1}^{q} h_i\left(z\left(t\right)\right) \left(\mathcal{A}_i - L\mathcal{C}_i\right) e\left(t\right) \tag{3.83}$$

where $\mathcal{A}_i$ corresponds to Φ_1, and $\mathcal{C}_i$ corresponds to Φ_2.

According to this new expression of the state estimation error dynamics, it is evident that the mismatching terms have been eliminated, resulting in dynamics that are completely proportional to the estimation error. This proportional relationship simplifies subsequent stability analysis using the second Lyapunov theorem. However, it is important to note that the weighting functions in this expression, denoted as $h_i(t)$, differ from those in the original system and observer $\mu_i(t)$. Nevertheless, this difference does not pose an issue as the weighting functions still satisfy the convex sum property, ensuring that they do not involve in the stability conditions, consistent with approaches taken in the previous theorems.

The following theorem provides sufficient stability conditions of the error dynamics:

Theorem 3.5

The estimation error converges asymptotically toward zero with decay rate α if there exist matrices $P = P^T \in \mathbb{R}^{n_x \times n_x} > 0$ and $M \in \mathbb{R}^{n_x \times n_y}$ such that the following LMI holds $\forall i = 1, \ldots, q$:

$$\mathcal{A}_i^{\,T} P + P\mathcal{A}_i - M\mathcal{C}_i - \mathcal{C}_i^{\,T} M^T + 2\alpha P < 0 \tag{3.84}$$

where the observer gain is given by $L = P^{-1}M$.

Proof. To study the stability of the error dynamics, the quadratic Lyapunov function is used:

$$V(t) = e(t)^T P e(t) \tag{3.85}$$

The derivative of $V(t)$ with respect to t is given as follows:

$$\dot{V}(t) = \sum_{i=1}^{q} h_i(z(t)) e^T \left((\mathcal{A}_i - L\mathcal{C}_i)^T P + P(\mathcal{A}_i - L\mathcal{C}_i) \right) e \tag{3.86}$$

To improve the performance of the estimation, the following decay rate is used:

$$\dot{V}(t) \leq -2\alpha V(t) \tag{3.87}$$

By substituting (3.85) and (3.86) in (3.87), the following inequality is obtained:

$$\sum_{i=1}^{q} h_i(z(t)) e^T \left(\mathcal{A}_{\mathrm{i}}^T P - \mathcal{C}_i^T L^T P + P\mathcal{A}_{\mathrm{i}} - PL\mathcal{C}_i + 2\alpha P \right) e < 0 \tag{3.88}$$

The inequality (3.88) is not linear due to the product of the variables P and L. However, applying the change of variable $M = PL$ provides a solution for achieving the linear stability conditions outlined in Theorem 3.5. □

Remark 3.1

The implementation of a unique gain L in the design of the observer stems from our utilization of the MVT. With the use of MVT, employing $\sum_{i=1}^{r} \mu_i(\hat{\xi}(t)) L_i$ for observer gains is not productive. This is because while the observer's weighting functions are $\mu_i(\xi)$, those of the estimation error dynamics are $h_i(z)$, and this distinction between the two membership functions prevents the application of relaxation theorems, like Tuan's method outlined in Lemma 1.5. Consequently, all the observer gains L_i need to satisfy every inequality, rather than each L_i meeting only its corresponding inequality i. This specific aspect makes it clear that employing the PDC form wouldn't lead to a reduction in conservatism. Instead, it might inadvertently deteriorate the computational complexity due to an increase in the number of inequalities involved, hence, the decision to employ a common gain L was a deliberate choice to manage these challenges.

Example 7: MVT based observer design for three-tank hydraulic system

1 - Dynamic model of the system

The three-tank hydraulic system illustrated in Figure 3.18, based on Guzman's design [Guzman et al., 2021], features three tanks with equal cross-sectional areas S, connected by pipes with areas $S_{p1,2,3}$. Water from a reservoir fills the first and second tanks

via pumps P_1 and P_2, with flow rates u_1 and u_2. Valves in each tank manage water release, and the system ensures water levels in the order $x_1 > x_3 > x_2$.

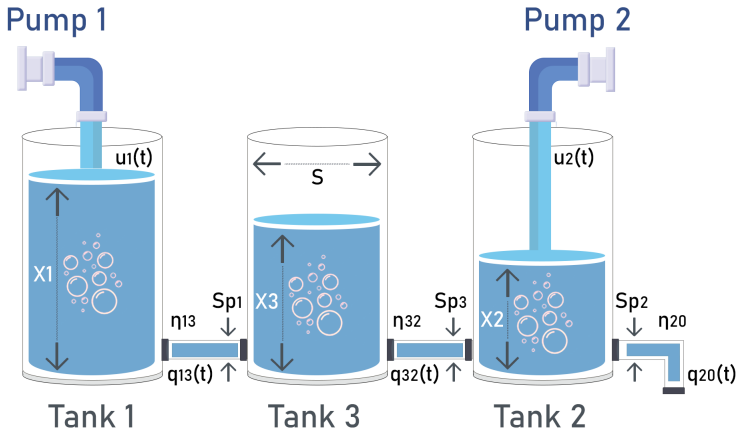

Fig 3.18: Three-tank hydraulic system.

Let us define $x(t) = \begin{bmatrix} x_1 & x_2 & x_3 \end{bmatrix}^T$, $u(t) = \begin{bmatrix} u_1 & u_2 \end{bmatrix}^T$ and the premise variables $\xi(x) = \begin{bmatrix} \xi_1(x) & \xi_2(x) & \xi_3(x) \end{bmatrix}^T$. Using these definitions, the system can be represented in the following state-space form:

$$\dot{x}(t) = \frac{1}{S}\begin{bmatrix} -C_1\xi_1(x) & 0 & 0 \\ 0 & -C_2\xi_2(x) & C_3\xi_3(x) \\ C_1\xi_1(x) & 0 & -C_3\xi_3(x) \end{bmatrix} x(t) + \frac{1}{S}\begin{bmatrix} 1 & 0 \\ 0 & 1 \\ 0 & 0 \end{bmatrix} u(t) \tag{3.89}$$

where

$$\xi_1(x) = \frac{\sqrt{|x_1 - x_3|}}{x_1},\ \xi_2(x) = \frac{\sqrt{x_2}}{x_2},\ \xi_3(x) = \frac{\sqrt{|x_3 - x_2|}}{x_3}$$

$$C_1 = \eta_{13}.S_{p1}.sign(x_1 - x_3).\sqrt{2g},\quad C_2 = \eta_{20}.S_{p2}.\sqrt{2g},\quad C_3 = \eta_{32}.S_{p3}.sign(x_3 - x_2).\sqrt{2g}$$

The parameters of the motor are giving in the following table:

Parameters	**Values**
The gravitational acceleration	$g = 9.8\ [m/s^2]$
The coefficient of discharge	$\eta_{13} = \eta_{32} = 0.456$ $\eta_{20} = 0.652$
The cross-section of the connection tubes	$S_{p1} = S_{p3} = 0.5 \times 10^{-4}\ [m^2]$ $S_{p2} = 0.8 \times 10^{-4}\ [m^2]$
The cross-section of the tanks	$S = 154\ \times 10^{-4}[m^2]$

Table 3.2: Three-tank hydraulic system parameters

Given the constraint $x_1 > x_3 > x_2$ and these parameters, we derive $C_1 = 1.0094 \times 10^{-4}$, $C_2 = 2.3092 \times 10^{-4}$, and $C_3 = 1.0094 \times 10^{-4}$.

2 - Observer design for the three-tank hydraulic system

In order to apply Theorem 3.5, the matrices $\mathcal{A}_i$ and $\mathcal{C}_i$ have to be determined. According to the mean value theorem, $\Phi_1(x(t))$ and its Jacobian $\frac{\partial \Phi_1}{\partial x}$ can be defined as follows:

$$\Phi_1(x(t)) = \frac{1}{S}\begin{bmatrix} -C_1\xi_1 x_1 + u_1(t) \\ -C_2\xi_2 x_2 + C_3\xi_3 x_3 + u_2(t) \\ C_1\xi_1 x_1 - C_3\xi_3 x_3 \end{bmatrix}$$

$$\frac{\partial \Phi_1}{\partial x} = \frac{1}{S}\begin{bmatrix} \frac{-C_1}{2}\varepsilon_1(x) & 0 & \frac{C_1}{2}\varepsilon_1(x) \\ 0 & \frac{-C_2}{2}\varepsilon_2(x) - \frac{C_3}{2}\varepsilon_3(x) & \frac{C_3}{2}\varepsilon_3(x) \\ \frac{C_1}{2}\varepsilon_1(x) & \frac{C_3}{2}\varepsilon_3(x) & -\frac{C_3}{2}\varepsilon_3(x) - \frac{C_1}{2}\varepsilon_1(x) \end{bmatrix}$$

where the new premise variables $\varepsilon_i(x)$ are given by:

$$\varepsilon_1(x) = \frac{1}{\sqrt{x_1 - x_3}}, \quad \varepsilon_2(x) = \frac{1}{\sqrt{x_2}} \text{ and } \quad \varepsilon_3(x) = \frac{1}{\sqrt{x_3 - x_2}},$$

and their limits are:

$$2 \leq \varepsilon_1(x) \leq 12, \quad 2 \leq \varepsilon_2(x) \leq 4 \text{ and } 2 \leq \varepsilon_3(x) \leq 14.$$

Through the use of the T-S representation on $\frac{\partial \Phi_1}{\partial x}$,The matrices $\mathcal{A}_i$ can be obtained as follows:

$$\mathcal{A}_1 = \frac{1}{S}\times \begin{bmatrix} \frac{-C_1}{2}\varepsilon_{1_{\max}} & 0 & \frac{C_1}{2}\varepsilon_{1_{\max}} \\ 0 & \frac{-C_2}{2}\varepsilon_{2_{\max}} - \frac{C_3}{2}\varepsilon_{3_{\max}} & \frac{C_3}{2}\varepsilon_{3_{\max}} \\ \frac{C_1}{2}\varepsilon_{1_{\max}} & \frac{C_3}{2}\varepsilon_{3_{\max}} & -\frac{C_3}{2}\varepsilon_{3_{\max}} - \frac{C_1}{2}\varepsilon_{1_{\max}} \end{bmatrix}, \quad \mathcal{A}_2 = \frac{1}{S}\times \begin{bmatrix} \frac{-C_1}{2}\varepsilon_{1_{\max}} & 0 & \frac{C_1}{2}\varepsilon_{1_{\max}} \\ 0 & \frac{-C_2}{2}\varepsilon_{2_{\max}} - \frac{C_3}{2}\varepsilon_{3_{\min}} & \frac{C_3}{2}\varepsilon_{3_{\min}} \\ \frac{C_1}{2}\varepsilon_{1_{\max}} & \frac{C_3}{2}\varepsilon_{3_{\min}} & -\frac{C_3}{2}\varepsilon_{3_{\min}} - \frac{C_1}{2}\varepsilon_{1_{\max}} \end{bmatrix}$$

$$\mathcal{A}_3 = \frac{1}{S}\times \begin{bmatrix} \frac{-C_1}{2}\varepsilon_{1_{\max}} & 0 & \frac{C_1}{2}\varepsilon_{1_{\max}} \\ 0 & \frac{-C_2}{2}\varepsilon_{2\min} - \frac{C_3}{2}\varepsilon_{3_{\max}} & \frac{C_3}{2}\varepsilon_{3_{\max}} \\ \frac{C_1}{2}\varepsilon_{1_{\max}} & \frac{C_3}{2}\varepsilon_{3_{\max}} & -\frac{C_3}{2}\varepsilon_{3_{\max}} - \frac{C_1}{2}\varepsilon_{1_{\max}} \end{bmatrix}, \quad \mathcal{A}_4 = \frac{1}{S}\times \begin{bmatrix} \frac{-C_1}{2}\varepsilon_{1_{\max}} & 0 & \frac{C_1}{2}\varepsilon_{1_{\max}} \\ 0 & \frac{-C_2}{2}\varepsilon_{2_{\min}} - \frac{C_3}{2}\varepsilon_{3_{\min}} & \frac{C_3}{2}\varepsilon_{3_{\min}} \\ \frac{C_1}{2}\varepsilon_{1_{\max}} & \frac{C_3}{2}\varepsilon_{3_{\min}} & -\frac{C_3}{2}\varepsilon_{3_{\min}} - \frac{C_1}{2}\varepsilon_{1_{\max}} \end{bmatrix}$$

$$\mathcal{A}_5 = \frac{1}{S}\times \begin{bmatrix} \frac{-C_1}{2}\varepsilon_{1_{\min}} & 0 & \frac{C_1}{2}\varepsilon_{1_{\min}} \\ 0 & \frac{-C_2}{2}\varepsilon_{2_{\max}} - \frac{C_3}{2}\varepsilon_{3_{\max}} & \frac{C_3}{2}\varepsilon_{3_{\max}} \\ \frac{C_1}{2}\varepsilon_{1_{\min}} & \frac{C_3}{2}\varepsilon_{3_{\max}} & -\frac{C_3}{2}\varepsilon_{3_{\max}} - \frac{C_1}{2}\varepsilon_{1_{\min}} \end{bmatrix}, \quad \mathcal{A}_6 = \frac{1}{S}\times \begin{bmatrix} \frac{-C_1}{2}\varepsilon_{1_{\min}} & 0 & \frac{C_1}{2}\varepsilon_{1_{\min}} \\ 0 & \frac{-C_2}{2}\varepsilon_{2_{\max}} - \frac{C_3}{2}\varepsilon_{3_{\min}} & \frac{C_3}{2}\varepsilon_{3_{\min}} \\ \frac{C_1}{2}\varepsilon_{1_{\min}} & \frac{C_3}{2}\varepsilon_{3_{\min}} & -\frac{C_3}{2}\varepsilon_{3_{\min}} - \frac{C_1}{2}\varepsilon_{1_{\min}} \end{bmatrix}$$

$$\mathcal{A}_7 = \frac{1}{S}\times \begin{bmatrix} \frac{-C_1}{2}\varepsilon_{1_{\min}} & 0 & \frac{C_1}{2}\varepsilon_{1_{\min}} \\ 0 & \frac{-C_2}{2}\varepsilon_{2_{\min}} - \frac{C_3}{2}\varepsilon_{3_{\max}} & \frac{C_3}{2}\varepsilon_{3_{\max}} \\ \frac{C_1}{2}\varepsilon_{1_{\min}} & \frac{C_3}{2}\varepsilon_{3_{\max}} & -\frac{C_3}{2}\varepsilon_{3_{\max}} - \frac{C_1}{2}\varepsilon_{1_{\min}} \end{bmatrix}, \quad \mathcal{A}_8 = \frac{1}{S}\times \begin{bmatrix} \frac{-C_1}{2}\varepsilon_{1_{\min}} & 0 & \frac{C_1}{2}\varepsilon_{1_{\min}} \\ 0 & \frac{-C_2}{2}\varepsilon_{2_{\min}} - \frac{C_3}{2}\varepsilon_{3_{\min}} & \frac{C_3}{2}\varepsilon_{3_{\min}} \\ \frac{C_1}{2}\varepsilon_{1_{\min}} & \frac{C_3}{2}\varepsilon_{3_{\min}} & -\frac{C_3}{2}\varepsilon_{3_{\min}} - \frac{C_1}{2}\varepsilon_{1_{\min}} \end{bmatrix}$$

According to the output equation, which is linear, $\Phi_2(x(t)) = Cx(t)$; hence:

$$\frac{\partial \Phi_2}{\partial x} = C = \begin{bmatrix} 1 & 0 & 0 \\ 0 & 1 & 0 \end{bmatrix}$$

Therefore:

$$\mathcal{C}_i = C$$

By solving the LMI in Theorem 3.5, the following observer matrices are obtained:

$$L = \begin{bmatrix} 0.4840 & 0.9309 \\ -0.9247 & 0.4900 \\ 0.0010 & 0.1682 \end{bmatrix}, P = \begin{bmatrix} 1.1432 & -0.0016 & -0.1489 \\ -0.0016 & 1.1300 & -0.1619 \\ -0.1489 & -0.1619 & 1.8552 \end{bmatrix}$$

3 - Simulation validation

The simulation has been validated by considering the initial condition as $x_0 = \begin{bmatrix} 0.08 & 0.06 & 0.07 \end{bmatrix}^T$ and $\hat{x}_0 = \begin{bmatrix} 0.181 & 0.1610 & 0.171 \end{bmatrix}^T$. The system inputs are shown in Figure 3.19. The tanks levels and their estimation are shown in Figure 3.20.

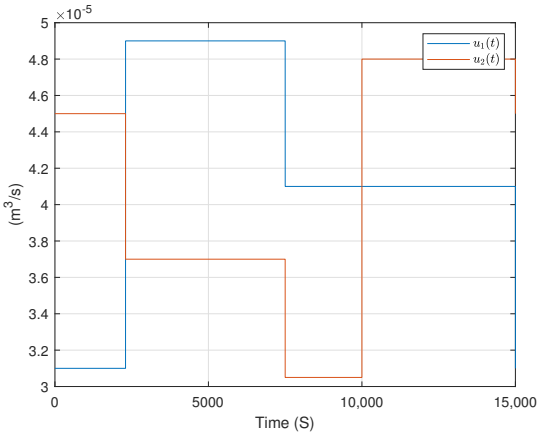

Fig 3.19: The flow rates of pumps.

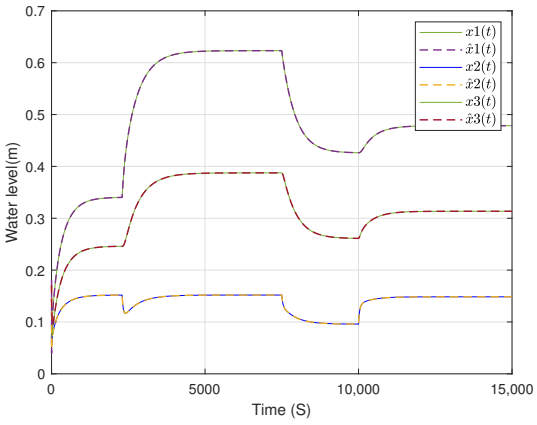

Fig 3.20: Tank levels and their estimations.

3.5.3 Observer design using the poly-quadratic Lyapunov function

In this section, an observer design utilizing the MVT and the poly-quadratic Lyapunov function is introduced to mitigate the conservatism inherent in the quadratic approach. As outlined in Section 3.2.2, designing an observer with the poly-quadratic Lyapunov function requires employing a specific observer structure to derive LMI stability conditions. When incorporating the MVT, this structure is defined as follows:

$$\begin{cases} \dot{\hat{x}} = \sum_{i=1}^{r} \mu_i(\hat{\xi}(t)) \left(A_i \hat{x}(t) + B_i u(t)\right) + \left(\sum_{j=1}^{q} h_j(z(t)) P_j\right)^{-1} L(y(t) - \hat{y}(t)) \\ \hat{y}(t) = \sum_{i=1}^{r} \mu_i(\hat{\xi}(t)) \left(C_i \hat{x}(t) + D_i u(t)\right) \end{cases} \tag{3.90}$$

However, a significant challenge in using this structure with the MVT is the presence of $z(t)$, the state between $x(t)$ and $\hat{x}\,(t)$, which is unknown according to Lemma 3.5. This necessitates approximating $z(t)$ with $\hat{x}\,(t)$, introducing a certain degree of error. To circumvent this issue, one might resort to the conventional observer structure (3.81), where stability conditions will be obtained as BMI. However, BMIs are typically more complex to solve than LMIs. To address this complexity, a method for solving BMIs using the same convex solvers employed for LMIs is proposed.

To analyze the estimation error dynamics stability using the poly-quadratic Lyapunov function, the following assumption is required:

Assumption 3.13. *The derivatives with respect to time for the weighting functions are constrained by positive constants, represented as $\emptyset_i$, described below:*

$$\left|\dot{h}_i\left(z(t)\right)\right| \leq \emptyset_i \tag{3.91}$$

By defining in prior the value of $\emptyset_i$, then the following theorem provides sufficient conditions described as BMI to ensure the asymptotic convergence of the error dynamics:

Theorem 3.6

The estimation error converges asymptotically toward zero if there exist matrices $P_j \; {}_{n_x \times n_x} = {P_j}^T > 0, L \in \mathbb{R}^{n_x \times n_y}$ a symmetric matrix $P_0 \in \mathbb{R}^{n_x \times n_x}$ such that $P_k \geq P_0$, and the following inequalities hold $\forall i, j = 1, \ldots, q$:

$$\mathcal{K}_{ii} < 0, \qquad i = 1, \ldots, q \tag{3.92}$$

$$\frac{1}{q-1}\mathcal{K}_{ii} + \frac{1}{2}\left(\mathcal{K}_{ij} + \mathcal{K}_{ji}\right) < 0, \qquad 1 \leq i \neq j \leq q \tag{3.93}$$

where:

$$\mathcal{K}_{ij} = \mathcal{A}_i^T P_j + P_j \mathcal{A}_i - \mathcal{C}_i^T L^T P_j - P_j L \mathcal{C}_i + \sum_{k=1}^{q} \emptyset_k \left(P_k - P_0\right) \tag{3.94}$$

Proof. In order to use a relaxation method from those detailed in Section 1.7.3, it is imperative that both membership functions of the inequality are symmetric and evaluated at the same state variable. Given that the membership functions of the error dynamics are immutable, as outlined in (3.83), the Lyapunov function must be chosen with identical membership functions as those of the error dynamics and evaluated at the same state

variable. Therefore, the poly-quadratic Lyapunov function is described as follows:

$$V\left(t\right)=e\left(t\right)^{T}\left(\sum_{j=1}^{q}h_{j}\left(z\left(t\right)\right)P_{j}\right)e\left(t\right)\ \ ,\ \ P_{j}=P_{j}^{T}>0 \tag{3.95}$$

Note that in contrast to the previously employed function (3.14) which incorporate $\mu_j\left(\hat{x}\left(t\right)\right)$, this one utilizes $h_j\left(z\left(t\right)\right)$.

The time derivative of $V(t)$ is:

$$\dot{V}\left(t\right)=\sum_{i=1}^{q}\sum_{j=1}^{q}h_{i}\left(z\right)h_{j}\left(z\right)e^{T}(\mathcal{A}_{i}^{T}P_{j}+P_{j}\mathcal{A}_{i}-\mathcal{C}_{i}^{T}L^{T}P_{j}-P_{j}L\mathcal{C}_{i})e+\sum_{k=1}^{q}\dot{h_{k}}\left(z\right)e^{T}P_{k}e \tag{3.96}$$

The conservatism associated with the time derivatives of the membership functions is mitigated by introducing a slack variable P_0 and employing the Assumption 3.13, similarly to the proof of Theorem 3.1. Consequently, equation (3.96) becomes:

$$\dot{V}(t)=\sum_{i=1}^{q}\sum_{j=1}^{q}h_{i}(z)h_{j}(z)e^{T}[\mathcal{K}_{ij}]e \tag{3.97}$$

where $\mathcal{K}_{ij}$ is given in (3.94).

The negativity of $\dot{V}$ is achieved by applying the relaxation technique outlined in Lemma 1.5, which results in the formulation of Theorem 3.6. □

The presence of BMI in stability conditions is a big limitation due to the fact that non-LMI solvers such as the general nonlinear programming "BMIBNB"[1] or "PENBMI" are not efficient especially for high order systems where the number of the inequalities is too large. The methodology commonly followed in this case is to express these non-LMI problems as LMI using suitable analytical methods such as multiplying the observer gain by the inverse of the Lyapunov function, as outlined in (3.90), which, unfortunately, is not applicable in our case as discussed before. Another method that is usually used in the literature to change the BMI that appears in (3.94) to LMI is the "change of variable method". Using this latter gives the following variables:

$$M_{j}=P_{j}L \tag{3.98}$$

After solving the optimization problem, the observer gain L is obtained as follows:

$$L={P_{j}}^{-1}M_{j} \tag{3.99}$$

The problem encountered here is that the solver yields varying solutions for L, rather than identical ones:

$$L_{j}={P_{j}}^{-1}M_{j} \tag{3.100}$$

[1] A built-in solver in YALMIP for non-convex problems. It implements a standard branch-and-bound algorithm. More details about this solver can be found at the following link.

where it is not possible to add a linear constraint to the optimization problem to guarantee the derivation of a unique gain.

In the following section, an approach for addressing BMI as an LMI problem is proposed.

3.5.3.1 Iterative Linear Matrix Inequalities

The appropriate method to solve the optimization problem given in Theorem 3.6 is to solve the BMI by steps, as the two-step procedure in [Lo and Lin, 2004], or an iterative method as that proposed in [Kim and Kim, 2001] [Rhee and Won, 2006]. The proposed algorithm shown in Figure 3.21 illustrates an iterative method which uses convex optimization to solve the inequalities by formulating the BMI problem as an LMI problem using an iterative LMI method. The methodology is described in the following:

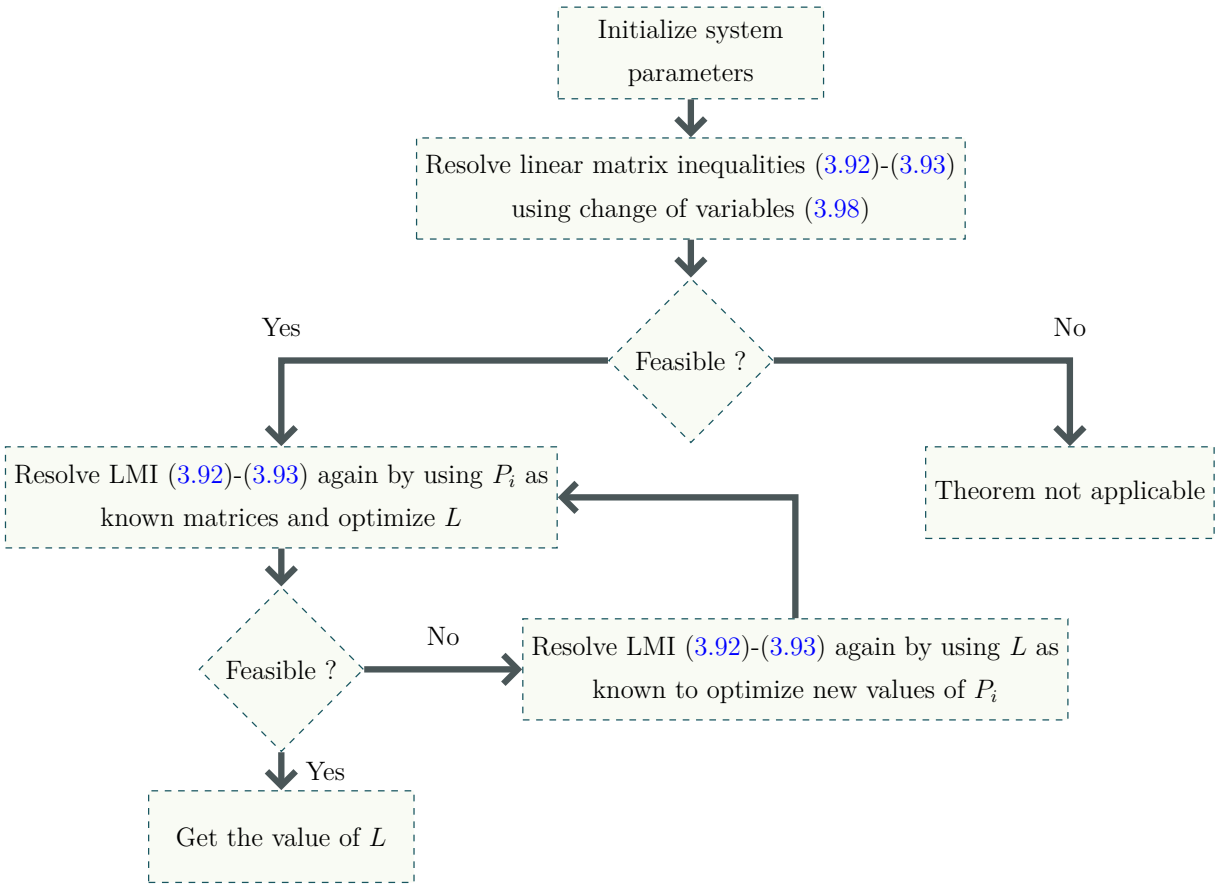

Fig 3.21: Algorithm for solving the Bilinear Matrix Inequalities.

❖ **The first step:** Involves applying the change variable (3.98) to the BMI (3.92)-(3.93), which results in the formulation of an LMI problem that can be solved using linear solvers.

- **The second step:** The obtained matrices P_i are now used as known, while considering the observer gain L as the only unknown variable. This leads to the formulation of an LMI stability conditions. Upon successful feasibility of this problem, the optimized gain L can be implemented in the observer. If not, the procedure progresses to the subsequent step.

- **The third step:** Different matrices P_i have to be chosen since the previous ones were incorrect. Also, since the solver optimized L to be as close as possible to a correct result, it can therefore be used as known, and new values of P_i can be found that are this time much closer to the correct results than the first ones; if not, other values can be used. After defining new matrices, the second step must then be repeated.

The computational complexity of solving an LMI problem is primarily determined by the size of the matrices involved as well as the nature of the specific algorithm employed to solve them. Renowned solvers, such as "SDPT3" and "MOSEK", are designed for convex optimization problems and employ deterministic algorithms. When addressing BMIs using iterative LMI methods, each LMI encountered in every iteration exhibits a computational complexity similar to the ones previously mentioned. Therefore, if numerous iterations are needed, the process can become computationally intensive. It is also important to highlight that convergence is not straightforward when solving BMI iteratively with LMIs. This challenge arises from the linearization of these non-convex constraints at each iteration by fixing one decision variable at a time, which in turn restricts the full potential of convex solvers. Furthermore, the proposed algorithm is heuristic in nature. To alleviate these limitations, the judicious selection of convex solvers in each iteration can improve the convergence of the solution.

3.5.3.2 Examples

Two examples are presented in this section. The first one is meant to illustrate the improvement obtained using the proposed observer compared to the conventional one. This is achieved by comparing the feasibility areas of these two theorems applied to a numerical example. The second example illustrates a real-time application of the proposed method on an induction motor to prove its feasibility in real-time and to show the efficiency of the algorithm in solving BMI in very high order systems (in this example 1024 inequalities).

Example 8: Feasibility area

The purpose of this example is to show the improvement obtained from the use of Theorem 3.6 compared to Theorem 3.5. The best way to prove such a feature is to compare the feasibility domain between these two theorems. This domain is visualized through a map, generated by applying each theorem to a system, which is evaluated based on two variables, a and b. By applying the theorem to every couple $(a\ , b)$ and checking the feasibility of the theorem in all of them, a point is added when the problem is feasible. The feasibility test is conducted by analyzing the eigenvalues of the LMIs. In this example, the solver "LMILAB" is used. The following constraint is used to add restrictions to the inequalities:

$$\dot{V}\left(t\right) \leq -2\alpha V\left(t\right) \tag{3.101}$$

1 - Observer design for the system

Let us consider the following nonlinear system:

$$\begin{cases} \dot{x}(t) = A\left(x(t)\right)x(t) + Bu(t) \\ y(t) = Cx(t) \end{cases} \tag{3.102}$$

where:

$$A\left(x(t)\right) = \begin{bmatrix} -5 & -2 + sinc(x_2) & a \\ -5 & -10 & 1.5 + 5.5sinc(x_3) \\ b & a-b & -20 \end{bmatrix}, B = \begin{bmatrix} 0.5 \\ 10 \\ 3.7 \end{bmatrix}, C = \begin{bmatrix} 0 & 1 & 0 \end{bmatrix}$$

In order to apply Theorem 3.6, the matrices $\mathcal{A}_i$ and $\mathcal{C}_i$ have to be determined. According to the mean value theorem, $\Phi_1\left(x(t)\right)$ and its Jacobian $\frac{\partial \Phi_1}{\partial x}$ can be defined as follows:

$$\Phi_1\left(x\left(t\right)\right) = A\left(x(t)\right)x(t) + Bu(t)$$

$$\frac{\partial \Phi_1}{\partial x} = \begin{bmatrix} -5 & \underbrace{-2 + \cos\left(x_2\right)}_{\varepsilon_1} & a \\ -5 & -10 & \underbrace{1.5 + 5.5\cos\left(x_3\right)}_{\varepsilon_2} \\ b & a-b & -20 \end{bmatrix}$$

where the premise variables $\varepsilon_i\left(x\right)$ are limited as follows:

$$-3 \leq \varepsilon_1 \leq -1, \quad -4 \leq \varepsilon_2 \leq 7$$

Through the use of the T-S representation on $\frac{\partial \Phi_1}{\partial x}$,The matrices $\mathcal{A}_i$ can be obtained as follows:

$$\mathcal{A}_1 = \begin{bmatrix} -5 & -1 & a \\ -5 & -10 & 7 \\ b & a-b & -20 \end{bmatrix}, \quad \mathcal{A}_2 = \begin{bmatrix} -5 & -1 & a \\ -5 & -10 & -4 \\ b & a-b & -20 \end{bmatrix}$$

$$\mathcal{A}_3 = \begin{bmatrix} -5 & -3 & a \\ -5 & -10 & 7 \\ b & a-b & -20 \end{bmatrix}, \quad \mathcal{A}_4 = \begin{bmatrix} -5 & -3 & a \\ -5 & -10 & -4 \\ b & a-b & -20 \end{bmatrix}$$

According to the output equation, which is linear, $\Phi_2(x(t)) = Cx(t)$; hence:

$$\frac{\partial \Phi_2}{\partial x} = C = \begin{bmatrix} 0 & 1 & 0 \end{bmatrix}$$

Therefore:

$$\mathcal{C}_i = C$$

The weighting functions of the estimation error dynamics are defined by:

$$\begin{cases} h_1(z(t)) = M^1_{\varepsilon_1} M^1_{\varepsilon_2}, h_2(z(t)) = M^1_{\varepsilon_1} M^2_{\varepsilon_2} \\ h_3(z(t)) = M^2_{\varepsilon_1} M^1_{\varepsilon_2}, h_4(z(t)) = M^2_{\varepsilon_1} M^2_{\varepsilon_2} \end{cases}$$

where the membership functions are given by:

$$M^1_{\varepsilon_1} = \frac{\varepsilon_1 - \varepsilon_{1min}}{\varepsilon_{1max} - \varepsilon_{1min}}; \; M^2_{\varepsilon_1} = \frac{\varepsilon_{1max} - \varepsilon_1}{\varepsilon_{1max} - \varepsilon_{1min}}; M^1_{\varepsilon_2} = \frac{\varepsilon_2 - \varepsilon_{2min}}{\varepsilon_{2max} - \varepsilon_{2min}}; \; M^2_{\varepsilon_2} = \frac{\varepsilon_{2max} - \varepsilon_2}{\varepsilon_{2max} - \varepsilon_{2min}}$$

2 - Feasibility domain mapping

By defining the following ranges $a \in [800, 1500]$ and $b \in [-1800, \; -400]$, and selecting $\alpha = 25$, the feasibility domains obtained from Theorem 3.5 and Theorem 3.6 are:

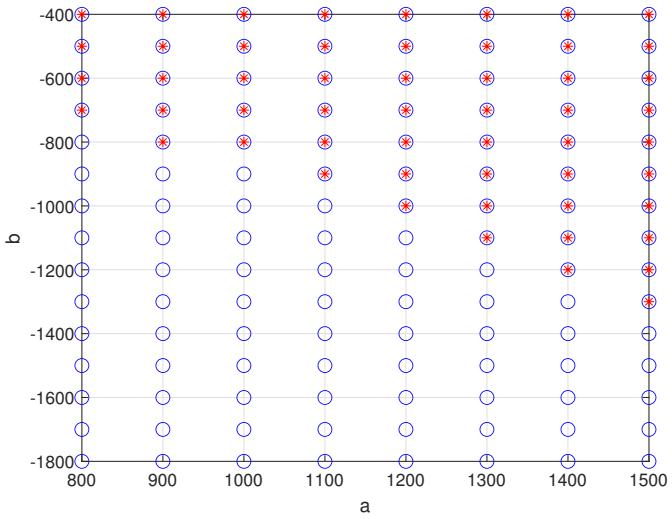

Fig 3.22: Comparative analysis of feasibility regions: 'o' represents Theorem 3.6, while '*' denotes Theorem 3.5.

Method	Feasible points	Number of decision variables	Number of matrix inequalities
Theorem 3.5	54	2	5
Theorem 3.6	120	6	24

Table 3.3: Comparative analysis of the complexity levels of the theorems

Based on the feasibility domain depicted in Figure 3.22, it is evident that the proposed method offers a wider range of applicability than the traditional approach. The proposed theorem encompasses the region covered by Theorem 3.5 and extends beyond it. Notably, Theorem 3.6 yielded 120 feasible points, whereas Theorem 3.5 resulted in 54 feasible points only. This result confirms the superiority of the proposed method in reducing conservatism. Nevertheless, upon inspection of Table 3.3, it is clear that Theorem 3.6 exhibits higher computational complexity compared to Theorem 3.5. This increase in complexity is attributed to the augmented number of decision variables and matrix inequalities involved in Theorem 3.6.

3 - Simulation validation

To demonstrate the feasibility of the proposed approach, a simulation was conducted with the parameters set at ($a = 1200,\ b = -1500$) where Theorem 3.5 is inapplicable and the proposed approach proves effective. By setting the initial conditions of the system at $[1 \quad 3 - 2]$ with a sinewave as input signal, the resulting matrices are:

$$P_1 = \begin{bmatrix} 24.9842 & 6.5231 & 0.1202 \\ 6.5231 & 20.1134 & -1.4884 \\ 0.1202 & -1.4884 & 20.0222 \end{bmatrix}, P_2 = \begin{bmatrix} 25.0291 & 6.5868 & 0.1136 \\ 6.5868 & 20.1402 & -1.5559 \\ 0.1136 & -1.5559 & 20.0097 \end{bmatrix}$$

$$P_3 = \begin{bmatrix} 24.9955 & 6.5100 & 0.1209 \\ 6.5100 & 20.1085 & -1.5007 \\ 0.1209 & -1.5007 & 20.0359 \end{bmatrix}, P_4 = \begin{bmatrix} 25.1798 & 6.6089 & 0.1143 \\ 6.6089 & 20.1434 & -1.5754 \\ 0.1143 & -1.5754 & 20.1300 \end{bmatrix}$$

$$P_0 = \begin{bmatrix} 24.9701 & 6.5469 & 0.1196 \\ 6.5469 & -162.6363 & -1.5941 \\ 0.1196 & -1.5941 & 20.0002 \end{bmatrix}, L = \begin{bmatrix} 0.5718 \\ 2.5091 \\ 3.2915 \end{bmatrix} \times 10^3$$

The simulation results are depicted in Figure 3.23. The blue line represents the real states of the system, while the red dashed line represents the estimated states. As illustrated, the observer provides accurate state estimations, with the error gradually approaching zero within a reasonable period of time despite the oscillatory behavior of the system. This effectively demonstrates the observer's feasibility and its advantage in reducing conservatism, as opposed to the conventional quadratic method.

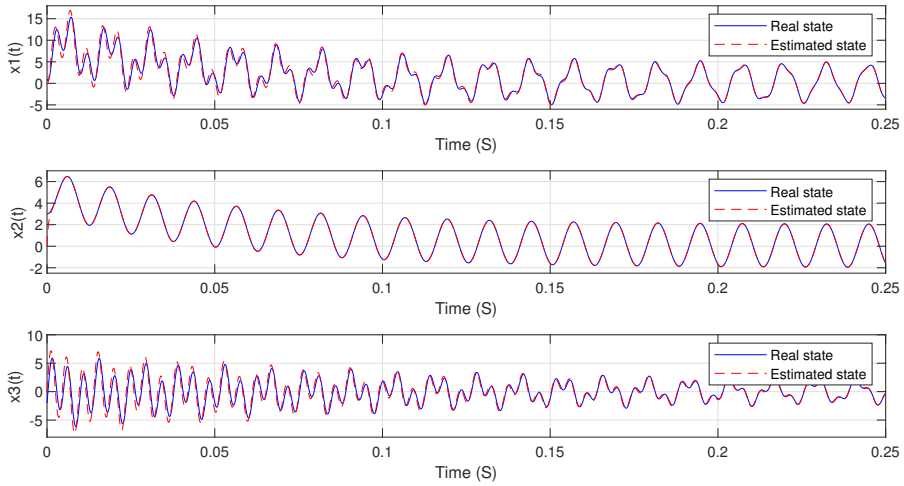

Fig 3.23: State estimation.

Example 9: Application to the induction motor

This example is a real-time application of the proposed observer dedicated to the induction motor. In this example, the output is assumed to be $y(t) = \omega(t)$. The aim of this example is to prove the feasibility of the proposed theorem in a real-time application, and additionally to demonstrate the efficiency of the proposed algorithm in solving BMI for very large systems in a short period of time. The error dynamics of the induction motor have 5 Premise Variables, which leads to 1024 inequalities according to Theorem 3.6 and 32 matrices P_i, thus results in a very large number of computations. The mathematical model of the induction motor is described in (1.27).

1 - Observer design for the induction motor

In order to apply Theorem 3.6, the matrices $\mathcal{A}_i$ and $\mathcal{C}_i$ have to be determined. According to the mean value theorem, $\Phi_1(x(t))$ and its Jacobian $\frac{\partial \Phi_1}{\partial x}$ are given by:

$$\Phi_1(x(t)) = A(x(t))\,x(t) + Bu(t)$$

$$\frac{\partial \Phi_1}{\partial x} = \begin{bmatrix} -\gamma & \omega_s & \frac{K_s}{T_r} & K_s\varepsilon_5 & K_s\varepsilon_4 \\ -\omega_s & -\gamma & -K_s\varepsilon_5 & \frac{K_s}{T_r} & -K_s\varepsilon_3 \\ \frac{L_m}{T_r} & 0 & -\frac{1}{T_r} & \omega_s - \varepsilon_5 & -\varepsilon_4 \\ 0 & \frac{L_m}{T_r} & -(\omega_s - \varepsilon_5) & -\frac{1}{T_r} & \varepsilon_3 \\ -\alpha\varepsilon_4 & \alpha\varepsilon_3 & \alpha\varepsilon_2 & -\alpha\varepsilon_1 & -\frac{f}{J_m} \end{bmatrix}$$

As shown, there exist 5 premise variables ordered as $\varepsilon = \begin{bmatrix} i_{sd} & i_{sq} & \Psi_{rd} & \Psi_{rq} & \omega \end{bmatrix}^T$, and they are limited as follows:

$$i_{sd_{\min}} \leq \varepsilon_1 \leq i_{sd_{\max}}, \quad i_{sq_{\min}} \leq \varepsilon_2 \leq i_{sq_{\max}}, \quad \Psi_{rd_{\min}} \leq \varepsilon_3 \leq \Psi_{rd_{\max}}$$

$$\Psi_{rq_{\min}} \leq \varepsilon_4 \leq \Psi_{rq_{\max}}, \quad \omega_{\min} \leq \varepsilon_5 \leq \omega_{\max}$$

Through the use of the T-S representation on $\frac{\partial \Phi_1}{\partial x}$,The matrices $\mathcal{A}_i$ are given by:

$$\mathcal{A}_i = \begin{bmatrix} -\gamma & \omega_s & \frac{K_s}{T_r} & K_s\varepsilon_5(r) & K_s\varepsilon_4(d) \\ -\omega_s & -\gamma & -K_s\varepsilon_5(r) & \frac{K_s}{T_r} & -K_s\varepsilon_3(o) \\ \frac{L_m}{T_r} & 0 & -\frac{1}{T_r} & \omega_s - \varepsilon_5(r) & -\varepsilon_4(d) \\ 0 & \frac{L_m}{T_r} & \varepsilon_5(r) - \omega_s & -\frac{1}{T_r} & \varepsilon_3(o) \\ -\alpha\varepsilon_4(d) & \alpha\varepsilon_3(o) & \alpha\varepsilon_2(k) & -\alpha\varepsilon_1(j) & -\frac{f}{J_m} \end{bmatrix}$$

where:

$$\varepsilon_1(j) = \begin{bmatrix} i_{sd_{\max}} & i_{sd_{\min}} \end{bmatrix}, \varepsilon_2(k) = \begin{bmatrix} i_{sq_{\max}} & i_{sq_{\min}} \end{bmatrix}, \varepsilon_3(o) = \begin{bmatrix} \Psi_{rd_{\max}} & \Psi_{rd_{\min}} \end{bmatrix}$$
$$\varepsilon_4(d) = \begin{bmatrix} \Psi_{rq_{\max}} & \Psi_{rq_{\min}} \end{bmatrix}, \varepsilon_5(r) = \begin{bmatrix} \omega_{\max} & \omega_{\min} \end{bmatrix}$$

By substituting each premise variable with its corresponding limits, the combination between them gives $q = 32$.

According to the output equation, which is linear, $\Phi_2(x(t)) = Cx(t)$; hence:

$$\frac{\partial \Phi_2}{\partial x} = C = \begin{bmatrix} 0 & 0 & 0 & 0 & 1 \end{bmatrix}$$

Therefore:

$$\mathcal{C}_i = C$$

By solving the LMI in Theorem 3.6, the following observer gain is obtained:

$$L = \begin{bmatrix} -0.4111 \\ -2.5898 \\ 0.0041 \\ 0.024 \\ 2.4791 \times 10^3 \end{bmatrix}$$

where the matrices P_i are omitted since their number is very big (32 matrices).

Using "tic-toc" command in MATLAB, the time spent to find the solution using the proposed iterative LMI algorithm described in Figure 3.21 is 32.63 seconds which is very appropriate to optimize the 1024 inequalities of Theorem 3.6. This proves the efficiency of the proposed algorithm compared to other solvers such as "BMIBNB solver" which was not able to solve this large number of BMI.

2 - Experimental results

The experiment is built in LMSE Laboratory. As shown in Figure 3.24, using only the speed sensor, the observer is designed to estimate all the other states of the system where the rotor position is measured using an incremental encoder with 1024 point resolution. To test the obtained results against the real values, the current is measured

using an i30s current clamp, and since the flux sensor is missing in this experiment, an approximation using the dynamic equations of the system is used. The dSPACE 1104 board card is used for data acquisition. In this experiment a 3 KW SIEMENS squirrel cage motor is used.

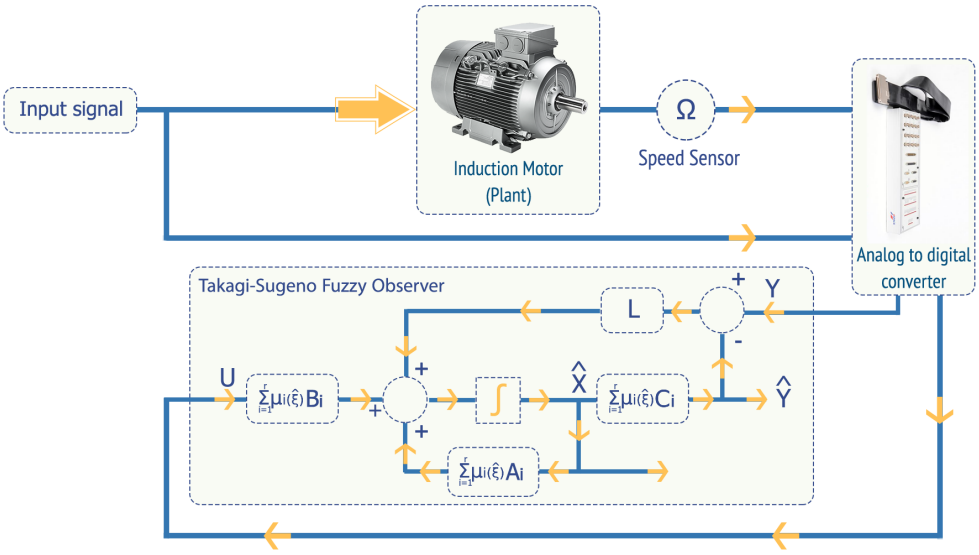

Fig 3.24: Overall schematic diagram of the observer.

The results are shown in Figure 3.25 through Figure 3.29, and clearly demonstrate the feasibility of the obtained observer gain and its effectiveness in yielding good state estimations for the induction motor. Unlike other works reported in the introduction, we also demonstrated the possibility of using only one sensor to estimate all the other four states. Furthermore, Table 3.4 showcases the performance evaluation indicators of the proposed observer which results in minimal estimation error within acceptable bounds. This highlights the robustness and reliability of the observer even under challenging real-time application conditions.

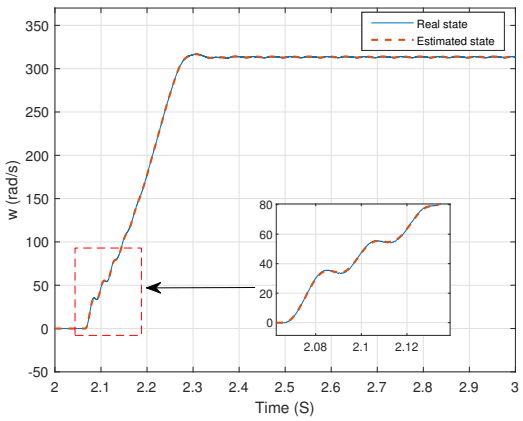

Fig 3.25: Rotor electrical angular speed.

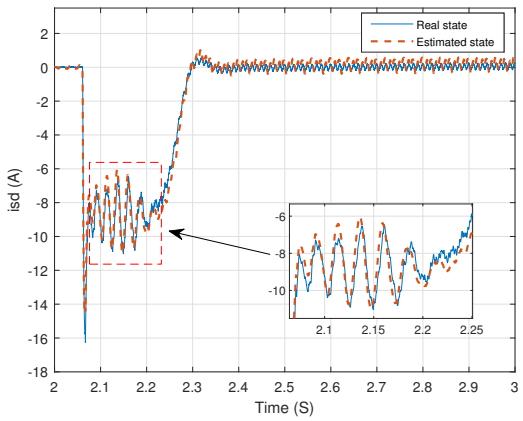

Fig 3.26: Direct axis stator current.

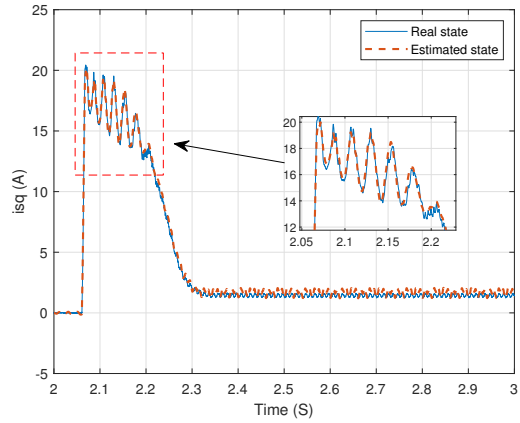

Fig 3.27: Quadrature axis stator current.

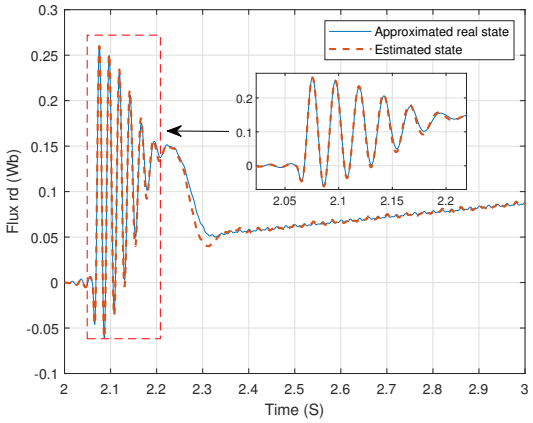

Fig 3.28: Direct axis rotor flux.

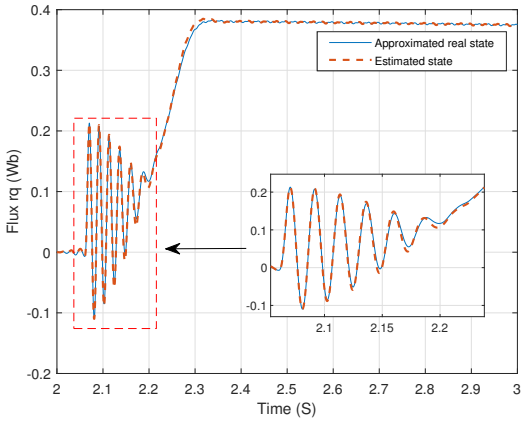

Fig 3.29: Quadrature axis rotor flux.

Observer performance	Integral Absolute Error	Mean Square Error
$i_{sd}(A)$	0.2743	0.1477
$i_{sq}(A)$	0.3144	0.1772
$\Psi_{sd}(\ Wb)$	0.0024	0.00002
$\Psi_{sq}(\ Wb)$	0.0018	0.00001
$\omega(rad/s)$	0.1152	0.0248

Table 3.4: Performance evaluation indicators

3.6 Discussion

In Theorem 3.1, we utilized the Lipschitz method to design an observer for UPV, offering reduced conservatism compared to Theorem 1 in [Ichalal et al., 2012]. Despite its benefits, the Lipschitz condition introduces significant conservatism, prompting a shift

to the method outlined in Theorem 3.2. This alternative approach further reduces conservatism by not relying on the Lipschitz condition. Subsequently, Theorem 3.4 presents enhancements through a poly-quadratic Lyapunov function, aiming to decrease conservatism inherent in the quadratic approach. It differentiates by associating different matrix P_i to each sub-model rather than a unique matrix P to all of them. The stability conditions derived are formulated as LMI. In Theorem 3.5 the MVT approach is adopted, entirely eliminating mismatching terms rather than merely reducing their impact as in Theorem 3.4. However, this comes at the cost of increased complexity in defining matrices $\mathcal{A}_i$ and $\mathcal{C}_i$. Building upon this, Theorem 3.6 proposes enhancements through the poly-quadratic Lyapunov function, indicating reduced conservatism relative to Theorem 3.5 which is evidenced in the feasibility area depicted in Figure 3.22. However, the stability conditions are now expressed as BMI, presenting a challenging optimization problem. We proposed an algorithm to address this optimization challenge, depicted in Figure 3.21, which proves to be more effective compared to other non-convex optimization solvers as "BMIBNB".

3.7 Conclusion

In this chapter, we delved into the complex world of state estimation in T-S fuzzy systems, with a special emphasis on systems characterized by UPV. Our comprehensive discussion highlighted the multifaceted challenges and the diversity of methodologies inherent to the estimation process. We particularly focused on mitigating mismatching terms, where each method contributes in different way towards stabilizing estimation error dynamics. Additionally, we conducted an extensive exploration of observer design, examining both quadratic and poly-quadratic Lyapunov functions. For each category, we dissected the observer structure, elucidating how the different approaches enhance accuracy and robustness while minimizing conservatism. Moreover, this chapter provided several applications, illustrating the effectiveness and adaptability of the discussed methods.

Chapter 4

State and unknown input estimation of Takagi-Sugeno fuzzy systems

4.1 Introduction

The quality of state estimation is fundamentally tied to the precision of the system's mathematical model and the accuracy of measurements of its inputs and outputs. However, real-world systems are complex and often subject to various types of disturbances, denoted $d(t)$, which significantly impact the estimation process.

Disturbances, or unwanted signals affecting the system, come in two main forms: internal and external. Internal disturbances include uncertainties in model parameters, variations in system dynamics, and other inherent system irregularities, often referred to as model uncertainties. External disturbances, on the other hand, originate from outside the system and include environmental noise, external faults, and various forms of interference. Both types of disturbances are considered as unknown inputs (UIs) that detrimentally influence the accuracy of state estimation if they are not taken into account in the design process.

The approaches to designing observers presented in Chapter 3 often overlooks these unknown inputs, leading to degraded performance in state estimation. Recognizing this limitation, this chapter emphasizes the necessity of incorporating the effect of these disturbances into the observer design process. By accounting for these unknown inputs, we can significantly enhance the performance and robustness of the observer, ensuring more accurate and reliable state estimation. This chapter presents the foundational concepts and methodologies for achieving effective state and unknown input estimation, setting the stage for the development of robust observers tailored for complex real-world systems, as depicted in Figure 4.1.

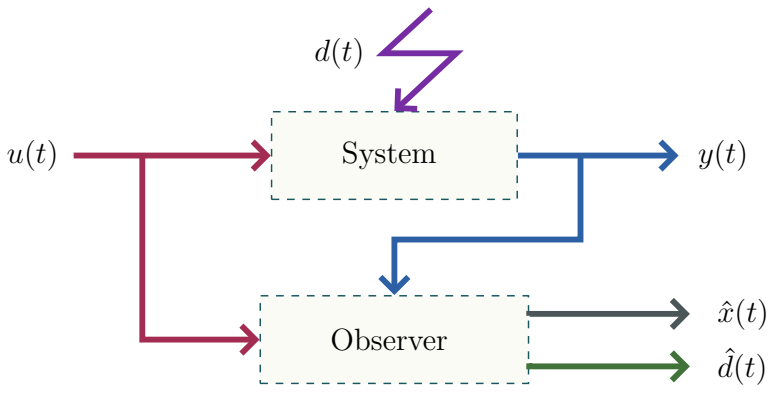

Fig 4.1: Principle of the unknown input observer.

State and unknown input estimation serves a critical role in fault detection, diagnosis and also in control systems. Accurate estimation enables control techniques such as

feedforward, robust, and predictive control to function optimally. Simultaneously, it is crucial for fault detection and diagnosis, enhancing system reliability and safety by aiding in the identification and correction of technical problems. Its application is versatile, as shown by Jing Na et al. in [Na et al., 2017], where it is used in vehicle engine torque estimation. In [Lu et al., 2016], the authors innovatively apply an unknown input decoupled filter design in linear time-varying systems, especially where common assumptions aren't met. The application of unknown input estimation is further extended to road roughness estimation in [Kang et al., 2019]. Moreover, a sophisticated application is presented by Qianyue Luo et al. in [Luo et al., 2021] where model predictive control based on an unknown input observer is utilized to address the control problem of heterogeneous vehicle platoons. Additionally, in [Zhonghai et al., 2018] ,an unknown input observer is used specifically for fault diagnosis of an intelligent hydraulic pump. Each of these references emphasizes the variety of applications and the importance of accurate unknown inputs estimation in maintaining efficient system operation.

In fault diagnosis, faults are typically treated as unknown inputs that disrupt the system operation. Figure 4.2 illustrates a diagram of an observer-based controller tailored to a system experiencing various types of faults. These faults necessitate identification or compensation to ensure continued acceptable operation of the observer. The definitions and characteristics of these fault types are described as follows [Baillieul and Samad, 2021]:

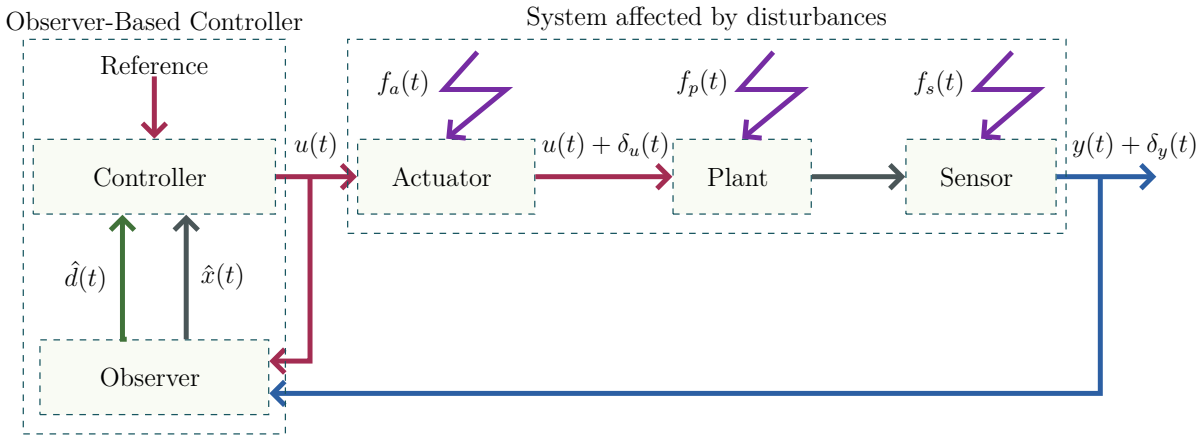

Fig 4.2: Diagram of an observer-based controller of a system affected by disturbances.

❖ **Actuator Fault $f_a(t)$:** corresponds to variations of the control input $u(t)$ applied to the controlled system either completely or partially. The complete failure of an actuator means that it produces no actuation regardless of the input applied to it. For partial actuator faults, the actuator becomes less effective and provides the plant with only a part of the normal actuation signal.

- **Sensor Fault $f_s(t)$:** implies that incorrect measurements are taken from the real system. This fault can also be subdivided into either a complete or partial sensor fault. When a sensor fails, the measurements no longer correspond to the required physical parameters. For a partial sensor fault the measurements give an inaccurate indication of required physical parameters.

- **Process Fault $f_p(t)$:** directly affects the physical system parameters and in turn the input/output properties of the system. Process faults are often termed component faults, arising as variations from the structure or parameters used during system modeling, and as such cover a wide class of possible faults.

There are two main categories of unknown input observers in the existing literature. The first category encompasses Simultaneous State and Unknown Input Observer (SSUIO), such as Proportional Integral Observers (PIO) and its extended version Proportional Multi Integral Observers (PMIO). These observers estimate both the states and the unknown inputs of the system simultaneously. Historically PIO was proposed firstly for linear systems by Wojciechowsky in [Wojciechowski, 1978], where the first derivative of the unknown inputs is supposed to be null which makes it possible using the state representation to estimate the unknown inputs and its derivative. This observer have found broad application in various domains. For instance, Abdelmalek et al. [Abdelmalek et al., 2018] proposed the application of PIO for fault-tolerant control in doubly fed induction generator-based wind turbines. Boukhlouf et al. [Boukhlouf et al., 2023] used the PIO for estimating states and UI in SynRM. Despite its widespread use, PIO has a significant limitation: it considers the unknown input to be either constant or with slow variation, according to the assumption that the first derivative of the UI equals zero. Consequently, when the UI variation is rapid, PIO can only deliver moderate results. After Designing the PIO, Jiang et al [Jiang et al., 2000] designed the PMIO which is an extended version of the PIO that uses multi integrals rather than just one. This observer is suitable for polynomial UI form by considering the s^{th} derivative of the UI to be zero; this characteristic contributes to enhancing the estimation precision of UIs and allows for the estimation of a wider variety of unknown inputs. PMIO observer has been utilized in various applications, such as fault detection in wind turbines [FADILI et al., 2019, Kühne et al., 2018] and robotics [Djeddi et al., 2020, Sun et al., 2021]. Although PMIO covers a broader class of UIs compared to PIO, it faces challenges when the order of the polynomial UI exceeds the design limit of the observer or when the form of the UI is non-polynomial. The second category of unknown input observer is the Decoupled Unknown Input Observer (DUIO). DUIO separates the UI from the state estimation error

and estimates them independently. Unlike other observers, DUIO does not require prior determination of the UI order, hence allowing for the estimation of a larger class of unknown signals. Comparative studies presented by the authors in [Hadi et al., 2019] have demonstrated DUIO's superiority over PMIO. In [Vu et al., 2017], the authors introduced a DUIO for discrete-time uncertain systems. They applied this to a DC motor controlling an inverted pendulum using a non-quadratic Lyapunov function, which offers less conservatism compared to the quadratic function.

This chapter focuses on the design of robust observer for T-S systems capable of providing state and unknown input estimation based on the two categories previously mentioned. In Section 4.2, the concept of the simultaneous state and unknown input estimation for both PIO and PMIO is presented. A comparative tests between them is evaluated on Synchronous Reluctance Motor using simulation and Hardware-in-the-loop tests (HIL). In section Section 4.3, the concept of decoupled unknown input observer is presented and compared with the SSUIO using HIL experimental test conducted on the SynRM.

4.2 Simultaneous state and unknown input observer

In this section, we will discuss the two types of SSUIO: PIO and PMIO. The methodologies outlined in Chapter 3 can be generalized for T-S systems with UPV in the presence of UI. Consequently, this chapter utilizes the MVT, outlined in Section 3.5, to design the observers since it provides an effective solution to the problem of the mismatching terms.

4.2.1 Proportional integral observer design

Let us consider the following T-S system where the unknown inputs are assumed to affect both state dynamics and measurements:

$$\begin{cases} \dot{x}(t) = \sum_{i=1}^{r} \mu_i(\xi(t)) \left(A_i x(t) + B_i u(t) + E_i d(t)\right) \\ y(t) = \sum_{i=1}^{r} \mu_i(\xi(t)) (C_i x(t) + D_i u(t) + G_i d(t)) \end{cases} \tag{4.1}$$

where $d(t) \in \mathbb{R}^{n_d}$ represents the unknown input. $G_i \in \mathbb{R}^{n_y \times n_d}$ and $E_i \in \mathbb{R}^{n_x \times n_d}$ are matrices representing the influence of the unknown inputs on the measurements and on the sate dynamics respectively.

To design a PIO, it is necessary to adhere to the following assumption:

Assumption 4.1. *The unknown input $d(t)$ is assumed to be constant, implying that its first time derivative is equal to zero:*

$$\dot{d}\,(t) = 0 \tag{4.2}$$

Employing this assumption is crucial as it characterizes the dynamics of the UI, enabling its incorporation into the state-space representation of the entire system:

$$\begin{cases} \dot{x}(t) = \sum_{i=1}^{r} \mu_i(\xi(t)) \left(A_i x(t) + B_i u(t) + E_i d(t)\right) \\ y(t) = \sum_{i=1}^{r} \mu_i(\xi(t))(C_i x(t) + D_i u(t) + G_i d(t)) \\ \dot{d}(t) = 0 \end{cases} \tag{4.3}$$

It is possible to approximate UI with slow variation using Assumption 4.1, as its derivative is nearly zero.

The augmented form of the system (4.3), which is used to consolidate both the state vector $x(t)$ and the derivative of the unknown input $d(t)$ into a single extended state vector $x_a(t)$, is described as follows:

$$\begin{cases} \dot{x}_a(t) = \sum_{i=1}^{r} \mu_i(\xi(t)) \left(\widetilde{A}_i x_a(t) + \widetilde{B}_i u(t)\right) \\ y(t) = \sum_{i=1}^{r} \mu_i(\xi(t))(\widetilde{C}_i x_a(t) + D_i u(t)) \end{cases} \tag{4.4}$$

where $x_a(t)$ represents the augmented state vector, which includes both the original system state $x(t)$ and the unknown input $d(t)$. The augmented state matrix for the i^{th} linear model of the T-S system, denoted as $\widetilde{A}_i$, is constructed from the original state matrix A_i and the disturbance matrix E_i. Similarly $(\widetilde{B}_i, \widetilde{C}_i)$ represent the augmented input and output matrices for the i^{th} linear model respectively.

$$x_a(t) = \begin{bmatrix} x(t) \\ d(t) \end{bmatrix}, \widetilde{A}_i = \begin{bmatrix} A_i & E_i \\ 0 & 0 \end{bmatrix}, \widetilde{B}_i = \begin{bmatrix} B_i \\ 0 \end{bmatrix}, \widetilde{C}_i = \begin{bmatrix} C_i & G_i \end{bmatrix}$$

The implementation of the augmented form is useful for analysis and observer design as it allows for working in a single unified state space representation.

Remark 4.1

If the UI is not a constant but a bounded nonlinear UI, it is advisable to always set $\dot{d}(t) = 0$ and increase the bandwidth of the observer. This compensates the approximation error model of the UI. Increasing the bandwidth is achieved by setting higher negative eigenvalues [Koenig and Mammar, 2002].

Remark 4.2

In control theory, it is known that increasing the bandwidth allows signals with higher frequency, such as noise, to infiltrate the system. Therefore, in observer design, this results in a more noisy state estimation error. Consequently, there needs to be a compromise between robustness to disturbances and sensitivity to noise.

Let us consider the following PIO for the system (4.3):

$$\begin{cases} \dot{\hat{x}} = \sum_{i=1}^{r} \mu_i(\hat{\xi}(t)) \left(A_i \hat{x}(t) + B_i u(t) + E_i \hat{d}(t) \right) + L_P(y(t) - \hat{y}(t)) \\ \hat{y}(t) = \sum_{i=1}^{r} \mu_i(\hat{\xi}(t))(C_i \hat{x}(t) + D_i u(t) + G_i \hat{d}(t)) \\ \dot{\hat{d}}(t) = L_I(y(t) - \hat{y}(t)) \end{cases} \tag{4.5}$$

where, $\hat{d}(t)$ represents the estimation of the unknown input. The matrices $L_P \in \mathbb{R}^{n_x \times n_y}$ and $L_I \in \mathbb{R}^{n_d \times n_y}$ are the proportional and integral gains respectively.

The augmented form of this observer is described as follows:

$$\begin{cases} \dot{\hat{x}}_a(t) = \sum_{i=1}^{r} \mu_i(\hat{\xi}(t)) \left(\widetilde{A}_i \hat{x}_a(t) + \widetilde{B}_i u(t) \right) + \widetilde{L}(y(t) - \hat{y}(t)) \\ \hat{y}(t) = \sum_{i=1}^{r} \mu_i(\hat{\xi}(t))(\widetilde{C}_i \hat{x}_a(t) + D_i u(t)) \end{cases} \tag{4.6}$$

where $\widetilde{L} = \begin{bmatrix} L_P \\ L_I \end{bmatrix}$.

The diagram of this observer is presented in Figure 4.3 below:

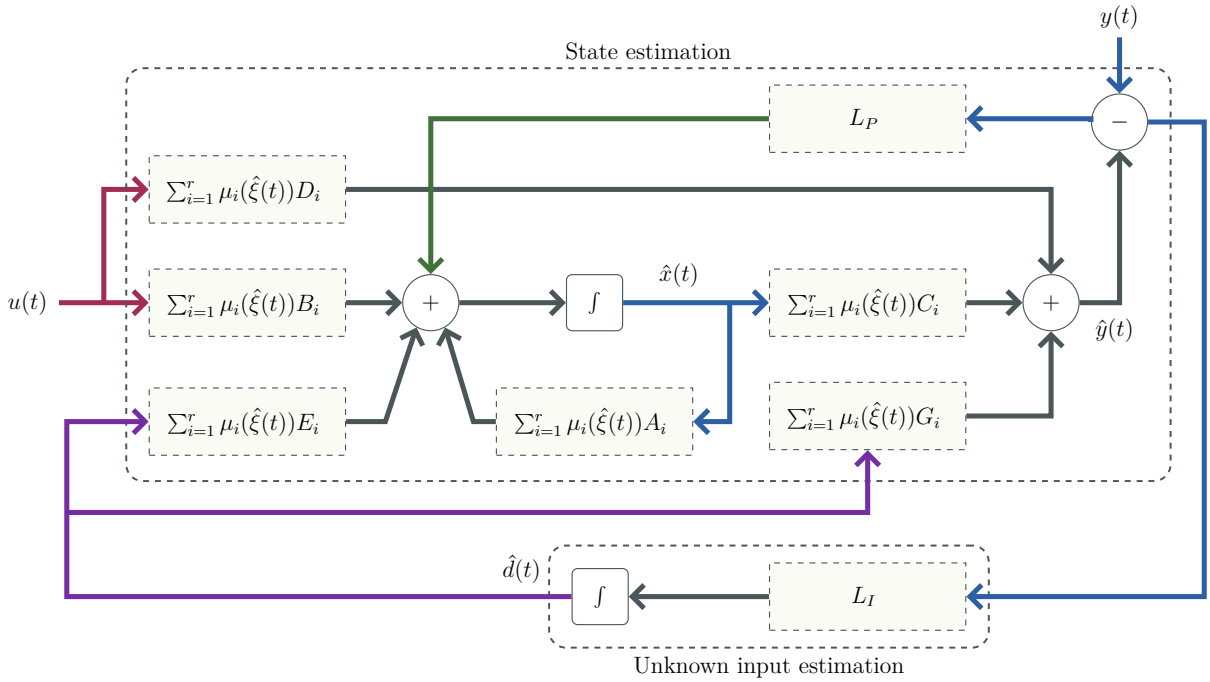

Fig 4.3: Proportional integral observer structure.

The dynamics of the estimation error $e_a(t) = x_a(t) - \hat{x}_a(t)$ are given as follows:

$$\begin{aligned} \dot{e}_a(t) = & \underbrace{\sum_{i=1}^{r} \mu_i(\xi(t)) \left(\widetilde{A}_i x_a(t) + \widetilde{B}_i u(t) \right)}_{\widetilde{\Phi}_1(x_a(t))} - \underbrace{\sum_{i=1}^{r} \mu_i(\hat{\xi}(t)) \left(\widetilde{A}_i \hat{x}_a(t) + \widetilde{B}_i u(t) \right)}_{\widetilde{\Phi}_1(\hat{x}_a(t))} \\ & - \widetilde{L}[\underbrace{\sum_{i=1}^{r} \mu_i(\xi(t)) \left(\widetilde{C}_i x_a(t) + D_i u(t) \right)}_{\widetilde{\Phi}_2(x_a(t))} - \underbrace{\sum_{i=1}^{r} \mu_i(\hat{\xi}(t)) \left(\widetilde{C}_i \hat{x}_a(t) + D_i u(t) \right)}_{\widetilde{\Phi}_2(\hat{x}_a(t))}] \end{aligned} \tag{4.7}$$

By defining $a = x_a(t)$ and $b = \hat{x}_a(t)$, the mean value theorem is applied to the terms $\widetilde{\Phi}_1$ and $\widetilde{\Phi}_2$, utilizing Lemma 3.5, to derive the subsequent result:

$$\dot{e}_a(t) = \sum_{i=1}^{q} h_i(z(t)) \left(\widetilde{\mathcal{A}}_i - \widetilde{L}\widetilde{\mathcal{C}}_i\right) e(t) \tag{4.8}$$

where $\widetilde{\mathcal{A}}_i$ corresponds to $\widetilde{\Phi}_1$, and $\widetilde{\mathcal{C}}_i$ corresponds to $\widetilde{\Phi}_2$.

The following theorem provides sufficient conditions described as LMI to ensure the asymptotic convergence of the error dynamics:

Theorem 4.1

The estimation error converges asymptotically toward zero with decay rate α if there exist matrices $P = P^T \in \mathbb{R}^{n_{xa} \times n_{xa}} > 0$ and $M \in \mathbb{R}^{n_{xa} \times n_y}$ such that the following LMI holds $\forall i = 1, \ldots, q$:

$$\widetilde{\mathcal{A}}_i^T P + P\widetilde{\mathcal{A}}_i - M\widetilde{\mathcal{C}}_i - \widetilde{\mathcal{C}}_i^T M^T + 2\alpha P < 0 \tag{4.9}$$

where the observer gain is given by:

$$\widetilde{L} = P^{-1}M \tag{4.10}$$

Proof. To study the stability of the error dynamics, the quadratic Lyapunov function is used:

$$V(t) = e_a(t)^T P e_a(t) \tag{4.11}$$

The derivative of $V(t)$ with respect to t is:

$$\dot{V}(t) = \sum_{i=1}^{q} h_i(z(t)) \, {e_a}^T \left(\left(\widetilde{\mathcal{A}}_i - \widetilde{L}\widetilde{\mathcal{C}}_i\right)^T P + P\left(\widetilde{\mathcal{A}}_i - \widetilde{L}\widetilde{\mathcal{C}}_i\right)\right) e_a \tag{4.12}$$

To improve the performance of the estimation, the following decay rate is used:

$$\dot{V}(t) \leq -2\alpha V(t) \tag{4.13}$$

By substituting (4.11) and (4.12) in (4.13) the following inequality is obtained:

$$\sum_{i=1}^{q} h_i(z(t)) \, {e_a}^T \left(\left(\widetilde{\mathcal{A}}_i - \widetilde{L}\widetilde{\mathcal{C}}_i\right)^T P + P\left(\widetilde{\mathcal{A}}_i - \widetilde{L}\widetilde{\mathcal{C}}_i\right) + 2\alpha P\right) e_a < 0 \tag{4.14}$$

The inequality (4.14) is not linear due to the product of the variables P and $\widetilde{L}$. However, applying the change of variable $M = P\widetilde{L}$ provides a solution for achieving the linear stability conditions outlined in Theorem 4.1. □

Remark 4.3

Setting higher negative eigenvalues, which leads to increasing the observer gain, can be achieved using the the α-stability described in Theorem 2.7. Therefore, increasing the bandwidth of the observer contributes in improving the estimation of non-constant UI by increasing the decay rate of the estimation error .

Example 10: Proportional integral observer design for synchronous reluctance motor

1 - Non-linear dynamical model of synchronous reluctance motor

The dynamical model of the synchronous reluctance motor (SynRM) is typically described in the rotational d-q reference frame. Below are the specific equations that described this nonlinear system:

$$\begin{cases} V_{sd} = R_s i_{sd} + L_d \frac{di_{sd}}{dt} - \omega L_q i_{sq} \\ V_{sq} = R_s i_{sq} + L_q \frac{di_{sq}}{dt} + \omega L_d i_{sd} \\ \frac{d\omega}{dt} = \frac{3}{2}\frac{p^2}{J_m}\left(L_d - L_q\right) i_{sd} i_{sq} - \frac{f}{J_m}\omega - \frac{p}{J_m} T_L(t) \end{cases} \tag{4.15}$$

here, V_{sd} and V_{sq} are the direct and the quadrature stator voltages respectively. i_{sd} and i_{sq} are the direct and the quadrature stator currents. ω is the rotor electrical angular speed. $T_L(t)$ is the resistant torque which is the unknown input affecting the state dynamics.

The parameters of the motor are giving in the following table [Yahia et al., 2014]:

Parameters	**Values**
Rated power	$P_r = 2.2[KW]$
Rated voltage	$V_r = 220/380[V]$
Rated speed	$\Omega_r = 1500[rpm]$
Stator resistance	$R_s = 1.71\ [\Omega]$
Inductance of direct axis	$L_d = 0.15\ [H]$
Inductance of quadratic axis	$L_q = 0.04\ [H]$
Moment of inertia	$Jm = 0.0137\ [Kg.m^2]$
Number of pair of poles	$p = 2$
Friction coefficient	$f = 0.00036\ [Nm/rad/s]$

Table 4.1: Synchronous reluctance motor parameters

By defining $x(t) = \begin{bmatrix} i_{sd} & i_{sq} & \omega \end{bmatrix}^T$, $u(t) = \begin{bmatrix} u_{sd} & u_{sq} \end{bmatrix}^T$ and $d(t) = T_L(t)$ the state space representation of the SynRM is presented as follows:

$$\begin{cases} \dot{x}(t) = A(x)x(t) + Bu(t) + Ed(t) \\ y(t) = Cx(t) + Gd(t) \end{cases} \tag{4.16}$$

where:

$$A(x) = \begin{bmatrix} \frac{-R_s}{L_d} & \frac{L_q}{L_d}\omega & 0 \\ -\frac{L_d}{L_q}\omega & \frac{-R_s}{L_q} & 0 \\ \alpha i_{sq} & 0 & -\frac{f}{Jm} \end{bmatrix}, B = \begin{bmatrix} \frac{1}{L_d} & 0 \\ 0 & \frac{1}{L_q} \\ 0 & 0 \end{bmatrix}, E = \begin{bmatrix} 0 \\ 0 \\ -\frac{p}{Jm} \end{bmatrix},$$

$$C = \begin{bmatrix} 0 & 0 & 1 \end{bmatrix}, \alpha = \frac{3p^2}{2Jm}(L_d - L_q), G = 0.$$

2 - Takagi-Sugeno fuzzy representation of the system

The T-S multi-model is given as follows:

$$\begin{cases} \dot{x}(t) = \sum_{i=1}^{r} \mu_i(\xi(t))(A_i x(t) + B_i u(t) + E_i d(t)) \\ y(t) = \sum_{i=1}^{r} \mu_i(\xi(t))(C_i x(t) + G_i d(t)) \end{cases} \tag{4.17}$$

By defining the premise variables $\xi_1 = i_{sq}$ and $\xi_2 = \omega$ as the nonlinear terms in the dynamical model of the SynRM in (4.16), the weighting functions can be described as follows:

$$\mu_i(\xi(t)) = \prod_{j=1}^{2} M_{ij}(\xi_j) \tag{4.18}$$

where the membership functions of the fuzzy rules are:

$$\begin{aligned} &\textbf{Rule1: } M_{11} = W_1(\xi_1), M_{12} = W_1(\xi_2) \\ &\textbf{Rule2: } M_{21} = W_1(\xi_1), M_{22} = W_2(\xi_2) \\ &\textbf{Rule3: } M_{31} = W_2(\xi_1), M_{32} = W_1(\xi_2) \\ &\textbf{Rule4: } M_{41} = W_2(\xi_1), M_{42} = W_2(\xi_2) \end{aligned}$$

And using the sector nonlinearity approach the following functions are obtained:

$$\begin{aligned} W_1(\xi_1) &= \frac{\xi_1 - \xi_{1min}}{\xi_{1max} - \xi_{1min}}, W_2(\xi_1) = \frac{\xi_{1max} - \xi_1}{\xi_{1max} - \xi_{1min}} \\ W_1(\xi_2) &= \frac{\xi_2 - \xi_{2min}}{\xi_{2max} - \xi_{2min}}, W_2(\xi_2) = \frac{\xi_{2max} - \xi_2}{\xi_{2max} - \xi_{2min}} \end{aligned}$$

The sub-matrices A_i, B_i, C_i, E_i and G_i of the multi-model (4.17) are given using the sector nonlinearity approach as follows:

$$A_1 = \begin{bmatrix} \frac{-R_s}{L_d} & \frac{L_q}{L_d}\omega_{max} & 0 \\ -\frac{L_q}{L_d}\omega_{max} & \frac{-R_s}{L_q} & 0 \\ \alpha i_{sq_{max}} & 0 & -\frac{f}{Jm} \end{bmatrix}, A_2 = \begin{bmatrix} \frac{-R_s}{L_d} & \frac{L_q}{L_d}\omega_{min} & 0 \\ -\frac{L_q}{L_d}\omega_{min} & \frac{-R_s}{L_q} & 0 \\ \alpha i_{sq_{max}} & 0 & -\frac{f}{Jm} \end{bmatrix}$$

$$A_3 = \begin{bmatrix} \frac{-R_s}{L_d} & \frac{L_q}{L_d}\omega_{max} & 0 \\ -\frac{L_q}{L_d}\omega_{max} & \frac{-R_s}{L_q} & 0 \\ \alpha i_{sq_{min}} & 0 & -\frac{f}{Jm} \end{bmatrix}, A_4 = \begin{bmatrix} \frac{-R_s}{L_d} & \frac{L_q}{L_d}\omega_{min} & 0 \\ -\frac{L_q}{L_d}\omega_{min} & \frac{-R_s}{L_q} & 0 \\ \alpha i_{sq_{min}} & 0 & -\frac{f}{Jm} \end{bmatrix}$$

$$B_i = \begin{bmatrix} \frac{1}{L_d} & 0 \\ 0 & \frac{1}{L_q} \\ 0 & 0 \end{bmatrix}, C_i = \begin{bmatrix} 0 & 0 & 1 \end{bmatrix}, E_i = \begin{bmatrix} 0 \\ 0 \\ -\frac{p}{Jm} \end{bmatrix}, G_i = 0 \ \forall i = 1 \dots 4$$

3 - Observer design for synchronous reluctance motor

The following figure illustrates the overall schematic diagram of the implementation of the observer with the SynRM.

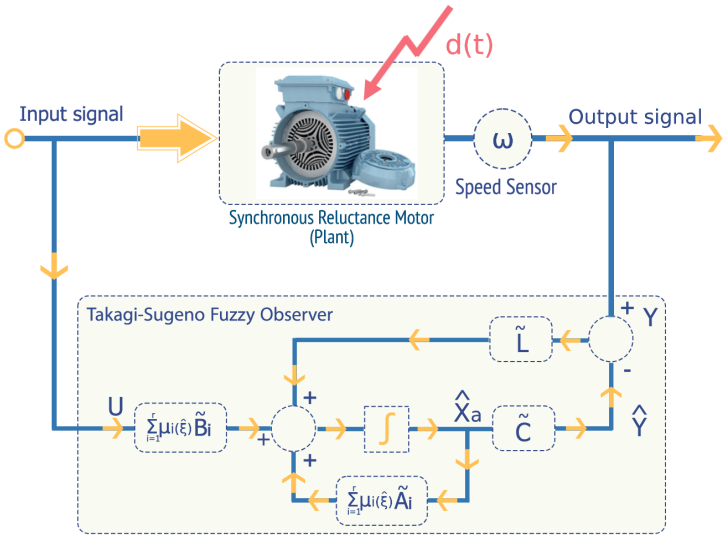

Fig 4.4: Overall schematic diagram of the observer.

In order to apply Theorem 4.1, the matrices $\widetilde{\mathcal{A}}_i$ and $\widetilde{\mathcal{C}}_i$ have to be determined.

According to the mean value theorem, $\widetilde{\Phi}_1(x_a(t))$ is defined as follows:

$$\widetilde{\Phi}_1(x_a) = \widetilde{A}(x_a)\, x_a + \widetilde{B}_i u(t)$$

where:

$$\widetilde{A}(x_a) = \begin{bmatrix} \mathrm{A}(x) & \mathrm{E} \\ 0 & 0 \end{bmatrix}$$

While its Jacobian $\frac{\partial \widetilde{\Phi}_1}{\partial x_a}$ is given by:

$$\frac{\partial \widetilde{\Phi}_1}{\partial x_a} = \begin{bmatrix} \frac{\partial \mathrm{A}(x)x}{\partial x} & \mathrm{E} \\ 0 & 0 \end{bmatrix}$$

where:

$$\frac{\partial A(x)x}{\partial x} = \begin{bmatrix} -\frac{R_s}{L_d} & \frac{L_q}{L_d}\omega & \frac{L_q}{L_d}i_{sq} \\ -\frac{L_d}{L_q}\omega & -\frac{R_s}{L_q} & -\frac{L_d}{L_q}i_{sd} \\ \alpha i_{sq} & \alpha i_{sd} & -\frac{f}{Jm} \end{bmatrix}$$

Through the use of the T-S representation on $\frac{\partial \widetilde{\phi}_1}{\partial x_a}$,The matrices $\widetilde{\mathcal{A}}_i$ can be obtained as follows:

$$\widetilde{\mathcal{A}}_i = \begin{bmatrix} \mathcal{A}_i & \mathrm{E} \\ 0 & 0 \end{bmatrix}$$

where:

$$\mathcal{A}_1 = \begin{bmatrix} -\frac{R_s}{L_d} & \frac{L_q}{L_d}\omega_{max} & \frac{L_q}{L_d}i_{sq_{max}} \\ -\frac{L_d}{L_q}\omega_{max} & -\frac{R_s}{L_q} & -\frac{L_d}{L_q}i_{sd_{max}} \\ \alpha i_{sq_{max}} & \alpha i_{sd_{max}} & -\frac{f}{Jm} \end{bmatrix}, \mathcal{A}_2 = \begin{bmatrix} -\frac{R_s}{L_d} & \frac{L_q}{L_d}\omega_{min} & \frac{L_q}{L_d}i_{sq_{max}} \\ -\frac{L_d}{L_q}\omega_{min} & -\frac{R_s}{L_q} & -\frac{L_d}{L_q}i_{sd_{max}} \\ \alpha i_{sq_{max}} & \alpha i_{sd_{max}} & -\frac{f}{Jm} \end{bmatrix}$$

$$\mathcal{A}_3 = \begin{bmatrix} -\frac{R_s}{L_d} & \frac{L_q}{L_d}\omega_{max} & \frac{L_q}{L_d}i_{sq_{min}} \\ -\frac{L_d}{L_q}\omega_{max} & -\frac{R_s}{L_q} & -\frac{L_d}{L_q}i_{sd_{max}} \\ \alpha i_{sq_{min}} & \alpha i_{sd_{max}} & -\frac{f}{Jm} \end{bmatrix}, \mathcal{A}_4 = \begin{bmatrix} -\frac{R_s}{L_d} & \frac{L_q}{L_d}\omega_{min} & \frac{L_q}{L_d}i_{sq_{min}} \\ -\frac{L_d}{L_q}\omega_{min} & -\frac{R_s}{L_q} & -\frac{L_d}{L_q}i_{sd_{max}} \\ \alpha i_{sq_{min}} & \alpha i_{sd_{max}} & -\frac{f}{Jm} \end{bmatrix}$$

$$\mathcal{A}_5 = \begin{bmatrix} -\frac{R_s}{L_d} & \frac{L_q}{L_d}\omega_{max} & \frac{L_q}{L_d}i_{sq_{max}} \\ -\frac{L_d}{L_q}\omega_{max} & -\frac{R_s}{L_q} & -\frac{L_d}{L_q}i_{sd_{min}} \\ \alpha i_{sq_{max}} & \alpha i_{sd_{min}} & -\frac{f}{Jm} \end{bmatrix}, \mathcal{A}_6 = \begin{bmatrix} -\frac{R_s}{L_d} & \frac{L_q}{L_d}\omega_{min} & \frac{L_q}{L_d}i_{sq_{max}} \\ -\frac{L_d}{L_q}\omega_{min} & -\frac{R_s}{L_q} & -\frac{L_d}{L_q}i_{sd_{min}} \\ \alpha i_{sq_{max}} & \alpha i_{sd_{min}} & -\frac{f}{Jm} \end{bmatrix}$$

$$\mathcal{A}_7 = \begin{bmatrix} -\frac{R_s}{L_d} & \frac{L_q}{L_d}\omega_{max} & \frac{L_q}{L_d}i_{sq_{min}} \\ -\frac{L_d}{L_q}\omega_{max} & -\frac{R_s}{L_q} & -\frac{L_d}{L_q}i_{sd_{min}} \\ \alpha i_{sq_{min}} & \alpha i_{sd_{min}} & -\frac{f}{Jm} \end{bmatrix}, \mathcal{A}_8 = \begin{bmatrix} -\frac{R_s}{L_d} & \frac{L_q}{L_d}\omega_{min} & \frac{L_q}{L_d}i_{sq_{min}} \\ -\frac{L_d}{L_q}\omega_{min} & -\frac{R_s}{L_q} & -\frac{L_d}{L_q}i_{sd_{min}} \\ \alpha i_{sq_{min}} & \alpha i_{sd_{min}} & -\frac{f}{Jm} \end{bmatrix}$$

According to the output equation, which is linear, $\widetilde{\Phi}_2(x_a(t)) = \widetilde{C}x_a(t)$; hence:

$$\frac{\partial \widetilde{\Phi}_2}{\partial x_a} = \widetilde{C} = \begin{bmatrix} C & G \end{bmatrix}$$

Therefore:

$$\widetilde{\mathcal{C}}_i = \widetilde{C}$$

By considering the output as the rotor's electrical angular speed, denoted as $y(t) = \omega(t)$, and a decay rate of $\alpha = 6.5$, Theorem 4.1 is applied to derive the following matrices for the PIO:

$$L_P = \begin{bmatrix} 8.2961 \times 10^{-12} \\ -3.0162 \times 10^{-12} \\ 1.2254 \times 10^{+4} \end{bmatrix}, L_I = \begin{bmatrix} -1.4678 \times 10^{+3} \end{bmatrix}$$

$$P = \begin{bmatrix} 2.763610^{+07} & 5.007510^{-11} & -2.501410^{-08} & -1.661210^{-10} \\ 5.007510^{-11} & 1.965210^{+06} & 6.385410^{-10} & -1.059610^{-11} \\ -2.501410^{-08} & 6.385410^{-10} & 8.173410^{+04} & 1.628510^{+03} \\ -1.661210^{-10} & -1.059610^{-11} & 1.628510^{+03} & 1.831210^{+04} \end{bmatrix}$$

4 - Simulation results

In this analysis, the Indirect Field-Oriented Control strategy is incorporated alongside the unknown input observer, which serves to regulate the SynRM. Figure 4.5 illustrates the control scheme structure utilized in the experiment. Since the primary focus of this example is on enhancing the state estimation performance, the control gains for the current and speed regulator were determined using the classical pole placement method. The employed speed regulator is of the "IP" type with $K_{P\Omega} = 5.7070$ and $K_{I\Omega} = 156.9792$ and the current regulation is of the "PI" type with $K_{Pi} = 86.8056$ and $K_{Ii} = 989.5833$.

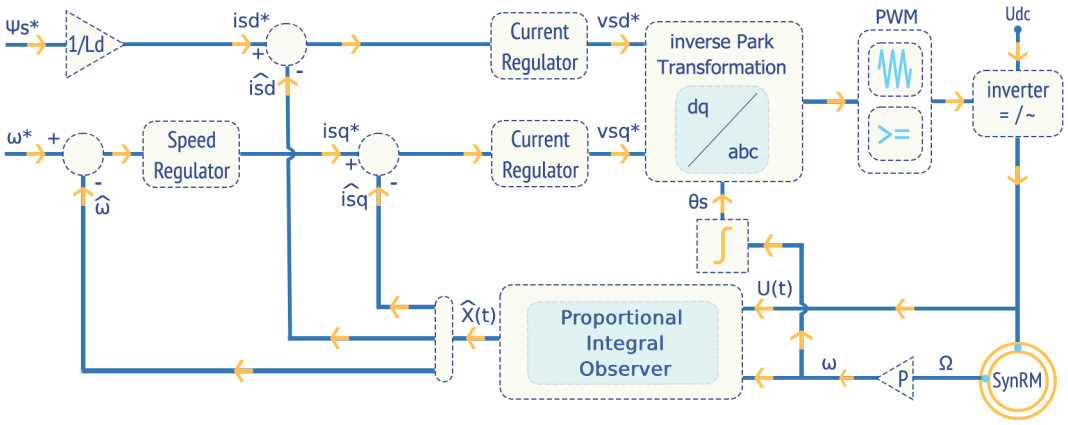

Fig 4.5: Schematic diagram of indirect field-oriented control with simultaneous state and unknown input observer.

The experiment was structured around the speed profile depicted in Figure 4.6, maintaining a constant magnetic flux reference at $0.8(Wb)$. To rigorously assess the observer's resilience and the stability of the estimation error dynamics, specific initial conditions were chosen, represented by $x_0(t) = \begin{bmatrix} -1 & 2 & 50 \end{bmatrix}^T$ and $\hat{x}_0(t) = \begin{bmatrix} 0 & 0 & 0 \end{bmatrix}^T$. A comprehensive analysis of the state estimation outcomes can be discerned from Figure 4.6 to Figure 4.9. Figure 4.10 and Figure 4.11 specifically delineate the estimation processes of the unknown input.

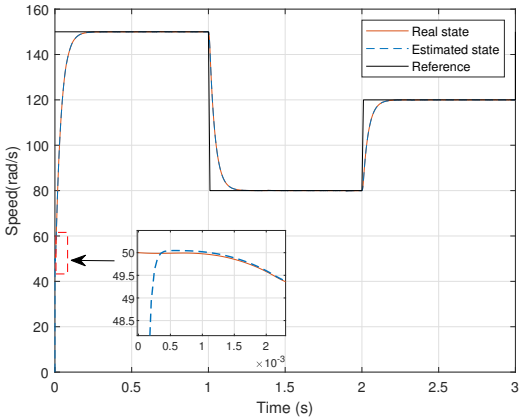

Fig 4.6: Rotor angular speed curve.

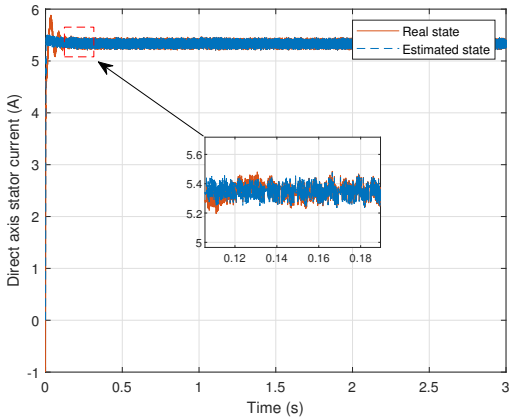

Fig 4.7: Direct axis stator current.

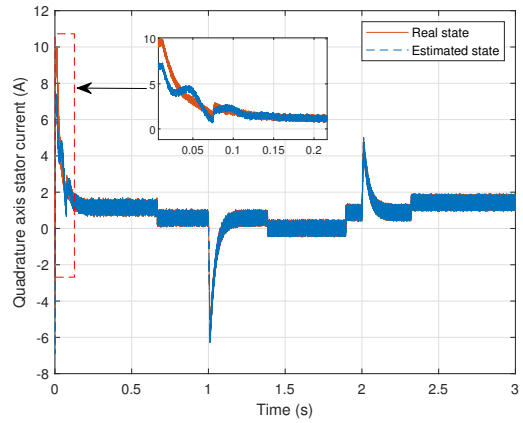

Fig 4.8: Quadrature axis stator current.

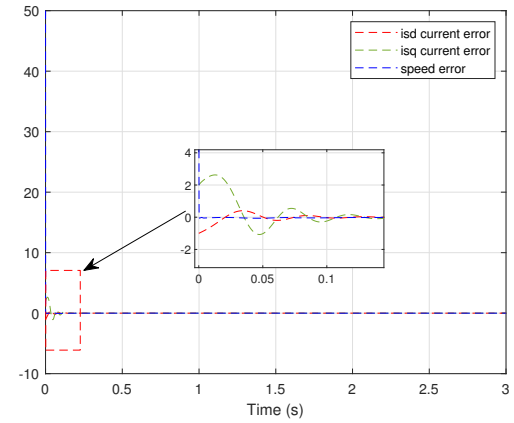

Fig 4.9: State estimation error.

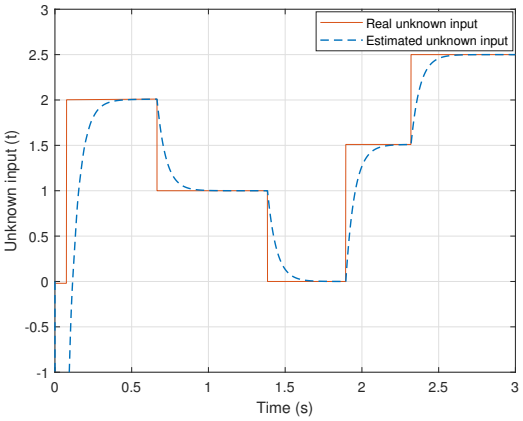

Fig 4.10: Unknown input of PIO.

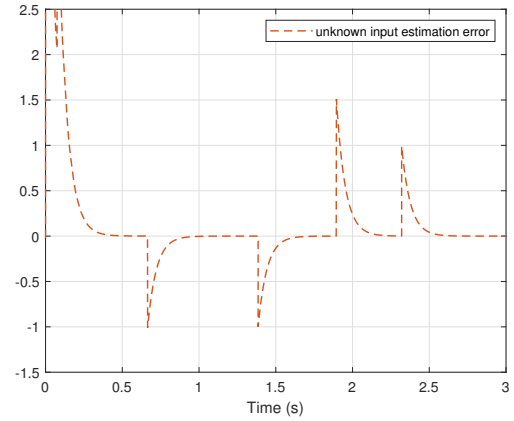

Fig 4.11: Unknown input error comparison.

An examination of the results in Figures 4.6 to 4.8, which depict speed, direct current, and quadratic current respectively, reveals that the observer efficiently estimates the state, despite the initial conditions of the observer and the motor being different. Figure 4.9, which shows the state estimation error, further corroborates this observation. The error converges to zero, indicating the observer's effectiveness in providing accurate

state estimation, regardless of initial disparities and unknown inputs.

Regarding the unknown input, Figure 4.10 presents the actual unknown input alongside its estimation. The unknown input, characterized as a stair-step function that remains constant within specific time intervals, is accurately estimated by the PIO within these intervals. However, during the transitions between these intervals, where the derivative is not null, the estimation is not identical since the PIO is designed for constant unknown inputs. Nevertheless, by choosing a decay rate of $\alpha = 6.5$, the observer gain and consequently the bandwidth are increased. This enhancement leads to a faster convergence of the estimation error, yielding acceptable results even during these transitional phases.

4.2.2 Proportional multi-integral observer design

The PIO's limitation, requiring the UI to be constant, is a conservative constraint that narrows the range of signals it can process. To improve the estimation performance of the UI, a more refined modeling approach is necessary. Consequently, this section introduces the PMIO, founded on the following assumption:

Assumption 4.2. *The unknown input $d(t)$ is assumed to follow a polynomial form. This assumption is characterized by the condition that its s^{th} time derivative is equal to zero:*

$$d^{(s)}(t) = 0 \tag{4.19}$$

This assumption enables an enhanced and more accurate modeling of the unknown input. Consequently, by adopting this assumption, it is no longer necessary for the UI to be constant. Instead, it can vary in any polynomial form. Consequently, the range of UI that the observer can handle is significantly expanded, resulting in less conservatism compared to the PIO.

The successive derivatives of $d(t)$ will be defined in the following state form:

$$\begin{bmatrix} \dot{d}(t) \\ \dot{d}_1(t) \\ \vdots \\ \dot{d}_{s-1}(t) \end{bmatrix} = \begin{bmatrix} d_1(t) \\ d_2(t) \\ \vdots \\ d_s(t) \end{bmatrix} \tag{4.20}$$

Employing this assumption enables the incorporation of the UI into the state-space representation of the system (4.1) as follows:

$$\begin{cases} \dot{x}(t) = \sum_{i=1}^{r} \mu_i(\xi(t)) \left(A_i x(t) + B_i u(t) + E_i d(t)\right) \\ y(t) = \sum_{i=1}^{r} \mu_i(\xi(t))(C_i x(t) + D_i u(t) + G_i d(t)) \\ \dot{d}(t) = d_1(t) \\ \vdots \\ \dot{d}_{s-1}(t) = d_s(t) \end{cases} \tag{4.21}$$

The augmented form of this system is described as follows:

$$\begin{cases} \dot{x}_a(t) = \sum_{i=1}^{r} \mu_i(\xi(t)) \left(\widetilde{A}_i x_a(t) + \widetilde{B}_i u(t)\right) \\ y(t) = \sum_{i=1}^{r} \mu_i(\xi(t))(\widetilde{C}_i x_a(t) + D_i u(t)) \end{cases} \tag{4.22}$$

where:

$$x_a(t) = \begin{bmatrix} x(t) \\ d(t) \\ d_1(t) \\ d_2(t) \\ \vdots \\ d_{s-1}(t) \end{bmatrix}, \widetilde{A}_i = \begin{bmatrix} A_i & E_i & 0 & \dots & 0 & 0 \\ 0 & 0 & I_{n_d} & \dots & 0 & 0 \\ 0 & 0 & 0 & \ddots & 0 & 0 \\ \vdots & \vdots & \vdots & \vdots & \vdots & \vdots \\ 0 & 0 & 0 & 0 & 0 & I_{n_d} \\ 0 & 0 & 0 & 0 & 0 & 0 \end{bmatrix}, \widetilde{B}_i = \begin{bmatrix} B_i \\ 0 \\ \vdots \\ 0 \end{bmatrix}, \widetilde{C}_i = \begin{bmatrix} C_i & G_i & 0 & \dots & 0 \end{bmatrix}$$

The structure of the PMIO observer of the system (4.21) is given as follows:

$$\begin{cases} \dot{\hat{x}} = \sum_{i=1}^{r} \mu_i(\hat{\xi}(t)) \left(A_i \hat{x}(t) + B_i u(t) + E_i \hat{d}(t)\right) + L_p(y(t) - \hat{y}(t)) \\ \hat{y}(t) = \sum_{i=1}^{r} \mu_i(\hat{\xi}(t))(C_i \hat{x}(t) + G_i \hat{d}(t) + D_i u(t)) \\ \dot{\hat{d}}(t) = L_{I0}(y(t) - \hat{y}(t)) + \hat{d}_1(t) \\ \dot{\hat{d}}_1(t) = L_{I1}(y(t) - \hat{y}(t)) + \hat{d}_2(t) \\ \vdots \\ \dot{\hat{d}}_{s-2}(t) = L_{Is-2}(y(t) - \hat{y}(t)) + \hat{d}_{s-1}(t) \\ \dot{\hat{d}}_{s-1}(t) = L_{Is-1}(y(t) - \hat{y}(t)) \end{cases} \tag{4.23}$$

where $\hat{d}_i \ \forall i = 1...s-1$ represent the estimation of the successive derivatives of the UI.

The augmented form of this observer is described as follows:

$$\begin{cases} \dot{\hat{x}}_a(t) = \sum_{i=1}^{r} \mu_i(\hat{\xi}(t)) \left(\widetilde{A}_i \hat{x}_a(t) + \widetilde{B}_i u(t)\right) + \widetilde{L}(y(t) - \hat{y}(t)) \\ \hat{y}(t) = \sum_{i=1}^{r} \mu_i(\hat{\xi}(t))(\widetilde{C}_i \hat{x}_a(t) + D_i u(t)) \end{cases} \tag{4.24}$$

where:

$$\widetilde{L} = \begin{bmatrix} L_P \\ L_I \end{bmatrix}, L_I = \begin{bmatrix} L_{I0} \\ L_{I1} \\ \vdots \\ L_{Is-1} \end{bmatrix}$$

The diagram of this observer is presented in Figure 4.12 below:

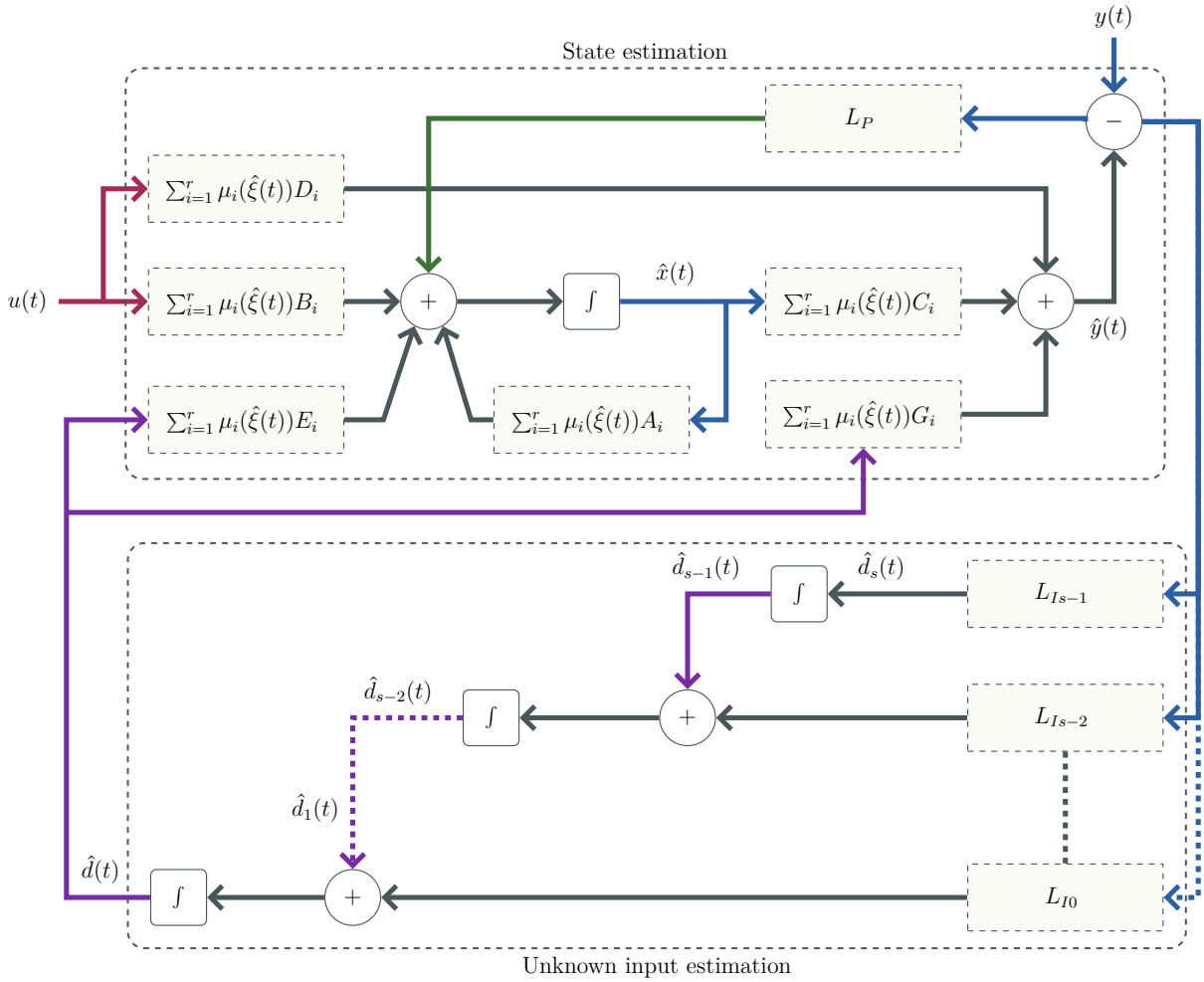

Fig 4.12: Proportional Multi-Integral Observer structure.

This diagram clearly illustrates the meaning of multi-integrals in the PMIO, which corresponds to employing multiple integral operations to estimate the UI. This process begins with the integral of the s^{th} derivative and progresses to derive the UI itself. In contrast, the PIO utilizes only a single integral operation.

To enhance the performance of UI estimation, it is required to increase the number of integrals. However, this increase necessitates significant modifications in the observer's structure, specifically by incorporating additional integral and summation operations. Consequently, a more adaptable structure is required. Let us rewrite the matrix $\widetilde{A}_i$ as follows:

$$\widetilde{A}_i = \begin{bmatrix} A_i & E_i & 0 \\ 0 & 0 & T \end{bmatrix}$$

where T is defined as:

$$T = \begin{bmatrix} I_{n_d} & \dots & 0 & 0 \\ 0 & \ddots & 0 & 0 \\ \vdots & \vdots & \vdots & \vdots \\ 0 & 0 & 0 & I_{n_d} \\ 0 & 0 & 0 & 0 \end{bmatrix}$$

Given this definition, the following matrix $\widetilde{T}$ is defined:

$$\widetilde{T} = \begin{bmatrix} 0 & T \end{bmatrix} = \begin{bmatrix} 0 & I_{n_d} & \dots & 0 & 0 \\ 0 & 0 & \ddots & 0 & 0 \\ \vdots & \vdots & \vdots & \vdots & \vdots \\ 0 & 0 & 0 & 0 & I_{n_d} \\ 0 & 0 & 0 & 0 & 0 \end{bmatrix}$$

With this definition, we can now define the following PMIO structure:

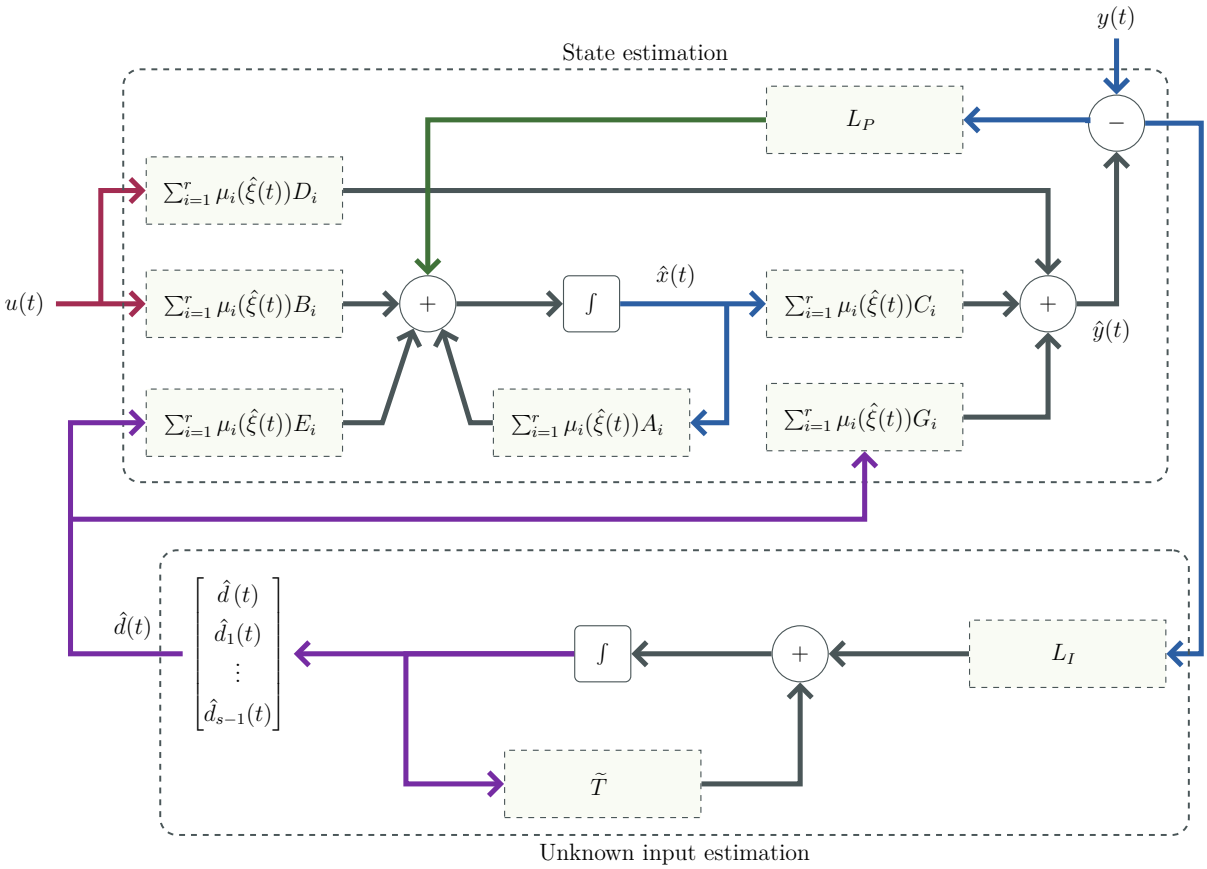

Fig 4.13: Compact proportional multi-integral observer structure.

This revised structure enhances adaptability for modifications compared to the previous one. It simplifies alterations by only requiring an update to the matrix $\widetilde{T}$ according to the degree of the polynomial UI under consideration.

The same theorem, Theorem 4.1, is employed for analyzing the stability of the estimation error dynamics in both the PIO and the PMIO scenarios. However, the distinction in these two cases arises from the differences in the matrices $\widetilde{A}_i$ and $\widetilde{C}_i$.

Example 11: Proportional multi-integral observer design for synchronous reluctance motor

In this analysis, a comparison is drawn between the PMIO and PIO methods. The objective is to highlight the effectiveness of the PMIO compared to the PIO. The same SynRM used in the previous example is employed here.

1 - Observer design for synchronous reluctance motor

The expression of $\widetilde{\Phi}_1\left(x_a(t)\right)$ is defined identically to its counterpart in the previous example, as follows:

$$\widetilde{\Phi}_1(x_a) = \widetilde{A}\left(x_a\right) x_a + \widetilde{B}_i u(t)$$

where, in the case of employing the PMIO, the matrix $\widetilde{A}\left(x_a\right)$ is defined as follows:

$$\widetilde{A}(x_a) = \begin{bmatrix} A(x) & E & 0 \\ 0 & 0 & T \end{bmatrix}$$

The Jacobian of $\widetilde{A}\left(x_a\right)$, denoted by $\frac{\partial \widetilde{\Phi}_1}{\partial x_a}$, is given by:

$$\frac{\partial \widetilde{\Phi}_1}{\partial x_a} = \begin{bmatrix} \frac{\partial \mathrm{A}(x)x}{\partial x} & E & 0 \\ 0 & 0 & T \end{bmatrix}$$

Through the use of the T-S representation on $\frac{\partial \widetilde{\Phi}_1}{\partial x_a}$, as demonstrated in the previous example, the matrices $\widetilde{\mathcal{A}}_i$ can be derived as follows:

$$\widetilde{\mathcal{A}}_i = \begin{bmatrix} \mathcal{A}_i & E & 0 \\ 0 & 0 & T \end{bmatrix}$$

where the matrices $\mathcal{A}_i$ here are the same as in the previous example.

According to the output equation, which is linear, $\widetilde{\Phi}_2(x_a(t)) = \widetilde{C}x_a(t)$; hence:

$$\frac{\partial \widetilde{\Phi}_2}{\partial x_a} = \widetilde{C} = \begin{bmatrix} C & G & 0 & \dots & 0 \end{bmatrix}$$

Therefore:

$$\widetilde{\mathcal{C}}_i = \widetilde{C}$$

By considering the same output and a decay rate as in the previous example, Theorem 4.1 is applied to derive the following gains for the PMIO with $s = 3$ (P3IO):

$$L_p = \begin{bmatrix} 8.5621 \times 10^{-12} \\ -5.8990 \times 10^{-12} \\ 1.3533 \times 10^{4} \end{bmatrix}, \quad L_I = \begin{bmatrix} -4.7362 \times 10^{3} \\ -6.1513 \times 10^{4} \\ -2.6645 \times 10^{5} \end{bmatrix}$$

2 - Hardware-in-the-loop validation

To assess the performance of the observer for SynRM, a comprehensive experimental approach was undertaken leveraging the HIL methodology. This method ensures the observer is assessed under conditions simulating real-world scenarios. The following Figure showcases the overall HIL architecture employed in the experiment:

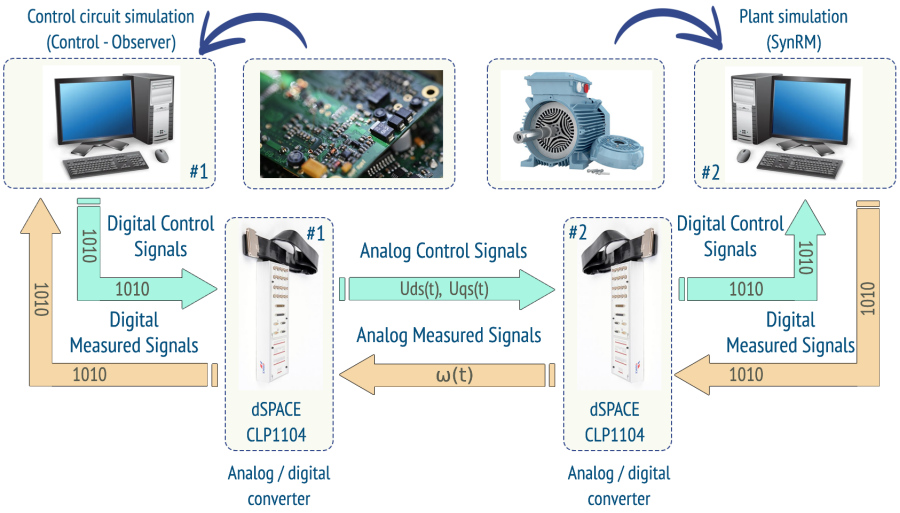

Fig 4.14: Structure of hardware-in-the-loop validation.

This configuration employed two Dspace 1104 cards, operating with a sampling time of $T_s = 0.0001(s)$. The initial card was tasked with the emulation of both the observer and the control circuit, guaranteeing that the observer's response and adjustments are analyzed in real-time. Concurrently, the secondary card was exclusively dedicated to the emulation of the SynRM. Its responsibility was to replicate the behavior and characteristics of the SynRM under various conditions. The entire setup for this experiment was carefully assembled at the LMSE Laboratory as showcased in the following figure:

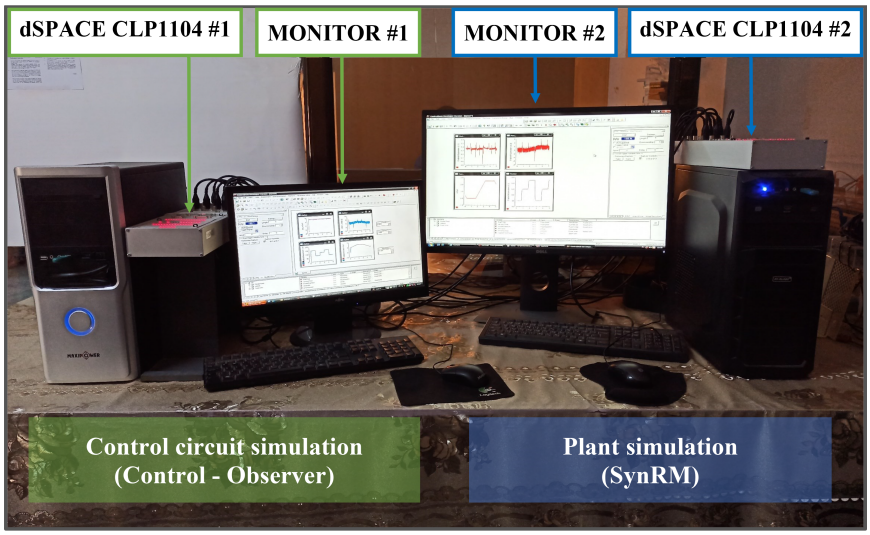

Fig 4.15: Test bench for hardware-in-the-Loop validation.

3 - Comparative results

3 - 1 - Case 1 (Slow unknown input variation)

A comparative analysis was performed under conditions where the variation in the unknown input was slow. Figure 4.16 illustrates the actual unknown input and its corresponding estimations. Under this circumstance, the disparity between both observers was found to be minimal, and both of them displayed competent performance, suggesting that they are both capable of handling unknown input with slower dynamics. The PIO, even though primarily tailored for estimating unknown inputs with null derivatives, seems to demonstrate flexibility in accommodating those with slow variations, essentially considering them almost like inputs with negligible derivatives.

Table 4.2 illustrates different performance criterion of the estimation error. The differences in errors, although slight, are still observable. The Integral Square Error (ISE), Integral Absolute Error (IAE), and Mean Squared Error (MSE) provide different perspectives on the performance. The PIO's slightly higher error values, compared to P3IO, imply that although it can handle slow variations, it is not as precise as the latter.

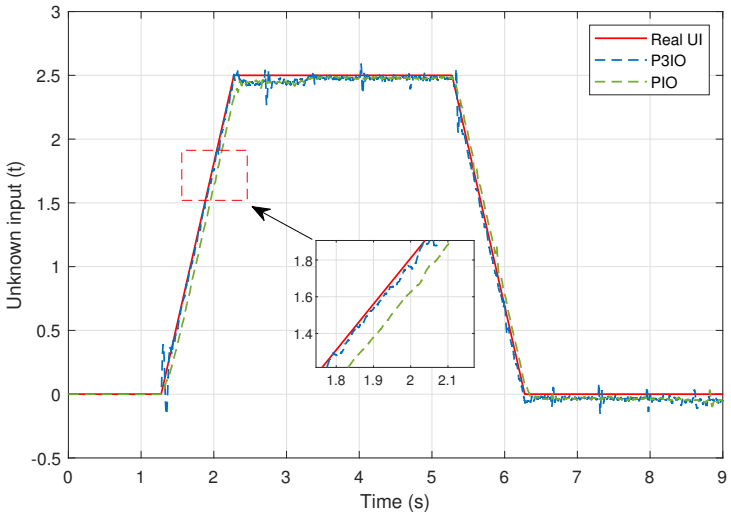

Fig 4.16: Unknown input estimation (case 1).

Observer performance	**Integral Square Error**	**Integral Absolute Error**	**Mean squared error**
PIO	0.0431	0.4116	0.0054
P3IO	**0.0186**	**0.2553**	**0.0023**

Table 4.2: Unknown input estimation performance (case 1)

4.2.2.1 Case 2 (Fast unknown input variation)

This case is specifically designed for scenarios where the unknown input variation is rapid. Figure 4.17 comprehensively displays both the actual unknown input and its corresponding estimates. The PIO's difficulty in accurately estimating rapidly changing unknown inputs becomes evident from the results. Its performance degradation is attributed to its inherent design limitations, which do not accommodate high variations. In contrast, the PMIO, with its design inherently built to handle such variations, showed a significant advantage in terms of adaptability and performance. Under these conditions, the performance disparity between the two observers became considerably more noticeable.

The results presented in Table 4.3 further highlight this distinction. A detailed analysis of the PIO's estimation error performances under these conditions indicates that fast-varying unknown inputs amplify the estimation error, leading to pronounced deviations from the anticipated outcomes. In contrast, the PMIO demonstrates a notable resilience against such changes, consistently maintaining low errors.

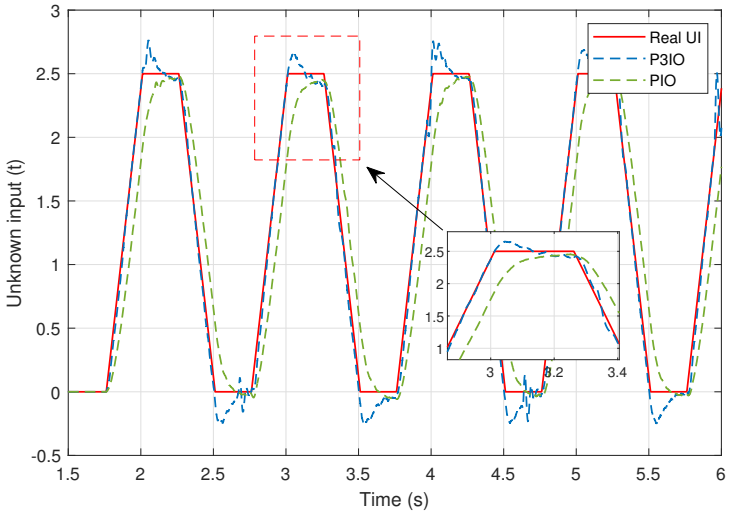

Fig 4.17: Unknown input estimation (case 2).

Observer performance	**Integral Square Error**	**Integral Absolute Error**	**Mean squared error**
PIO	1.0349	2.3026	0.1078
P3IO	**0.0873**	**0.6382**	**0.0095**

Table 4.3: Unknown input estimation performance (case 2)

4.2.3 Reducing excessive observer gains

One of the prevalent challenges in academic research is the constraints imposed by hardware capabilities. A widely utilized interface in this context is the dSPACE 1104 card. This card is generally restricted to a sampling time of up to $10^{-4}(s)$ using fixed step size numerical methods such as "Euler method". However, employing these specifications with very high observer gains can present difficulties. Beyond certain gain threshold, these solvers lose effectiveness, leading to the divergence of the numerical problem.

This limitation necessitates reducing the observer gains to enable the successful resolution of the differential equations integral to the model. Additionally, enhancing the performance of the observer, particularly for unknown input estimation, often involves pole assignment in the LMI region as α-stability used in Theorem 4.1. While effective, this technique tends to increase observer gains as discussed in Remark 4.3, thereby requiring a strategic balance to mitigate the associated challenges.

Although α-stability enhances the observer gain, achieving practical gains and precise estimation of states and unknown inputs in real-time applications necessitates incorporating a constraint that aids in reducing the observer gain. This approach is essential for achieving a balance between these two conflicting requirements. Based on equation (4.10) the observer gain could be calculated as follows:

$$\widetilde{L} = \frac{Cof\,(P)^T M}{\det(P)} \tag{4.25}$$

where $Cof\,(P)$ is the cofactor matrix of P and $\det(P)$ is its determinant. According to this equation it is clear that maximizing $\det(P)$ is a condition for reducing the observer gain $\widetilde{L}$, therefore the following constraint is provided:

$$\max \qquad \det(P) \tag{4.26}$$

It is apparent that this constraint, is non-convex problem which requires the use of monotonical transformation to convert it to a convex problem. In Yalmip, the geometric mean of the eigenvalues is the proposed solution because it is equal to $det(P)^{1/n}$ (where n is the order of P) which is a monotonic function of the determinant. The command "geomean" is applicable on Hermitian matrices provided by Yalmip to solve the determinant minimization problem.

It is important to highlight that the maximization constraint (4.26) have been used to derive the observer gains for both previous examples for the PIO and PMIO. Let's take for example the observer gains obtained without using this method in the case of P3IO by setting $\alpha = 6.5$ used for the SynRM:

$$det(P) = 2.0956 \times 10^{-6}$$

$$L_p = \begin{bmatrix} 5.9986 \times 10^{-13} \\ 1.0767 \times 10^{-11} \\ 2.3580 \times 10^{4} \end{bmatrix}, \quad L_I = \begin{bmatrix} -7.2357 \times 10^{4} \\ -1.3747 \times 10^{6} \\ -6.3888 \times 10^{6} \end{bmatrix}$$

However, the results in the case of using the maximization constraint are:

$$det(P) = 5.7705 \times 10^{24}$$

$$L_p = \begin{bmatrix} 8.5621 \times 10^{-12} \\ -5.8990 \times 10^{-12} \\ 1.3533 \times 10^{4} \end{bmatrix}, \quad L_I = \begin{bmatrix} -4.7362 \times 10^{3} \\ -6.1513 \times 10^{4} \\ -2.6645 \times 10^{5} \end{bmatrix}$$

It is apparent that the use of the maximization constraint significantly increases the determinant, in contrast to results obtained without such constraint. This difference is evident when comparing observer gains, the maximization method effectively reduces them. The gains derived from determinant maximization are suitable for real-time application using dSPACE 1104. Conversely, gains computed without the constraint are impractical for real-time use. Their excessively high values, reaching up to 10^6, combined with the limitations of the fixed numerical solver and the used sampling time, preclude real-time resolution.

4.2.4 Proportional multi-integral observer design using poly-quadratic Lyapunov function

In this section, an observer design utilizing the MVT and the poly-quadratic Lyapunov function is introduced to mitigate the conservatism inherent in the quadratic approach. This approach is a generalization of the method presented in Section 3.5.3 to accommodate unknown inputs. To analyze the estimation error dynamics stability using the poly-quadratic Lyapunov function, the following assumption is required:

Assumption 4.3. *The derivatives with respect to time for the weighting functions are constrained by positive constants, represented as $\emptyset_i$, described below:*

$$\left|\dot{h}_i\left(z(t)\right)\right| \leq \emptyset_i \tag{4.27}$$

By defining in prior the value of $\emptyset_k$, then the following theorem provides sufficient conditions described as BMI to ensure the asymptotic convergence of the error dynamics:

Theorem 4.2

The estimation error converges asymptotically toward zero if there exist symmetric positive definite matrices $P_j \in \mathbb{R}^{n_{x_a} \times n_{x_a}}$, a matrix $\widetilde{L} \in \mathbb{R}^{n_{x_a} \times n_y}$ and a symmetric matrix $P_0 \in \mathbb{R}^{n_{x_a} \times n_{x_a}}$, such that the following inequalities holds $\forall i, j = 1, ..., q$:

$$P_i \geq P_0, \qquad i = 1, \ldots, q \tag{4.28}$$

$$\mathcal{K}_{ii} < 0, \qquad i = 1, \ldots, q \tag{4.29}$$

$$\frac{1}{q-1}\mathcal{K}_{ii} + \frac{1}{2}\left(\mathcal{K}_{ij} + \mathcal{K}_{ji}\right) < 0, \qquad 1 \leq i \neq j \leq q \tag{4.30}$$

where:

$$\mathcal{K}_{ij} = \widetilde{\mathcal{A}}_i^T P_j + P_j \widetilde{\mathcal{A}}_i - \widetilde{\mathcal{C}}_i^T \widetilde{L}^T P_j - P_j \widetilde{L} \widetilde{\mathcal{C}}_i + \sum_{k=1}^{q} \emptyset_k \left(P_k - P_0\right) \tag{4.31}$$

The proof of this theorem is similar to that of Theorem 3.6.

The BMI optimization problem is solved using iterative LMI as previously discussed in Section 3.5.3.1, where the algorithm is described as follows:

- **Step1:** By fixing the observer gains L_P and L_I by an initial condition, the BMI in equations (4.29)-(4.30) becomes an LMI problem. Upon solving this problem, suitable initial matrices P_i can be obtained.
- **Step2:** The obtained matrices P_i are now used as known quantities, and only the observer gains L_P and L_I as unknown, which also leads to an LMI problem. If the problem is feasible, the obtained gains can be used by the observer; otherwise, the next step is added.
- **Step3:** Different matrices P_i have to be chosen because the earlier ones were inaccurate. Given that the solver tailored L_P and L_I to be nearly accurate in step 2, it can now be considered as a reference. Hence, as in Step 1, updated values of P_i can be derived that are more accurate than the initial ones. If these are not suitable enough, alternative values can be explored, and the second step must then be repeated.

4.2.4.1 Examples:

In this section, two examples are presented. In the first one, the feasibility area of the proposed theorem is compared with that of the quadratic approach to demonstrate the improvement achieved. The second example is a simulation that illustrates actuator

and sensor fault detection in a three-tank hydraulic system using unmeasurable premise variables as opposed to the use of measurable variables reported in previous works.

Example 12: Feasibility area

The feasibility domain is obtained by applying the quadratic and poly-quadratic approach to a system evaluated in terms of two parameters a and b. For every pair $(a\ , b)$ the feasibility is verified by checking the eigenvalues of the LMIs. In this example, both "SDPT3" and "MOSEK" solvers are used to solve the LMI of Theorem 4.2 and to design a proportional two-integrals observer $P2IO$.

1 - Observer design for the system

Let us consider the following nonlinear system:

$$\begin{cases} \dot{x} = A\left(x\right)x + Ed \\ y = Cx + Gd \end{cases} \tag{4.32}$$

where:

$$A\left(x\right) = \begin{bmatrix} -7 & -20 + 10\frac{tanh(x_2)}{x_2} & a \\ -4 & -13.58 & -1.17 + 2.87\frac{tanh(x_3)}{x_3} \\ b & a-b & -3.1 \end{bmatrix}, E = \begin{bmatrix} 6 \\ -10 \\ -3 \end{bmatrix}, C = \begin{bmatrix} 0 & 1 & 0 \end{bmatrix}, G = 1$$

In order to apply Theorem 4.2, the matrices $\widetilde{\mathcal{A}}_i$ and $\widetilde{\mathcal{C}}_i$ have to be determined. According to the mean value theorem, $\widetilde{\Phi}_1(x_a(t))$ is defined as follows:

$$\widetilde{\Phi}_1(x_a) = \widetilde{A}\left(x_a\right)x_a + \widetilde{B}_i u(t)$$

where:

$$\widetilde{A}\left(x_a\right) = \begin{bmatrix} A\left(x\right) & E & 0 \\ 0 & 0 & T \end{bmatrix}$$

While its Jacobian $\frac{\partial\widetilde{\Phi}_1}{\partial x_a}$ is given by:

$$\frac{\partial\widetilde{\Phi}_1}{\partial x_a} = \begin{bmatrix} \frac{\partial \mathrm{A}(x)x}{\partial x} & E & 0 \\ 0 & 0 & T \end{bmatrix}$$

where:

$$\frac{\partial \mathrm{A}(x)x}{\partial x} = \begin{bmatrix} -7 & \underbrace{-20 + 10\tanh\left(x_2\right)}_{\varepsilon_1} & a \\ -4 & -13.58 & \underbrace{-1.17 + 2.87\tanh\left(x_3\right)}_{\varepsilon_2} \\ b & a-b & -3.1 \end{bmatrix}$$

and the premise variables $\varepsilon_i(x)$ are limited as follows:

$$-30 \leq \varepsilon_1 \leq -10,\ -4.04 \leq \varepsilon_2 \leq 1.7$$

Through the use of the T-S representation on $\frac{\partial\widetilde{\Phi}_1}{\partial x_a}$, the matrices $\widetilde{\mathcal{A}}_i$ can be obtained as follows:

$$\widetilde{\mathcal{A}}_i = \begin{bmatrix} \mathcal{A}_i & E & 0 \\ 0 & 0 & T \end{bmatrix}$$

where the sub matrices $\mathcal{A}_i$ are given by:

$$\mathcal{A}_1 = \begin{bmatrix} -7 & -10 & a \\ -4 & -13.58 & 1.7 \\ b & a-b & -3.1 \end{bmatrix}, \ \mathcal{A}_2 = \begin{bmatrix} -7 & -10 & a \\ -4 & -13.58 & -4.04 \\ b & a-b & -3.1 \end{bmatrix}$$

$$\mathcal{A}_3 = \begin{bmatrix} -7 & -30 & a \\ -4 & -13.58 & 1.7 \\ b & a-b & -3.1 \end{bmatrix}, \ \mathcal{A}_4 = \begin{bmatrix} -7 & -30 & a \\ -4 & -13.58 & -4.04 \\ b & a-b & -3.1 \end{bmatrix}$$

Similarly to the previous examples of the MVT, the matrices $\widetilde{\mathcal{C}}_i$ are given by:

$$\widetilde{\mathcal{C}}_i = \widetilde{C} = \begin{bmatrix} C & G & 0 & \dots & 0 \end{bmatrix}$$

The weighting functions of the estimation error dynamics are defined by:

$$\begin{cases} h_1(z(t)) = M^1_{\varepsilon_1} \times M^1_{\varepsilon_2}, h_2(z(t)) = M^1_{\varepsilon_1} \times M^2_{\varepsilon_2} \\ h_3(z(t)) = M^2_{\varepsilon_1} \times M^1_{\varepsilon_2}, h_4(z(t)) = M^2_{\varepsilon_1} \times M^2_{\varepsilon_2} \end{cases}$$

where the membership functions are given by:

$$M^1_{\varepsilon_1} = \frac{\varepsilon_1 - \varepsilon_{1min}}{\varepsilon_{1max} - \varepsilon_{1min}}, \ M^2_{\varepsilon_1} = \frac{\varepsilon_{1max} - \varepsilon_1}{\varepsilon_{1max} - \varepsilon_{1min}}, M^1_{\varepsilon_2} = \frac{\varepsilon_2 - \varepsilon_{2min}}{\varepsilon_{2max} - \varepsilon_{2min}}, \ M^2_{\varepsilon_2} = \frac{\varepsilon_{2max} - \varepsilon_2}{\varepsilon_{2max} - \varepsilon_{2min}}$$

2 - Feasibility domain mapping

By setting the following intervals $a \in [50, 400]$ and $b \in [-4500, \ -500]$, the feasibility domains obtained from the quadratic and non-quadratic approaches are illustrated in Figure 4.18:

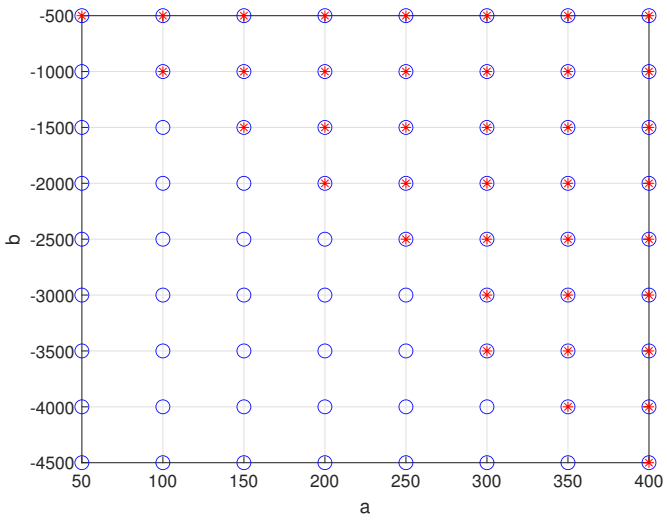

Fig 4.18: Feasibility area comparison: 'o' represents Theorem 4.2, while '*' denotes Theorem 4.1.

Method	Feasible points	Number of decision variables	Number of matrix inequalities
Theorem 4.1	33	2	5
Theorem 4.2	72	9	24

Table 4.4: Comparison of theorems' complexity

From Figure 4.18, it becomes apparent that the proposed technique offers a broader application scope than the traditional method. The novel theorem, which is based on the non-quadratic function, not only covers the area addressed by the quadratic model but it extends beyond it as well. Notably, from Table 4.4, the proposed method yields 72 feasible points, in contrast to the traditional method's 33 points. This underscores the superior efficiency of the new technique in reducing conservatism. However, it is clear that the non-quadratic function introduces more computational challenges than its quadratic counterpart. This increased complexity is due to the increased number of decision variables and matrix inequalities inherent to the new method, as well as the presence of BMI stability conditions.

3 - Simulation validation

To prove the feasibility of the proposed method, simulation is carried out at ($a = 100,\ b = -2500$) where the proposed method is applicable while the quadratic approach is not. By setting the initial conditions at $x_0 = \begin{bmatrix}3 & 3.3 & 4.5\end{bmatrix}^T$ and $\hat{x}_0 = \begin{bmatrix}2.7 & 2.97 & 4.05\end{bmatrix}^T$ the obtained matrices P_i are given as follows:

$$P_1 = \begin{bmatrix} 0.2227 & -0.1660 & 0 & 0.0686 & -0.0003 \\ -0.1660 & 0.2368 & 0.0013 & -0.1213 & 0.0161 \\ 0 & 0.0013 & 0.0088 & 0.0033 & 0 \\ 0.0686 & -0.1213 & 0.0033 & 0.1154 & -0.0313 \\ -0.0003 & 0.0161 & 0 & -0.0313 & 0.0116 \end{bmatrix}, \quad P_2 = \begin{bmatrix} 0.2150 & -0.1543 & 0 & 0.0625 & 0.0006 \\ -0.1543 & 0.2199 & 0.0014 & -0.1127 & 0.0150 \\ 0 & 0.0014 & 0.0088 & 0.0033 & 0 \\ 0.0625 & -0.1127 & 0.0033 & 0.1111 & -0.0308 \\ -0.0006 & 0.0150 & 0 & -0.0308 & 0.0116 \end{bmatrix}$$

$$P_3 = \begin{bmatrix} 0.2297 & -0.1714 & 0 & 0.0708 & -0.0003 \\ -0.1714 & 0.2474 & 0 & -0.1256 & 0.0161 \\ 0 & 0 & 0.0091 & 0.0038 & 0 \\ 0.0708 & -0.1256 & 0.0038 & 0.1171 & -0.0313 \\ -0.0003 & 0.0161 & 0 & -0.0313 & 0.0116 \end{bmatrix}, \quad P_4 = \begin{bmatrix} 0.2201 & -0.1577 & 0 & 0.0639 & 0.0006 \\ -0.1577 & 0.2283 & 0.0001 & -0.1165 & 0.0152 \\ 0 & 0.0001 & 0.0091 & 0.0037 & 0 \\ 0.0639 & -0.1165 & 0.0037 & 0.1128 & -0.0309 \\ -0.0006 & 0.0152 & 0 & -0.0309 & 0.0116 \end{bmatrix}$$

$$P_0 = \begin{bmatrix} 0.2126 & -0.1537 & 0 & 0.0617 & 0.0004 \\ -0.1537 & -0.7887 & 0.0013 & -1.1197 & 0.0150 \\ 0 & 0.0013 & 0.0087 & 0.0033 & 0 \\ 0.0617 & -1.1197 & 0.0033 & -0.8987 & -0.0308 \\ 0.0004 & 0.0150 & 0 & -0.0308 & 0.0115 \end{bmatrix}$$

while the resulting observer gains are given by:

$$L_P = \begin{bmatrix} -0.8318 \\ 3.4695 \\ -4.5987 \end{bmatrix} \times 10^4, L_I = \begin{bmatrix} 1.1198 \\ 2.5399 \end{bmatrix} \times 10^5$$

The results of the simulation are given in Figure 4.19 through Figure 4.21. The state estimation error is demonstrated in Figure 4.19 indicating that good results are obtained. In Figure 4.20, the blue line represents the real unknown input, while the yellow dashed line is the estimated unknown input. As shown, the observer gives a good estimation of the states with an error that converges toward zero, which proves, on one hand, the feasibility of the observer, and on the other, the reduction of the conservatism compared to the quadratic approach.

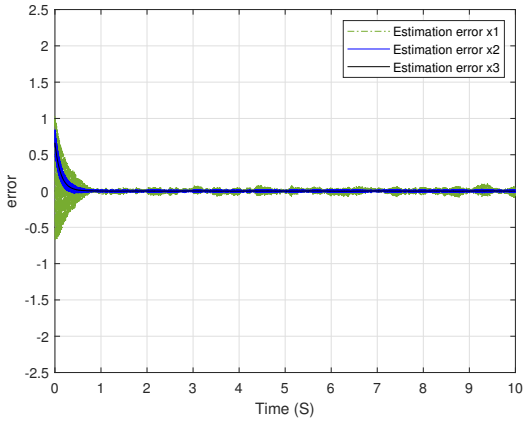

Fig 4.19: Estimation error.

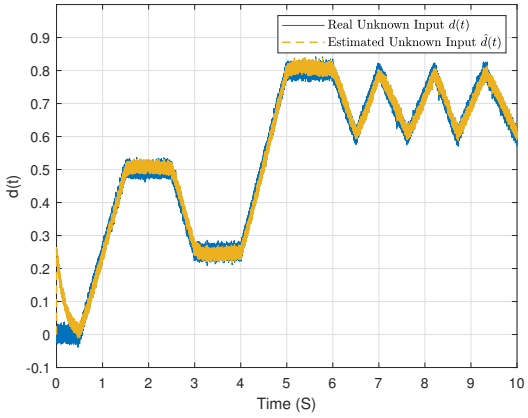

Fig 4.20: Unknown input estimation.

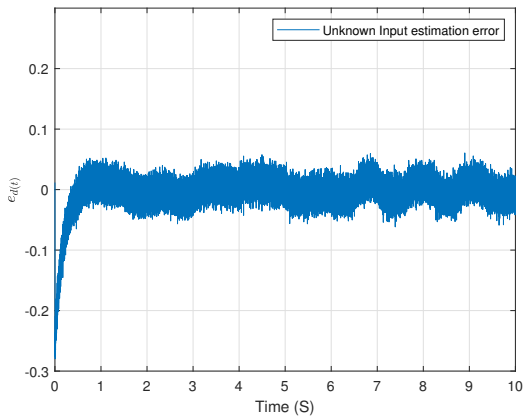

Fig 4.21: Unknown input estimation error.

Example 13: Actuator and sensor fault detection: application to three-tank hydraulic system

This example is given to prove the improvement of the observer to estimate unknown inputs in the case of unmeasured premise variables, as opposed to the work reported by Guzman [Guzman et al., 2021] who designed a PI observer using poly-quadratic Lyapunov function for only measured premise variables. For this purpose, we revisit the same three-tank hydraulic system model used in Guzman's work.

1 - Takagi-Sugeno fuzzy representation of the system:

Three-tank hydraulic mathematical model have been presented before in Section 3.5.2. Unlike in the previous example, this system is now assumed to be subject to faults in both the actuator and the sensor. To accurately represent these faults in the model, we introduce them respectively as $d(t) = \begin{bmatrix} d_a(t)^T & d_s(t)^T \end{bmatrix}^T$. With this modifications, the dynamical model of the system is accordingly updated to incorporate the effects of these faults:

$$\begin{cases} \dot{x}(t) = \sum_{i=1}^{r} \mu_i(\xi(t)) \left(A_i x(t) + B_i u(t) + E_i d(t)\right) \\ y(t) = \sum_{i=1}^{r} \mu_i(\xi(t)) \left(C_i x(t) + G_i d(t)\right) \end{cases}$$

where:

$$E_i = \frac{1}{S} \begin{bmatrix} -0.3 & 0 \\ 0 & 0 \\ 0 & 0 \end{bmatrix}, \qquad G_i = \begin{bmatrix} 0 & 0 \\ 0 & -0.3 \end{bmatrix} (i = 1, \ldots, r)$$

2 - Observer design for the system:

Deriving the matrices $\widetilde{\mathcal{A}}_i$ for the three-tank hydraulic system is similar to the previous MVT examples, these matrices are given by:

$$\widetilde{\mathcal{A}}_i = \begin{bmatrix} \mathcal{A}_i & E & 0 \\ 0 & 0 & T \end{bmatrix},$$

where the matrices $\mathcal{A}_i$ have been derived previously in Section 3.5.2.

Similarly, the matrices $\widetilde{\mathcal{C}}_i$ are given by:

$$\widetilde{\mathcal{C}}_i = \widetilde{C} = \begin{bmatrix} C & G & 0 & \ldots & 0 \end{bmatrix}$$

In order to design a P3IO, the following matrices are obtained by solving the BMI in Theorem 4.2:

$$L_p = \begin{bmatrix} 9.8319 & 1.6483 \\ -0.0032 & 0.0252 \\ 0.0075 & -0.0624 \end{bmatrix} \times 10^4, \quad L_I = \begin{bmatrix} -0.4672 & -0.0817 \\ 1.2089 & -9.9546 \\ -1.4165 & -0.2659 \\ 0.4905 & -4.0268 \\ -0.3476 & -0.0630 \\ 0.1374 & -1.1330 \end{bmatrix} \times 10^4$$

3 - Simulation results:

System simulation was carried using the initial condition $x_0 = \begin{bmatrix}0.09 & 0.07 & 0.08\end{bmatrix}^T$ and $\hat{x}_0 = \begin{bmatrix}0.092 & 0.072 & 0.081\end{bmatrix}^T$. The system inputs are shown in Figure 4.22. The actuator and sensor faults are shown in Figure 4.23 and Figure 4.24 with their respective estimations. The tanks levels and their estimation are shown in Figure 4.25.

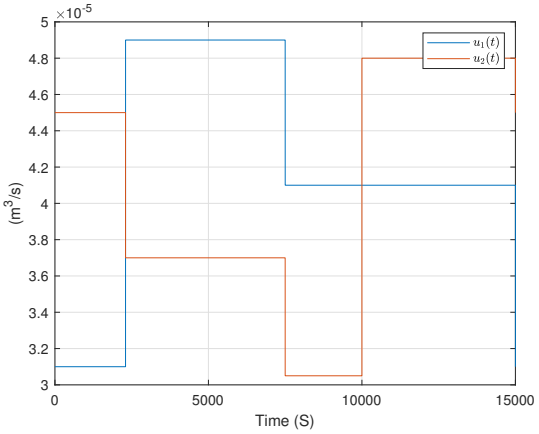

Fig 4.22: Flow rates of pumps.

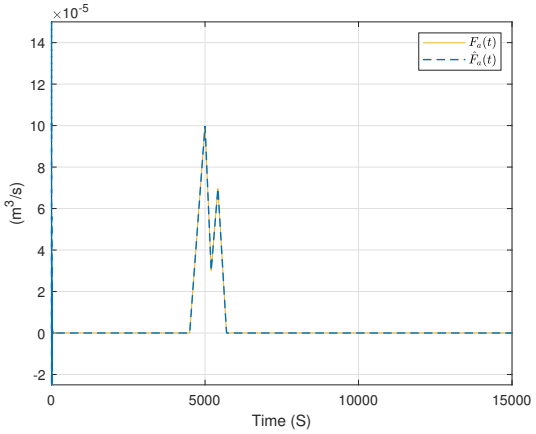

Fig 4.23: Actuator fault and its estimation.

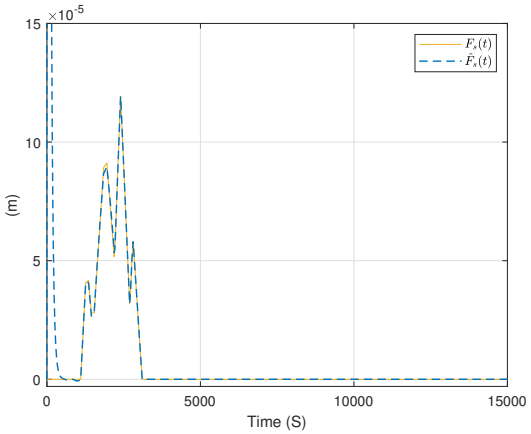

Fig 4.24: Sensor fault and its estimation.

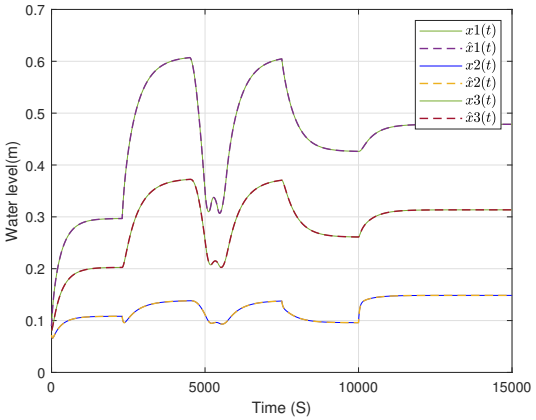

Fig 4.25: Tanks levels and their estimations.

The simulation results demonstrate the efficacy of the derived observer gains in estimating both the hydraulic system states and the actuator and sensor faults. Achieving this was made possible using an unmeasured premise variable based on a non-quadratic Lyapunov function. The use of the mean value theorem ensures that the estimation error dynamics become fully factorized and proportional to the estimation error, hence eliminating the effect of mismatching terms. This contrasts with Guzman's observer, designed solely for measurable premise variables, which failed to mitigate the effect of these mismatches. Consequently, our approach allows the observer to be applicable to a broader class of systems with either measurable or unmeasurable premise variables or even in the way the approach handles the mismatching terms.

4.3 Decoupled unknown input observer

Although PMIO covers a broader class of UIs compared to PIO, it faces challenges when the order of the polynomial UI exceeds the design limit of the observer or when the form of the UI is non-polynomial. Therefore, in this section, we will discuss the second class of unknown input observers which is the DUIO. As discussed in the introduction before, this class of observers is based on separating the UI from the state estimation error and estimates them independently. Unlike other observers, DUIO does not require prior determination of the UI order, hence allowing for the estimation of a larger class of unknown signals.

Consider the following T-S system, where the unknown inputs are assumed to influence both the state dynamics and the measurements:

$$\begin{cases} \dot{x}(t) = \sum_{i=1}^{r} \mu_i(\xi(t)) \left(A_i x(t) + B_i u(t) + E_i d(t)\right) \\ y(t) = Cx(t) + Gd(t) \end{cases} \tag{4.33}$$

In the subsequent sections, the design of the observer will be discussed for both MPV and UPV cases. A comparative analysis between the SSUIO and the DUIO will be discussed in the UPV section.

4.3.1 Observer design for MPV

The structure of the DUIO for the T-S system (4.33) is defined as:

$$\begin{cases} \dot{z}(t) = \sum_{i=1}^{r} \mu_i(\hat{\xi}(t)) \left(N_i z(t) + G_i u(t) + L_i y(t)\right) \\ \hat{x}(t) = z(t) - Hy(t) \end{cases} \tag{4.34}$$

The state estimation error between the system (4.33) and the observer (4.34) is given by:

$$\begin{aligned} e(t) &= x(t) - \hat{x}(t) = x(t) - z(t) + Hy(t) = x(t) - z(t) + HCx(t) + HGd(t) \\ &= Rx(t) - z(t) + HGd(t) \end{aligned} \tag{4.35}$$

where:

$$R = I + HC \tag{4.36}$$

The estimation error dynamics are given by:

$$\dot{e}(t) = R\dot{x}(t) - \dot{z}(t) + HG\dot{d}(t) \tag{4.37}$$

After substituting (4.33), (4.34), $y(t)$ and $z(t)$ in (4.37), and taking into account the equality given in (2.20) for MPV case, the following expression is obtained:

$$\begin{aligned}\dot{\mathrm{e}}(\mathrm{t}) = \sum_{\mathrm{i}=1}^{\mathrm{r}} \mu_{\mathrm{i}}(\hat{\xi}(\mathrm{t}))\,[(RA_i - N_i - K_iC)\,x(t) + (RB_i - G_i)\,u(t) \\ + (RE_i - K_iG)\,d(t) + N_ie(t)] + HG\dot{d}(t)\end{aligned} \tag{4.38}$$

where:

$$K_i = N_iH + L_i \tag{4.39}$$

Given that the following conditions are satisfied, as outlined in (4.40) to (4.43),

$$HG = 0 \tag{4.40}$$

$$N_i = RA_i - K_iC \tag{4.41}$$

$$RB_i = G_i \tag{4.42}$$

$$RE_i = K_iG \tag{4.43}$$

then, the error dynamics can be described as follows:

$$\dot{e}\,(t) = \sum_{i=1}^{r} \mu_i\left(\hat{\xi}\,(t)\right) N_ie(t) \tag{4.44}$$

Based on the work presented in [Akhenak et al., 2003], the following theorem is formulated, offering sufficient conditions for the asymptotic convergence of the error dynamics:

Theorem 4.3

The estimation error will tend towards zero asymptotically if there exist matrices $P = P^T \in \mathbb{R}^{n_x \times n_x} > 0, M_i \in \mathbb{R}^{n_x \times n_y}$ and $S \in \mathbb{R}^{n_x \times n_y}$ such that the following conditions hold $\forall i = 1, ..., r$:

$$(PA_i + SCA_i - M_iC)^T + (PA_i + SCA_i - M_iC) < 0 \tag{4.45}$$

$$SG = 0 \tag{4.46}$$

$$(P + SC)\,E_i = M_iG \tag{4.47}$$

The observer matrices are given by:

$$H = P^{-1}S \tag{4.48}$$

$$K_i = P^{-1}M_i \tag{4.49}$$

$$N_i = (I + HC)A_i - K_iC \tag{4.50}$$

$$L_i = K_i - N_iH \tag{4.51}$$

$$G_i = (I + HC)B_i \tag{4.52}$$

Proof. Let's define the quadratic Lyapunov function as follows:

$$V(t) = e(t)^T P e(t) \tag{4.53}$$

The time derivative of $V(t)$ is:

$$\dot{V}(t) = \dot{e}(t)^T P e(t) + e(t)^T P \dot{e}(t) \tag{4.54}$$

By substituting (4.44), (4.41) and (4.36) in (4.54), the following equation is obtained:

$$\begin{aligned} \dot{V}(t) = \textstyle\sum_{\mathrm{i}=1}^{\mathrm{r}} \mu_{\mathrm{i}}(\hat{\xi}(\mathrm{t})) e(t)^T \Big[& (P\ \mathrm{A_i} + PHC\ \mathrm{A_i} - PK_iC)^T \\ & + (P\ \mathrm{A_i} + PHC\ \mathrm{A_i} - PK_iC) \Big] e(t) \end{aligned} \tag{4.55}$$

Let us define the following change of variables:

$$S = PH \tag{4.56}$$

$$M_i = PK_i \tag{4.57}$$

By integrating (4.56) with (4.40), condition (4.46) is obtained. Similarly, combining (4.56) and (4.57) with (4.43), condition (4.47) is achieved. When these changes of variables are applied to the negativity of (4.55), result in condition (4.45) emerges. □

4.3.1.1 Unknown input estimation

Once the state estimation is achieved and the impact of the unknown input on the estimation error is effectively isolated, the unknown input can be inferred using the estimated state vector. In the context of system (4.33), the unknown input is presented alongside its respective influence matrix.

$$W(t) = \begin{bmatrix} \sum_{i=1}^{r} \mu_i \left(\hat{\xi}(t)\right) E_i \\ G \end{bmatrix} \tag{4.58}$$

The unknown input can be inferred using the following equation:

$$\hat{d}(t) = W^-(t) \begin{bmatrix} \dot{\hat{x}}(t) - \sum_{i=1}^{r} \mu_i \left(\hat{\xi}(t)\right) \left(A_i \hat{x}(t) + B_i u(t)\right) \\ y(t) - C\hat{x}(t) \end{bmatrix} \tag{4.59}$$

where $W^-(t)$ is left pseudo-inverse of $W(t)$, that exist if the following condition is verified at every instant t:

$$rank\left(W(t)\right) = n_d \tag{4.60}$$

where n_d is the dimension of the unknown input vector, and $W^-(t)$ is given in the following equation:

$$W^-(t) = \left(W^T(t) W(t)\right)^{-1} W^T(t) \tag{4.61}$$

4.3.1.2 Example of application

Example 14: DUIO design of fuel cell 3P-IBC

In this example the same 3P-IBC used in Section 2.3.1.1 is used here. However, in this example, the power source of the IBC is a Fuel Cell Electric Vehicles (FCEVs). The FCEVs are generally comprised of two core components: the power-train and the drive-train as visualized in Figure 4.26. The power-train can be further segmented into various subsystems, such as the fuel cell stack, the hydrogen storage system, power electronics and the auxiliary source. Conversely, the drive-train encompasses the elements that transfer power to the wheels, typically including the transmission, axles, and differentials. This example, however, focuses solely on two specific parts within the power-train: the fuel cell and the interleaved boost converter.

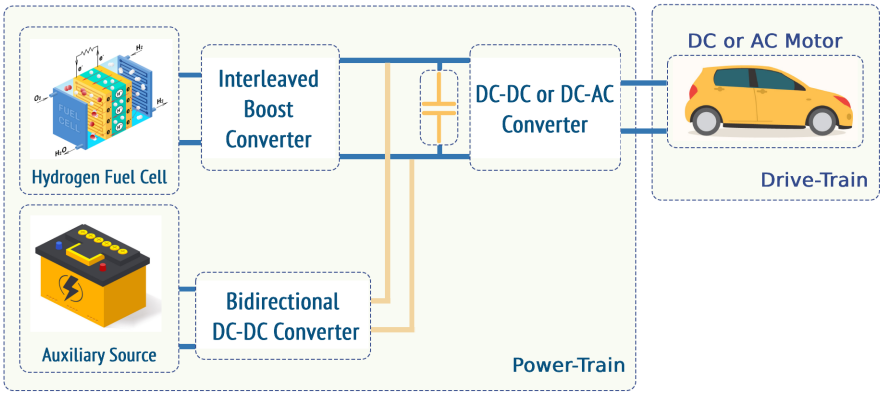

Fig 4.26: Fuel Cell Electric Vehicles Structure.

1 - Takagi-Sugeno fuzzy representation of the system

The T-S representation of the 3P-IBC was detailed earlier in Section 2.3.1.1. In this specific example, we redefine the current load $I_{Load}(t)$ as the unknown input $d(t)$:

$$\begin{cases} \dot{x}(t) = \sum_{i=1}^{r} \mu_i(\xi(t)) (A_i x(t) + B_i u(t) + E_i I_{Load}(t)) \\ y(t) = \sum_{i=1}^{r} \mu_i(\xi(t)) (C_i x(t)) \end{cases} \tag{4.62}$$

2 - Modeling of the fuel cell

Various Proton Exchange Membrane Fuel Cell (PEMFC) models have been documented in the literature. These can essentially be categorized into two types based on the primary characteristic of the fuel cell that the model targets: those are steady-state (or static) models and dynamic models [Hasanien et al., 2022]. Figure 4.27 shows a graphical representation of the relationship between the cell voltage and the current density of a 1.2$[kW]$ NexaTM PEMFC, typically obtained by conducting a series of steady-state measurements at different applied loads [Hammoudi et al., 2020].

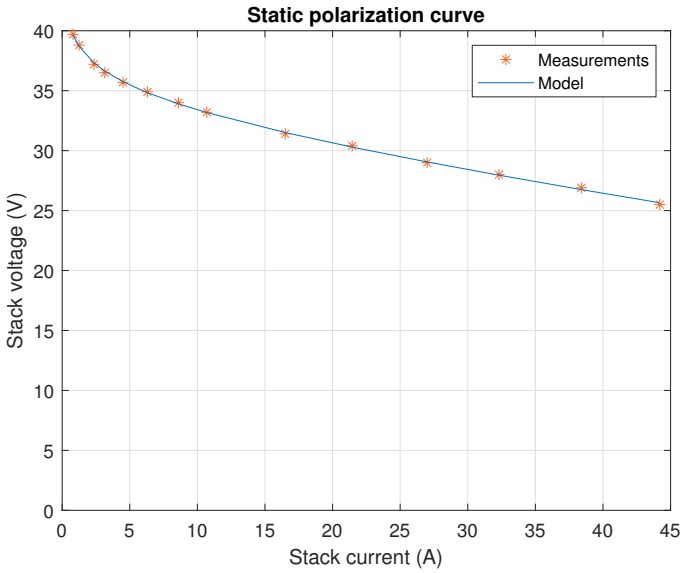

Fig 4.27: Static polarization curve of fuel cell.

The model utilized in this paper was derived through the interpolation of the collected data.

3 - DUIO Design for 3P-IBC

By considering the output as the output voltage V_{out}, Theorem 4.3 is applied to derive the following observer gains:

$$N_i = \begin{bmatrix} -6.5741 & 0 & 0 & 0 \\ 0 & -6.5741 & 0 & 0 \\ 0 & 0 & -6.5741 & 0 \\ 0 & 0 & 0 & -3.50 \end{bmatrix} \quad \forall i = 1 \dots 8 \ ,$$

$$L_1 = \begin{bmatrix} -925.9259 \\ -925.9259 \\ -925.9259 \\ 0 \end{bmatrix}, L_2 = \begin{bmatrix} -925.9259 \\ -925.9259 \\ 0 \\ 0 \end{bmatrix}, L_3 = \begin{bmatrix} -925.9259 \\ 0 \\ -925.9259 \\ 0 \end{bmatrix}, L_4 = \begin{bmatrix} -925.9259 \\ 0 \\ 0 \\ 0 \end{bmatrix},$$

$$L_5 = \begin{bmatrix} 0 \\ -925.9259 \\ -925.9259 \\ 0 \end{bmatrix}, L_6 = \begin{bmatrix} 0 \\ -925.9259 \\ 0 \\ 0 \end{bmatrix}, L_7 = \begin{bmatrix} 0 \\ 0 \\ -925.9259 \\ 0 \end{bmatrix}, L_8 = \begin{bmatrix} 0 \\ 0 \\ 0 \\ 0 \end{bmatrix}$$

$$H = \begin{bmatrix} 0 \\ 0 \\ 0 \\ -1 \end{bmatrix}, R = \begin{bmatrix} 1 & 0 & 0 & 0 \\ 0 & 1 & 0 & 0 \\ 0 & 0 & 1 & 0 \\ 0 & 0 & 0 & 0 \end{bmatrix}.$$

4 - Simulation results

Figure 4.28 illustrates the schematic of the control loop. In contrast to the topology presented in Section 2.3.1.1, this configuration employs only a single sensor, which measures the output voltage $V_{out}(t)$. Unlike the previous setup, the input I_{Load} is not necessary in this case, as its influence has been decoupled from the observer. Additionally, the input voltage $V_{in}(t) = V_{fc}(t)$ is derived from the mathematical model of the fuel cell, based on the consumed current. The simulation utilizes the same initial conditions for both the system and the observer as in the previous example, as well as the voltage and current regulators.

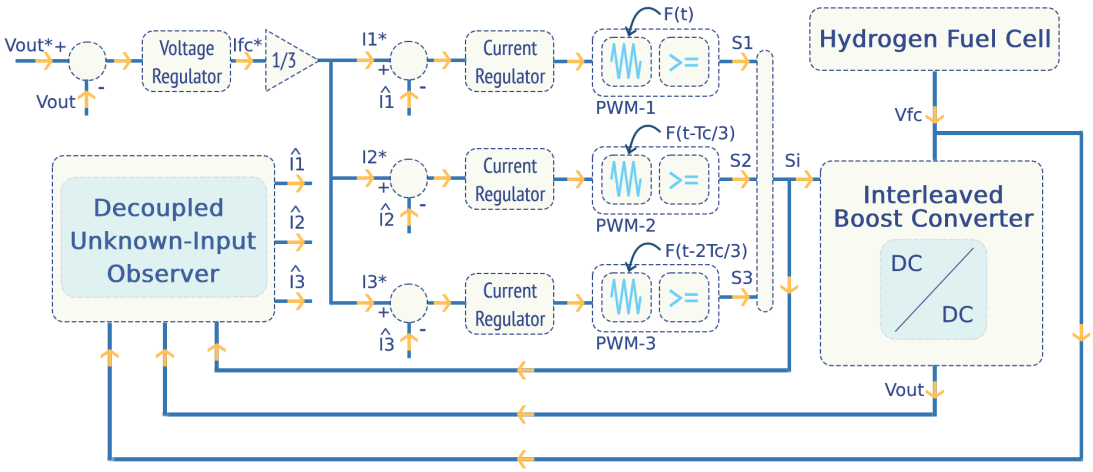

Fig 4.28: Dual-loop control scheme of three-phase interleaved boost converter.

The observer's effectiveness in tracking the unknown input and its variations is assessed through the same load resistance scenario used in the previous example. The scenario commences with $R = 20(\Omega)$, undergoes a decrease to $R = 15(\Omega)$ at $t = 0.4(s)$, and then returns to the initial $R = 20(\Omega)$ at $t = 0.8(s)$. The estimated states are shown in Figure 4.29 though Figure 4.31, and the unknown input is shown in Figure 4.32.

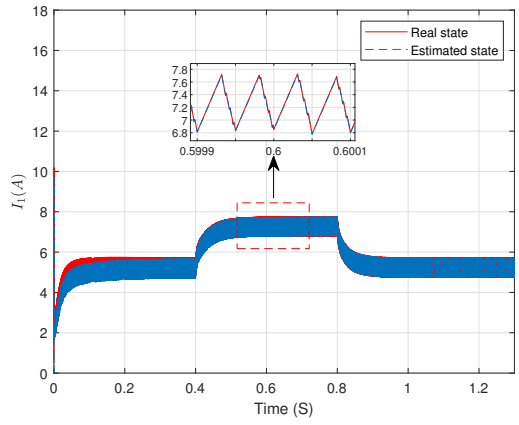

Fig 4.29: Interleaved boost converter phase current I_1.

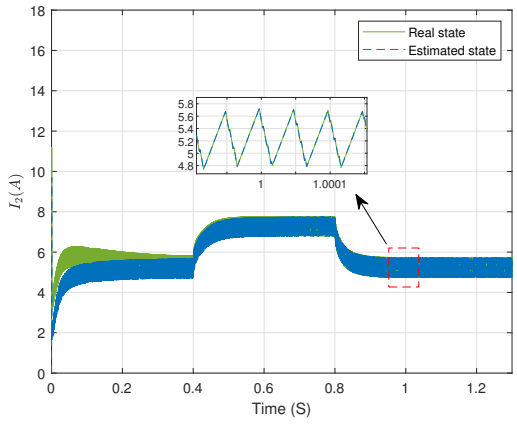

Fig 4.30: Interleaved boost converter phase current I_2.

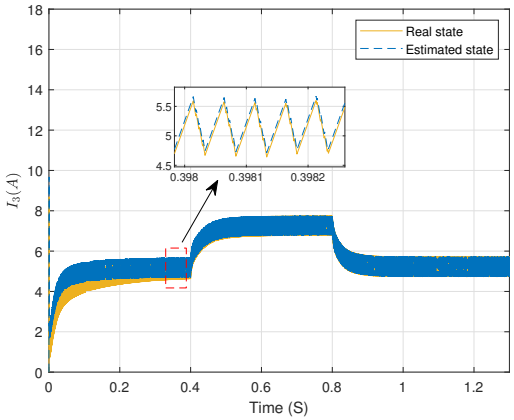

Fig 4.31: Interleaved boost converter phase current I_3.

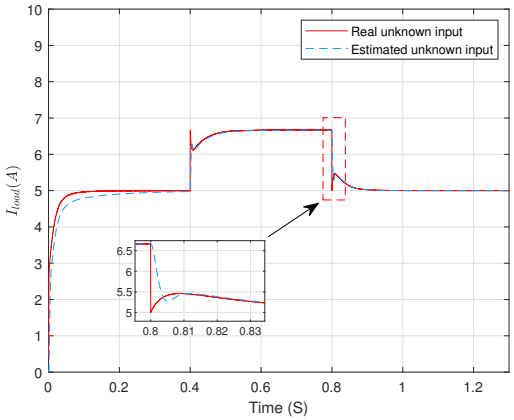

Fig 4.32: The load current (unknown input).

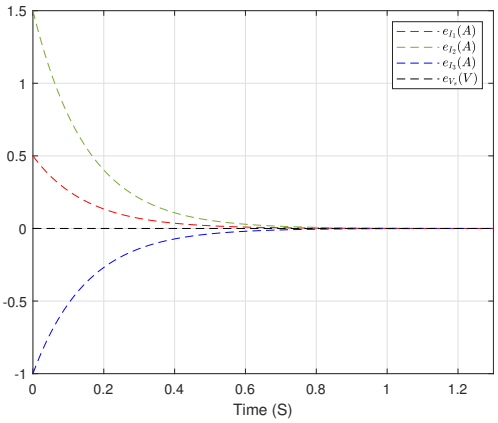

Fig 4.33: State estimation error.

The observations presented in Figures 4.29, 4.30, and 4.31 demonstrate that the estimated states align closely with the actual states, despite the fact that the observer is not utilizing all the same input that the system uses. Typically, an observer necessitates all inputs that the system uses in order to replicate its states. However, through the implementation of a decoupling approach, the impact of the unknown input has been successfully eliminated. As a result, the observer operates effectively without requiring this input. This precise alignment is further evidenced in Figure 4.33, where the estimation error curves are observed to asymptotically converge towards zero, thereby validating the effectiveness of the observer's design.

Additionally, Figure 4.32 distinctly shows the unknown input and its identical estimation despite the variation in the load value, further substantiating the effectiveness of the implemented method outlined in Section 4.3.1.1. Importantly, it's worth noting that all these accomplishments were achieved using only one sensor among the five quantities. This efficient use of resources significantly reduces the cost of the process, making it an even more viable solution.

Collectively, these results provide robust proof of the method's ability to accurately estimate the three-phase currents of the converter as well as the load current under fluctuating charges. Hence, the proposed system not only ensures precision and reliability but also offers cost-effectiveness, further enhancing its applicability and potential for wider implementations.

4.3.2 Observer design for UPV

The structure of the DUIO for the T-S system (4.33) is defined as:

$$\begin{cases} \dot{z}(t) = \sum_{i=1}^{r} \mu_i(\hat{\xi}(t)) \left(N_i z(t) + RA_i \hat{x}(t) + RB_i u(t) + L_i y(t)\right) \\ \hat{x}(t) = z(t) - Hy(t) \end{cases} \tag{4.63}$$

The state estimation error between the system (4.33) and the observer (4.63) is given by:

$$\begin{aligned} e\,(t) &= x\,(t) - \hat{x}\,(t) = x\,(t) - z\,(t) + Hy\,(t) = x\,(t) - z\,(t) + HCx\,(t) + HGd\,(t) \\ &= Rx\,(t) - z\,(t) + HGd(t) \end{aligned} \tag{4.64}$$

where:

$$R = I + HC \tag{4.65}$$

Therefore, the estimation error dynamics are given by:

$$\dot{e}\,(t) = R\dot{x}\,(t) - \dot{z}\,(t) + HG\dot{d}(t) \tag{4.66}$$

After substituting (4.33), (4.63) $y(t)$ and $z(t)$ in (4.66) the following expression is obtained:

$$\begin{aligned} \dot{e}(t) = &\sum_{i=1}^{r} \mu_i(\hat{\xi}(t)) \left[(-N_i R - L_i C)\, x(t) + (RE_i - (L_i + N_i H)\, G)\, d(t) + N_i e(t)\right] \\ &+ HG\dot{d}(t) + R(\Phi(x) - \Phi(\hat{x})) \end{aligned} \tag{4.67}$$

where:

$$\Phi(x) = \sum_{i=1}^{r} \mu_i\left(\xi\,(t)\right) \left[A_i x\,(t) + B_i u\,(t) + E_i d\,(t)\right] \tag{4.68}$$

By using the change of variable $K_i = N_i H + L_i$ and verifying the conditions (4.69) to (4.71)

$$HG = 0 \tag{4.69}$$

$$N_i = -K_i C \tag{4.70}$$

$$RE_i = K_i G \tag{4.71}$$

the error dynamics are then given by:

$$\dot{e}(t) = \sum_{i=1}^{r} \mu_i \left(\hat{\xi}(t)\right) N_i e(t) + R\left(\Phi(x) - \Phi(\hat{x})\right) \tag{4.72}$$

By defining $a = x(t)$ and $b = \hat{x}(t)$, the mean value theorem is applied to the term Φ, utilizing Lemma 3.5, to derive the subsequent result:

$$\dot{e}(t) = \sum_{i=1}^{r} \sum_{j=1}^{q} \mu_i \left(\hat{\xi}(t)\right) h_j(z(t)) (N_i + R\mathcal{A}_j) e(t) \tag{4.73}$$

Based on the work presented in [Ichalal, 2009], the following theorem provides sufficient conditions to guarantee the asymptotic convergence of the error dynamics (4.73):

Theorem 4.4

The estimation error converges asymptotically towards zero with decay rate α if there exist matrices $P = P^T \in \mathbb{R}^{n_x \times n_x} > 0, M_i \in \mathbb{R}^{n_x \times n_y}$ and $S \in \mathbb{R}^{n_x \times n_y}$ such that the following conditions holds $\forall\ i = 1, \ldots, r$ and $j = 1, \ldots, q$:

$$(P\mathcal{A}_j + SC\mathcal{A}_j - M_i C)^T + (P\mathcal{A}_j + SC\mathcal{A}_j - M_i C) < -2\alpha P \tag{4.74}$$

$$SG = 0 \tag{4.75}$$

$$(P + SC) E_i = M_i G \tag{4.76}$$

The observer matrices are given by:

$$H = P^{-1} S \tag{4.77}$$

$$K_i = P^{-1} M_i \tag{4.78}$$

$$N_i = -K_i C \tag{4.79}$$

$$L_i = K_i - N_i H \tag{4.80}$$

Proof. Let's define the quadratic Lyapunov function as follows:

$$V(t) = e(t)^T P e(t) \tag{4.81}$$

The time derivative of $V(t)$ is:

$$\dot{V}(t) = \dot{e}(t)^T P e(t) + e(t)^T P \dot{e}(t) \tag{4.82}$$

By substituting (4.73) and (4.65) in (4.82), equation (4.83) is obtained:

$$\dot{V}(t) = \sum_{i=1}^{r} \sum_{j=1}^{q} \mu_i(\xi(t)) h_j(z(t)) \left[(P\mathcal{A}_j + PHC\mathcal{A}_j - PK_i C)^T + (P\mathcal{A}_j + PHC\mathcal{A}_j - PK_i C)\right] \tag{4.83}$$

Employing the following change of variables:

$$S = PH \tag{4.84}$$

$$M_i = PK_i \tag{4.85}$$

coupled with the decay rate expressed as:

$$\dot{V}(t) < -2\alpha P \tag{4.86}$$

the inequalities outlined in (4.74) of Theorem 4.4 are obtained. By integrating (4.84) with (4.69), equation (4.75) is obtained. Further, combining (4.84) and (4.85) with (4.71) results in equation (4.76). □

Example 15: DUIO design for synchronous reluctance motor

In this example, the same SynRM used in the previous examples is used here. This example is dedicated to validate the performance of the DUIO compared to both PIO and PMIO through a HIL test.

The scheme below demonstrates a comprehensive diagram of the proposed observer in conjunction with the SynRM:

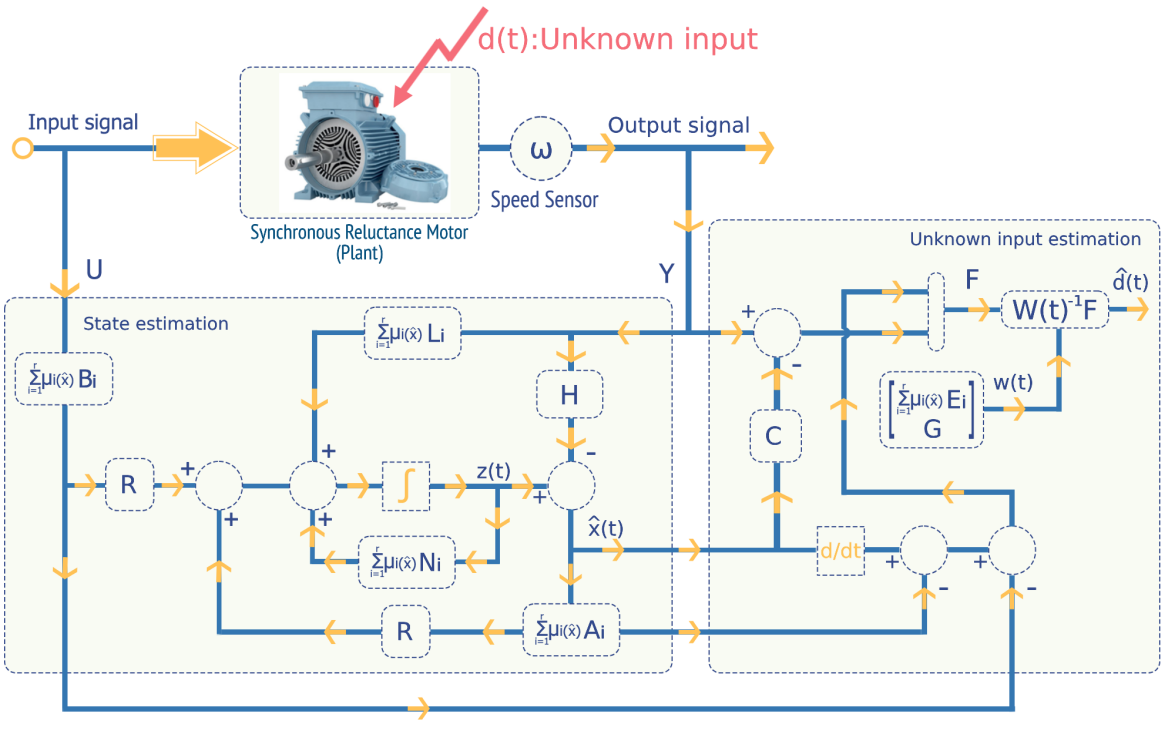

Fig 4.34: Comprehensive diagram of the proposed observer in conjunction with the SynRM

1 - Observer design for SynRM

In order to validate Theorem 4.4, it is necessary to first identify the $\mathcal{A}_i$ terms.

The expression of $\Phi(x)$ in (4.68) is defined as follows:

$$\Phi(x) = A(x)\,x + Bu(t) + Ed(t) \tag{4.87}$$

While its Jacobian $\frac{\partial \Phi}{\partial x}$ is given by:

$$\frac{\partial A(x)x}{\partial x} = \begin{bmatrix} -\frac{R_s}{L_d} & \frac{L_q}{L_d}\omega & \frac{L_q}{L_d}i_{sq} \\ -\frac{L_d}{L_q}\omega & -\frac{R_s}{L_q} & -\frac{L_d}{L_q}i_{sd} \\ \alpha i_{sq} & \alpha i_{sd} & -\frac{f}{Jm} \end{bmatrix}$$

It is important to highlight that the derivation here is performed with respect to $x(t)$, given that the estimation error is defined as $e(t) = x(t) - \hat{x}(t)$. This differs from the approach used in SSUIO, where the estimation error is expressed as $e(t) = x_a(t) - \hat{x}_a(t)$, leading to the derivation being performed with respect to $x_a(t)$.

The Jacobian $\frac{\partial \Phi}{\partial x}$ in this case is identical to that obtained in the earlier examples of the SynRM. Consequently, employing the T-S representation alongside the sector non-linearity approach to this Jacobian, leads to the derivation of the same terms $\mathcal{A}_i$ as those identified in the previous examples.

Taking into consideration the output as the electrical angular speed of the rotor, indicated as $y(t) = \omega(t)$, and using a decay rate of $\alpha = 6.5$, Theorem 4.4 is employed to deduce the observer gains for the DUIO of the SynRM:

$$N_i = \begin{bmatrix} 0 & 0 & 0.0020 \\ 0 & 0 & 0.0592 \\ 0 & 0 & -8.4650 \end{bmatrix}, L_i = \begin{bmatrix} 9.5410 \times 10^{-18} \\ 2.9143 \times 10^{-16} \\ -4.0856 \times 10^{-14} \end{bmatrix} \quad \forall i = 1 \ldots 8$$

$$H = \begin{bmatrix} 0 \\ 0 \\ 0 \\ -1 \end{bmatrix}, R = \begin{bmatrix} 1 & 0 & 0 \\ 0 & 1 & 0 \\ 0 & 0 & 0 \end{bmatrix}, P = \begin{bmatrix} 0.2304 & 0 & 0 \\ 0 & 0.0164 & 0 \\ 0 & 0 & 6.8698 \end{bmatrix} \times 10^3$$

2 - Hardware-in-the-loop validation

This section presents an experimental test conducted to validate the effectiveness of the proposed DUIO. The evaluation is split into two subsections. The first subsection focuses on assessing the effectiveness of state and unknown input estimation of the proposed observer. The second subsection offers a comparative analysis in the context of unknown input estimation of the DUIO against the PIO and the PMIO presented before.

The unknown input observer is integrated within the same Indirect Field-Oriented Control strategy used in the previous SynRM examples. The same HIL structure presented in Figure 4.14 is implemented here.

2 - 1 - Decoupled Unknown Input Observer Performance's Evaluation

The experiment proceeded by utilizing the speed profile depicted in Figure 4.35, in conjunction with a flux reference set to $0.8(Wb)$. The unknown input profile is visually depicted in Figure 4.39. For the purpose of substantiating the stability of the error dynamics, the system's initial conditions were configured as $x_0(t) = \begin{bmatrix} -1 & 2 & 50 \end{bmatrix}^T$. Figures 4.35 through 4.38 present the outcome of the state estimate. Furthermore, Figure 4.39 illustrates the estimation of the unknown input, while its estimation error is clearly represented by Figure 4.40.

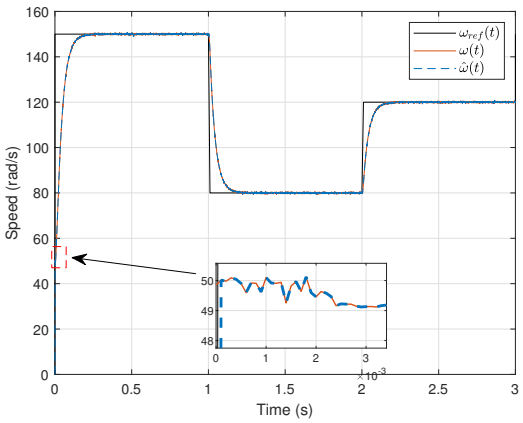

Fig 4.35: Rotor angular speed curve.

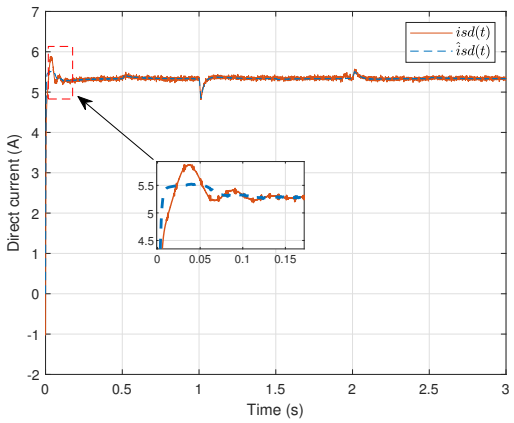

Fig 4.36: Direct axis stator current.

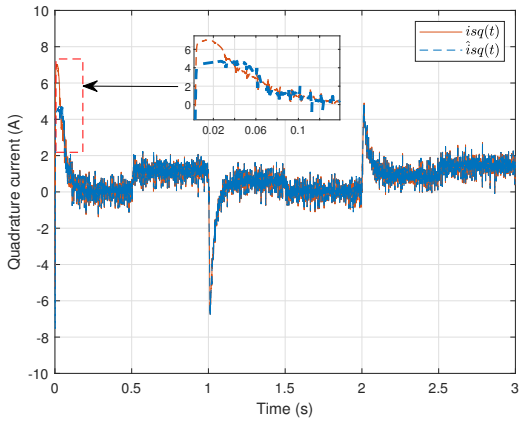

Fig 4.37: Quadrature axis stator current.

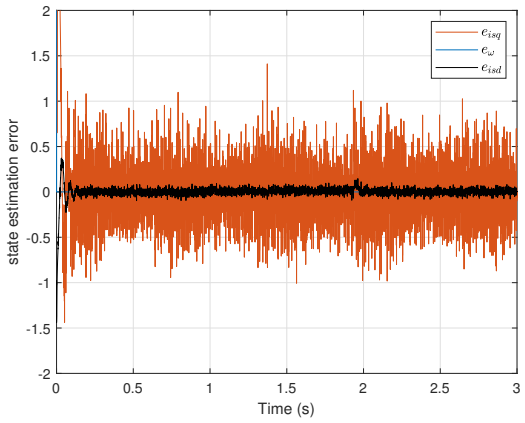

Fig 4.38: State estimation error.

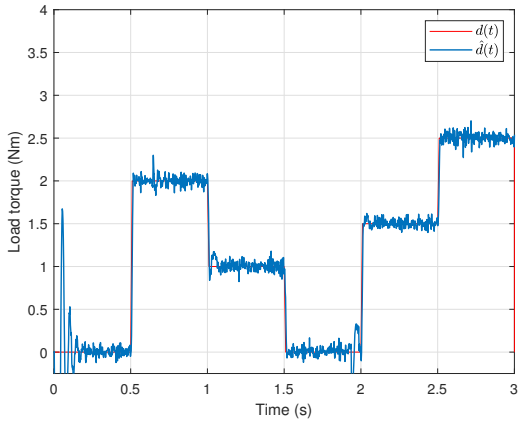

Fig 4.39: Unknown input estimation.

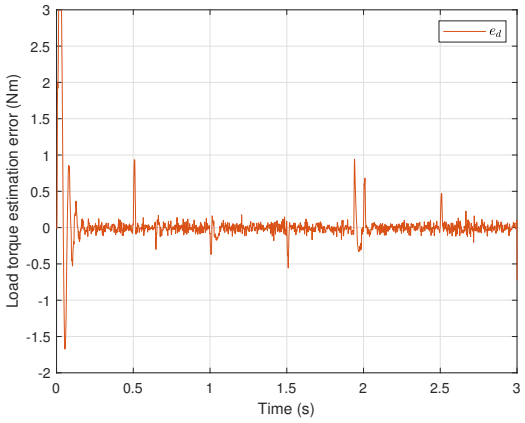

Fig 4.40: Unknown input estimation error.

Observer performance	**Integral Square Error**	**Integral Absolute Error**	**Mean squared error**
$e_{i_{sd}}(A)$	0.0074	0.0588	0.0019
$e_{i_{sq}}(A)$	0.2339	0.4289	0.0585
$e_d(Nm)$	0.4360	0.3779	0.1089

Table 4.5: State estimation performance

The results depicted in Figures 4.35 through 4.40, along with those from Table 4.5, demonstrate the observer's successful estimation of SynRM states despite disturbances in information transmission between the two platforms (dSPACE1 and dSPACE2) and the differences in the initial conditions between the system and the observer. This effective state estimation, even under varying initial conditions, highlights the robustness and adaptability of the observer under challenging real-time application conditions. A further significant observation, illustrated by Figure 4.39, is the observer's ability to adeptly handle the varying nature of the unknown input. Even with these variations, the observer's estimation of this unknown input tracked perfectly, with only minor errors that remained within acceptable limits. This strong performance in the presence of unknown input changes significantly emphasizes the overall reliability of the DUIO.

2 - 2 - Comparative results

In this section, a comparative assessment is conducted to evaluate the performances of the DUIO observer against PIO and PMIO observers. The examination is centered around these observers' capability to estimate unknown input under various conditions: slow, fast and random unknown input variations. The ensuing results will highlights

their adaptability and effectiveness, thereby offering a more comprehensive understanding of their potential utility in real-world applications. The observer gains of both PIO and PMIO are the same obtained in the previous examples.

2 - 2 - 1 - Case 1 (Slow unknown input variation)

A thorough comparative analysis involving the DUIO, PMIO, and PIO was conducted under slow variation conditions of the unknown input. Figure 4.41 represents the actual unknown input and its corresponding estimations. Table 4.6 demonstrates the diverse performance criteria for the estimation error. In these circumstances, it was found that the differences among the three observers were minimal. Despite being primarily designed for estimating unknown inputs with null derivatives, the PIO remarkably managed to effectively accommodate inputs with slow variations, essentially considering their derivatives as null. PMIO markedly demonstrated a good fit with this type of unknown input. Given its original design to handle variable unknown inputs, it is entirely expected that the PMIO performs well with simpler, slow variations. Moreover, the DUIO, despite not considering the form of the unknown input during its design process, demonstrated its robustness and adaptability by providing a commendable estimation, thus highlighting the strength of its design.

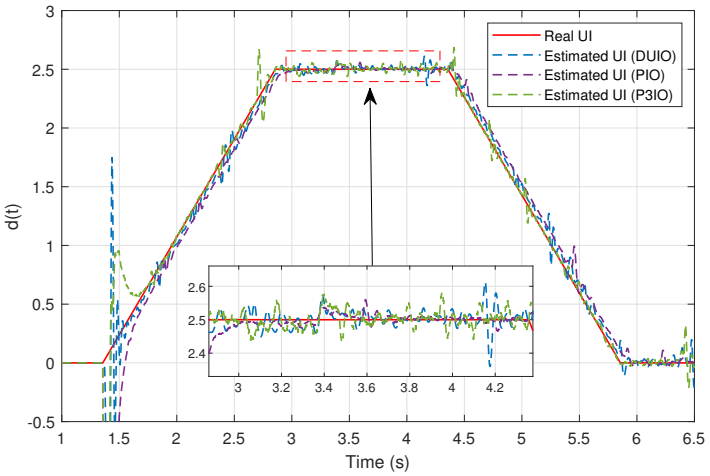

Fig 4.41: Unknown input estimation (case 1).

Observer performance	Integral Square Error	Integral Absolute Error	Mean squared error
PIO	1.6015	0.7519	0.2669
P3IO	1.5907	0.5422	0.2651
DUIO	**0.4841**	**0.4198**	**0.0807**

Table 4.6: Unknown input estimation performance (case 1)

2 - 2 - 2 - Case 2 (Fast unknown input variation)

This experiment, precisely configured for situations where the variation in the UI is fast, gives insight into the distinctive performances of PIO, PMIO, and DUIO. Figure 4.42 offers a detailed illustration of both the actual unknown input and its respective estimates, while Table 4.7 outlines a range of performance criteria related to the estimation error of the unknown input. The PIO, as shown, struggled with the fast changes in the unknown input, hence exposing its limitations in these situations. In contrast, the PMIO, whose design is fundamentally conceived to handle such variations, demonstrated significant adaptability and performance. However, there was a noticeable, albeit slight, drop in PMIO's performance during the phase when the unknown input transitioned from a horizontal to a diagonal form. The increased derivative at this moment exceeds what the observer was originally designed for. Even so, the PMIO recovered swiftly, managing to reduce the estimation error promptly. Under these conditions, the performance disparity between these observers became considerably more pronounced, a contrast further elaborated in Table 4.7. Meanwhile, the DUIO consistently performed at a high level, much as in the first experiment. The resulting estimations aligned closely with the original unknown input, despite its fast variation, illustrating once again the DUIO's effectiveness in providing accurate estimations across diverse scenarios.

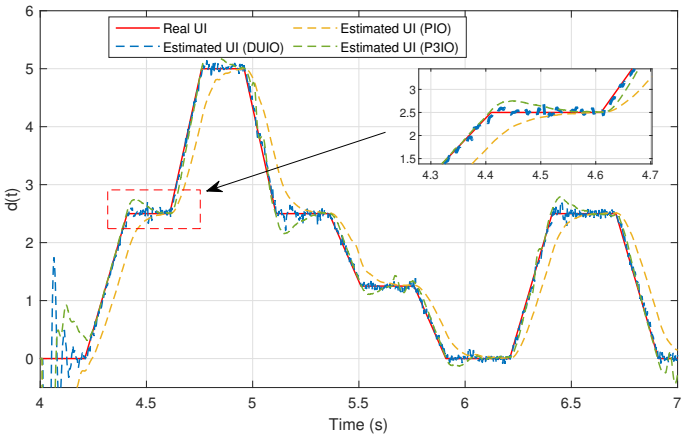

Fig 4.42: Unknown input estimation (case 2).

Observer performance	Integral Square Error	Integral Absolute Error	Mean squared error
PIO	0.4610	0.8667	0.1537
P3IO	0.0535	0.2930	0.0178
DUIO	**0.0120**	**0.1452**	**0.0040**

Table 4.7: Unknown input estimation performance (case 2)

2 - 2 - 3 - Case 3 (Random unknown input variation)

In the third examination performance test, visualized in Figure 4.43 and quantified in Table 4.8, the unknown input displayed an unpredictable and random pattern, thereby posing a rigorous challenge for the three observers. Both PIO and PMIO experienced diminished performance, as the unexpected variability in the unknown input outpaced what these observers were initially designed to manage. However, even within this complex environment, PMIO maintained a level of performance that surpassed PIO, showcasing its resilience amidst unpredictable variations. Concurrently, the DUIO preserved its consistent high performance and remarkable accuracy, deftly managing the random form of the unknown input. This experiment reaffirmed the effectiveness of DUIO's robust design, demonstrating its ability to flexibly accommodate various forms and fluctuations of unknown inputs. In comparison, the constrained performances of PIO and PMIO were highlighted, emphasizing their limitations when faced with scenarios their specific designs did not account for.

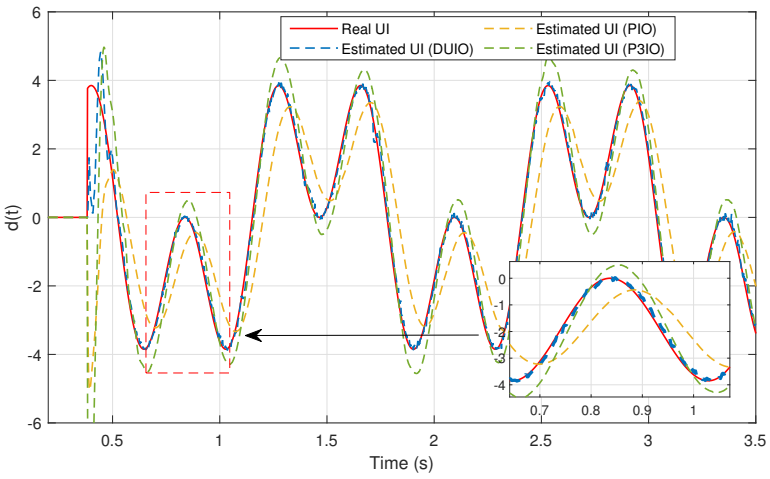

Fig 4.43: Unknown input estimation (case 3).

Observer performance	Integral Square Error	Integral Absolute Error	Mean squared error
PIO	6.0136	2.3199	3.5114
P3IO	4.1586	1.3628	2.4282
DUIO	**0.0889**	**0.2012**	**0.0519**

Table 4.8: Unknown input estimation performance (case 3)

4.4 Conclusion

In this chapter, we have explored two primary methodologies for state and unknown input estimation in T-S fuzzy systems. We began by presenting the design of the PIO, discussing how adjusting its bandwidth impacts the performance of unknown input estimation. Following this, the PMIO was introduced as an enhancement of the PIO, aimed at improving the accuracy of unknown input estimation and expanding the range of unknown input forms that the observer can accommodate. A comparative analysis of these two observers was then conducted through a HIL test applied to a SynRM.

Subsequently, we presented an approach to reduce conservatism in these observers. This improvement was achieved by employing a poly-quadratic Lyapunov function, as opposed to a traditional quadratic one. The use of this advanced function resulted in a more refined and expanded feasibility area, demonstrating its effectiveness in enhancing estimation accuracy.

Finally, we shifted our focus to the second category of unknown input observers, which is based on the decoupling approach. Stability conditions for both the MPV and UPV cases were derived, followed by a comprehensive comparative analysis among the PIO, PMIO, and the DUIO, again validated through a HIL test. This analysis encompassed various scenarios, ranging from slow to random unknown input variations, providing a thorough evaluation of each observer's performance in these different conditions.

General Conclusion

The importance of observers in control theory is paramount, as they are integral to almost all control strategies. This holds particularly true in complex environments where direct measurement of all system states is impractical or impossible. By providing accurate estimates of these unmeasured states, observers enable more effective and efficient control strategies, thus enhancing system performance and reliability. Our work presented in this thesis contributes significantly to this field by expanding the capabilities of state estimation in nonlinear systems through advanced observer design methodologies. This thesis focuses on the analysis and design of observers for nonlinear systems, specifically utilizing the Takagi-Sugeno multi-model approach. Our objective was to enhance existing methodologies by reducing their conservatism, thereby enabling the feasibility of observer design for a broader range of systems and expanding the applicability of these crucial tools in control theory.

In Chapter 1, we introduced the T-S multi-model construction for nonlinear systems, employing the sector nonlinearity approach. This method provides an exact representation of original nonlinear dynamics, exemplified through an application on an induction motor. We also explored the stability conditions of T-S systems under quadratic and poly-quadratic approaches using the second Lyapunov theorem. In Chapter 2, we delved into the observer design for T-S systems, starting by focusing on observability and detectability aspects. These fundamentals are crucial for determining the feasibility of designing an observer. An example of designing an observer for T-S systems with MPV is illustrated through an application to a 3P-IBC.

The core contributions of our thesis were presented in Chapters 3 and 4, targeting the reduction of conservatism in observer design for UPV systems. In Chapter 3, we improved the design of the Lipschitz-based observer, achieving less conservative stability conditions. This was demonstrated through a comparative example, proving the feasibility of our approach over a previous method. We then transitioned to an $\mathcal{L}_2$-gain synthesis approach, effectively reducing conservatism over the Lipschitz-based method. This was exemplified through applications to a DC motor, highlighting the method's ability to mitigate mismatching terms and sensor noise impacts on state estimation error. Further, we explored the mean value theorem-based observer design, fully eliminating the effect of mismatching terms. We contributed in improving this method through the employment

of the poly-quadratic Lyapunov function. The feasibility domain has been plotted to demonstrate the superiority of our approach compared to the quadratic approach used in existing works. An innovative algorithm for solving the resulting BMI stability conditions has been presented and compared to other existing BMI solvers. Chapter 4 focuses on the design of unknown input observers. We began with the design of PIO and PMIO observers, presenting a comprehensive comparative analysis between them. In this context, the practical applicability of the observer was enhanced by optimizing the observer gains for real-time scenarios, demonstrated through hardware-in-the-loop validation on a synchronous reluctance motor. We then developed a PMIO observer based on the mean value theorem, significantly reducing conservatism by employing the poly-quadratic Lyapunov approach. The unknown input observer design based on the decoupling approach has been presented and compared to both previous observers through the same test. In this comparative analysis, we demonstrated the superiority of the DUIO over the PIO and PMIO.

Despite these advancements, several limitations remain. The observers developed lack robustness against parametric variations in nonlinear systems, highlighting a need for more adaptive solutions, especially for real-world applications where parametric variations are common. The algorithm for solving the BMI remains sub-optimal, limiting the full potential of the convex solvers used in the optimization process, which suggests a need for better optimization techniques. Lastly, high-frequency inputs present a challenge in applying the observer in real-world scenarios. The limitations of the microcontrollers result in reduced accuracy in transmitting the input signal to the observer. Therefore, the system's input will not be exactly as the observer's, consequently affecting the estimation accuracy. In this context, the development of more robust observers against high-frequency transmission is required.

Appendix

Appendix A

YALMIP Toolbox: a short tutorial

In order to solve the LMI constraints defined in the proposed theorems, the Yalmip toolbox is employed. Yalmip, **Y**et **A**nother **LMI P**arser , is a renowned modeling language in MATLAB, specially tailored for optimization problems. It provides an intuitive framework for formulating and solving optimization problems, ranging from linear and polynomial to semidefinite programming tasks. Its integration with several solvers allows for a broad spectrum of optimization problems to be tackled efficiently. In the context of our work, utilizing Yalmip facilitates the accurate definition and solution of the constraints, particularly beneficial for complex systems where manual computation might be prone to errors. Here, some basic commands of YALMIP are defined.

A.1 Defining decision variables

In any optimization problem, the unknown variables that need to be determined are referred to as "decision variables". In YALMIP, "**sdpvar**" is used to define the symbolic decision variables.

For example, a rectangular matrix A with n rows and m columns is represented by the command:

```
A = sdpvar(n,m)
```

A symmetric matrix $P \in \mathrm{R}^{n\times n}$ is represented by:

```
P = sdpvar(n,n,'symmetric','real')
```

or by default as follows:

```
P = sdpvar(n,n)
```

For a non-symmetric matrix, the following command is used:

```
P = sdpvar(n,n,'full')
```

Almost all MATLAB operators can be applied on sdpvar objects. Hence, we create diagonal matrix of P with:

```
D = diag(P)
```

The sdpvar objects are manipulated in MATLAB as any other variable and most functions are overloaded. Hence, the following command is valid:

```
P = sdpvar(3,3) + diag(sdpvar(3,1))
```

When employing a poly-quadratic Lyapunov function, there exist r positive definite matrices, each denoted as P_i. These matrices are defined as follows:

```
for i = 1:r
P{i} = sdpvar(n,n);
end
```

A.2 Defining constraints

For example, the declaration of a symmetric matrix along with the imposition of a positive definiteness constraint can be achieved through the following code:

```
n=3
P = sdpvar(n,n)
C = [P>=0]
```

Declaring a symmetric matrix whose elements are all positive can be defined as follows:

```
P = sdpvar(n,n);
C = [P(:)>=0];
```

An example of defining the stability of a linear system using a Lyapunov LMI approach is given as follows:

```
C = [A'*P+P*A<=0];
```

Note that we have defined non-strict inequalities, although our theoretical problem involves strict inequalities. YALMIP will warn or submit and error if you use strict inequalities. If you want to satisfy a strict inequality, you have to define a non-strict inequality with a margin.

```
Tolerance=0.001;% just an example
C = [A'*P+P*A<=-Tolerance];
```

To define a collection of constraints, we simply create and concatenate them as follows:

```
C = [A1'*P+P*A1<= -Tolerance, A2'*P+P*A2<=-Tolerance,
    .., Ar'*P+P*Ar<=-Tolerance];
```

or simply, by using the cell array method:

```
A={A1,A2,..,Ar}
C=[];
for i = 1:r
C = [C, A{i}'*P+P*A{i}<=-Tolerance];
end
```

A.3 Setting options for YALMIP and solver

To configure options in YALMIP and its associated solvers, the command **sdpsettings** is utilized. For instance, to specify the use of the "MOSEK" solver, the following code snippet can be employed:

```
options = sdpsettings('solver','MOSEK');
```

A.4 Solving the optimization problem

After defining all variables and constraints, the optimization problem can be solved using the "**optimize**" command. The syntax for this command is as follows:

```
optimize(Constraints,Objective,options);
```

By default, the objective in an optimization problem is set for minimization. To convert it into a maximization problem, the objective function is multiplied by -1.

For instance, consider the following optimization problem:

$$\max \det(P) \text{ subject to } AP+PA < 0$$

This problem can be solved using the following code:

```
P = sdpvar(n,n);
C = [A*P+P*A<=-Tolerance];
Obj = -logdet(P); %In the context of convex optimization, the
    logarithm of the determinant, expressed as logdet(P), is
   commonly used instead of the determinant det(P) to ensure
   convexity. Additionally, in YALMIP, the function geomean(P
   ) can also be utilized as an alternative approach.
opt = sdpsettings('solver','MOSEK');
diagnostics = optimize(C,Obj,opt);
```

A.5 Analyze the obtained results

After solving the optimization problem, the command "**value**" is used to extract the numerical value of a decision variable:

```
P=value(P)
```

After executing the optimize command, a diagnostic structure is returned. This structure can be used to determine whether the solver successfully solved the problem or encountered any issues. The code to achieve this is as follows:

```
if diagnostics.problem == 0
disp('Solver thinks it is feasible')
P=value(P)
else
disp('Hmm, something went wrong!')
diagnostics.info
yalmiperror(diagnostics.problem)
end
```

While the "optimize" command provides results, it is not guaranteed that these results are always correct. Therefore, it is crucial to verify the feasibility of the optimization problem, particularly whether the constraints have been satisfied. This verification can be accomplished using the "**check**" command, as demonstrated in the following code example:

```
check(C);
[primalfeas,dualfeas] = check(C);
if any(primalfeas<0)
disp(['The problem is infeasible']);
else
disp(['The problem is feasible']);
end
```

In the context of LMI-based optimization, the feasibility of the problem is determined by the eigenvalues of the LMI. If all eigenvalues of the LMI are negative, the problem is considered feasible. Conversely, if at least one eigenvalue is positive, the LMI is not negative definite, rendering the problem infeasible.

For the matrix P, positive definiteness is sought, implying the need for all positive eigenvalues to ensure feasibility.

The "check" command, returns the smallest eigenvalue of the LMI in the variable "**primalfeas**". It's important to note that all definite constraints are reformulated as positive definite constraints. This means that an LMI originally negative definite is made positive definite by multiplying with -1. However, the matrix P remains unchanged in its positive definite form.

Therefore, regardless of whether we are evaluating the matrix P or the LMI, a negative value returned by "primalfeas" indicates an infeasible solution. Conversely, a positive value indicates a feasible solution.

A.6 Example of application

In this section, we present the code used for designing the observer of the 3P-IBC, as discussed in Section Section 2.3.1.1:

```
clear;clc;
c=4.84e-4;L1=1.08e-3;L2=L1;L3=L2;
RL=7.1e-3;r1=RL;r2=RL;r3=RL;
E = [0;0;0;-(1/c)];
B = [0 0 0 1/L1;
0 0 0 1/L2;
0 0 0 1/L3;
0 0 0 0];
A0 = [-r1/L1 0 0 0;
0 -r2/L2 0 0;
0 0 -r3/L3 0;
0 0 0 0];
A1 = [0 0 0 -1/L1;
0 0 0 0;
0 0 0 0;
1/c 0 0 0];
A2 = [0 0 0 0;
0 0 0 -1/L2;
0 0 0 0;
0 1/c 0 0];
A3 = [0 0 0 0;
0 0 0 0;
0 0 0 -1/L3;
```

```
0 0 1/c 0];
C=[0 0 0 1];
n_y=size(C,1);
n_x=size(C,2);
Z1_lim=[1 0];Z2_lim=[1 0];Z3_lim=[1 0];
r=1;
for j=1:2
for k=1:2
for o=1:2
A_TS{r}=A0+A1*Z1_lim(j)+A2*Z2_lim(k)+A3*Z3_lim(o);
r=r+1;
end
end
end
r=r-1;
yalmip('clear');
Tolerance = 1e-5000000;
P = sdpvar(n_x,n_x);
for i=1:r
M{i} = sdpvar(n_x,n_y);
end
F=[P >= +Tolerance];
teta=20;
for i=1:r
F=[F , P*A_TS{i}+A_TS{i}'*P-C'*M{i}'-M{i}*C<= -Tolerance ];
%pole placement
F=[F, [sin(teta)*(P*A_TS{i}+A_TS{i}'*P-C'*M{i}'-M{i}*C) cos(
   teta)*(P*A_TS{i}-A_TS{i}'*P+C'*M{i}'-M{i}*C);
cos(teta)*(-P*A_TS{i}+A_TS{i}'*P-C'*M{i}'+M{i}*C) sin(teta)*(
   P*A_TS{i}+A_TS{i}'*P-C'*M{i}'-M{i}*C)] <= -Tolerance];
end
options = sdpsettings('solver','lmilab');
sol = optimize(F,[],options)
if sol.problem == 0
P=value(P);
for i=1:r
```

```
M{i}=value(M{i});
L{i}=inv(P)*M{i};
end
[primalfeas,dualfeas] = check(F);
if any(primalfeas<0)
disp(['The problem is infeasible']);
else
disp(['The problem is feasible']);
end
else
display('Hmm, something went wrong!');
sol.info
yalmiperror(sol.problem)
end
```

Appendix B

Evaluation of the Lipschitz constant

In this appendix, the steps to evaluate the Lipschitz constant introduced in Section 3.3 are presented [Ichalal et al., 2010].

Let $f(x) : R^n \to R^n$ be a vector function, $f_i(x) : \mathbb{R}^n \to \mathbb{R}$ the i^{th} component of f, $x \in \mathbb{R}^n$ be the state vector and $\hat{x} \in \mathbb{R}^n$ be its estimation.

The Taylor formula at order zero with an integral remainder term of $f(x)$ around $\hat{x}$ is:

$$f_i(x) - f_i(\hat{x}) = \int_{\hat{x}_1}^{x_1} \frac{\partial f_i}{\partial x_1}(t)dt + \ldots + \int_{\hat{x}_n}^{x_n} \frac{\partial f_i}{\partial x_n}(t)dt, i \quad \forall 1, \ldots, n \tag{B.1}$$

Each function variation can be bounded as follows:

$$|f_i(x) - f_i(\hat{x})| \leq \int_{\hat{x}_1}^{x_1} \left|\frac{\partial f_1}{\partial x_1}(t)\right| dt + \ldots + \int_{\hat{x}_n}^{x_n} \left|\frac{\partial f_1}{\partial x_n}(t)\right| dt \tag{B.2}$$

Let's define:

$$a_{ij} = \max_{t \in [x_j \hat{x}_j]} \left|\frac{\partial f_i}{\partial x_j}(t)\right|, \quad \forall i, j \in \{1, .., n\} \tag{B.3}$$

Since the interval $\left[\begin{array}{cc} x_j & \hat{x}_j \end{array}\right]$ is unknown, a_{ij} will be calculated for all $t \in$ R:

$$a_{ij} = \max_{t \in R} \left|\frac{\partial f_i}{\partial x_j}(t)\right| \tag{B.4}$$

Consequently, B.2 will be defined as follows:

$$|f_i(x) - f_i(\hat{x})| \leq a_{i1} |x_1 - \hat{x}_1| + \ldots + a_{in} |x_n - \hat{x}_n| \tag{B.5}$$

By expressing the inequalities B.5 in matrix form, we obtain the following result:

$$|f(x) - f(\hat{x})| \leq J|x - \hat{x}| \tag{B.6}$$

where:

$$J = \begin{bmatrix} a_{11} & \cdots & a_{1n} \\ \vdots & \ddots & \vdots \\ a_{n1} & \cdots & a_{nn} \end{bmatrix} \tag{B.7}$$

The Lipschitz constant of $f(x)$ is given by the largest singular value of J.

Bibliography

[Abdelmalek et al., 2018] Abdelmalek, S., Azar, A. T., and Dib, D. (2018). A novel actuator fault-tolerant control strategy of dfig-based wind turbines using takagi-sugeno multiple models. *International Journal of Control, Automation and Systems*, 16:1415–1424. (page 124).

[Ahrens and Khalil, 2009] Ahrens, J. H. and Khalil, H. K. (2009). High-gain observers in the presence of measurement noise: A switched-gain approach. *Automatica*, 45(4):936–943. (page 52).

[Akhenak, 2004] Akhenak, A. (2004). *Conception d'observateurs non linéaires par approche multimodèle: application au diagnostic*. PhD thesis, éditeur inconnu. (pages 21, 53).

[Akhenak et al., 2003] Akhenak, A., Chadli, M., Maquin, D., and Ragot, J. (2003). State estimation via multiple observer with unknown inputs: Application to the three tank system. In *5th IFAC Symposium on Fault Detection, Supervision and Safety for Technical Processes, Safeprocess' 2003*, page CDROM. (page 153).

[Allag et al., 2019] Allag, M., Allag, A., Zeghib, O., and Hamidani, B. (2019). Robust h_∞ control based on the mean value theorem for induction motor drive. *Journal of Control, Automation and Electrical Systems*, 30(5):657–665. (pages 80, 81).

[Amel, 2020] Amel, H. F. (2020). *Analyse d'Observabilité et Synthèse d'Observateurs à Modes Glissants pour des Systèmes Non Linéaires Décrits par un Modèle de Takagi-Sugeno*. PhD thesis, Université Abou Bekr Belkaid - Tlemcen. (pages 53, 57).

[Anstett et al., 2009] Anstett, F., Millérioux, G., and Bloch, G. (2009). Polytopic observer design for lpv systems based on minimal convex polytope finding. *Journal of Algorithms & Computational Technology*, 3(1):23–43. (page 35).

[Baillieul and Samad, 2021] Baillieul, J. and Samad, T. (2021). *Encyclopedia of systems and control*. Springer. (page 123).

[Bergsten et al., 2002] Bergsten, P., Palm, R., and Driankov, D. (2002). Observers for takagi-sugeno fuzzy systems. *IEEE Transactions on Systems, Man, and Cybernetics, Part B (Cybernetics)*, 32(1):114–121. (page 79).

[Bockmayr et al., 2001] Bockmayr, A., Weispfenning, V., and Maher, M. (2001). Chapter 12 - solving numerical constraints. In Robinson, A. and Voronkov, A., editors, *Handbook of Automated Reasoning*, Handbook of Automated Reasoning, pages 751–842. North-Holland, Amsterdam. (pages 42, 43).

[Boukhlouf et al., 2023] Boukhlouf, A., Hammoudi, M., Saadi, R., and Benbouzid, M. (2023). Hardware-in-the-loop implementation of an unknown input observer for synchronous reluctance motor. *ISA transactions*, 133:485–494. (pages 53, 80, 124).

[Boyd et al., 1994] Boyd, S., Balakrishnan, V., Feron, E., and El Ghaoui, L. (1994). History of linear matrix inequalities in control theory. In *Proceedings of 1994 American Control Conference-ACC'94*, volume 1, pages 31–34. IEEE. (page 38).

[Boyd and Vandenberghe, 2004] Boyd, S. P. and Vandenberghe, L. (2004). *Convex optimization*. Cambridge university press. (pages 33, 34, 35, 42).

[Byrnes et al., 1999] Byrnes, C. I., Gilliam, D. S., and Shubov, V. I. (1999). Boundary control, stabilization and zero-pole dynamics for a non-linear distributed parameter system. *International Journal of Robust and Nonlinear Control: IFAC-Affiliated Journal*, 9(11):737–768. (page 69).

[Chadli and Borne, 2012] Chadli, M. and Borne, P. (2012). *Multiple models approach in automation: Takagi-Sugeno fuzzy systems*. John Wiley & Sons. (pages 17, 19, 72, 75).

[Chaves Jr et al., 2021] Chaves Jr, E. R., de A. Dantas, A. F., and Maitelli, A. L. (2021). Unknown input observer-based actuator and sensor fault estimation technique for uncertain discrete time takagi-sugeno systems. *International Journal of Control, Automation and Systems*, 19(7):2444–2454. (page 80).

[Cherifi et al., 2017] Cherifi, A., Guelton, K., and Arcese, L. (2017). Local d-stabilization of uncertain ts fuzzy models via fuzzy luapunov functions. In *2017 IEEE International Conference on Fuzzy Systems (FUZZ-IEEE)*, pages 1–6. IEEE. (page 73).

[Cherifi et al., 2019] Cherifi, A., Guelton, K., Arcese, L., and Leite, V. J. (2019). Global non-quadratic d-stabilization of takagi–sugeno systems with piecewise continuous membership functions. *Applied Mathematics and Computation*, 351:23–36. (page 73).

[Chilali and Gahinet, 1996] Chilali, M. and Gahinet, P. (1996). H/sub/spl infin//design with pole placement constraints: an lmi approach. *IEEE Transactions on automatic control*, 41(3):358–367. (pages 69, 70, 72).

[Chilali et al., 1999] Chilali, M., Gahinet, P., and Apkarian, P. (1999). Robust pole placement in lmi regions. *IEEE transactions on Automatic Control*, 44(12):2257–2270. (pages 69, 70).

[De Berg, 2000] De Berg, M. (2000). *Computational geometry: algorithms and applications*. Springer Science & Business Media. (page 35).

[Djeddi et al., 2020] Djeddi, A., Soufi, Y., Chenikher, S., and Aouiche, A. (2020). Synthesis of unknown inputs pi and pmi observers for takagi-sugeno augmented models applied on a manipulator arm. *Electrotehnica, Electronica, Automatica*, 68(1):89–97. (page 124).

[Długosz and Baranowski, 2020] Długosz, M. and Baranowski, J. (2020). Observer design for estimation of nonobservable states in buildings. *Mathematical Problems in Engineering*, 2020:1–8. (page 55).

[DUONG, 2013] DUONG, C. C. (2013). *Exploring some alternatives to non-quadratic LMI conditions for analyzing nonlinear systems based on Takagi-Sugeno modelling*. PhD thesis, Citeseer. (page 41).

[Elias et al., 2021] Elias, L. J., Faria, F. A., Araujo, R., and Oliveira, V. A. (2021). Stability analysis of takagi–sugeno systems using a switched fuzzy lyapunov function. *Information Sciences*, 543:43–57. (page 8).

[FADILI et al., 2019] FADILI, Y., LAHMADI, K., and BOUMHIDI, I. (2019). Fault detection and isolation for wind turbine system based on proportional multi-integral observer (pmio). *International Journal of Automation and Smart Technology*, 9(3):121–137. (page 124).

[Filev, 1991] Filev, D. (1991). Fuzzy modeling of complex systems. *International Journal of Approximate Reasoning*, 5(3):281–290. (page 21).

[Fossard and Normand-Cyrot, 1993] Fossard, A. and Normand-Cyrot, D. (1993). *Systèmes non linéaires. 1. Modélisation, estimation*. Masson. (page 54).

[Gasso, 2000] Gasso, K. (2000). *Identification des systèmes dynamiques non-linéaires: approche multi-modèle*. PhD thesis. (page 24).

[Guzman et al., 2021] Guzman, J., López-Estrada, F.-R., Estrada-Manzo, V., and Valencia-Palomo, G. (2021). Actuator fault estimation based on a proportional-integral observer with nonquadratic lyapunov functions. *International Journal of Systems Science*, 52(9):1938–1951. (pages 80, 83, 105, 150).

[Hadi et al., 2019] Hadi, A. S., Shaker, M. S., and Jawad, Q. A. (2019). Estimation/decoupling approach for robust takagi–sugeno uio-based fault reconstruction in nonlinear systems affected by a simultaneous time-varying actuator and sensor faults. *International Journal of Systems Science*, 50(13):2473–2485. (page 125).

[Hamidani et al., 2019] Hamidani, B., Allag, A., Allag, A., and Zeghib, O. (2019). Sensorless non-linear control applied to a pmsm machine based on new extended mvt observer. *Journal of Electrical Engineering & Technology*, 14(4):1615–1623. (page 80).

[Hammoudi et al., 2020] Hammoudi, M. Y., Saadi, R., Cardoso, A. J. M., Benbouzid, M. E. H., and Sahraoui, M. (2020). Practical implementation of h-infinity control for fuel cell-interleaved boost converter. *International Journal of Modelling and Simulation*, 40(1):44–61. (page 155).

[Hasanien et al., 2022] Hasanien, H. M., Shaheen, M. A., Turky, R. A., Qais, M. H., Alghuwainem, S., Kamel, S., Tostado-Véliz, M., and Jurado, F. (2022). Precise modeling of pem fuel cell using a novel enhanced transient search optimization algorithm. *Energy*, 247:123530. (page 155).

[Hendricks et al., 2008] Hendricks, E., Jannerup, O., and Sørensen, P. H. (2008). *Linear systems control: deterministic and stochastic methods*. Springer. (page 68).

[Ichalal, 2009] Ichalal, D. (2009). *Estimation et diagnostic de systèmes non linéaires décrits par un modèle de Takagi-Sugeno*. PhD thesis, Institut National Polytechnique de Lorraine-INPL. (page 160).

[Ichalal et al., 2018] Ichalal, D., Marx, B., Mammar, S., Maquin, D., and Ragot, J. (2018). How to cope with unmeasurable premise variables in takagi–sugeno observer design: Dynamic extension approach. *Engineering Applications of Artificial Intelligence*, 67:430–435. (page 79).

[Ichalal et al., 2007] Ichalal, D., Marx, B., Ragot, J., and Maquin, D. (2007). Design of observers for takagi-sugeno discrete-time systems with immeasurable premise variables. In *5th Workshop on Advanced Control and Diagnosis, ACD 2007*, page CDROM. (page 91).

[Ichalal et al., 2008] Ichalal, D., Marx, B., Ragot, J., and Maquin, D. (2008). Design of observers for takagi-sugeno systems with immeasurable premise variables: an $\mathcal{L}_2$ approach. *IFAC Proceedings Volumes*, 41(2):2768–2773. (pages 80, 91).

[Ichalal et al., 2009a] Ichalal, D., Marx, B., Ragot, J., and Maquin, D. (2009a). Simultaneous state and unknown inputs estimation with pi and pmi observers for takagi sugeno model with unmeasurable premise variables. In *2009 17th Mediterranean conference on control and automation*, pages 353–358. IEEE. (page 80).

[Ichalal et al., 2009b] Ichalal, D., Marx, B., Ragot, J., and Maquin, D. (2009b). State estimation of nonlinear systems using multiple model approach. In *2009 American Control Conference*, pages 4636–4641. IEEE. (page 79).

[Ichalal et al., 2010] Ichalal, D., Marx, B., Ragot, J., and Maquin, D. (2010). State estimation of takagi–sugeno systems with unmeasurable premise variables. *IET Control Theory & Applications*, 4(5):897–908. (page 179).

[Ichalal et al., 2012] Ichalal, D., Marx, B., Ragot, J., and Maquin, D. (2012). Advances in observer design for takagi-sugeno systems with unmeasurable premise variables. In *2012 20th Mediterranean Conference on Control & Automation (MED)*, pages 848–853. IEEE. (pages 79, 81, 83, 84, 87, 88, 89, 90, 119).

[Jiang et al., 2000] Jiang, G.-P., Wang, S.-P., and Song, W.-Z. (2000). Design of observer with integrators for linear systems with unknown input disturbances. *Electronics Letters*, 36(13):1. (page 124).

[Johansen and Foss, 1993] Johansen, T. A. and Foss, B. (1993). Constructing narmax models using armax models. *International journal of control*, 58(5):1125–1153. (page 24).

[Johansen et al., 2000] Johansen, T. A., Shorten, R., and Murray-Smith, R. (2000). On the interpretation and identification of dynamic takagi-sugeno fuzzy models. *IEEE Transactions on Fuzzy systems*, 8(3):297–313. (page 23).

[Kalman, 1960] Kalman, R. E. (1960). A new approach to linear filtering and prediction problems. (pages 7, 51).

[Kang et al., 2019] Kang, S.-W., Kim, J.-S., and Kim, G.-W. (2019). Road roughness estimation based on discrete kalman filter with unknown input. *Vehicle System Dynamics*, 57(10):1530–1544. (page 123).

[Khalil and Praly, 2014] Khalil, H. K. and Praly, L. (2014). High-gain observers in nonlinear feedback control. *International Journal of Robust and Nonlinear Control*, 24(6):993–1015. (page 52).

[Kim and Kim, 2001] Kim, E. and Kim, D. (2001). Stability analysis and synthesis for an affine fuzzy system via lmi and ilmi: Discrete case. *IEEE Transactions on Systems, Man, and Cybernetics, Part B (Cybernetics)*, 31(1):132–140. (page 111).

[Koenig and Mammar, 2002] Koenig, D. and Mammar, S. (2002). Design of proportional-integral observer for unknown input descriptor systems. *IEEE transactions on automatic control*, 47(12):2057–2062. (page 126).

[Ksouri, 1999] Ksouri, M. (1999). *Contribution à la commande multimodèles des processus complexes*. PhD thesis, Thèse de Doctorat, Université des Sciences et Technologies de Lille, Lille. (page 16).

[Kühne et al., 2018] Kühne, P., Pöschke, F., and Schulte, H. (2018). Fault estimation and fault-tolerant control of the fast nrel 5-mw reference wind turbine using a proportional multi-integral observer. *International Journal of Adaptive Control and Signal Processing*, 32(4):568–585. (page 124).

[Lendek et al., 2011] Lendek, Z., Guerra, T. M., Babuska, R., and De Schutter, B. (2011). *Stability analysis and nonlinear observer design using Takagi-Sugeno fuzzy models*, volume 262. Springer. (pages 38, 39, 57).

[Lo and Lin, 2004] Lo, J.-C. and Lin, M.-L. (2004). Observer-based robust h_∞ infin//control for fuzzy systems using two-step procedure. *IEEE Transactions on Fuzzy Systems*, 12(3):350–359. (page 111).

[Louzimi et al., 2017] Louzimi, A., El Assoudi, A., Soulami, J., and El Yaagoubi, E. (2017). Unknown input observer design for a class of nonlinear descriptor systems: a takagi-sugeno approach with lipschitz constraints. *Nonlinear Analysis and Differential Equations*, 5(3):99–116. (page 79).

[Lu et al., 2016] Lu, P., van Kampen, E.-J., de Visser, C. C., and Chu, Q. (2016). Framework for state and unknown input estimation of linear time-varying systems. *Automatica*, 73:145–154. (page 123).

[Luenberger, 1971] Luenberger, D. (1971). An introduction to observers. *IEEE Transactions on automatic control*, 16(6):596–602. (pages 7, 51).

[Luo et al., 2021] Luo, Q., Nguyen, A.-T., Fleming, J., and Zhang, H. (2021). Unknown input observer based approach for distributed tube-based model predictive control of heterogeneous vehicle platoons. *IEEE Transactions on Vehicular Technology*, 70(4):2930–2944. (page 123).

[Mimoune et al., 2023] Mimoune, K., Hammoudi, M. Y., Saadi, R., Benbouzid, M., and Boukhlouf, A. (2023). Real-time implementation of non linear observer based state feedback controller for induction motor using mean value theorem. *Journal of Electrical Engineering & Technology*, 18(1):615–628. (pages 80, 81).

[Mozelli et al., 2009] Mozelli, L. A., Palhares, R. M., Souza, F., and Mendes, E. M. (2009). Reducing conservativeness in recent stability conditions of ts fuzzy systems. *Automatica*, 45(6):1580–1583. (pages 47, 48).

[Na et al., 2017] Na, J., Chen, A. S., Herrmann, G., Burke, R., and Brace, C. (2017). Vehicle engine torque estimation via unknown input observer and adaptive parameter estimation. *IEEE Transactions on Vehicular Technology*, 67(1):409–422. (page 123).

[Nacer et al., 2021] Nacer, M. L., Kherfane, H., Moreau, S., and Saad, S. (2021). Robust observer design for uncertain lipschitz nonlinear systems based on differential mean value theorem: Application to induction motors. *Journal of Control, Automation and Electrical Systems*, 32:132–144. (page 53).

[Naidu, 2002] Naidu, D. (2002). *Optimal Control Systems*. Electrical Engineering Textbook Series. CRC press. (page 55).

[Nguang and Shi, 2006] Nguang, S. K. and Shi, P. (2006). Robust h_∞ output feedback control design for fuzzy dynamic systems with quadratic d stability constraints: An lmi approach. *Information Sciences*, 176(15):2161–2191. (page 73).

[Nguyen et al., 2021] Nguyen, A.-T., Campos, V., Guerra, T.-M., Pan, J., and Xie, W. (2021). Takagi–sugeno fuzzy observer design for nonlinear descriptor systems with unmeasured premise variables and unknown inputs. *International Journal of Robust and Nonlinear Control*, 31(17):8353–8372. (page 102).

[Orjuela, 2008] Orjuela, R. (2008). *Contribution à l'estimation d'état et au diagnostic des systèmes représentés par des multimodèles*. PhD thesis, Institut National Polytechnique de Lorraine-INPL. (pages 17, 22, 52).

[Ouhib, 2020] Ouhib, L. (2020). State and unknown inputs estimation for takagi–sugeno systems with immeasurable premise variables: Proportional multiple integral observer design. *Mathematics and Computers in Simulation*, 167:372–380. (page 79).

[Ouhib and Kara, 2023] Ouhib, L. and Kara, R. (2023). Proportional observer design based on d-stability and finsler's lemma for takagi-sugeno systems. *Fuzzy Sets and Systems*, 452:61–90. (page 80).

[Ouzaz et al., 2021] Ouzaz, M., El Assoudi, A., et al. (2021). Simultaneous state and fault estimation for takagi-sugeno implicit models with lipschitz constraints. *An International Journal of Optimization and Control: Theories & Applications (IJOCTA)*, 11(1):100–108. (page 79).

[Pan et al., 2022] Pan, J., Nguyen, A.-T., Guerra, T.-M., Sentouh, C., Wang, S., and Popieul, J.-C. (2022). Vehicle actuator fault detection with finite-frequency specifications via takagi-sugeno fuzzy observers: Theory and experiments. *IEEE Transactions on Vehicular Technology*, 72(1):407–417. (page 80).

[Pan et al., 2023] Pan, J., Nguyen, A.-T., Wang, S., Deng, H., and Zhang, H. (2023). Fuzzy unknown input observer for estimating sensor and actuator cyber-attacks in intelligent connected vehicles. *Automotive Innovation*, pages 1–12. (pages 53, 80).

[Pérez-Estrada et al., 2018] Pérez-Estrada, A.-J., Osorio-Gordillo, G.-L., Darouach, M., Alma, M., and Olivares-Peregrino, V.-H. (2018). Generalized dynamic observers for quasi-lpv systems with unmeasurable scheduling functions. *International Journal of Robust and Nonlinear Control*, 28(17):5262–5278. (page 80).

[Rhee and Won, 2006] Rhee, B.-J. and Won, S. (2006). A new fuzzy lyapunov function approach for a takagi–sugeno fuzzy control system design. *Fuzzy sets and systems*, 157(9):1211–1228. (page 111).

[Sala and Ariño, 2007] Sala, A. and Ariño, C. (2007). Asymptotically necessary and sufficient conditions for stability and performance in fuzzy control: Applications of polya's theorem. *Fuzzy sets and systems*, 158(24):2671–2686. (page 41).

[Schaum, 2018] Schaum, A. (2018). Strong detectability and unknown input observer design for a class of networks of systems. *IFAC-PapersOnLine*, 51(23):46–51. (page 55).

[Sohrab, 2003] Sohrab, H. H. (2003). *Basic real analysis*, volume 231. Springer. (page 85).

[Sun et al., 2021] Sun, C., Huang, S., Wu, L., Guo, L., and Yi, S. (2021). Robust actuator and sensor fault estimation for fuzzy delay singularly perturbed systems via proportional multiple-integral observer. *Int. J. Innov. Comput. Inf. Control*, 17(3):767–787. (page 124).

[Takagi and Sugeno, 1985] Takagi, T. and Sugeno, M. (1985). Fuzzy identification of systems and its applications to modeling and control. *Systems, Man and Cybernetics, IEEE Transactions on*, (1):116–132. (page 19).

[Tanaka et al., 2001] Tanaka, K., Hori, T., and Wang, H. O. (2001). A fuzzy lyapunov approach to fuzzy control system design. In *Proceedings of the 2001 American Control Conference.(Cat. No. 01CH37148)*, volume 6, pages 4790–4795. IEEE. (page 48).

[Tanaka et al., 2003] Tanaka, K., Hori, T., and Wang, H. O. (2003). A multiple lyapunov function approach to stabilization of fuzzy control systems. *IEEE Transactions on fuzzy systems*, 11(4):582–589. (pages 8, 46).

[Tanaka et al., 1998] Tanaka, K., Ikeda, T., and Wang, H. O. (1998). Fuzzy regulators and fuzzy observers: relaxed stability conditions and lmi-based designs. *IEEE Transactions on fuzzy systems*, 6(2):250–265. (page 46).

[Tanaka and Wang, 2004] Tanaka, K. and Wang, H. O. (2004). *Fuzzy control systems design and analysis: a linear matrix inequality approach*. John Wiley & Sons. (pages 22, 26, 60).

[Tanwani and Trenn, 2019] Tanwani, A. and Trenn, S. (2019). Detectability and observer design for switched differential–algebraic equations. *Automatica*, 99:289–300. (page 55).

[Tuan et al., 2001] Tuan, H. D., Apkarian, P., Narikiyo, T., and Yamamoto, Y. (2001). Parameterized linear matrix inequality techniques in fuzzy control system design. *IEEE Transactions on fuzzy systems*, 9(2):324–332. (page 41).

[Vandenberghe and Balakrishnan, 1997] Vandenberghe, L. and Balakrishnan, V. (1997). Algorithms and software for lmi problems in control. *IEEE Control Systems Magazine*, 17(5):89–95. (page 41).

[Vu et al., 2017] Vu, V.-P., Wang, W.-J., Zurada, J. M., Chen, H.-C., and Chiu, C.-H. (2017). Unknown input method based observer synthesis for a discrete time uncertain t–s fuzzy system. *IEEE Transactions on Fuzzy Systems*, 26(2):761–770. (page 125).

[Wang et al., 1996] Wang, H. O., Tanaka, K., and Griffin, M. F. (1996). An approach to fuzzy control of nonlinear systems: Stability and design issues. *IEEE transactions on fuzzy systems*, 4(1):14–23. (page 40).

[Wang et al., 2016] Wang, L., Zhang, H., and Liu, X. (2016). H1 observer design for continuous-time takagi-sugeno fuzzy model with unknown premise variables via non-quadratic lyapunov function. *IEEE Transactions on Systems, Man, and Cybernetics, Part B (Cybernetics)*, 46(9):1986–1996. (page 83).

[Wojciechowski, 1978] Wojciechowski, B. (1978). Analysis and synthesis of proportional-intergral observers for single-input single-output time-invariant continuous systems. *Ph. D. dissertation, Gliwice, Poland*. (page 124).

[Wu et al., 2008] Wu, L., Wang, C., and Zeng, Q. (2008). Observer-based sliding mode control for a class of uncertain nonlinear neutral delay systems. *Journal of the Franklin Institute*, 345(3):233–253. (page 52).

[Xiaodong and Qingling, 2003] Xiaodong, L. and Qingling, Z. (2003). New approaches to h_∞ controller designs based on fuzzy observers for ts fuzzy systems via lmi. *Automatica*, 39(9):1571–1582. (page 41).

[Yahia et al., 2014] Yahia, K., Matos, D., Estima, J. O., and Cardoso, A. M. (2014). Modeling synchronous reluctance motors including saturation, iron losses and mechanical losses. In *2014 International Symposium on Power Electronics, Electrical Drives, Automation and Motion*, pages 601–606. IEEE. (page 129).

[Yan et al., 2021] Yan, J.-J., Yang, G.-H., and Li, X.-J. (2021). Fault detection in finite frequency domain for ts fuzzy systems with partly unmeasurable premise variables. *Fuzzy Sets and Systems*, 421:158–177. (page 53).

[Yan and Utkin, 2002] Yan, Z. and Utkin, V. (2002). Sliding mode observers for electric machines-an overview. In *IEEE 2002 28th Annual Conference of the Industrial Electronics Society. IECON 02*, volume 3, pages 1842–1847. IEEE. (page 52).

[Yang et al., 2019] Yang, R., Rotondo, D., and Puig, V. (2019). Observer design for takagi-sugeno lipschitz systems affected by disturbances using quadratic boundedness. In *2019 International Conference on Control, Automation and Diagnosis (ICCAD)*, pages 1–6. IEEE. (page 53).

[Youssef et al., 2017] Youssef, T., Chadli, M., Karimi, H. R., and Wang, R. (2017). Actuator and sensor faults estimation based on proportional integral observer for ts fuzzy model. *Journal of the Franklin Institute*, 354(6):2524–2542. (page 80).

[Yves and Granjon, 2001] Yves, G. and Granjon, Y. (C 2001). *Automatique: systèmes linéaires, non linéaires, à temps continu, à temps discret, représentation d'état, cours et exercices corrigés*. Sciences Sup sciences de l'ingénieur. Dunod, Paris. (pages 54, 68).

[Zemouche, 2017] Zemouche, A. (2017). Observer design for nonlinear systems by using high-gain and lpv/lmi-based technique. In *2017 American Control Conference (ACC)*, pages 2624–2629. IEEE. (page 52).

[Zemouche et al., 2005] Zemouche, A., Boutayeb, M., and Bara, G. I. (2005). Observer design for nonlinear systems: An approach based on the differential mean value theorem. In *Proceedings of the 44th IEEE Conference on Decision and Control*, pages 6353–6358. IEEE. (pages 102, 103).

[Zhang et al., 2016] Zhang, J., Swain, A. K., and Nguang, S. K. (2016). *Robust observer-based fault diagnosis for nonlinear systems using MATLAB®*. Springer. (page 41).

[Zhonghai et al., 2018] Zhonghai, M., Shaoping, W., Jian, S., Tongyang, L., and Xingjian, W. (2018). Fault diagnosis of an intelligent hydraulic pump based on a nonlinear unknown input observer. *Chinese Journal of Aeronautics*, 31(2):385–394. (page 123).

[Zhou et al., 2022] Zhou, N., Wang, S., Zhao, J., Huang, Z., and Huang, R. (2022). Observability and detectability analyses for dynamic state estimation of the marginally observable model of a synchronous machine. *IET Generation, Transmission & Distribution*, 16(7):1373–1384. (page 55).